Sensitivity Analysis of Dynamic Systems Subjected to Seismic Loads

by

Christopher Roth and Mircea Grigoriu

Cornell University
School of Civil and Environmental Engineering
Ithaca, New York 14853

NOTICE

MCEER

MULTIDISCIPLINARY CENTER FOR EARTHQUAKE ENGINEERING RESEARCH

A National Center of Excellence in Advanced Technology Applications

Sensitivity Analysis of Dynamic Systems Subjected to Seismic Loads

by

Christopher Roth[1] and Mircea Grigoriu[2]

1   Graduate Research Assistant, School of Civil and Environmental Engineering, Cornell University
2   Professor, School of Civil and Environmental Engineering, Cornell University

MULTIDISCIPLINARY CENTER FOR EARTHQUAKE ENGINEERING RESEARCH
University at Buffalo, State University of New York
Red Jacket Quadrangle, Buffalo, NY 14261

Preface

The Multidisciplinary Center for Earthquake Engineering Research (MCEER) is a national center of excellence in advanced technology applications that is dedicated to the reduction of earthquake losses nationwide. Headquartered at the University at Buffalo, State University of New York, the Center was originally established by the National Science Foundation in 1986, as the National Center for Earthquake Engineering Research (NCEER).

Comprising a consortium of researchers from numerous disciplines and institutions throughout the United States, the Center's mission is to reduce earthquake losses through research and the application of advanced technologies that improve engineering, pre-earthquake planning and post-earthquake recovery strategies. Toward this end, the Center coordinates a nationwide program of multidisciplinary team research, education and outreach activities.

MCEER's research is conducted under the sponsorship of two major federal agencies: the National Science Foundation (NSF) and the Federal Highway Administration (FHWA), and the State of New York. Significant support is derived from the Federal Emergency Management Agency (FEMA), other state governments, academic institutions, foreign governments and private industry.

MCEER's NSF-sponsored research objectives are twofold: to increase resilience by developing seismic evaluation and rehabilitation strategies for the post-disaster facilities and systems (hospitals, electrical and water lifelines, and bridges and highways) that society expects to be operational following an earthquake; and to further enhance resilience by developing improved emergency management capabilities to ensure an effective response and recovery following the earthquake (see the figure below).

A cross-program activity focuses on the establishment of an effective experimental and analytical network to facilitate the exchange of information between researchers located in various institutions across the

iii
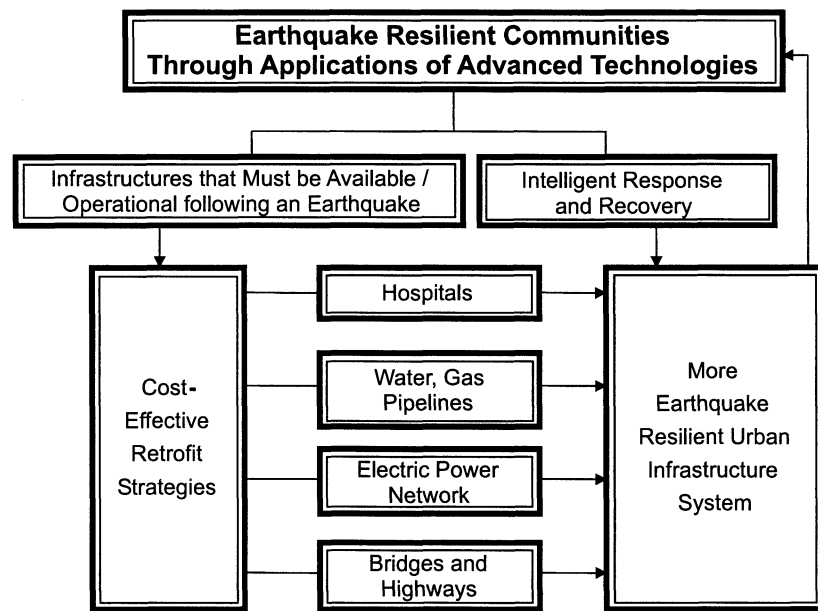
country. These are complemented by, and integrated with, other MCEER activities in education, outreach, technology transfer, and industry partnerships.

This research provides analytical and numerical methods directed to the development of optimal strategies for improving the seismic performance of hospitals and other critical facilities. The sensitivity factors developed in this research provide the basis for a cost effective implementation of advanced technologies.

This report investigates the parameters of both a seismic input and its effect on a dynamic system, such as a building. A quantitative measure of the sensitivity of the response to the seismic input or system parameter was developed, called the sensitivity factor. This factor is defined as the derivative of the response with respect to the parameter value. It can be used to identify critical parameters, estimate the effect of a small change in the parameter value, and select optimum values for the parameter. The direct differentiation method is proposed to calculate the sensitivity factors. By differentiating the governing equation of the system, the governing equation of the sensitivity factor is obtained. This equation can be solved numerically by a similar method to that used to calculate the system response. The errors in the numerical method were investigated and not found to be significant. The method was implemented in two computer programs:

1. *An entire program to calculate both displacement and sensitivity factors was written using the MATLAB code, for a relatively simple, beam-element level of analysis; and*
2. *New subroutines were added to an existing finite element analysis program, DIANA, for more detailed analysis.*

An example is given illustrating applications of the sensitivity factors to a hospital in Buffalo, New York. Both the primary structural and a secondary piping system are considered. The sensitivity factors are used in identification of critical parameters, selection of retrofit strategies, and calculation of fragility curves.

ABSTRACT

A typical problem in earthquake engineering consists of a dynamic system, such as a building, subjected to a seismic ground motion input. In practical problems, the parameters of both the input and the system are not well known. This report investigates a quantitative measure of the sensitivity of the response to an input or system parameter. The measure, termed the sensitivity factor, is defined as the derivative of the response with respect to the parameter value. It can be used to identify critical parameters, estimate the effect of a small change in the parameter value, and select optimum values for the parameter. The direct differentiation method is proposed to calculate the sensitivity factors. By differentiating the governing equation of the system, the governing equation of the sensitivity factor is obtained. This equation can be solved numerically by a similar method to that used to calculate the system response. The errors in the numerical method were investigated and not found to be significant. The method was implemented in two computer programs: (1) an entire program to calculate both displacement and sensitivity factors was written using the MATLAB code, for a relatively simple, beam-element level of analysis; and (2) new subroutines were added to an existing finite element analysis program, DIANA, for more detailed analysis. An example is given illustrating applications of the sensitivity factors to a hospital in Buffalo. Both the primary structural and a secondary piping system are considered. The sensitivity factors are used in identification of critical parameters, selection of retrofit strategies, and calculation of fragility curves.

TABLE OF CONTENTS

LIST OF ILLUSTRATIONS

LIST OF ILLUSTRATIONS

LIST OF ILLUSTRATIONS

SECTION 1
INTRODUCTION

A typical problem in earthquake engineering consists of a dynamic system subjected to a seismic ground motion input. Systems of interest include buildings, bridges and piping systems. In practical problems, the parameters of both the input and the system are not well known. For example, the magnitude and distance of the earthquake event causing the ground motion are extremely uncertain. The soil conditions at the system site affect the ground motion, and these are not always well known. Parameters of the system that are rarely, if ever, certain include material parameters such as strength and stiffness, damping parameters, and section dimensions.

As the parameters of the input and the system are not well known, the response of the system cannot be calculated with absolute certainty. It is useful to determine the sensitivity of the response to the uncertain parameters. This information helps to identify the critical parameters and can be used in many modeling, design, and retrofit applications. For example, when seeking to improve the performance of the system, there is no point in adjusting parameters which have very little effect on the response. The critical parameters have the greatest effect on the response and should be considered first.

This report investigates a measure of sensitivity termed the sensitivity factor, which is defined as the derivative of the response with respect to a parameter of the input or of the system. This measure has been used before, and is a useful quantitative measure of sensitivity. It can be used to identify the critical parameters, as well as in applications such as calibration and optimization of system parameters.

A sensitivity measure is of little practical use if it is difficult to calculate. For a sensitivity measure to be useful it must be possible to calculate it for the typical mathematical models used to represent and analyze practical dynamic systems. With this in mind, a large part of this report is devoted to implementation of calculation routines for sensitivity factors in computer programs that can be used for the analysis of real systems.

In existing work on this topic, the application of the sensitivity factors to practical problems is not covered in any detail. This report attempts to remedy this by presenting an example illustrating the application of the sensitivity factors in the analysis of hospital structural and piping systems.

1.1   Literature review

The idea of using derivatives for sensitivity analysis is not new. A brief review of the history of the theory of sensitivity is given by Eslami [19]. Pioneering theoretical work was done by Bykhovsky in 1947 in Russian [8] and in 1964 in English [9]. This work was primarily in control theory. References to sensitivity analysis in the structural mechanics literature are

more recent. In 1974 Ray investigated sensitivity analysis for a relatively simple hysteretic system [54]. Work on the types of nonlinear systems modeled by finite elements that are of interest here is even more recent. Much of the work has originated from Arora and his co-workers at the Optimal Design Laboratory at the University of Iowa ([3], [28], [66]), who use the sensitivity factors primarily for structural optimization; Kleiber and his co-workers at the Polish Academy of Sciences ([26], [29], [30]); and Zhang and Der Kiureghian at the University of California at Berkeley ([68], [69]) who use the sensitivity factors in probabilistic analysis, for example, first-order reliability analysis.

Three methods have been used to calculate the sensitivity factors: the finite difference method (FDM), the direct differentiation method (DDM), and the adjoint structure method (ASM). A useful review of the three methods is given by Adelman and Haftka [1].

The existing work on sensitivity analysis can be conveniently divided into three groups: linear systems, nonlinear path-independent systems, and nonlinear path-dependent systems. These three groups will be discussed in the following sections.

1.1.1 Linear systems

The simplest problems of all are linear static problems. Lee and Lim [33] [34] use the sensitivity factors and a Taylor series approximation to estimate the displacement of a system with random properties and to select optimum properties for the system. Sergeyev and Mróz [59] use sensitivity factors to optimize the geometry and cross-sectional dimensions of space frames. Both of these references use the DDM. Choi et al [12] suggest a method to apply the ASM using an existing finite element program without making any changes to the source code of the program.

Moving to linear dynamic systems, Liu and Begg [37] derive sensitivity equations for linear systems subjected to active structural control. Benfratello et al [6] use sensitivity factors to estimate the response of a system to white noise input. Both of these use the DDM. Hien and Kleiber [26] give a general formulation of the ASM for linear dynamic systems.

It should also be noted that several authors have investigated the sensitivity of eigenvalues and eigenvectors to the system parameters ([33], [35], [37], [64], [65]). This work will not be considered in this report as the systems of interest are nonlinear, but it may need to be considered in future work.

1.1.2 Nonlinear path-independent systems

For nonlinear problems, many authors fail to make a clear distinction between static and dynamic systems. Many examples are given in which loads are applied incrementally over

"time", but the examples are frequently only quasi-static rather than dynamic as inertia and damping terms are not considered. A true dynamic system is considered by Ma et al [39], who investigate the sensitivity of oscillation of a beam fully fixed at both ends using the DDM. The only nonlinearities considered are geometric. Unfortunately it is not clear that the formulation can be applied to a problem of a more realistic scale.

The other references considered in this section are quasi-static rather than dynamic. Kleiber et al [30] do derive some sensitivity equations for dynamic applications, but the examples given in their paper are only quasi-static. Both the ASM and the DDM were used. Phelan et al [52] and Arora et al [3] present other formulations of the ASM for static problems. The formulation of Arora et al was implemented in the ADINA finite element program.

1.1.3   Nonlinear path-dependent systems

It has been concluded by many authors ([3], [28], [29], [30], [66]) that the ASM is impractical or impossible to use for nonlinear path-dependent systems. All of the references found used the DDM for this type of problem.

Ray et al [55] calculate sensitivity factors for a multistory shear frame structure with a simple bilinear hysteretic relationship between story shear and interstory drift subjected to dynamic ground motion input. However, it is not clear that the formulation can be applied to more general structures and material models.

Tsay et al [66] and Kleiber [29] derive equations for quasi-static problems with geometric and material nonlinearity. However, the formulations are very general and more work would be needed to derive numerically implementable equations for specific material models. Tsay et al give some simple numerical examples using single degree-of-freedom rods in Part 2 of their paper [67]. Kleiber gives no numerical examples.

Zhang and Der Kiureghian [68] give the most useful formulation for sensitivity analysis of dynamic systems using finite elements. Specific equations are derived for the J_2 plasticity model implemented in the FEAP finite element analysis program. Simple numerical examples of a perforated strip and a truss, both subjected to sawtooth oscillating loads, are given.

More recently sensitivity equations have been derived for other specific material models and structures. Jao et al [28] derive equations for an endochronic material model which describes plastic and viscoplastic behavior with one set of equations and no yield surface. The equations are used to optimize the design of a truss subjected to simple ramp force dynamic loading. Kulkarni et al [31] [32] derive equations for plate elements and shells of revolution with a viscoplastic material model. The equations of motion are numerically integrated by the central difference method, which is not commonly used for dynamic analysis under earthquake ground motions.

This report will concentrate on the DDM for nonlinear, path-dependent problems. Although the method has been used before, several changes and new aspects not found in the literature will be included.

- The method will be formulated in terms of history-dependent variables, which may be clearer to follow and implement in incremental numerical integration finite element programs.

- Sensitivity equations have not been derived for the material models used in DIANA or used in piping system analysis. These equations will be derived and implemented.

- A formulation will be included for sensitivity analysis under multiple support excitations.

- The errors in the numerical integration routine used will be investigated.

- The interpretation and use of the sensitivity factors in common earthquake engineering applications will be demonstrated.

1.2   Report organization

This report is divided into three parts:

- Sections 2–4 contain a general description of the problem and the solution approach to be followed. Chapter 2 describes the basic principles of sensitivity analysis. Chapter 3 contains details of the governing equations and the proposed method of solution, and Chapter 4 describes some of the applications of the sensitivity information.

- Sections 5–8 give details of the implementation of the general theory in two software programs that can be used for practical research, analysis and design. Chapter 6 covers the MATLAB program, and Chapter 7 covers the DIANA program. Each chapter contains details of the material models used, derivation of the necessary equations for sensitivity analysis, and details of the software implementation.

- Sections 9 contains an example application of sensitivity analysis to two systems of realistic size and complexity. The systems are the primary structural system and secondary nonstructural piping system of a hospital in Buffalo. The example demonstrates the use of the sensitivity factors in practical design and retrofit.

SECTION 2
SENSITIVITY ANALYSIS

2.1 Definition of sensitivity factors

Consider the basic conceptual model of a dynamic physical system illustrated in figure 2-1. The model consists of an *input*, which passes through the *system*, and results in an *output*. Uncertain parameters may exist in the input and/or the system. Let $\boldsymbol{x}$ be a vector whose coordinates consist of all of the uncertain parameters in both the input and the system. As the properties of the input and the system depend on $\boldsymbol{x}$, the output $\boldsymbol{u}(t, \boldsymbol{x})$ will also be a function of $\boldsymbol{x}$ as well as time t. The input, system, and output will be described in more detail in Section 2.6 for the typical seismic analysis problem considered in this report.

Sensitivity analysis determines the effect on the output $\boldsymbol{u} \in \mathbb{R}^m$ of changing the parameters in $\boldsymbol{x}$. It is useful to introduce a quantitative measure of the sensitivity of $\boldsymbol{u}$ to an arbitrary element x_i of $\boldsymbol{x}$. Several different measures have been proposed. One fairly intuitive measure of sensitivity is the derivative of $\boldsymbol{u}$ with respect to x_i, denoted by $\boldsymbol{v}_i$:

$$\boldsymbol{v}_i(t) = \left\{ \begin{array}{c} v_{1i}(t) \\ v_{2i}(t) \\ v_{3i}(t) \\ \vdots \\ v_{mi}(t) \end{array} \right\} = \left\{ \begin{array}{c} \dfrac{\partial u_1(t)}{\partial x_i}\Big|_{\boldsymbol{x}=\boldsymbol{x}_0} \\ \dfrac{\partial u_2(t)}{\partial x_i}\Big|_{\boldsymbol{x}=\boldsymbol{x}_0} \\ \dfrac{\partial u_3(t)}{\partial x_i}\Big|_{\boldsymbol{x}=\boldsymbol{x}_0} \\ \vdots \\ \dfrac{\partial u_m(t)}{\partial x_i}\Big|_{\boldsymbol{x}=\boldsymbol{x}_0} \end{array} \right\} = \dfrac{\partial \boldsymbol{u}(t, \boldsymbol{x})}{\partial x_i}\Big|_{\boldsymbol{x}=\boldsymbol{x}_0} \tag{2-1}$$

where $\boldsymbol{x}_0$ is the nominal value of $\boldsymbol{x}$.
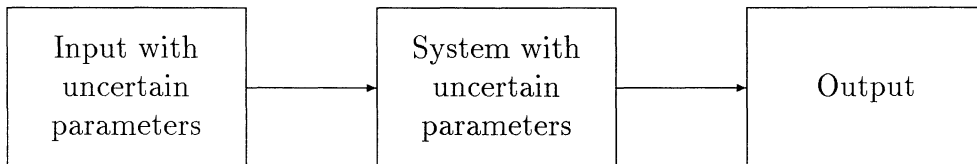
FIGURE 2-1 Model of physical system

This measure is a function of time, like the output $\boldsymbol{u}$. It has been given several names, such as *coefficient of influence* [9], *sensitivity coefficient* [32], and *sensitivity function* [19]. For consistency with previous work at Cornell University [57], it will be termed the *sensitivity factor* in this report.

2.2   Properties of sensitivity factors

The derivative $\boldsymbol{v}_i(t)$ possesses two characteristics that should be expected of a good sensitivity measure: an increasing absolute value of the derivative implies increasing sensitivity; and a positive derivative implies that $\boldsymbol{u}$ increases as x_i increases.

However, a limitation of the derivative is that it measures the sensitivity of $\boldsymbol{u}$ at only a single value of x_i, rather than over a range of values. The extent to which this is a problem depends on the relationship between $\boldsymbol{u}$ and x_i, and on the intended use of the sensitivity information.

Consider the graph of u versus x_i in figure 2-2(a). To illustrate the concepts, the case of scalar, static $u(x)$ will be shown; however, similar comments apply to vector, dynamic $\boldsymbol{u}(t, \boldsymbol{x})$. An excessively detailed sensitivity analysis could conceivably be done by constructing the entire graph of u versus x. This would provide all of the information that could be required of a sensitivity analysis, such as the identification of the values of x that maximize or minimize u; ranges of x over which u changes rapidly as x is changed; and ranges of x over which u decreases as x increases.

However, it is typically not necessary to consider the whole graph of u vs x. In practical situations, x has a limited range of realistic values, and the behavior of u outside of this range need not be considered. For example, the damping ratio in a typical building varies between approximately 2% and 15%. Values outside of this range are unrealistic and thus the behavior of the system outside of this range is irrelevant. The range of realistic variation of x, and the behavior of u over this range, are thus key considerations in sensitivity analysis.

A potential problem with the derivative as a sensitivity measure is illustrated in figure 2-2(a). Suppose that the only sensitivity information available is the derivative at a, and that we wish to use this information to adjust the value of x so that $u(x)$ is maximized. The negative derivative at a would suggest that the optimum x value is less than a, while the opposite is actually true. The derivative is a local measure that gives accurate sensitivity information about the behaviour of the response near the point a, but cannot in general be extrapolated to response farther from a.

In view of this, the derivative is a useful sensitivity measure particularly if the possible range of parameter variation is small (figure 2-2(b)) or if the graph of u vs x is approximately linear, when it may be considered to be accurate over the entire range.

6
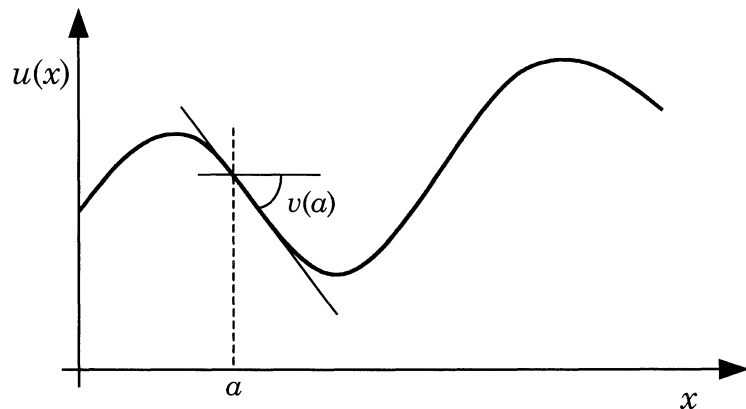
(a)
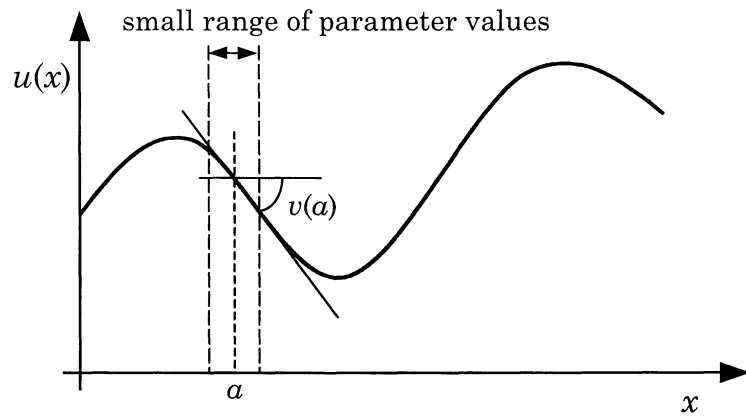
(b)
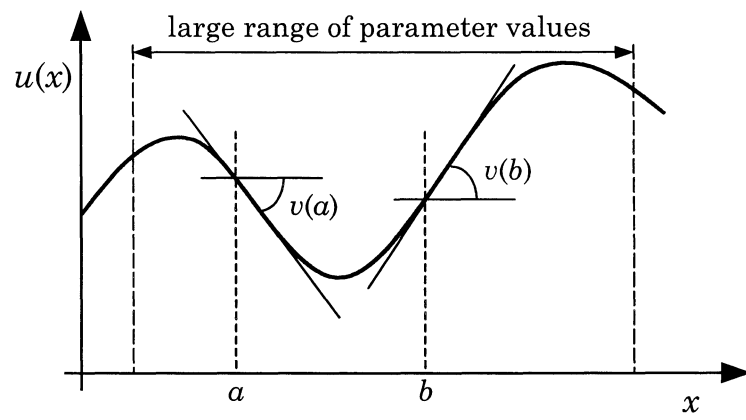
(c)

FIGURE 2-2 System output

7
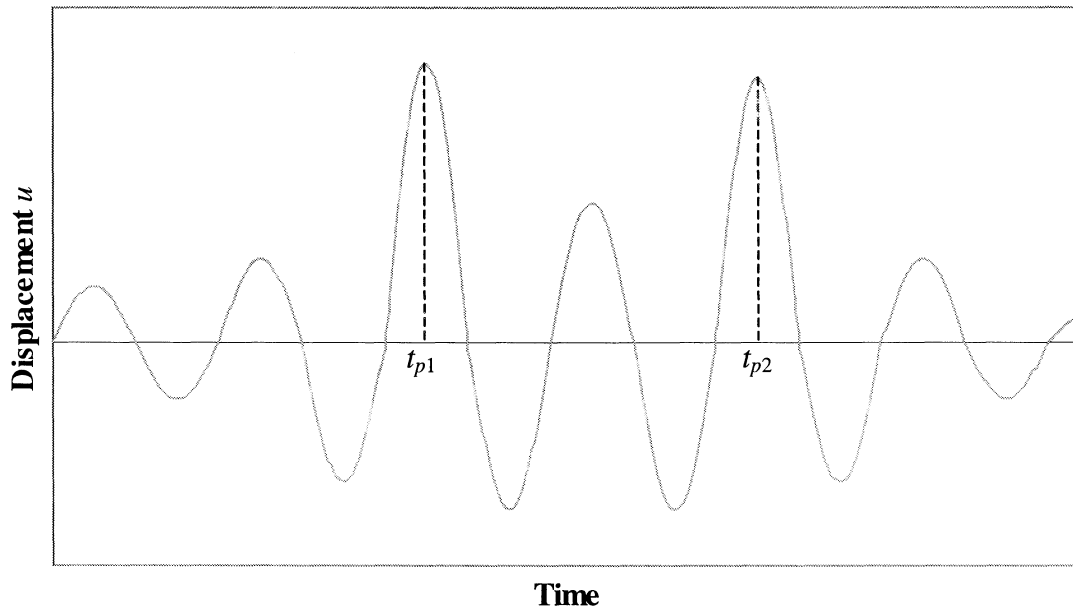
FIGURE 2-3 Response $u(t,x)$ at fixed x

If the possible range of parameter variation is large (figure 2-2(c)), it is unavoidable that analyses will have to be done to determine u at more than one x value to obtain an understanding of the sensitivity, but derivatives are still useful. For example, suppose that in figure 2-2(c) the parameter value that minimizes the response is required. Based on analyses of the system at $x = a$ and $x = b$ without calculating derivatives, it would appear that the optimum parameter value should be greater than b. However, with information from sensitivity analysis it becomes clearer that the optimum value should be sought between a and b.

In dynamic problems where u is a function of both t and x some additional complications arise. In many applications in earthquake engineering, the peak value of u over all t is the critical output, so we are interested in calculating the sensitivity of the peak value to x. It is not immediately clear that the sensitivity factor at the time of the peak value of u is the true sensitivity of the peak value, as the time at which the peak occurs may also depend on x. This can be investigated as follows. Consider the response $u(t,x)$ plotted against t for a fixed value of x in figure 2-3. A typical earthquake response consists of many oscillation cycles. The peak value of u is reached at the peak of one of the cycles.

Suppose for simplicity that there are two cycles with particularly large peak u values, reached at times $t = t_{p1}$ and $t = t_{p2}$ respectively. In general, as x is varied, the times of the peaks will vary so we write $t_{p1}(x)$ and $t_{p2}(x)$. We assume that $t_{p1}(x)$ and $t_{p2}(x)$ are continuous. The peak u values $u(t_{p1}(x),x)$ and $u(t_{p2}(x),x)$ are also obviously functions of x. The graph of $u(t_{p1}(x),x)$ and $u(t_{p2}(x),x)$ versus x will look something like figure 2-4.

8
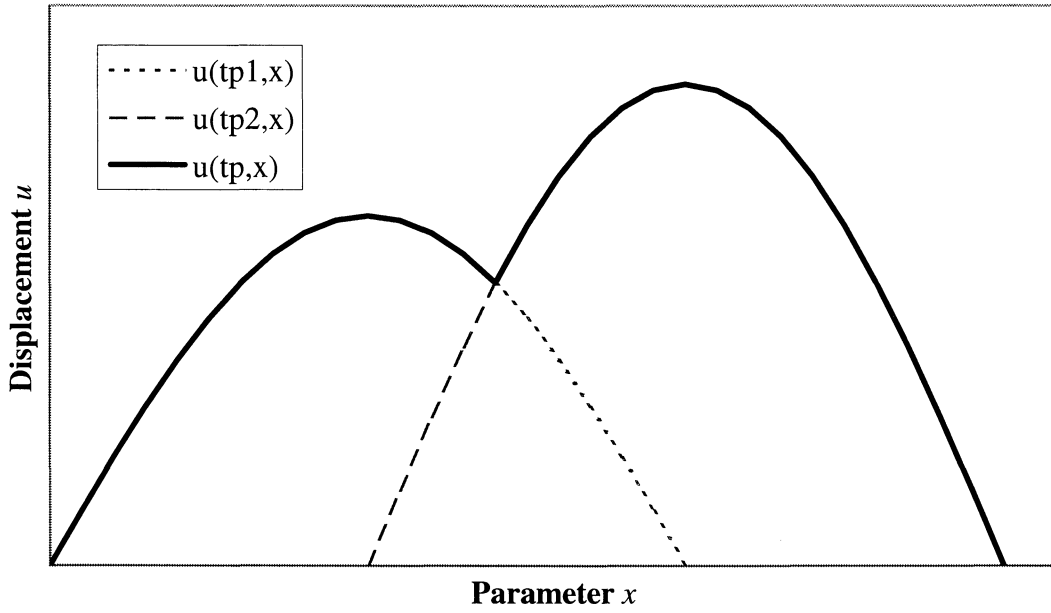
FIGURE 2-4 Peak u values versus x

The peak value of u over all t is the larger of $u(t_{p1}(x), x)$ and $u(t_{p2}(x), x)$. It occurs at time $t_p(x)$, with either $t_p(x) = t_{p1}(x)$ or $t_p(x) = t_{p2}(x)$. The sensitivity of the peak value, $\dfrac{\partial u(t_p(x), x)}{\partial x}$, is the gradient of $u(t_p(x), x)$ in figure 2-4. It is defined for all x except at the x value where $u(t_{p1}(x), x) = u(t_{p2}(x), x)$, where one has to consider left-hand and right-hand derivatives. Away from this x value, the gradient is well defined. The question that arises is: does the following hold?

$$\left.\frac{\partial u(t, x)}{\partial x}\right|_{t=t_p} = \frac{\partial u(t_p(x), x)}{\partial x} \tag{2-2}$$

In words, is the sensitivity factor at the time at which the peak value occurs equal to the true sensitivity of the overall peak value? It is not immediately obvious that equation 2-2 is valid as the left-hand side is the sensitivity factor at a *fixed* time, while the right-hand side is the sensitivity factor of the overall peak value and the time at which this overall peak occurs is not fixed.

Away from the x value where $u(t_{p1}(x), x) = u(t_{p2}(x), x)$, $t_p(x)$ is continuous so the correct gradient of the peak is given by

$$\frac{\partial u(t_p(x), x)}{\partial x} = \left.\frac{\partial u(t, x)}{\partial t}\right|_{t=t_p} \cdot \frac{\partial t_p(x)}{\partial x} + \left.\frac{\partial u(t, x)}{\partial x}\right|_{t=t_p} \tag{2-3}$$

9

$$= \left. \frac{\partial u(t,x)}{\partial x} \right|_{t=t_p}$$

as $\left. \dfrac{\partial u(t,x)}{\partial t} \right|_{t=t_p} = 0$ and $\dfrac{\partial t_p(x)}{\partial x}$ is finite. We can thus use the sensitivity factor at the time of the peak as the true sensitivity factor of the peak, provided that care is taken around values of x where t_p jumps.

Similar comments also apply under suitable assumptions when considering the maximum value of displacement over a two or three dimensional continuum rather than over time.

2.3 Practical applications of sensitivity factors

The sensitivity factors as defined in Section 2.1 have many practical applications, some of which were mentioned in Section 2.2. It is worth listing the applications that are especially useful in seismic analysis:

1. The determination of the effect of a small change in the parameter values. If $\boldsymbol{x}$ is varied by a small amount $h\boldsymbol{e}_i$, the first-order Taylor expansion can be used:

$$\boldsymbol{u}(t, \boldsymbol{x}_0 + h\boldsymbol{e}_i) \approx \boldsymbol{u}(t, \boldsymbol{x}_0) + \boldsymbol{v}_i(t)h \qquad (2\text{-}4)$$

   where $\boldsymbol{e}_i$ is the i-th unit vector and $\boldsymbol{v}_i$ the sensitivity factor. This approximation allows the engineer to estimate the effect of varying a parameter of the system without having to run a time-consuming second dynamic analysis.

2. The identification of the most critical parameters of the system. This is closely related to the above point. A critical parameter is one for which the product of the sensitivity factor ($\boldsymbol{v}_i$) and the uncertainty or variation in the parameter (h) is large. It is clear from equation 2-4 that these parameters will have the greatest influence on the response. The critical parameters need to be determined accurately for satisfactory modeling of the system. They should also be considered first when selecting optimum retrofit strategies. For example, suppose that it is found that the response of a structure is more sensitive to the stiffness of a concrete column than to its strength. The best retrofit strategy to consider would then be one like steel column jacketing that affects the column stiffness, rather than one like glassfiber wrapping that affects only the column strength.

3. The calibration of a computer model against data from experiments and/or more detailed computer models. The problem is to adjust the parameters $\boldsymbol{x}$ so that, for example, the displacement of a critical degree of freedom u_j matches the given data as closely as possible. The sign of the sensitivity factor v_{ji} indicates the direction in

which x_i should be adjusted, and several methods exist for using the magnitude of v_{ji} to indicate by how much x_i should be adjusted. The same process can be used to adjust the value of x_i so that u_j is minimized, as often required during design.

2.4 Calculation of sensitivity factors

The next obvious question is how the sensitivity factor may be calculated. From the literature review in Section 1.1 it appears that the finite difference and direct differentiation methods are suitable for nonlinear, path-dependent problems. In order to select one of the two methods, more details on both of them will be given.

The finite difference method is a common and general method for estimating the sensitivity factors. For a forward finite difference the derivative is approximated by

$$\boldsymbol{v}_i(t) \approx \frac{\boldsymbol{u}(t, \boldsymbol{x}_0 + h\boldsymbol{e}_i) - \boldsymbol{u}(t, \boldsymbol{x}_0)}{h} \qquad (2\text{-}5)$$

The error in the forward finite difference approach is of order h. A better approximation is given by the central finite difference method, where the error is of order h^2

$$\boldsymbol{v}_i(t) \approx \frac{\boldsymbol{u}(t, \boldsymbol{x}_0 + h\boldsymbol{e}_i) - \boldsymbol{u}(t, \boldsymbol{x}_0 - h\boldsymbol{e}_i)}{2h} \qquad (2\text{-}6)$$

The accuracy depends on the increment $h\boldsymbol{e}_i$ of $\boldsymbol{x}$, which is difficult to select *a priori*. The finite difference approach actually gives the secant gradient between two points rather than the tangent gradient at a point. If h is small enough, the resulting approximation is satisfactory. Unfortunately, we do not know how small h should be without performing several calculations and comparing them to the exact solution. In addition, if h is too small, the difference between $\boldsymbol{u}(t, \boldsymbol{x}_0 + h\boldsymbol{e}_i)$ and $\boldsymbol{u}(t, \boldsymbol{x}_0 - h\boldsymbol{e}_i)$ will be small and numerical errors can cause loss of accuracy. Another disadvantage of the finite difference method is that it is necessary to perform at least two analyses of the structure, which may be time-consuming for large structures.

For the direct differentiation method, the governing equation of the system, used to determine the output $\boldsymbol{u}$ from the input, is differentiated to obtain the governing equation of the sensitivity factor. This second equation can then be solved in a similar manner to the original equation. The method eliminates the disadvantages of the finite difference method. The remainder of this report will concentrate on the direct differentiation method to calculate sensitivity factors.

11

Stiffness x_1 $\longrightarrow u$

m $- - - \to p \sin x_2 t$
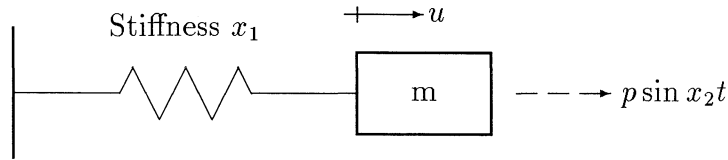
FIGURE 2-5 Single oscillator

2.5 Example

A simple example should make the concepts of sensitivity analysis and the direct differentiation method clearer.

Consider a single undamped oscillator subjected to a harmonic force where the stiffness of the oscillator and frequency of the driving force are uncertain (figure 2-5). This is a dynamic system with one output, and uncertain parameters in the input (x_2) and in the system (x_1).

The governing equation of the system is

$$m\ddot{u} + x_1 u = p\sin(x_2 t) \tag{2-7}$$

with initial conditions $u = 0$, $\dot{u} = 0$ at $t = 0$. An overdot indicates differentiation with respect to t.

Apply the direct differentiation method to obtain the governing equation of the sensitivity factors. Differentiating equation 2-7 with respect to x_i gives the general form of the equation

$$m\ddot{v}_i + x_1 v_i = -\frac{\partial x_1}{\partial x_i}u + \frac{\partial}{\partial x_i}\left[p\sin(x_2 t)\right] \tag{2-8}$$

from which the governing equations for v_1 and v_2 are

$$m\ddot{v}_1 + x_1 v_1 = -u \tag{2-9}$$

$$m\ddot{v}_2 + x_1 v_2 = pt\cos(x_2 t) \tag{2-10}$$

12

For this simple example closed form solutions can be found for equations 2-8, 2-9 and 2-10. The solutions are

$$u = -\frac{p}{x_1}\frac{x_2/\omega}{1-(x_2/\omega)^2}\sin(\omega t) + \frac{p}{x_1}\frac{1}{1-(x_2/\omega)^2}\sin(x_2 t) \qquad (2\text{-}11)$$

$$v_1 = \frac{p}{x_1^2}\frac{1}{\left[1-(x_2/\omega)^2\right]^2}\sin(x_2 t)$$

$$+ \frac{1}{2}\frac{p}{x_1^2}\frac{x_2/\omega}{1-(x_2/\omega)^2}\omega t\cos(\omega t) - \frac{p}{2x_1^2}\frac{3x_2/\omega-(x_2/\omega)^3}{\left[1-(x_2/\omega)^2\right]^2}\sin(\omega t) \qquad (2\text{-}12)$$

$$v_2 = -\frac{p}{x_1\omega}\frac{1+(x_2/\omega)^2}{\left[1-(x_2/\omega)^2\right]^2}\sin(\omega t)$$

$$+ 2\frac{p}{x_1}\frac{x_2/\omega^2}{\left[1-(x_2/\omega)^2\right]^2}\sin(x_2 t) + \frac{p}{x_1}\frac{1}{1-(x_2/\omega)^2}t\cos(x_2 t) \qquad (2\text{-}13)$$

where $\omega = \sqrt{\frac{x_1}{m}}$, the natural frequency of the oscillator. It is assumed that $x_2 \neq \omega$.

To illustrate the results, graphs have been plotted for the following parameter values: $x_1 = 2$, $x_2 = 0.3$, $m = 1$, and $p = 2$. Figure 2-6 shows the response u. Figure 2-7 shows the sensitivity factor v_1 calculated by the direct differentiation method (equation 2-9) only, while figure 2-8 shows sensitivity factor v_2 calculated by both the direct differentiation method (equation 2-10) and by the central difference method (equation 2-6) with $h = 0.02$. As h is reduced further, the two functions converge. This was used as a test to confirm the accuracy of the calculated sensitivity factors.

Suppose x_1 and x_2 are uncertain and may vary within $\pm 3\%$ of their nominal values. We can approximately determine the effect on u by using equation 2-4. Figure 2-9 shows typical results for increasing x_1 by 0.06 (3% of 2). The approximate (equation 2-4) and exact results are shown. Figure 2-10 shows the results for varying x_2 by 0.009 (3% of 0.3).

The figures illustrate a point mentioned in Section 2.3. It is clear from figures 2-7 and 2-8 that the magnitude of v_2 is generally larger than v_1. From this, one may be tempted to conclude that u is substantially more sensitive to x_2 than x_1. However, this would be incorrect. As described in Section 2.3, there are two factors to be considered in the identification of critical parameters: the sensitivity factor itself (v_i), and the uncertainty in the parameter value (h). Figures 2-9 and 2-10 show the effects on the response u of increasing a parameter from its nominal value by 3%, the assumed maximum possible variation. The effects are similar for each parameter. It is thus incorrect to conclude that u is more sensitive to x_2 than x_1.
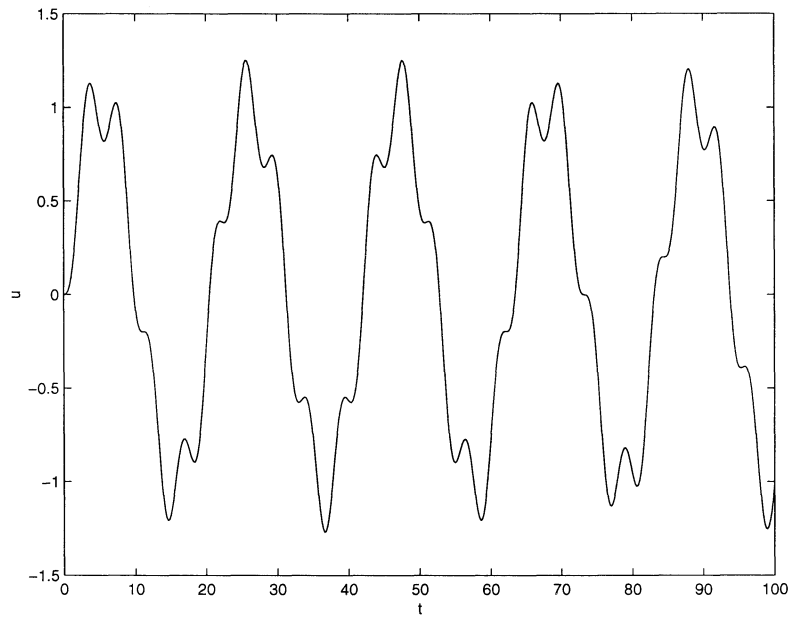
FIGURE 2-6 Response u
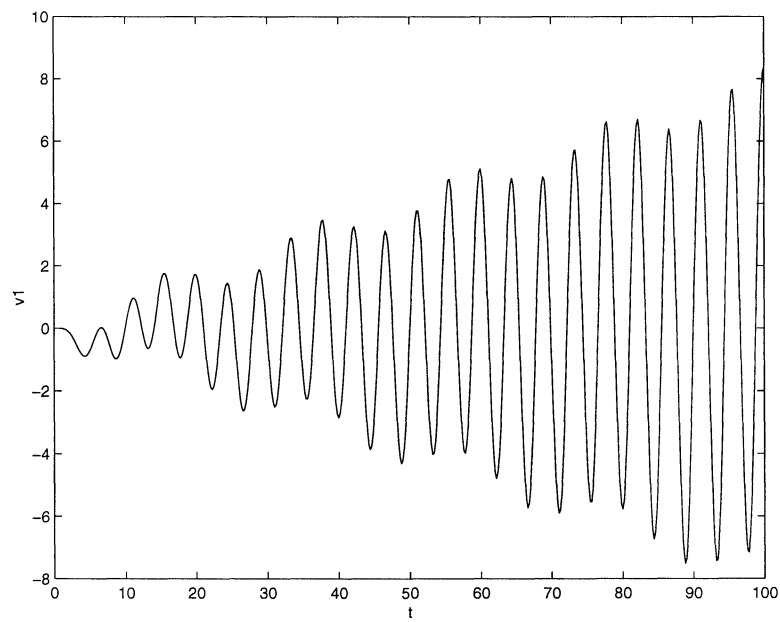
FIGURE 2-7 Sensitivity factor v_1

14
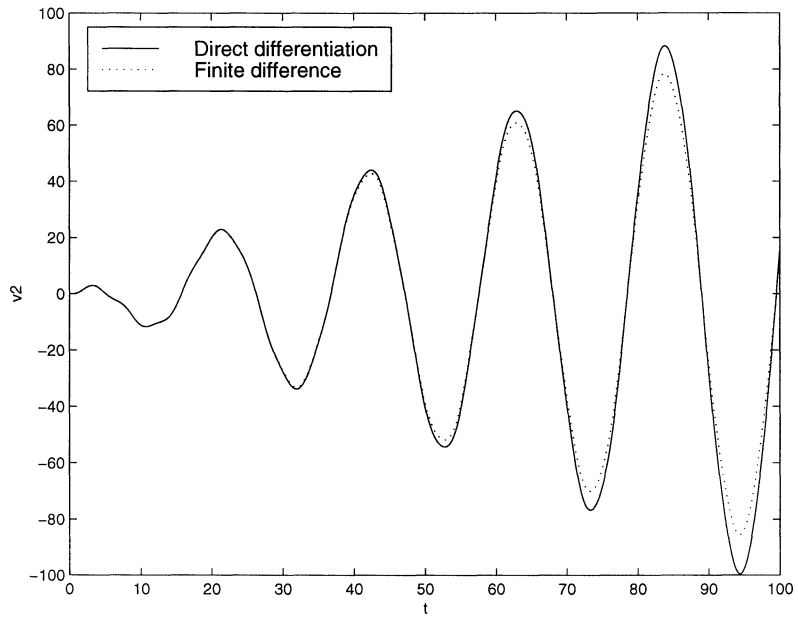
FIGURE 2-8 Sensitivity factor v_2
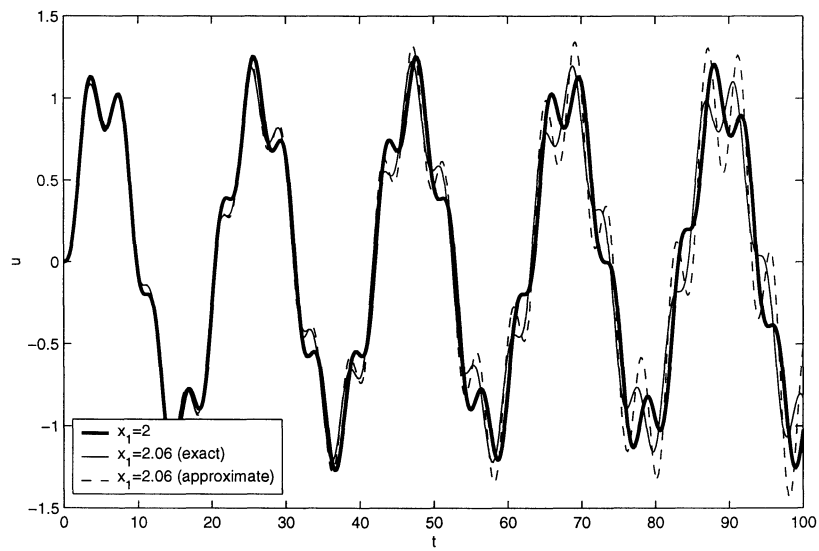
FIGURE 2-9 Effect of increasing x_1 from 2 to 2.06
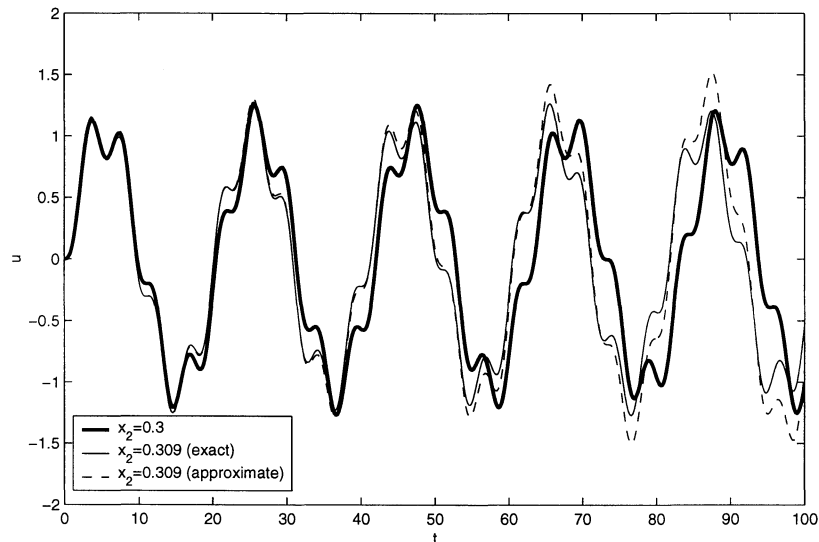
FIGURE 2-10 Effect of increasing x_2 from 0.3 to 0.309

2.6 Sensitivity analysis for earthquake engineering

This section gives details of the physical problem to which we wish to apply the concepts of sensitivity analysis described earlier in the section. Although sensitivity analysis can be applied to almost any physical problem, it is worth thoroughly describing the problem under consideration as the theory in section 3 will be developed specifically for this problem. We wish to investigate the response of a civil engineering structure to an earthquake load. This section describes the problem in more detail in terms of the three parts of the model — the input, system and output.

2.6.1 Input

The input to the problem is an earthquake ground motion record. It specifies the acceleration of the supports of the structure as a function of time. The ground motion may be based on a real earthquake record or on an artificially generated record. The motion is also a function of the uncertain parameters in $\boldsymbol{x}$ and will be denoted $a(t, \boldsymbol{x})$.

One possible example of an uncertain parameter is a scaling factor. Suppose that a given ground motion $w(t)$ is based on a real or artificial earthquake. The motion may be scaled to a different PGA by a factor x:

$$a(t, x) = x\, w(t) \qquad (2\text{-}14)$$

In this case the sensitivity factor with respect to x will indicate the sensitivity of the output to the PGA of the input motion.

Other examples of uncertain parameters arise if the input is modeled as a random process and a parametric representation of the process is used. Suppose that the input is a Gaussian random process with one-sided power spectral density $g(\omega, \boldsymbol{\theta})$ where ω is the frequency and $\boldsymbol{\theta} = (\theta_1, \theta_2, \ldots)$ is a vector of parameters governing the shape of the spectral density. It is possible to simulate the process [63] by selecting a cut-off frequency ω_c, dividing the range $(0, \omega_c)$ into n intervals and approximating the process by:

$$a(t) = \sum_{k=1}^{n} \sqrt{g(\omega_k, \boldsymbol{\theta}) \Delta \omega} \left(A_k \cos \omega_k t + B_k \sin \omega_k t \right) \tag{2-15}$$

where $\Delta \omega = \frac{\omega_c}{n}$; $\omega_k = (k - \frac{1}{2}) \Delta \omega$; and A_k and B_k are standard Gaussian random variables.

Equation 2-15 is a rich source of parameters that may be considered uncertain. For example, $g(\omega_k, \boldsymbol{\theta}), k = 1, 2, \ldots, n$ are uncertain if the parameters in $\boldsymbol{\theta}$ are uncertain. Sensitivity factors with respect to these parameters would thus indicate the sensitivity of the output with respect to the shape of the power spectral density. Variables $A_k, B_k, k = 1, 2, \ldots, n$ are random variables. Sensitivity factors with respect to these variables may be used to estimate the second moment characteristics of the output from a linear Taylor series approximation of the output in terms of the input variables.

2.6.2 System

The system under consideration is a civil engineering structure such as a building, a dam wall, a piping system, or a bridge. We will assume that it is mathematically modeled by discrete elements. In general these elements will be finite elements, although a smaller subset of finite elements such as beam elements or truss elements may also be used. The position of the system at any time t is given by vector $\boldsymbol{u}(t)$, which describes the displacement of each degree of freedom of the system. If the structure is subjected to the input ground motion it vibrates and the resulting displacement vector $\boldsymbol{u}(t)$ is the output of the problem.

Other relevant quantities for the discretized system are the mass matrix $\boldsymbol{m}$, the damping matrix $\boldsymbol{c}$ and the restoring force vector $\boldsymbol{r}$. These are standard quantities in structural dynamics [13] and will not be defined in more detail here. We will assume that the mass matrix $\boldsymbol{m}$ is fixed, but that $\boldsymbol{c}$ and $\boldsymbol{r}$ may depend on the uncertain parameters in $\boldsymbol{x}$. This is reasonable as it is typically easier to accurately determine the mass of a structure than it is to determine the damping or restoring force characteristics. For a general nonlinear structure $\boldsymbol{r}$ may also be a function of displacement $\boldsymbol{u}$, velocity $\dot{\boldsymbol{u}}$ and certain path- or history-dependent parameters which will be stored in vector $\boldsymbol{z}$. These history-dependent parameters are common in

17

hysteresis models [58]. For example, $z(t)$ may contain the maximum value of displacement in the positive direction between the start of the analysis and time t.

It will also be assumed that the geometry of the discretization into elements is fixed. This means that the number of elements, the shapes of the elements, and the position of the nodes connecting the elements are fixed. In this report it will generally be assumed that the same input motion is applied at all supports of the system. However, in Section 3.6 this restriction will be relaxed and equations will be derived for multiple support excitations.

The governing equation of motion of the system subjected to a seismic ground acceleration $a(t, \boldsymbol{x})$ is [13]

$$\boldsymbol{m}\ddot{\boldsymbol{u}}(t, \boldsymbol{x}) + \boldsymbol{c}(\boldsymbol{x})\dot{\boldsymbol{u}}(t, \boldsymbol{x}) + \boldsymbol{r}(\boldsymbol{u}(t, \boldsymbol{x}), \dot{\boldsymbol{u}}(t, \boldsymbol{x}), \boldsymbol{z}(t, \boldsymbol{x}), \boldsymbol{x}) = -\boldsymbol{mi}\,a(t, \boldsymbol{x}) \qquad (2\text{-}16)$$

where $\boldsymbol{i}$ is the influence vector representing the displacement of the masses resulting from static application of a unit ground displacement. An overdot indicates differentiation with respect to t.

Many structural dynamics analysis programs exist to solve equation 2-16 for the output $\boldsymbol{u}$. Differentiating equation 2-16 with respect to x_i gives the governing equation for sensitivity factor $\boldsymbol{v}_i$. This process, and the resulting equations, will be described in more detail in section 3.

2.6.3   Output

As mentioned in the previous section, the output from the system is the displacement as a function of time, $\boldsymbol{u}(t, \boldsymbol{x})$. This is the quantity that existing programs solve for using equation 2-16. The displacement itself is frequently a critical variable in structural analysis and design. However, other quantities based on the displacement may also be critical. For example, the interstory drift in a multistory building is frequently checked as it is a good indicator of structural damage [4]. If $u_i(t, \boldsymbol{x})$ is the lateral displacement of story i in a multistory building and s is the interstory distance, then the interstory drift is given by

$$d_i(t) = \frac{u_{i+1}(t, \boldsymbol{x}) - u_i(t, \boldsymbol{x})}{s} \qquad (2\text{-}17)$$

The sensitivity analysis theory developed in section 3 enables the calculation of sensitivity factors for the displacement. These factors can also be used to find the sensitivity factors

18

for the interstory drift as follows:

$$\frac{\partial d_i(t)}{\partial x_j} = \frac{\dfrac{\partial u_{i+1}(t, \boldsymbol{x})}{\partial x_j} - \dfrac{\partial u_i(t, \boldsymbol{x})}{\partial x_j}}{s}$$

$$= \frac{v_{i+1,j}(t) - v_{i,j}(t)}{s} \qquad (2\text{-}18)$$

Similar calculations may be done for other quantities based on the displacement. For example, various damage indices are based on interstory displacement or joint rotation [10]. Sensitivity factors for these indices may be expressed in terms of the sensitivity factors for the displacement in a similar manner to equation 2-18.

SECTION 3
THEORY

3.1 Governing equations

The governing equations of the displacement $\boldsymbol{u}$ and the sensitivity factors $\boldsymbol{v}$ are second degree differential equations. This section presents the equations, and Section 3.2 describes a method to solve them numerically.

3.1.1 Original system

The governing differential equation for the displacement of the original system contains the mass matrix $\boldsymbol{m}$, the damping matrix $\boldsymbol{c}$, the restoring force vector $\boldsymbol{r}$, the influence vector $\boldsymbol{i}$, and the seismic ground acceleration a; all of which were introduced in Section 2.6. It will be assumed that the mass matrix $\boldsymbol{m}$ is perfectly known, but that $\boldsymbol{c}$, $\boldsymbol{r}$ and a may depend on the uncertain parameters in vector $\boldsymbol{x}$. For a general nonlinear structure $\boldsymbol{r}$ may also be a function of displacement $\boldsymbol{u}$, velocity $\dot{\boldsymbol{u}}$ and the history-dependent parameters in vector $\boldsymbol{z}$. From equation 2-16, the governing equation of the system with $\boldsymbol{x}$ at its nominal value $\boldsymbol{x}_0$ is

$$\boldsymbol{m}\ddot{\boldsymbol{u}}(t, \boldsymbol{x}_0) + \boldsymbol{c}(\boldsymbol{x}_0)\dot{\boldsymbol{u}}(t, \boldsymbol{x}_0) + \boldsymbol{r}(\boldsymbol{u}(t, \boldsymbol{x}_0), \dot{\boldsymbol{u}}(t, \boldsymbol{x}_0), \boldsymbol{z}(t, \boldsymbol{x}_0), \boldsymbol{x}_0) = \boldsymbol{f}(t, \boldsymbol{x}_0) \tag{3-1}$$

where $\boldsymbol{f}(t, \boldsymbol{x}_0) = -\boldsymbol{m}\,\boldsymbol{i}\,a(t, \boldsymbol{x}_0)$. This is the equation that is solved by common existing structural dynamics programs to determine the displacement $\boldsymbol{u}$ of a structure subjected to a ground motion. It is a second degree nonhomogenous differential equation. For general nonlinear restoring force functions, it is also a nonlinear differential equation.

3.1.2 Sensitivity factors

We will start by finding the governing equation of a single sensitivity factor $\boldsymbol{v}_i$. Later, we will combine the equations to obtain a single equation for all of the sensitivity factors.

The governing equation of $\boldsymbol{v}_i$ is obtained by differentiating equation 3-1 with respect to x_i. The derivative of the restoring force $\boldsymbol{r}(\boldsymbol{u}(t, \boldsymbol{x}_0), \dot{\boldsymbol{u}}(t, \boldsymbol{x}_0), \boldsymbol{z}(t, \boldsymbol{x}_0), \boldsymbol{x}_0)$ with respect to x_i is

$$\frac{\partial \boldsymbol{r}}{\partial x_i} = \frac{\partial \boldsymbol{r}}{\partial \boldsymbol{u}}\bigg|_{\dot{\boldsymbol{u}}, \boldsymbol{z}, \boldsymbol{x}} \cdot \frac{\partial \boldsymbol{u}}{\partial x_i} + \frac{\partial \boldsymbol{r}}{\partial \dot{\boldsymbol{u}}}\bigg|_{\boldsymbol{u}, \boldsymbol{z}, \boldsymbol{x}} \cdot \frac{\partial \dot{\boldsymbol{u}}}{\partial x_i} + \frac{\partial \boldsymbol{r}}{\partial \boldsymbol{z}}\bigg|_{\boldsymbol{u}, \dot{\boldsymbol{u}}, \boldsymbol{x}} \cdot \frac{\partial \boldsymbol{z}}{\partial x_i} + \frac{\partial \boldsymbol{r}}{\partial x_i}\bigg|_{\boldsymbol{u}, \dot{\boldsymbol{u}}, \boldsymbol{z}} \tag{3-2}$$

where, for example, $\dfrac{\partial \boldsymbol{r}}{\partial \boldsymbol{u}}\bigg|_{\dot{\boldsymbol{u}}, \boldsymbol{z}, \boldsymbol{x}}$ is the partial derivative of $\boldsymbol{r}$ with respect to $\boldsymbol{u}$ with $\dot{\boldsymbol{u}}$, $\boldsymbol{z}$ and

21

$\boldsymbol{x}$ held fixed; and $\left(\dfrac{\partial \boldsymbol{r}}{\partial \boldsymbol{u}}\right)_{kl} = \dfrac{\partial r_k}{\partial u_l}$. It is common in engineering [24] to drop the variables that are held fixed from the notation. This convention will be followed here, with the exception of $\dfrac{\partial \boldsymbol{r}}{\partial x_i}\bigg|_{\boldsymbol{u},\dot{\boldsymbol{u}},\boldsymbol{z}}$, as this quantity may be confused with the partial derivative on the left hand side of equation 3-2.

With this in mind, equation 3-1 may be differentiated with respect to x_i giving

$$
\begin{aligned}
&\boldsymbol{m}\frac{\partial \ddot{\boldsymbol{u}}(t,\boldsymbol{x}_0)}{\partial x_i} + \frac{\partial \boldsymbol{c}(\boldsymbol{x}_0)}{\partial x_i}\dot{\boldsymbol{u}}(t,\boldsymbol{x}_0) + \boldsymbol{c}(\boldsymbol{x}_0)\frac{\partial \dot{\boldsymbol{u}}(t,\boldsymbol{x}_0)}{\partial x_i} \\
&+ \frac{\partial \boldsymbol{r}}{\partial \boldsymbol{u}}(t,\boldsymbol{x}_0)\cdot\frac{\partial \boldsymbol{u}}{\partial x_i}(t,\boldsymbol{x}_0) + \frac{\partial \boldsymbol{r}}{\partial \dot{\boldsymbol{u}}}(t,\boldsymbol{x}_0)\cdot\frac{\partial \dot{\boldsymbol{u}}}{\partial x_i}(t,\boldsymbol{x}_0) \\
&+ \frac{\partial \boldsymbol{r}}{\partial \boldsymbol{z}}(t,\boldsymbol{x}_0)\cdot\frac{\partial \boldsymbol{z}}{\partial x_i}(t,\boldsymbol{x}_0) + \frac{\partial \boldsymbol{r}}{\partial x_i}\bigg|_{\boldsymbol{u},\dot{\boldsymbol{u}},\boldsymbol{z}}(t,\boldsymbol{x}_0) = \frac{\partial \boldsymbol{f}}{\partial x_i}(t,\boldsymbol{x}_0)
\end{aligned}
\tag{3-3}
$$

Changing the order of differentiation with respect to t and x_i and rearranging

$$
\begin{aligned}
&\boldsymbol{m}\ddot{\boldsymbol{v}}_i(t) + \left[\boldsymbol{c}(\boldsymbol{x}_0) + \frac{\partial \boldsymbol{r}}{\partial \dot{\boldsymbol{u}}}(t,\boldsymbol{x}_0)\right]\dot{\boldsymbol{v}}_i(t) + \frac{\partial \boldsymbol{r}}{\partial \boldsymbol{u}}(t,\boldsymbol{x}_0)\boldsymbol{v}_i(t) = \\
&\frac{\partial \boldsymbol{f}}{\partial x_i}(t,\boldsymbol{x}_0) - \frac{\partial \boldsymbol{c}}{\partial x_i}(\boldsymbol{x}_0)\dot{\boldsymbol{u}}(t,\boldsymbol{x}_0) - \left[\frac{\partial \boldsymbol{r}}{\partial x_i}\bigg|_{\boldsymbol{u},\dot{\boldsymbol{u}},\boldsymbol{z}}(t,\boldsymbol{x}_0) + \frac{\partial \boldsymbol{r}}{\partial \boldsymbol{z}}(t,\boldsymbol{x}_0)\frac{\partial \boldsymbol{z}}{\partial x_i}(t,\boldsymbol{x}_0)\right]
\end{aligned}
\tag{3-4}
$$

It is worth examining equation 3-4 in some detail as it is the governing equation of the sensitivity factor, the subject of this report. The equation is similar in form to equation 3-1 in that it is a second degree nonhomogenous differential equation. However, as the coefficients of $\ddot{\boldsymbol{v}}_i$, $\dot{\boldsymbol{v}}_i$ and $\boldsymbol{v}_i$ and the right-hand side (RHS) of equation 3-4 do not depend on $\boldsymbol{v}_i$, it is a linear differential equation with time-varying coefficients. This is true even if the structure is nonlinear in a structural engineering sense. The coefficient of $\dot{\boldsymbol{v}}_i$ is frequently just $\boldsymbol{c}(\boldsymbol{x}_0)$ as $\dfrac{\partial \boldsymbol{r}}{\partial \dot{\boldsymbol{u}}}$ is zero for most of the restoring force models of interest. The exception would be for rate-dependent material models, but these are rarely encountered in earthquake engineering. The coefficient of $\boldsymbol{v}_i$, $\dfrac{\partial \boldsymbol{r}}{\partial \boldsymbol{u}}$, is the tangent stiffness matrix of the structure and is often used in the calculation of $\boldsymbol{u}$. On the right-hand side (RHS) of the equation, $\dfrac{\partial \boldsymbol{f}}{\partial x_i}$ depends on the input model and is usually not difficult to calculate. If x_i is a parameter of the material model and not the input, then $\dfrac{\partial \boldsymbol{f}}{\partial x_i}$ is zero. Similarly, $\dfrac{\partial \boldsymbol{c}}{\partial x_i}$ is also usually not difficult to find, and generally needs to be calculated only once at the beginning of the analysis. If x_i is a parameter of the input or the restoring force only, then $\dfrac{\partial \boldsymbol{c}}{\partial x_i}$ will be zero. The term

22

in brackets, $\dfrac{\partial \boldsymbol{r}}{\partial x_i}\Big|_{\boldsymbol{u},\dot{\boldsymbol{u}},\boldsymbol{z}} + \dfrac{\partial \boldsymbol{r}}{\partial \boldsymbol{z}}\dfrac{\partial \boldsymbol{z}}{\partial x_i}$, is usually the most difficult to calculate. It contains two of the four terms of the derivative of $\boldsymbol{r}$ with respect to x_i, and may be thought of as the derivative of $\boldsymbol{r}$ with respect to x_i with $\boldsymbol{u}$ and $\dot{\boldsymbol{u}}$ held constant.

Before considering methods to solve equation 3-4, it is necessary to determine whether a unique solution exists. The equation is a linear differential equation. However, the coefficients of $\dot{\boldsymbol{v}}_i$ and $\boldsymbol{v}_i$ and the RHS are in general not continuous functions of time but may exhibit discontinuities or "jumps" at a finite number of time instants. For example, the coefficient of $\boldsymbol{v}_i$ is the tangent stiffness of the structure. For an elasto-plastic structure the value of this stiffness will jump from the elastic stiffness to the tangent plastic stiffness when yielding occurs. The RHS and the coefficient of $\dot{\boldsymbol{v}}_i$ will in general also exhibit discontinuities.

We may prove the existence of a unique solution for $\boldsymbol{v}_i$ in the presence of these discontinuities by considering intervals of continuity. Suppose that discontinuities in one or more coefficients on the left-hand side of equation 3-4 occur at times $\tau_1, \tau_2, \tau_3, \ldots$ with $\tau_1 < \tau_2 < \tau_3 < \ldots$. Consider first the interval $0 < t \le \tau_1$. Over this interval the coefficients are continuous and equation 3-4 can be solved if initial conditions $\boldsymbol{v}_i(0)$ and $\dot{\boldsymbol{v}}_i(0)$ are given. A well-known theorem (for example, Theorem 2 of section 2.1 of [18]) states that the solution for $\boldsymbol{v}_i$ exists and is unique. At time τ_1 record $\boldsymbol{v}_i(\tau_1)$ and $\dot{\boldsymbol{v}}_i(\tau_1)$. Consider next the interval $\tau_1 < t \le \tau_2$. Over this interval the coefficients are again continuous and we can find a unique solution for $\boldsymbol{v}_i$ given initial conditions $\boldsymbol{v}_i(\tau_1)$ and $\dot{\boldsymbol{v}}_i(\tau_1)$. The same procedure can be followed for intervals $\tau_2 < t \le \tau_3$, $\tau_3 < t \le \tau_4$, $\ldots$. In this way it becomes clear that a unique solution for $\boldsymbol{v}_i$ exists from time $t = 0$ until the end of any time period of interest.

3.2 Numerical solution

For general earthquake input motions, it is not possible to find analytical solutions for equations 3-1 and 3-4. Solutions based on numerical integration of the equations are thus required. These numerical solutions are found at a series of discrete time steps $t_1, t_2, t_3, \ldots$ separated by intervals of size Δt. The Newmark method [46] of numerical integration is widely used in earthquake engineering [13] and will be presented here to solve equation 3-1 for the displacement $\boldsymbol{u}$. The method will then be extended to solve equation 3-4 for the sensitivity factor $\boldsymbol{v}_i$.

3.2.1 Original system

The approach followed by the Newmark method is based on an assumption of the variation of the acceleration $\ddot{\boldsymbol{u}}$ over a time step Δt; for example, that $\ddot{\boldsymbol{u}}$ remains constant over the step. Integrating the acceleration results in equations for the increments of velocity and displacement over the step. These equations are then substituted into the governing equation

23

(equation 3-1) giving a linear equation for the increment of displacement over the step. After solving for the displacement increment, the new displacement, velocity and acceleration can be calculated.

To simplify the notation, the dependence of $\boldsymbol{m}$, $\boldsymbol{c}$, $\boldsymbol{f}$ and $\boldsymbol{u}$ on $\boldsymbol{x}$, and $\boldsymbol{r}$ on $\boldsymbol{u}$, $\dot{\boldsymbol{u}}$, $\boldsymbol{z}$ and $\boldsymbol{x}$ will be suppressed. At a general time step t_j, equation 3-1 can be rewritten as

$$\boldsymbol{m}\ddot{\boldsymbol{u}}(t_j) + \boldsymbol{c}\dot{\boldsymbol{u}}(t_j) + \boldsymbol{r}(t_j) = \boldsymbol{f}(t_j) \tag{3-5}$$

The incremental form of equation 3-5, obtained by subtracting equation 3-5 written at time t_j from that at time t_{j+1}, is

$$\boldsymbol{m}\Delta\ddot{\boldsymbol{u}}(t_j) + \boldsymbol{c}\Delta\dot{\boldsymbol{u}}(t_j) + \Delta\boldsymbol{r}(t_j) = \Delta\boldsymbol{f}(t_j) \tag{3-6}$$

where $\Delta\ddot{\boldsymbol{u}}(t_j) = \ddot{\boldsymbol{u}}(t_{j+1}) - \ddot{\boldsymbol{u}}(t_j)$; and other incremental quantities are defined analogously.

For small time steps the following approximation can be made

$$\Delta\boldsymbol{r}(t_j) \approx \frac{\partial \boldsymbol{r}}{\partial \boldsymbol{u}}(t_j)\Delta\boldsymbol{u}(t_j) \tag{3-7}$$

As mentioned in Section 3.1, the matrix $\dfrac{\partial \boldsymbol{r}}{\partial \boldsymbol{u}}$ is commonly known as the tangent stiffness matrix.

Substituting equation 3-7 into equation 3-6, we have

$$\boldsymbol{m}\Delta\ddot{\boldsymbol{u}}(t_j) + \boldsymbol{c}\Delta\dot{\boldsymbol{u}}(t_j) + \frac{\partial \boldsymbol{r}}{\partial \boldsymbol{u}}(t_j)\Delta\boldsymbol{u}(t_j) = \Delta\boldsymbol{f}(t_j) \tag{3-8}$$

As stated in the introduction to this section, the Newmark method is based on an assumption of the variation of $\ddot{\boldsymbol{u}}$ between t_j and t_{j+1}, and results in the following equations

$$\dot{\boldsymbol{u}}(t_{j+1}) = \dot{\boldsymbol{u}}(t_j) + [(1-\gamma)\Delta t]\,\ddot{\boldsymbol{u}}(t_j) + (\gamma\Delta t)\ddot{\boldsymbol{u}}(t_{j+1}) \tag{3-9}$$

$$\boldsymbol{u}(t_{j+1}) = \boldsymbol{u}(t_j) + (\Delta t)\dot{\boldsymbol{u}}(t_j) + \left[(0.5-\beta)(\Delta t)^2\right]\ddot{\boldsymbol{u}}(t_j) + \left[\beta(\Delta t)^2\right]\ddot{\boldsymbol{u}}(t_{j+1}) \tag{3-10}$$

where γ and β are the parameters of the method. These parameters determine the accuracy and stability of the solution. A special case is the average acceleration method, obtained by

selecting $\gamma = \frac{1}{2}$ and $\beta = \frac{1}{4}$. This method is unconditionally stable and is recommended for multi degree-of-freedom, nonlinear systems [13].

Rearranging equations 3-9 and 3-10

$$\Delta \dot{\boldsymbol{u}}(t_j) = \frac{\gamma}{\beta \Delta t} \Delta \boldsymbol{u}(t_j) - \frac{\gamma}{\beta} \dot{\boldsymbol{u}}(t_j) + \Delta t \left(1 - \frac{\gamma}{2\beta} \right) \ddot{\boldsymbol{u}}(t_j) \tag{3-11}$$

$$\Delta \ddot{\boldsymbol{u}}(t_j) = \frac{1}{\beta (\Delta t)^2} \Delta \boldsymbol{u}(t_j) - \frac{1}{\beta \Delta t} \dot{\boldsymbol{u}}(t_j) - \frac{1}{2\beta} \ddot{\boldsymbol{u}}(t_j) \tag{3-12}$$

Substituting equations 3-11 and 3-12 into equation 3-8

$$\hat{\boldsymbol{k}}(t_j) \Delta \boldsymbol{u}(t_j) = \Delta \hat{\boldsymbol{f}}(t_j) \tag{3-13}$$

$$\text{where} \quad \hat{\boldsymbol{k}}(t_j) \quad = \quad \frac{\partial \boldsymbol{r}}{\partial \boldsymbol{u}}(t_j) + \frac{\gamma}{\beta \Delta t} \boldsymbol{c} + \frac{1}{\beta (\Delta t)^2} \boldsymbol{m}$$

$$\Delta \hat{\boldsymbol{f}}(t_j) \quad = \quad \Delta \boldsymbol{f}(t_j) + \left[\frac{1}{\beta \Delta t} \boldsymbol{m} + \frac{\gamma}{\beta} \boldsymbol{c} \right] \dot{\boldsymbol{u}}(t_j)$$

$$+ \left[\frac{1}{2\beta} \boldsymbol{m} + \Delta t \left(\frac{\gamma}{2\beta} - 1 \right) \boldsymbol{c} \right] \ddot{\boldsymbol{u}}(t_j)$$

Equation 3-13 represents a set of simultaneous linear equations and suitable linear algebra methods exist for solving it for the displacement increment $\Delta \boldsymbol{u}(t_j)$. From this $\boldsymbol{u}(t_{j+1})$ may easily be calculated and the equilibrium (equation 3-1) at time t_{j+1} checked. If the equilibrium is not satisfied within a specified tolerance, iteration may be required. This may happen if the time step is too large for equation 3-7 to be accurate or if geometric or material nonlinearities arise between t_j and t_{j+1}. Once $\boldsymbol{u}(t_{j+1})$ is satisfactorily found, $\dot{\boldsymbol{u}}(t_{j+1})$ and $\ddot{\boldsymbol{u}}(t_{j+1})$ can be calculated and the solution can proceed to the next time step.

3.2.2   Sensitivity factors

As it is also not possible in general to find an analytical solution to equation 3-4 for the sensitivity factor, a numerical solution will be required for this equation as well. As equation 3-4 is similar in form to equation 3-1 and the two equations will frequently be solved by the same computer program, the Newmark method will also be used to solve for the sensitivity factor.

The method can be extended in a simple manner to solve equation 3-4 for the sensitivity factor $\boldsymbol{v}_i$. First it is necessary to derive the incremental form of the equation. At time t_j,

we have

$$m\ddot{\boldsymbol{v}}_i(t_j) + \left[\boldsymbol{c} + \frac{\partial \boldsymbol{r}}{\partial \dot{\boldsymbol{u}}}(t_j)\right] \dot{\boldsymbol{v}}_i(t_j) + \frac{\partial \boldsymbol{r}}{\partial \boldsymbol{u}}(t_j)\boldsymbol{v}_i(t_j) =$$

$$\frac{\partial \boldsymbol{f}}{\partial x_i}(t_j) - \frac{\partial \boldsymbol{c}}{\partial x_i}\dot{\boldsymbol{u}}(t_j) - \left[\left.\frac{\partial \boldsymbol{r}}{\partial x_i}\right|_{\boldsymbol{u},\dot{\boldsymbol{u}},\boldsymbol{z}}(t_j) + \frac{\partial \boldsymbol{r}}{\partial \boldsymbol{z}}(t_j)\frac{\partial \boldsymbol{z}}{\partial x_i}(t_j)\right] \tag{3-14}$$

or

$$m\ddot{\boldsymbol{v}}_i(t_j) + \tilde{\boldsymbol{c}}(t_j)\dot{\boldsymbol{v}}_i(t_j) + \tilde{\boldsymbol{k}}(t_j)\boldsymbol{v}_i(t_j) = \tilde{\boldsymbol{f}}_i(t_j) \tag{3-15}$$

where
$$\tilde{\boldsymbol{c}}(t_j) = \boldsymbol{c} + \frac{\partial \boldsymbol{r}}{\partial \dot{\boldsymbol{u}}}(t_j)$$

$$\tilde{\boldsymbol{k}}(t_j) = \frac{\partial \boldsymbol{r}}{\partial \boldsymbol{u}}(t_j)$$

$$\tilde{\boldsymbol{f}}_i(t_j) = \frac{\partial \boldsymbol{f}}{\partial x_i}(t_j) - \frac{\partial \boldsymbol{c}}{\partial x_i}\dot{\boldsymbol{u}}(t_j) - \left[\left.\frac{\partial \boldsymbol{r}}{\partial x_i}\right|_{\boldsymbol{u},\dot{\boldsymbol{u}},\boldsymbol{z}}(t_j) + \frac{\partial \boldsymbol{r}}{\partial \boldsymbol{z}}(t_j)\frac{\partial \boldsymbol{z}}{\partial x_i}(t_j)\right]$$

Subtract equation 3-15 at time t_j from that at time t_{j+1} to obtain the incremental form

$$m\Delta\ddot{\boldsymbol{v}}_i(t_j) + \tilde{\boldsymbol{c}}(t_{j+1})\Delta\dot{\boldsymbol{v}}_i(t_j) + \tilde{\boldsymbol{k}}(t_{j+1})\Delta\boldsymbol{v}_i(t_j) = \Delta\tilde{\boldsymbol{f}}_i(t_j) - \Delta\tilde{\boldsymbol{c}}(t_j)\dot{\boldsymbol{v}}_i(t_j) - \Delta\tilde{\boldsymbol{k}}(t_j)\boldsymbol{v}_i(t_j) \tag{3-16}$$

It should be noted that jumps in the values of $\tilde{\boldsymbol{c}}$, $\tilde{\boldsymbol{k}}$ and $\tilde{\boldsymbol{f}}$ may occur at a time instant between t_j and t_{j+1}. The correct approach would be to determine the time instant of each jump and restart the problem at these times with new equations and the state vector at that instant as the initial conditions. However, this would be extremely difficult and time consuming so we will assume that as Δt is small the errors introduced by not finding the exact time instant are negligible. Section 3.5 will examine these errors in more detail.

Analogous to equations 3-9 and 3-10, we have from the Newmark method

$$\Delta\dot{\boldsymbol{v}}_i(t_j) = \frac{\gamma}{\beta\Delta t}\Delta\boldsymbol{v}_i(t_j) - \frac{\gamma}{\beta}\dot{\boldsymbol{v}}_i(t_j) + \Delta t\left(1 - \frac{\gamma}{2\beta}\right)\ddot{\boldsymbol{v}}_i(t_j) \tag{3-17}$$

$$\Delta\ddot{\boldsymbol{v}}_i(t_j) = \frac{1}{\beta(\Delta t)^2}\Delta\boldsymbol{v}_i(t_j) - \frac{1}{\beta\Delta t}\dot{\boldsymbol{v}}_i(t_j) - \frac{1}{2\beta}\ddot{\boldsymbol{v}}_i(t_j) \tag{3-18}$$

Substituting equations 3-17 and 3-18 into equation 3-16 and rearranging

$$\hat{\tilde{\boldsymbol{k}}}(t_j)\Delta\boldsymbol{v}_i(t_j) = \Delta\hat{\tilde{\boldsymbol{f}}}_i(t_j) \tag{3-19}$$

where $\quad \hat{\tilde{\boldsymbol{k}}}(t_j) \quad = \quad \dfrac{\partial \boldsymbol{r}}{\partial \boldsymbol{u}}(t_{j+1}) + \dfrac{\gamma}{\beta \Delta t}\tilde{\boldsymbol{c}}(t_{j+1}) + \dfrac{1}{\beta(\Delta t)^2}\boldsymbol{m}$

$$\Delta \hat{\tilde{\boldsymbol{f}}}_i(t_j) \;=\; \Delta \tilde{\boldsymbol{f}}_i(t_j) - \Delta \tilde{\boldsymbol{c}}(t_j)\dot{\boldsymbol{v}}_i(t_j) - \Delta \tilde{\boldsymbol{k}}(t_j)\boldsymbol{v}_i(t_j)$$

$$+ \left[\frac{1}{\beta \Delta t}\boldsymbol{m} + \frac{\gamma}{\beta}\tilde{\boldsymbol{c}}(t_{j+1}) \right]\dot{\boldsymbol{v}}_i(t_j)$$

$$+ \left[\frac{1}{2\beta}\boldsymbol{m} + \Delta t \left(\frac{\gamma}{2\beta} - 1 \right)\tilde{\boldsymbol{c}}(t_{j+1}) \right]\ddot{\boldsymbol{v}}_i(t_j)$$

Equation 3-19 can be solved for $\Delta \boldsymbol{v}_i(t_j)$, and $\boldsymbol{v}_i(t_{j+1})$, $\dot{\boldsymbol{v}}_i(t_{j+1})$ and $\ddot{\boldsymbol{v}}_i(t_{j+1})$ can be found. As equation 3-4 is linear in $\boldsymbol{v}$, no iteration is required.

It can be seen that $\hat{\tilde{\boldsymbol{k}}}(t_j)$ is independent of i. The n equations based on equation 3-19 for all n sensitivity factors may thus be combined into one

$$\hat{\tilde{\boldsymbol{k}}}(t_j)\Delta \boldsymbol{v}(t_j) = \Delta \hat{\tilde{\boldsymbol{f}}}(t_j) \qquad\qquad\qquad (3\text{-}20)$$

where $\quad \Delta \boldsymbol{v}(t_j) \quad = \quad \begin{bmatrix} \Delta \boldsymbol{v}_1(t_j) & \Delta \boldsymbol{v}_2(t_j) & \Delta \boldsymbol{v}_3(t_j) & \cdots & \Delta \boldsymbol{v}_n(t_j) \end{bmatrix}$

$\qquad\qquad \Delta \hat{\tilde{\boldsymbol{f}}}(t_j) \quad = \quad \begin{bmatrix} \Delta \hat{\tilde{\boldsymbol{f}}}_1(t_j) & \Delta \hat{\tilde{\boldsymbol{f}}}_2(t_j) & \Delta \hat{\tilde{\boldsymbol{f}}}_3(t_j) & \cdots & \Delta \hat{\tilde{\boldsymbol{f}}}_n(t_j) \end{bmatrix}$

We can solve for all of the sensitivity factors at the same time using the same linear algebra routine used to solve equation 3-13.

3.3 Solution strategy

To summarize, the basic steps required to calculate the sensitivity factor $\boldsymbol{v}$ are

- Solve numerically for displacement $\boldsymbol{u}$ (equation 3-13)

- Calculate necessary derivative quantities such as $\left.\dfrac{\partial \boldsymbol{r}}{\partial x}\right|_{\boldsymbol{u},\dot{\boldsymbol{u}},\boldsymbol{z}} + \dfrac{\partial \boldsymbol{r}}{\partial \boldsymbol{z}}\dfrac{\partial \boldsymbol{z}}{\partial x}$

- Solve numerically for $\boldsymbol{v}$ (equation 3-19).

There are two possible approaches to carrying out these steps: (1) solve for $\boldsymbol{u}$ over the entire duration of interest, storing the necessary information at each step, and then solve for $\boldsymbol{v}$; and (2) solve for $\boldsymbol{u}$ at a time step t_j, calculate the necessary information, solve for $\boldsymbol{v}$ at t_j, and then move on to t_{j+1}. The second approach is preferred as the first would require storage of prohibitively large amounts of information for large problems.

The required procedure at a typical time step is summarized in figure 3-1. Two comments should be made to clarify the procedure:

1. It can be seen that $\frac{\partial \boldsymbol{z}}{\partial \boldsymbol{x}}(t_{j+1})$ is calculated after $\boldsymbol{v}(t_j)$. An example will illustrate the need for this order. Consider a path- or history-dependent plasticity model in which the restoring force at step t_j, $\boldsymbol{r}(t_j)$, depends on the plastic strain at the previous step, $\boldsymbol{\varepsilon}^P(t_{j-1})$, as well as $\boldsymbol{x}$ and the displacement at the current step, $\boldsymbol{u}(t_j)$. The history-dependence of the model is introduced through the $\boldsymbol{\varepsilon}^P(t_{j-1})$ term. Such a model will be introduced in section 7. In the terms used in the formulation in this section, the plastic strain at t_{j-1}, $\boldsymbol{\varepsilon}^P(t_{j-1})$, is the history-dependent variable $\boldsymbol{z}(t_j)$ used in the calculation of $\boldsymbol{r}$ at time t_j, or

$$\boldsymbol{z}(t_j) \equiv \boldsymbol{\varepsilon}^P(t_{j-1}) \tag{3-21}$$

so

$$\frac{\partial \boldsymbol{z}}{\partial x_i}(t_j) \equiv \frac{\partial \boldsymbol{\varepsilon}^P(t_{j-1})}{\partial x_i} \tag{3-22}$$

therefore

$$\left.\frac{\partial \boldsymbol{r}}{\partial x_i}\right|_{\boldsymbol{u},\dot{\boldsymbol{u}},\boldsymbol{z}}(t_j) + \frac{\partial \boldsymbol{r}}{\partial \boldsymbol{z}}(t_j)\frac{\partial \boldsymbol{z}}{\partial x_i}(t_j) \equiv \left.\frac{\partial \boldsymbol{r}}{\partial x_i}\right|_{\boldsymbol{u},\dot{\boldsymbol{u}},\boldsymbol{z}}(t_j) + \frac{\partial \boldsymbol{r}(t_j)}{\partial \boldsymbol{\varepsilon}^P(t_{j-1})}\frac{\partial \boldsymbol{\varepsilon}^P(t_{j-1})}{\partial x_i} \tag{3-23}$$

Assuming that $\frac{\partial \boldsymbol{\varepsilon}^P(t_{j-1})}{\partial \boldsymbol{x}}$ is known, the quantity in equation 3-23 can be found and $\boldsymbol{v}(t_j)$ can be calculated by equation 3-19. Next, for this model it is found that the derivative of the plastic strain at time t_j, $\frac{\partial \boldsymbol{\varepsilon}^P(t_j)}{\partial \boldsymbol{x}}$, is a function of the derivative of the displacement at time t_j, $\boldsymbol{v}(t_j)$. After $\boldsymbol{v}(t_j)$ is calculated, $\frac{\partial \boldsymbol{\varepsilon}^P(t_j)}{\partial \boldsymbol{x}}$ can be found and stored for use at the next step as $\frac{\partial \boldsymbol{z}}{\partial x_i}(t_{j+1})$. The value of $\frac{\partial \boldsymbol{\varepsilon}^P}{\partial \boldsymbol{x}}$ to be used at the first step can be found from the initial conditions.

2. A large proportion of the work required to calculate the sensitivity factor is in the calculation of the derivatives $\frac{\partial \boldsymbol{r}}{\partial \boldsymbol{x}}$, $\frac{\partial \boldsymbol{r}}{\partial \boldsymbol{z}}$, etc. Some authors, such as Greene and Haftka [25], suggest a "semi-analytical" approach: use finite differences to calculate these derivatives, and then solve for $\boldsymbol{v}$ using the numerical method of equation 3-19. Unfortunately, this method is subject to the same disadvantages of the finite difference method as described in section 2. Direct differentiation of the material restoring force and damping models is a more accurate and satisfactory method of calculating the necessary derivatives. The derivatives can be found on an element-by-element basis and assembled

Solve for displacement $\boldsymbol{u}(t_j)$

Calculate $\left.\dfrac{\partial \boldsymbol{r}}{\partial x_i}\right|_{\boldsymbol{u},\dot{\boldsymbol{u}},\boldsymbol{z}}(t_j) + \dfrac{\partial \boldsymbol{r}}{\partial \boldsymbol{z}}(t_j)\dfrac{\partial \boldsymbol{z}}{\partial x_i}(t_j)$, $i = 1, 2, 3, \ldots$

Solve for $\boldsymbol{v}(t_j)$

Calculate $\dfrac{\partial \boldsymbol{z}}{\partial x_i}(t_{j+1})$, $i = 1, 2, 3, \ldots$
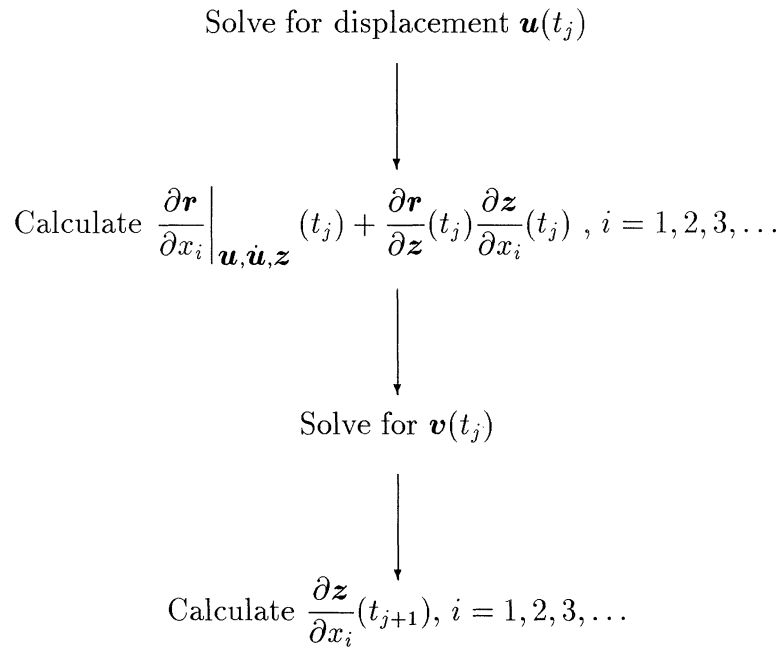
FIGURE 3-1 Basic procedure at a typical time step t_j

into a global matrix in the same way as the element restoring force and stiffness matrices. For example, figure 3-2 shows the assembly of the global $\left.\dfrac{\partial \boldsymbol{r}}{\partial x}\right|_{\boldsymbol{u},\dot{\boldsymbol{u}},\boldsymbol{z}} + \dfrac{\partial \boldsymbol{r}}{\partial \boldsymbol{z}}\dfrac{\partial \boldsymbol{z}}{\partial x}$ matrix. Details of the material models considered and their derivatives will be given in sections 6 and 7.

3.4   Example

A simple example will illustrate the theory and test the accuracy of the numerical solution. The example is the single degree-of-freedom oscillator of Section 2.5 with viscous damping of magnitude c added, and the linear spring replaced by a non-conservative bilinear spring (figure 3-3). The oscillator is driven by a harmonic forcing function $p_0 \sin(\omega t)$ (figure 3-4). We wish to find the sensitivity factor with respect to the stiffness x. For this relatively simple problem, an analytical solution can be found to check the accuracy of the numerical solution. The problem will be solved for the following values of the parameters:

$$m \;=\; 0.35$$

First element $l = 1$

Calculate transformation matrix $\boldsymbol{\Gamma}_l$

Find element displacement vector $\boldsymbol{u}_l$ and velocity vector $\dot{\boldsymbol{u}}_l$

Convert to local coordinates: $\boldsymbol{u}_l' = \boldsymbol{\Gamma}_l \boldsymbol{u}_l$, $\dot{\boldsymbol{u}}_l' = \boldsymbol{\Gamma}_l \dot{\boldsymbol{u}}_l$

$l = l + 1$

Call subroutine to calculate element derivative vector $\left(\left. \dfrac{\partial \boldsymbol{r}}{\partial x} \right|_{\boldsymbol{u},\dot{\boldsymbol{u}},\boldsymbol{z}} + \dfrac{\partial \boldsymbol{r}}{\partial \boldsymbol{z}} \dfrac{\partial \boldsymbol{z}}{\partial x} \right)_l'$

Convert to global coordinates:

$$\left(\left. \dfrac{\partial \boldsymbol{r}}{\partial x} \right|_{\boldsymbol{u},\dot{\boldsymbol{u}},\boldsymbol{z}} + \dfrac{\partial \boldsymbol{r}}{\partial \boldsymbol{z}} \dfrac{\partial \boldsymbol{z}}{\partial x} \right)_l = \boldsymbol{\Gamma}_l^T \left(\left. \dfrac{\partial \boldsymbol{r}}{\partial x} \right|_{\boldsymbol{u},\dot{\boldsymbol{u}},\boldsymbol{z}} + \dfrac{\partial \boldsymbol{r}}{\partial \boldsymbol{z}} \dfrac{\partial \boldsymbol{z}}{\partial x} \right)_l'$$

Add data in element vector to correct position in global $\left. \dfrac{\partial \boldsymbol{r}}{\partial x} \right|_{\boldsymbol{u},\dot{\boldsymbol{u}},\boldsymbol{z}} + \dfrac{\partial \boldsymbol{r}}{\partial \boldsymbol{z}} \dfrac{\partial \boldsymbol{z}}{\partial x}$ vector
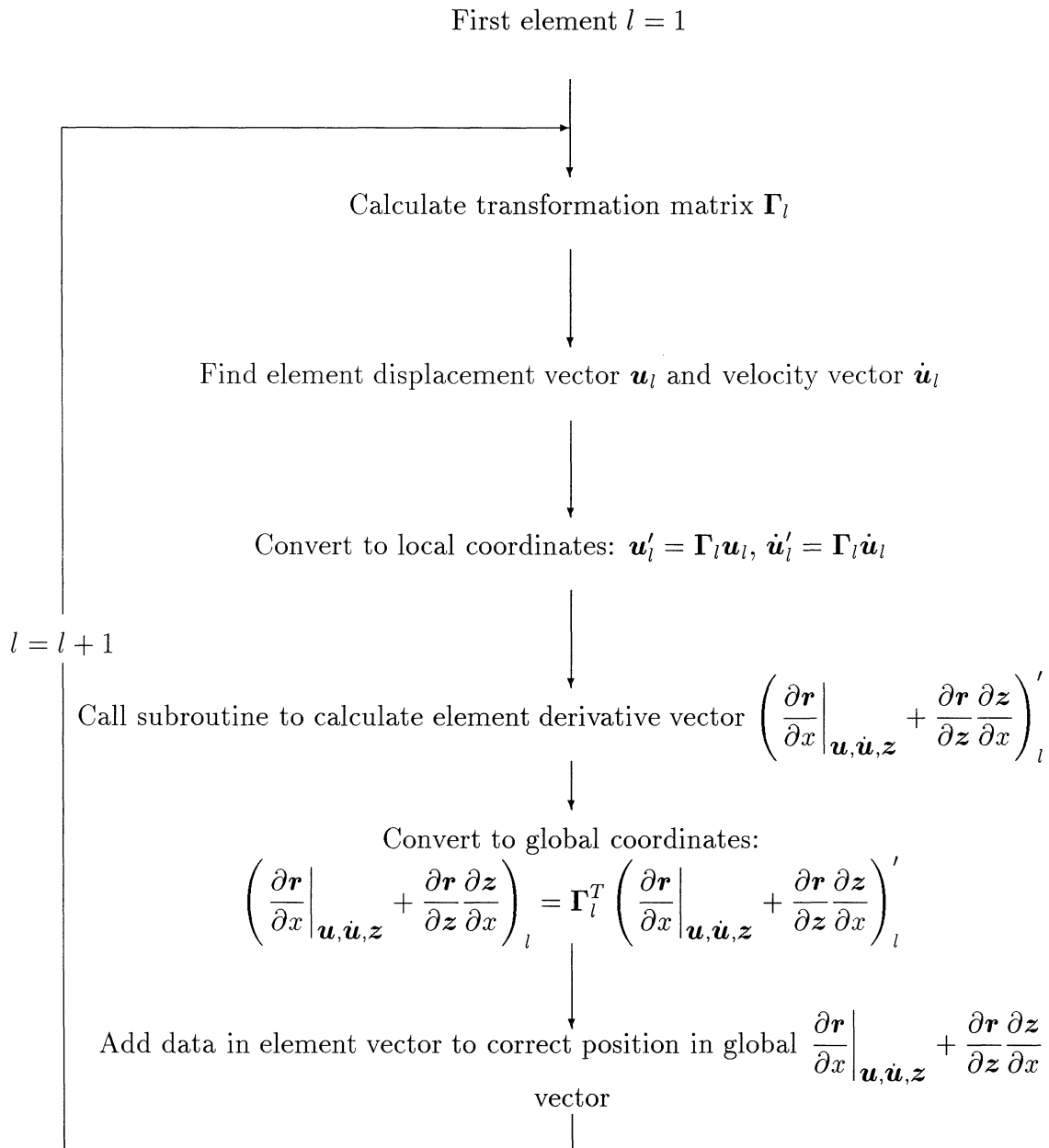
FIGURE 3-2 Flowchart of loop through elements to calculate $\left. \dfrac{\partial \boldsymbol{r}}{\partial x} \right|_{\boldsymbol{u},\dot{\boldsymbol{u}},\boldsymbol{z}} + \dfrac{\partial \boldsymbol{r}}{\partial \boldsymbol{z}} \dfrac{\partial \boldsymbol{z}}{\partial x}$
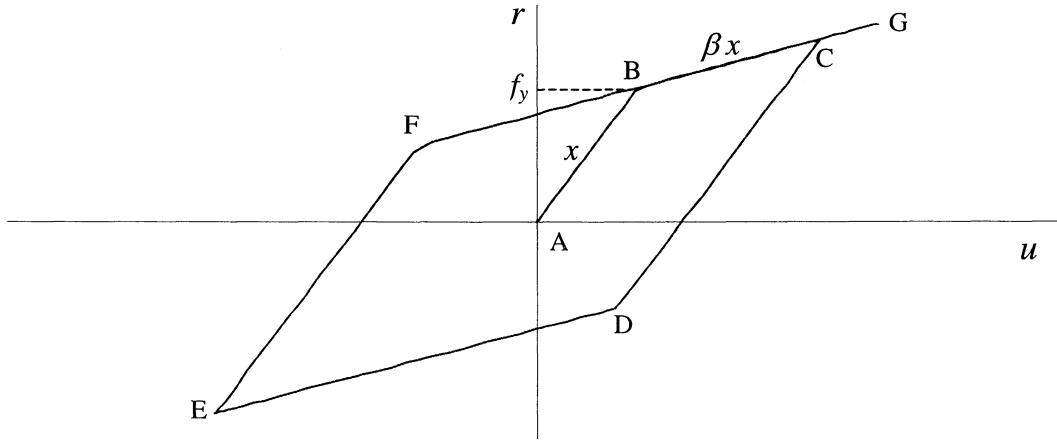
FIGURE 3-3 Restoring force vs. displacement

$$
\begin{aligned}
c &= 0.529 \\
x_0 &= 80 \\
f_y &= 92.6 \\
\beta &= 0.2 \\
p_0 &= 308.8 \\
\omega &= 6.283
\end{aligned}
$$

and zero initial conditions.

3.4.1 Analytical and numerical solutions

The oscillator is at rest at at time $t = 0$ so that the starting point on the restoring force vs. displacement diagram (figure 3-3) is point A. At time τ_B it reaches point B, at time τ_C it reaches point C, etc. As different equations for the restoring force r apply on the different ranges A – B, B – C, etc., different governing equations for u and v apply on each range. It is thus necessary to consider each of these ranges in turn. This will now be done in more detail.

- **A – B:** The restoring force is given by

$$
r(t, x) = xu(t, x) \tag{3-24}
$$

  so the governing equation for u for $x = x_0$ is

$$
m\ddot{u}(t, x_0) + c\dot{u}(t, x_0) + x_0 u(t, x_0) = p_0 \sin(\omega t) \tag{3-25}
$$

31
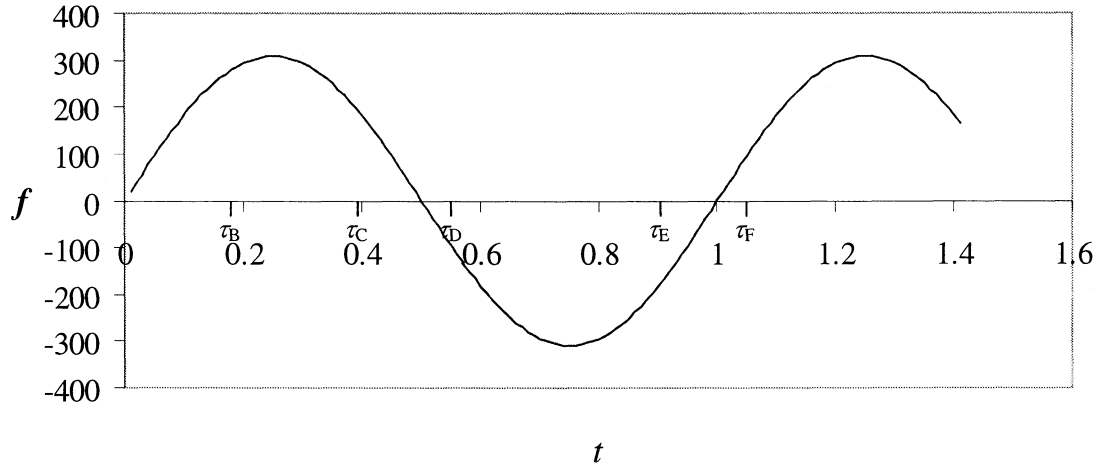
FIGURE 3-4 Driving force

and for v

$$m\ddot{v}(t) + c\dot{v}(t) + x_0 v(t) = -u(t, x_0) \qquad (3\text{-}26)$$

These equations can be solved analytically for u and v. Details are given later in this section.

- **B − C:** The restoring force is given by

$$r = f_y(1 - \beta) + \beta x_0 u(t, x_0) \qquad (3\text{-}27)$$

so the governing equations for u and v are

$$m\ddot{u}(t, x_0) + c\dot{u}(t, x_0) + f_y(1 - \beta) + \beta x_0 u(t, x_0) = p_0 \sin(\omega t) \qquad (3\text{-}28)$$

$$m\ddot{v}(t) + c\dot{v}(t) + \beta x_0 v(t) = -\beta u(t, x_0) \qquad (3\text{-}29)$$

Equation 3-29 can be solved analytically with $v(\tau_B)$ and $\dot{v}(\tau_B)$ as initial conditions.

- **C − D:** The restoring force is given by

$$r = z_2(t, x_0) + x_0 \left[u(t, x_0) - z_1(t, x_0) \right] \qquad (3\text{-}30)$$

where $\quad z_1(t, x_0) \quad = \quad$ displacement at last velocity sign change
$\qquad\qquad\qquad = \quad u(\tau_C, x_0)$
$\qquad z_2(t, x_0) \quad = \quad$ restoring force at last velocity sign change
$\qquad\qquad\qquad = \quad r(\tau_C, x_0)$
$\qquad\qquad\qquad = \quad f_y(1 - \beta) + \beta x_0 u(\tau_C, x_0)$

32

The governing equation for u is

$$m\ddot{u}(t, x_0) + c\dot{u}(t, x_0) + z_2(t, x_0) + x_0\left[u(t, x_0) - z_1(t, x_0)\right] = p_0\sin(\omega t) \qquad \text{(3-31)}$$

The right-hand side (RHS) of the governing equation of v is more difficult to find in this case and is

$$
\begin{aligned}
\text{RHS} &= -\left.\frac{\partial r}{\partial x}\right|_{u,\dot{u},z_1,z_2}(t, x_0) - \frac{\partial r}{\partial z_1}(t, x_0)\frac{\partial z_1}{\partial x}(t, x_0) \\
&\quad - \frac{\partial r}{\partial z_2}(t, x_0)\frac{\partial z_2}{\partial x}(t, x_0) \qquad\qquad\qquad\qquad \text{(3-32)} \\
&= -\left[u(t, x_0) - u(\tau_C, x_0)\right] - \left[-x_0\right]v(\tau_C) - 1\left[\beta u(\tau_C, x_0) + \beta x_0 v(\tau_C)\right]
\end{aligned}
$$

so the governing equation of v is

$$m\ddot{v}(t) + c\dot{v}(t) + x_0 v(t) = \qquad\qquad\qquad\qquad\qquad \text{(3-33)}$$
$$-\left[u(t, x_0) - u(\tau_C, x_0)\right] - \left[-x_0\right]v(\tau_C) - 1\left[\beta u(\tau_C, x_0) + \beta x_0 v(\tau_C)\right]$$

These three ranges illustrate the typical equations involved. Equations for D–E, E–F and F–G are similar and will not be given here.

The general analytical solutions of the above equations for u and v have the form

$$
\begin{aligned}
u(t) &= C_1\sin(\omega t) + C_2\cos(\omega t) \\
&\quad + e^{-\zeta\omega_n t}\left[\,C_3\cos(\omega_d t) + C_4\sin(\omega_d t)\,\right] + C_5 \qquad\qquad \text{(3-34)}
\end{aligned}
$$

$$
\begin{aligned}
v(t) &= C_6\sin(\omega t) + C_7\cos(\omega t) \\
&\quad + e^{-\zeta\omega_n t}\left[\,C_8\cos(\omega_d t) + C_9\sin(\omega_d t)\,\right] \\
&\quad + te^{-\zeta\omega_n t}\left[\,C_{10}\cos(\omega_d t) + C_{11}\sin(\omega_d t)\,\right] + C_{12} \qquad \text{(3-35)}
\end{aligned}
$$

where $\zeta\omega_n = \frac{c}{2m} = 7.559 \times 10^{-1}$
$\omega_d =$ frequency of damped vibration
$= 1.510 \times 10^1$ for A–B, C–D, E–F; and 6.719 for B–C, D–E, F–G

$C_1, C_2, C_3, \ldots, C_{12}$ are constants that depend on the parameter values and initial conditions. As the governing equations are different for each range A–B, B–C, C–D, etc., the constants

will have different values on each range. The calculated values of the constants are given in table 3-1 and the critical time instants which separate the ranges are calculated as

$$\tau_B = 0.182$$
$$\tau_C = 0.397$$
$$\tau_D = 0.568$$
$$\tau_E = 0.901$$
$$\tau_F = 1.063$$

TABLE 3-1 Values of constants

Range	A–B	B–C	C–D
C_1	1.629	1.491×10^1	1.629
C_2	-8.183×10^{-2}	-2.272×10^1	-8.183×10^{-2}
C_3	8.183×10^{-2}	2.549×10^1	8.911×10^{-1}
C_4	-6.737×10^{-1}	-7.258	5.112×10^{-1}
C_5	0	-4.630	1.660
C_6	-2.449×10^{-2}	5.435×10^{-1}	-2.449×10^{-2}
C_7	2.467×10^{-3}	1.254	2.467×10^{-3}
C_8	-2.467×10^{-3}	-1.296	-3.078×10^{-2}
C_9	1.429×10^{-2}	-6.279×10^{-1}	5.915×10^{-3}
C_{10}	-6.374×10^{-2}	-3.086×10^{-1}	4.837×10^{-2}
C_{11}	-7.742×10^{-3}	-1.084	-8.431×10^{-2}
C_{12}	0	5.788×10^{-2}	-1.895×10^{-2}
Range	D–E	E–F	F–G
C_1	1.491×10^1	1.629	1.491×10^1
C_2	-2.272×10^1	-8.183×10^{-2}	-2.272×10^1
C_3	3.774×10^1	3.277×10^{-1}	5.385×10^1
C_4	-2.415	-1.660	8.154
C_5	4.630	-1.991	-4.630
C_6	5.435×10^{-1}	-2.449×10^{-2}	5.435×10^{-1}
C_7	1.254	2.467×10^{-3}	1.254
C_8	-1.530	1.168×10^{-1}	-2.144
C_9	-5.317×10^{-1}	6.494×10^{-2}	-7.117×10^{-2}
C_{10}	-1.027×10^{-1}	-1.571×10^{-1}	3.467×10^{-1}
C_{11}	-1.605	-3.100×10^{-2}	-2.290
C_{12}	-5.788×10^{-2}	4.658×10^{-2}	5.788×10^{-2}
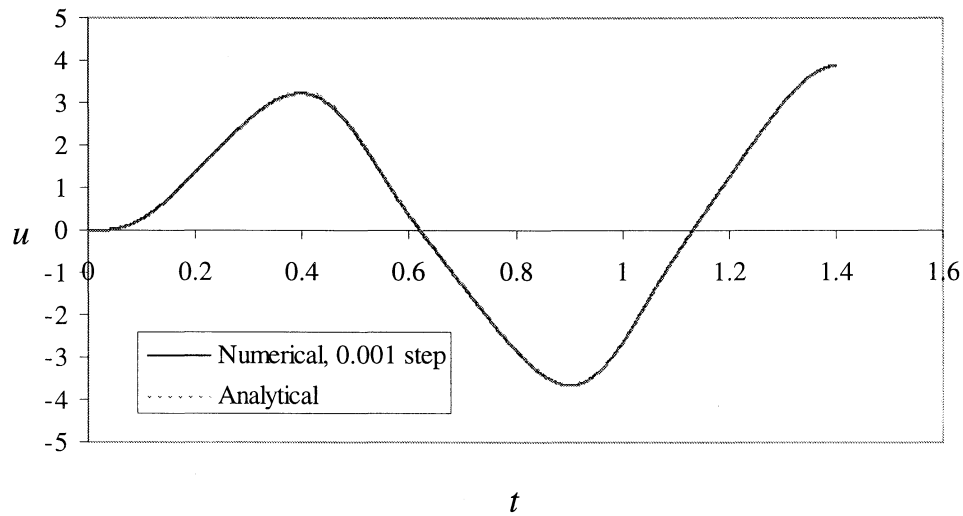
FIGURE 3-5 Displacement u

The resulting solutions for u and v are plotted in figures 3-5 and 3-6. The problem was also solved using the numerical method described in Section 3.2, and results are shown in the figures for time step size $\Delta t = 0.001$. It is clear that the numerical method gives suitably accurate results.

The coefficient of $\dot{v}$ in the governing equations for v is simply c, which is a constant. The coefficient of v is $\dfrac{\partial r}{\partial u}$, which is only piecewise constant, with discontinuities at τ_B, τ_C, τ_D, ... Figure 3-7 shows $\dfrac{\partial r}{\partial u}$ as a function of time. The right-hand side (RHS) or "driving force" of the equation for v is shown in figure 3-8. It is piecewise continuous, with discontinuities at τ_B, τ_C, τ_D, ...

3.4.2 Graphical calculation of derivatives

Several different mathematical formulations of the physical system shown in figure 3-3 are possible. Equations 3-24, 3-27 and 3-30 represent just one possible formulation. There is a tendency for the mathematics to obscure the physical problem, particularly when calculating the derivatives ($\dfrac{\partial r}{\partial u}$ and the RHS) required for the sensitivity factor calculation. No matter what mathematical representation is used, the derivatives should be the same. Fortunately, the derivatives can also be obtained from graphical analysis of figure 3-3. This process can be used to check the derivatives obtained from any mathematical representation. It can also help to confirm intuitively the forms of $\dfrac{\partial r}{\partial u}$ and the RHS and the existence of the discontinuities.

35
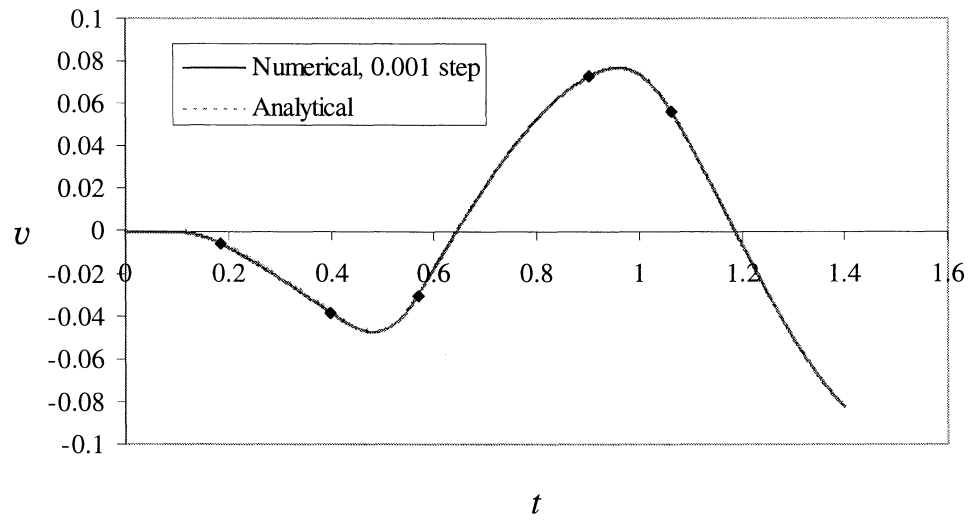
FIGURE 3-6 Sensitivity factor v

FIGURE 3-7 $\dfrac{\partial r}{\partial u}$

36
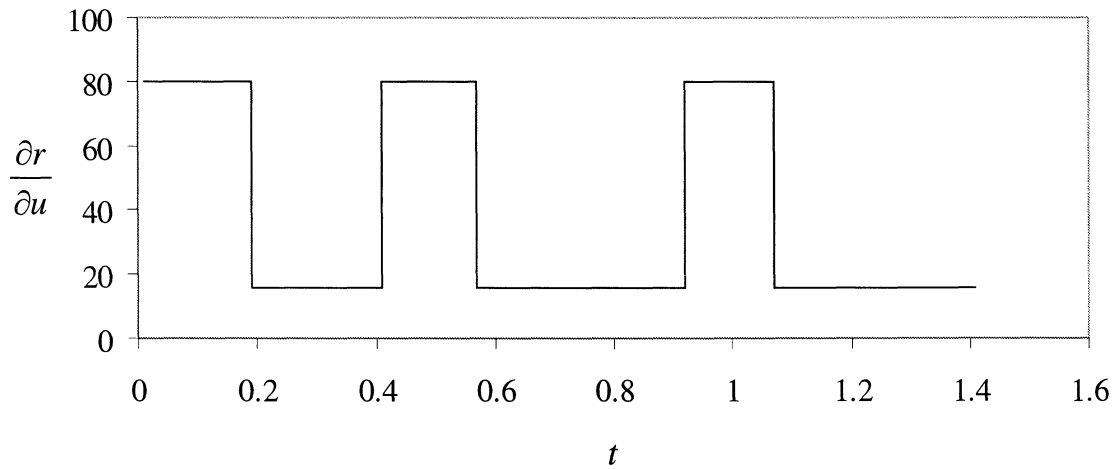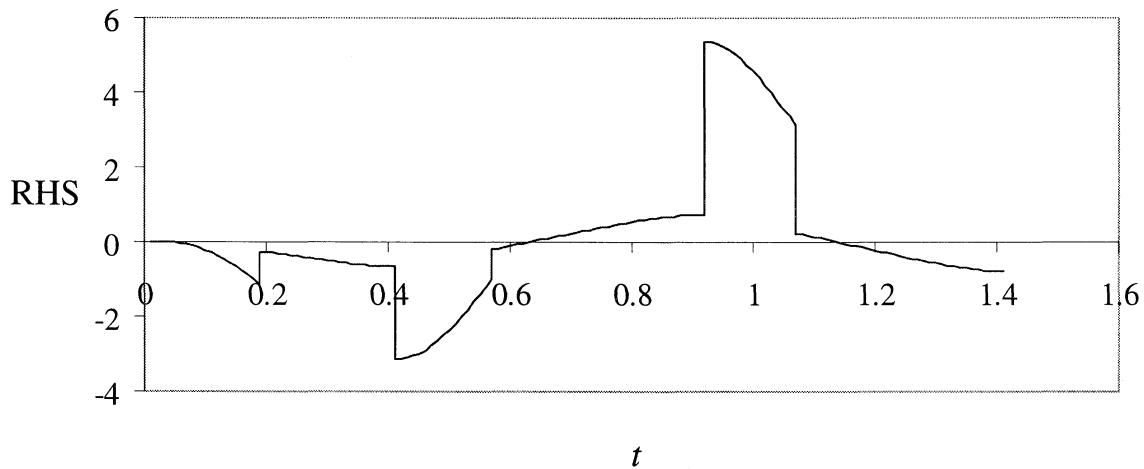
FIGURE 3-8 Right-hand side

Both $\dfrac{\partial r}{\partial u}$ and the RHS have graphical interpretations on the restoring force vs. displacement graph. The coefficient of v, $\dfrac{\partial r}{\partial u}$, is the easier of the two to interpret. It is the gradient of the graph, which is x_0 on A–B and C–D and βx_0 on B–C.

The RHS is more difficult. As $\dfrac{\partial f}{\partial x}$ and $\dfrac{\partial c}{\partial x}$ are zero, the RHS is

$$-\left[\left.\frac{\partial r}{\partial x}\right|_{u,\dot{u},z_1,z_2} + \frac{\partial r}{\partial z_1}\frac{\partial z_1}{\partial x} + \frac{\partial r}{\partial z_2}\frac{\partial z_2}{\partial x} \right]$$

or the negative of the rate of change of r with x at constant u. This can be determined by applying a small change Δx to x and finding how r changes at a fixed u. More precisely, the RHS is $-\lim\limits_{\Delta x \to 0} \dfrac{\Delta r}{\Delta x}$ where $\Delta r = r(u, x_0 + \Delta x) - r(u, x_0)$. This will be done for A–B, B–C, and C–D (figure 3-9).

- A – H: $\Delta r = \Delta x\, u$, or $\dfrac{\Delta r}{\Delta x} = u$; therefore $-\lim\limits_{\Delta x \to 0} \dfrac{\Delta r}{\Delta x} = -u$ as in equation 3-26.

- H – B: Leave out for now. As $\Delta x \to 0$, H $\to$ B so the behavior on the H – B line becomes irrelevant.

- B – C: $\Delta r = \beta\, \Delta x\, u$, or $\dfrac{\Delta r}{\Delta x} = \beta u$; therefore $-\lim\limits_{\Delta x \to 0} \dfrac{\Delta r}{\Delta x} = -\beta u$ as in equation 3-29.

- D – E: This is more complicated than the previous ranges. In general, due to the changed restoring force characteristics of the system between A and C, the point

37
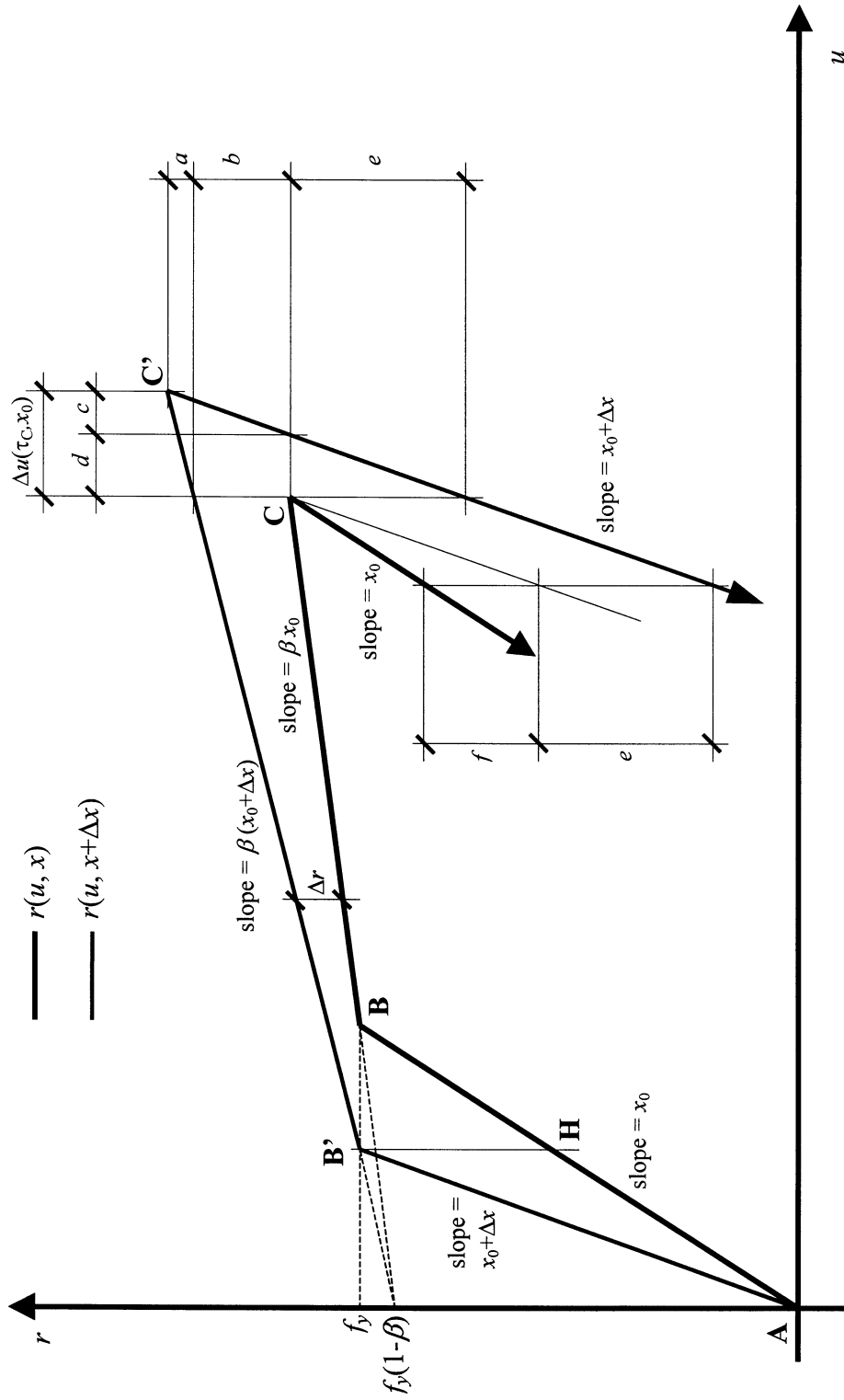
FIGURE 3-9 Graphical calculation of derivatives

at which the velocity changes sign will move from C to C', increasing $u(\tau_C, x_0)$ by $\Delta u(\tau_C, x_0)$. The change in r may then be derived from:

$$
\begin{aligned}
a &= \beta \left[x_0 + \Delta x \right] \Delta u(\tau_C, x_0) && \text{(3-36)} \\
&= \beta x_0 \, \Delta u(\tau_C, x_0) + \beta \, \Delta x \, \Delta u(\tau_C, x_0) \\
&\approx \beta x_0 \, \Delta u(\tau_C, x_0) \\
b &= \beta \, \Delta x \, u(\tau_C, x_0) \\
c &= \frac{a + b}{x_0 + \Delta x} \\
&= \frac{\beta x_0 \, \Delta u(\tau_C, x_0) + \beta \, \Delta x \, u(\tau_C, x_0)}{x_0 + \Delta x} \\
d &= \Delta u(\tau_C, x_0) - c \\
&= \Delta u(\tau_C, x_0) - \frac{\beta x_0 \, \Delta u(\tau_C, x_0) + \beta \, \Delta x \, u(\tau_C, x_0)}{x_0 + \Delta x} \\
e &= \left[x_0 + \Delta x \right] d \\
&= \left[x_0 + \Delta x \right] \left[\Delta u(\tau_C, x_0) - \frac{\beta x_0 \, \Delta u(\tau_C, x_0) + \beta \, \Delta x \, u(\tau_C, x_0)}{x_0 + \Delta x} \right] \\
&= \left[x_0 + \Delta x \right] \Delta u(\tau_C, x_0) - \beta x_0 \, \Delta u(\tau_C, x_0) + \beta \, \Delta x \, u(\tau_C, x_0) \\
&\approx x_0 \, \Delta u(\tau_C, x_0) - \beta x_0 \, \Delta u(\tau_C, x_0) + \beta \, \Delta x \, u(\tau_C, x_0) \\
f &= \Delta x \left[u(\tau_C, x_0) - u \right] \\
\Delta r &= -f - e \\
&= \Delta x \left[u - u(\tau_C, x_0) \right] - x_0 \, \Delta u(\tau_C, x_0) + \beta x_0 \, \Delta u(\tau_C, x_0) \\
&\quad + \beta \, \Delta x \, u(\tau_C, x_0) \\
\frac{\Delta r}{\Delta x} &= \left[u - u(\tau_C, x_0) \right] - x_0 \frac{\Delta u(\tau_C, x_0)}{\Delta x} + \beta x_0 \frac{\Delta u(\tau_C, x_0)}{\Delta x} + \beta u(\tau_C, x_0) \\
-\lim_{\Delta x \to 0} \frac{\Delta r}{\Delta x} &= -\left[u - u(\tau_C, x_0) \right] + x_0 v(\tau_C, x_0) - \beta x_0 v(\tau_C, x_0) - \beta u(\tau_C, x_0)
\end{aligned}
$$

as in equation 3-33.

Similar graphical checks can be done for other parameters of interest and for other restoring force vs. displacement models.

3.5   Error analysis

As indicated in Section 3.1, the coefficients of the governing equation for the sensitivity factor have time-varying coefficients with discontinuities or "jumps" at several time instants. The correct approach to solving for the sensitivity factor would be to restart the problem at each discontinuity. After each restart, the problem would be solved with the new governing

differential equations and the state vector at the time of the restart as the initial conditions for the new problem. This approach may be reasonable for a single-degree-of-freedom system. However, in a multi-degree-of-freedom system there may be a large number of discontinuities occurring at slightly different time instants and the task of determining all of the time instants and restarting the problem each time would rapidly become enormously computation-intensive and impractical. It may be more reasonable to sacrifice some accuracy and find the sensitivity factor at predetermined time steps $t_1, t_2, t_3, \ldots$ separated by intervals of size Δt only. In general, these time steps will not coincide with the discontinuity time instants. This section attempts to determine the extent of the resulting error.

3.5.1 Basic approach

A common approach for determining errors in numerical integration methods is to calculate the error in a single time step of a single degree-of-freedom system ([22], [27], [70]). The initial conditions at the start of the step are assumed to be correct, and exact and numerical solutions for the displacement at the end of the step are calculated. The *local error* is defined as the difference between the two solutions. The lowest power of Δt in the local error is particularly important as it determines the convergence properties of the numerical method. This approach will be used here to investigate the error in a Newmark numerical solution caused by a discontinuity occurring during a time step.

Consider the following equation, similar to the governing equation of a sensitivity factor for a single degree-of-freedom system

$$m\ddot{v}(t) + c\dot{v}(t) + \tilde{k}(t)v(t) = \tilde{f}(t) \tag{3-37}$$

and a single time step of length Δt. Discontinuities in $\tilde{k}$ and $\tilde{f}$ occur at a general time instant during the step. The time instant is $\eta\Delta t$ after the start of the step, where $0 < \eta < 1$. Such simultaneous jumps in both $\tilde{k}$ and $\tilde{f}$ are often observed in the governing equations of sensitivity factors; for instance, in the example of Section 3.4. For the first part of the time step, $\tilde{k} = k_1$, and after $\eta\Delta t$, $\tilde{k} = k_4$. $\tilde{f}$ varies linearly from $\tilde{f}_1$ to $\tilde{f}_2$ over $\eta\Delta t$, after which it jumps to $\tilde{f}_3$ and varies linearly to $\tilde{f}_4$ at the end of the step. The situation is illustrated in figure 3-10.

The assumption that $\tilde{k}$ remains piecewise constant is necessary to allow the use of the exact solution for a linear system. In the context of sensitivity factors, if the original system has a piecewise linear restoring force-displacement relationship then the assumption is valid. However, even if this is not the case it may still be reasonable to assume that the stiffness $\tilde{k}$ is approximately constant over the short time periods $\eta\Delta t$ and $(1 - \eta)\Delta t$.

The conditions at the start of the step are v_1 and $\dot{v}_1$. Just before the discontinuity, the solution and its derivative are v_2 and $\dot{v}_2$; just after the jump, v_3 and $\dot{v}_3$; and at the end of
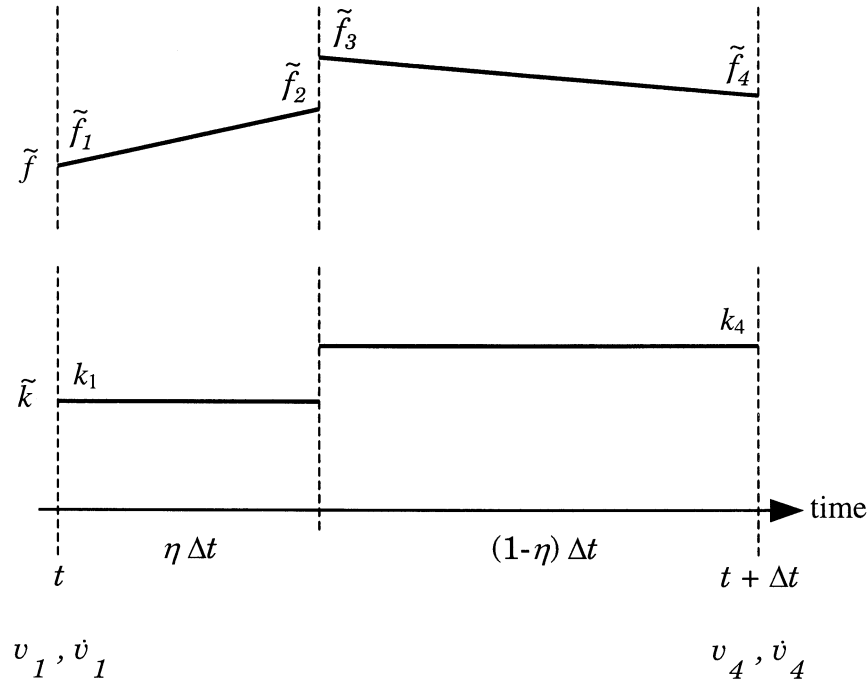
FIGURE 3-10 Single time step

the step, v_4 and $\dot{v}_4$. Clearly $v_2 = v_3$ and $\dot{v}_2 = \dot{v}_3$. The next problem is to determine exact and numerical solutions for v_4 in terms of the initial conditions and the system parameters.

For the numerical solution, equilibrium of the initial conditions requires

$$m\ddot{v}_1 = \tilde{f}_1 - c\dot{v}_1 - k_1 v_1 \tag{3-38}$$

so from equation 3-19

$$
\begin{aligned}
v_4 &= v_1 + \frac{\tilde{f}_4 - \tilde{f}_1 - (k_4 - k_1)v_1 + (\frac{4m}{\Delta t} + 2c)\dot{v}_1 + 2(\tilde{f}_1 - c\dot{v}_1 - k_1 v_1)}{k_4 + \frac{2}{\Delta t}c + \frac{4}{\Delta t^2}m} \\
&= v_1 + \frac{\tilde{f}_4 + \tilde{f}_1 - (k_4 + k_1)v_1 + \frac{4m}{\Delta t}\dot{v}_1}{k_4 + \frac{2}{\Delta t}c + \frac{4}{\Delta t^2}m} \\
&= v_1 + \frac{(\tilde{f}_4 + \tilde{f}_1)\Delta t^2 - (k_4 + k_1)v_1\,\Delta t^2 + 4m\,\Delta t\,\dot{v}_1}{k_4\,\Delta t^2 + 2\,\Delta t\,c + 4m} \\
&= v_1 + \dot{v}_1\Delta t + \left[\frac{\tilde{f}_4 + \tilde{f}_1}{4m} - \frac{k_4 + k_1}{4m}v_1 - \frac{c}{2m}\dot{v}_1\right]\Delta t^2 + O(\Delta t^3) \tag{3-39}
\end{aligned}
$$

41

where $g(\Delta t) = O(\Delta t^k)$ means that $g(\Delta t) \sim C\Delta t^k$ as $\Delta t \to 0$ for some finite constant C.

The exact solution can be determined by applying a linearly varying force over a time duration $\eta\Delta t$ to the system with $\tilde{k} = k_1$ and v_1 and $\dot{v}_1$ as initial conditions, determining v_2 and $\dot{v}_2$, and applying a second linearly varying force over time $(1-\eta)\Delta t$ to the system with $\tilde{k} = k_4$ and v_2 and $\dot{v}_2$ as initial conditions.

The solution for a linearly varying force applied to a system can be found in [13] and gives

$$
\begin{aligned}
v_2 \;=\; & e^{-\zeta_1\omega_{n1}\eta\Delta t}\sin\left(\omega_{d1}\eta\Delta t\right)\left[\frac{\zeta_1 v_1}{\sqrt{1-\zeta_1^2}} + \frac{\dot{v}_1}{\omega_{d1}} - \frac{\tilde{f}_1}{k_1}\cdot\frac{\zeta_1}{\sqrt{1-\zeta_1^2}} + \frac{\tilde{f}_2-\tilde{f}_1}{k_1}\cdot\frac{2\zeta_1^2-1}{\omega_{d1}\eta\Delta t}\right] \\
& + e^{-\zeta_1\omega_{n1}\eta\Delta t}\cos\left(\omega_{d1}\eta\Delta t\right)\left[v_1 - \frac{\tilde{f}_1}{k_1} + \frac{\tilde{f}_2-\tilde{f}_1}{k_1}\cdot\frac{2\zeta_1}{\omega_{n1}\eta\Delta t}\right] \\
& + \frac{\tilde{f}_1}{k_1} + \frac{\tilde{f}_2-\tilde{f}_1}{k_1}\left[1 - \frac{2\zeta_1}{\omega_{n1}\eta\Delta t}\right]
\end{aligned}
\tag{3-40}
$$

$$
\begin{aligned}
\dot{v}_2 \;=\; & e^{-\zeta_1\omega_{n1}\eta\Delta t}\sin\left(\omega_{d1}\eta\Delta t\right)\left[\frac{-\omega_{n1}v_1 - \zeta_1\dot{v}_1}{\sqrt{1-\zeta_1^2}} + \frac{\tilde{f}_1}{k_1}\left(\frac{\omega_{n1}}{\sqrt{1-\zeta_1^2}} + \frac{\zeta_1}{\eta\Delta t\sqrt{1-\zeta_1^2}}\right)\right. \\
& \left. - \frac{\tilde{f}_2}{k_1\eta\Delta t}\cdot\frac{\zeta_1}{\sqrt{1-\zeta_1^2}}\right] \\
& + e^{-\zeta_1\omega_{n1}\eta\Delta t}\cos\left(\omega_{d1}\eta\Delta t\right)\left[\dot{v}_1 - \frac{\tilde{f}_2-\tilde{f}_1}{k_1\eta\Delta t}\right] \\
& + \frac{\tilde{f}_2-\tilde{f}_1}{k_1\eta\Delta t}
\end{aligned}
\tag{3-41}
$$

The solution at the end of the step is then given by

$$
\begin{aligned}
v_4 \;=\; & e^{-\zeta_4\omega_{n4}(1-\eta)\Delta t}\sin\left(\omega_{d4}(1-\eta)\Delta t\right)\left[\frac{\zeta_4 v_2}{\sqrt{1-\zeta_4^2}} + \frac{\dot{v}_2}{\omega_{d4}} - \frac{\tilde{f}_3}{k_4}\cdot\frac{\zeta_4}{\sqrt{1-\zeta_4^2}}\right. \\
& \left. + \frac{\tilde{f}_4-\tilde{f}_3}{k_4}\cdot\frac{2\zeta_4^2-1}{\omega_{d4}(1-\eta)\Delta t}\right] \\
& + e^{-\zeta_4\omega_{n4}(1-\eta)\Delta t}\cos\left(\omega_{d4}(1-\eta)\Delta t\right)\left[v_2 - \frac{\tilde{f}_3}{k_4} + \frac{\tilde{f}_4-\tilde{f}_3}{k_4}\cdot\frac{2\zeta_4}{\omega_{n4}(1-\eta)\Delta t}\right]
\end{aligned}
$$

$$+ \frac{\tilde{f}_3}{k_4} + \frac{\tilde{f}_4 - \tilde{f}_3}{k_4} \left[1 - \frac{2\zeta_4}{\omega_{n4}(1-\eta)\Delta t} \right]$$

$$= e^{-\zeta_4\omega_{n4}(1-\eta)\Delta t} \sin\left(\omega_{d4}(1-\eta)\Delta t\right) \left\{ \frac{\zeta_4}{\sqrt{1-\zeta_4^2}} \left[\frac{\tilde{f}_1}{k_1} + \frac{\tilde{f}_2 - \tilde{f}_1}{k_1}\left(1 - \frac{2\zeta_1}{\omega_{n1}\eta\Delta t}\right) \right] \right.$$

$$\left. + \frac{\tilde{f}_2 - \tilde{f}_1}{\omega_{d4}k_1\eta\Delta t} - \frac{\tilde{f}_3}{k_4} \cdot \frac{\zeta_4}{\sqrt{1-\zeta_4^2}} + \frac{\tilde{f}_4 - \tilde{f}_3}{k_4} \cdot \frac{2\zeta_4^2 - 1}{\omega_{d4}(1-\eta)\Delta t} \right\}$$

$$+ e^{-\zeta_4\omega_{n4}(1-\eta)\Delta t} \cos\left(\omega_{d4}(1-\eta)\Delta t\right) \left\{ \frac{\tilde{f}_1}{k_1} + \frac{\tilde{f}_2 - \tilde{f}_1}{k_1}\left(1 - \frac{2\zeta_1}{\omega_{n1}\eta\Delta t}\right) \right.$$

$$\left. - \frac{\tilde{f}_3}{k_4} + \frac{\tilde{f}_4 - \tilde{f}_3}{k_4} \cdot \frac{2\zeta_4}{\omega_{n4}(1-\eta)\Delta t} \right\}$$

$$+ e^{-\zeta_1\omega_{n1}\eta\Delta t - \zeta_4\omega_{n4}(1-\eta)\Delta t} \sin\left(\omega_{d1}\eta\Delta t\right) \sin\left(\omega_{d4}(1-\eta)\Delta t\right)$$

$$\left\{ \frac{\zeta_4}{\sqrt{1-\zeta_4^2}} \left[\frac{\zeta_1 v_1}{\sqrt{1-\zeta_1^2}} + \frac{\dot{v}_1}{\omega_{d1}} - \frac{\tilde{f}_1}{k_1} \cdot \frac{\zeta_1}{\sqrt{1-\zeta_1^2}} + \frac{\tilde{f}_2 - \tilde{f}_1}{k_1} \cdot \frac{2\zeta_1^2 - 1}{\omega_{d1}\eta\Delta t} \right] \right.$$

$$+ \frac{1}{\omega_{d4}} \left[\frac{-\omega_{n1}v_1 - \zeta_1\dot{v}_1}{\sqrt{1-\zeta_1^2}} + \frac{\tilde{f}_1}{k_1}\left(\frac{\omega_{n1}}{\sqrt{1-\zeta_1^2}} + \frac{\zeta_1}{\eta\Delta t\sqrt{1-\zeta_1^2}} \right) \right.$$

$$\left. \left. - \frac{\tilde{f}_2}{k_1\eta\Delta t} \cdot \frac{\zeta_1}{\sqrt{1-\zeta_1^2}} \right] \right\}$$

$$+ e^{-\zeta_1\omega_{n1}\eta\Delta t - \zeta_4\omega_{n4}(1-\eta)\Delta t} \cos\left(\omega_{d1}\eta\Delta t\right) \sin\left(\omega_{d4}(1-\eta)\Delta t\right)$$

$$\left\{ \frac{\zeta_4}{\sqrt{1-\zeta_4^2}} \left[v_1 - \frac{\tilde{f}_1}{k_1} + \frac{\tilde{f}_2 - \tilde{f}_1}{k_1} \cdot \frac{2\zeta_1}{\omega_{n1}\eta\Delta t} \right] \right.$$

$$\left. + \frac{1}{\omega_{d4}} \left[\dot{v}_1 - \frac{\tilde{f}_2 - \tilde{f}_1}{k_1\eta\Delta t} \right] \right\}$$

$$+ e^{-\zeta_1\omega_{n1}\eta\Delta t - \zeta_4\omega_{n4}(1-\eta)\Delta t} \sin\left(\omega_{d1}\eta\Delta t\right) \cos\left(\omega_{d4}(1-\eta)\Delta t\right)$$

$$\left\{ \frac{\zeta_1 v_1}{\sqrt{1-\zeta_1^2}} + \frac{\dot{v}_1}{\omega_{d1}} - \frac{\tilde{f}_1}{k_1} \cdot \frac{\zeta_1}{\sqrt{1-\zeta_1^2}} + \frac{\tilde{f}_2 - \tilde{f}_1}{k_1} \cdot \frac{2\zeta_1^2 - 1}{\omega_{d1}\eta\Delta t} \right\}$$

$$+ e^{-\zeta_1\omega_{n1}\eta\Delta t - \zeta_4\omega_{n4}(1-\eta)\Delta t} \cos\left(\omega_{d1}\eta\Delta t\right) \cos\left(\omega_{d4}(1-\eta)\Delta t\right)$$

$$\left\{ v_1 - \frac{\tilde{f}_1}{k_1} + \frac{\tilde{f}_2 - \tilde{f}_1}{k_1} \cdot \frac{2\zeta_1}{\omega_{n1}\eta\Delta t} \right\}$$

$$+ \frac{\tilde{f}_3}{k_4} + \frac{\tilde{f}_4 - \tilde{f}_3}{k_4} \left[1 - \frac{2\zeta_4}{\omega_{n4}(1-\eta)\Delta t} \right] \tag{3-42}$$

Noting that $\zeta_1\omega_{n1} = \zeta_4\omega_{n4} = \frac{c}{2m}$ and replacing the exponential and trigonometric functions

43

by their Taylor expansions about zero, this becomes

$$
\begin{aligned}
v_4 &= \left\{ \omega_{d4}(1-\eta)\Delta t - \frac{c}{2m}\omega_{d4}(1-\eta)^2\Delta t^2 \right.\\
&\quad \left. + \left(\frac{c^2\omega_{d4}}{8m^2} - \frac{\omega_{d4}^3}{6}\right)(1-\eta)^3\Delta t^3 + O(\Delta t^4) \right\}\\
&\quad \cdot \left\{ \frac{\zeta_4}{\sqrt{1-\zeta_4^2}}\left[\frac{\tilde{f}_2}{k_1} - \frac{(\tilde{f}_2 - \tilde{f}_1)c}{k_1^2\eta\Delta t} - \frac{\tilde{f}_3}{k_4}\right] + \frac{1}{\omega_{d4}}\left[\frac{\tilde{f}_2 - \tilde{f}_1}{k_1\eta\Delta t} + \frac{(\tilde{f}_4 - \tilde{f}_3)(2\zeta_4^2 - 1)}{k_4(1-\eta)\Delta t}\right] \right\}\\
&\quad + \left\{ 1 - \frac{c}{2m}(1-\eta)\Delta t + \left(\frac{c^2}{8m^2} - \frac{\omega_{d4}^2}{2}\right)(1-\eta)^2\Delta t^2 \right.\\
&\quad \left. + \left(\frac{c\omega_{d4}^2}{4m} - \frac{c^3}{48m^3}\right)(1-\eta)^3\Delta t^3 + O(\Delta t^4) \right\}\\
&\quad \cdot \left\{ \frac{\tilde{f}_2}{k_1} - \frac{(\tilde{f}_2 - \tilde{f}_1)c}{k_1^2\eta\Delta t} - \frac{\tilde{f}_3}{k_4} + \frac{(\tilde{f}_4 - \tilde{f}_3)c}{k_4^2(1-\eta)\Delta t} \right\}\\
&\quad + \left\{ \omega_{d1}\omega_{d4}\eta(1-\eta)\Delta t^2 - \frac{c}{2m}\omega_{d1}\omega_{d4}\eta(1-\eta)\Delta t^3 + O(\Delta t^4) \right\}\\
&\quad \cdot \left\{ \frac{\zeta_4}{\sqrt{1-\zeta_4^2}}\left[\frac{\zeta_1 v_1}{\sqrt{1-\zeta_1^2}} + \frac{\dot{v}_1}{\omega_{d1}} - \frac{\tilde{f}_1}{k_1}\cdot\frac{\zeta_1}{\sqrt{1-\zeta_1^2}} + \frac{\tilde{f}_2 - \tilde{f}_1}{k_1}\cdot\frac{2\zeta_1^2 - 1}{\omega_{d1}\eta\Delta t}\right] \right.\\
&\quad + \frac{1}{\omega_{d4}}\left[\frac{-\omega_{n1}v_1 - \zeta_1\dot{v}_1}{\sqrt{1-\zeta_1^2}} + \frac{\tilde{f}_1}{k_1}\left(\frac{\omega_{n1}}{\sqrt{1-\zeta_1^2}} + \frac{\zeta_1}{\eta\Delta t\sqrt{1-\zeta_1^2}}\right)\right.\\
&\quad \left.\left. - \frac{\tilde{f}_2}{k_1\eta\Delta t}\cdot\frac{\zeta_1}{\sqrt{1-\zeta_1^2}}\right]\right\}\\
&\quad + \left\{ \omega_{d4}(1-\eta)\Delta t - \frac{c}{2m}\omega_{d4}(1-\eta)\Delta t^2 \right.\\
&\quad \left. + \left(\frac{c^2\omega_{d4}(1-\eta)}{8m^2} - \frac{\omega_{d4}^3(1-\eta)^3}{6} - \frac{\omega_{d1}^2\omega_{d4}\eta^2(1-\eta)}{2}\right)\Delta t^3 + O(\Delta t^4) \right\}\\
&\quad \cdot \left\{ \frac{\zeta_4}{\sqrt{1-\zeta_4^2}}\left[v_1 - \frac{\tilde{f}_1}{k_1} + \frac{(\tilde{f}_2 - \tilde{f}_1)c}{k_1^2\eta\Delta t}\right] + \frac{1}{\omega_{d4}}\left[\dot{v}_1 - \frac{\tilde{f}_2 - \tilde{f}_1}{k_1\eta\Delta t}\right] \right\}\\
&\quad + \left\{ \omega_{d1}\eta\Delta t - \frac{c}{2m}\omega_{d1}\eta\Delta t^2 \right.\\
&\quad \left. + \left(\frac{c^2\omega_{d1}\eta}{8m^2} - \frac{\omega_{d1}^3\eta^3}{6} - \frac{\omega_{d1}\omega_{d4}^2\eta(1-\eta)^2}{2}\right)\Delta t^3 + O(\Delta t^4) \right\}\\
&\quad \cdot \left\{ \frac{\zeta_1 v_1}{\sqrt{1-\zeta_1^2}} + \frac{\dot{v}_1}{\omega_{d1}} - \frac{\tilde{f}_1}{k_1}\cdot\frac{\zeta_1}{\sqrt{1-\zeta_1^2}} + \frac{\tilde{f}_2 - \tilde{f}_1}{k_1}\cdot\frac{2\zeta_1^2 - 1}{\omega_{d1}\eta\Delta t} \right\}\\
&\quad + \left\{ 1 - \frac{c}{2m}\Delta t + \left(\frac{c^2}{8m^2} - \frac{\omega_{d1}^2\eta^2}{2} - \frac{\omega_{d4}^2(1-\eta)^2}{2}\right)\Delta t^2 \right.\\
&\quad \left. + \left(\frac{c\omega_{d1}^2\eta^2}{4m} + \frac{c\omega_{d4}^2(1-\eta)^2}{4m} - \frac{c^3}{48m^3}\right)\Delta t^3 + O(\Delta t^4) \right\}
\end{aligned}
$$

$$\cdot \left\{ v_1 - \frac{\tilde{f}_1}{k_1} + \frac{(\tilde{f}_2 - \tilde{f}_1)c}{k_1^2 \eta \Delta t} \right\}$$

$$+ \frac{\tilde{f}_4}{k_4} - \frac{(\tilde{f}_4 - \tilde{f}_3)c}{k_4^2 (1 - \eta) \Delta t}$$

$$= v_1 + \dot{v}_1 \Delta t + \left\{ -\frac{c}{2m} \dot{v}_1 + \left[\frac{k_1}{m} \left(\frac{\eta^2}{2} - \eta \right) + \frac{k_4}{m} \left(-\frac{\eta^2}{2} + \eta - \frac{1}{2} \right) \right] v_1 \right.$$

$$+ \frac{\tilde{f}_1}{m} \left(-\frac{\eta^2}{2} + \eta \right) + \frac{\tilde{f}_2 - \tilde{f}_1}{m} \left(-\frac{\eta^2}{3} + \frac{\eta}{2} \right) + \frac{\tilde{f}_4 - \tilde{f}_3}{m} \left(-\frac{\eta^2}{3} + \frac{2\eta}{3} - \frac{1}{3} \right)$$

$$\left. + \frac{\tilde{f}_4}{m} \left(\frac{\eta^2}{2} - \eta + \frac{1}{2} \right) \right\} \Delta t^2 + O(\Delta t^3)$$

$$= v_1 + \dot{v}_1 \Delta t + \left\{ -\frac{c}{2m} \dot{v}_1 + \left[\frac{k_1}{m} \left(\frac{\eta^2}{2} - \eta \right) + \frac{k_4}{m} \left(-\frac{\eta^2}{2} + \eta - \frac{1}{2} \right) \right] v_1 \right.$$

$$\left. + \frac{\tilde{f}_1}{m} \left(-\frac{\eta^2}{2} + \eta \right) + \frac{\tilde{f}_4}{m} \left(\frac{\eta^2}{2} - \eta + \frac{1}{2} \right) \right\} \Delta t^2 + O(\Delta t^3) \tag{3-43}$$

where the last line follows after noting that $\tilde{f}_2 - \tilde{f}_1$ and $\tilde{f}_4 - \tilde{f}_3$ are both $O(\Delta t)$, based on the continuity of $\tilde{f}$ away from the jump.

The local error is the difference between the exact and numerical solutions (equations 3-39 and 3-43) and is

$$\text{Error} = \left\{ \left[\frac{k_4 - k_1}{m} \left(-\frac{\eta^2}{2} + \eta - \frac{1}{4} \right) \right] v_1 - \frac{\tilde{f}_4 - \tilde{f}_1}{m} \left(-\frac{\eta^2}{2} + \eta - \frac{1}{4} \right) \right\} \Delta t^2$$

$$+ O(\Delta t^3) \tag{3-44}$$

Several conclusions can be drawn from equation 3-44:

- If $k_1 = k_4$ and there are no discontinuities in $\tilde{f}$ so $\tilde{f}_4 - \tilde{f}_1 = O(\Delta t)$ then the local error is $O(\Delta t^3)$. This agrees with existing results for the Newmark method [27].

- If $\eta = 1 - \frac{1}{\sqrt{2}} \approx 0.2929$ then the local error is also $O(\Delta t^3)$. This condition is only of academic interest as it will not in general be met.

- In general, if there are discontinuities in either $\tilde{k}$ or $\tilde{f}$, the local error will be $O(\Delta t^2)$, one order less than that found in the absence of discontinuities. It is often stated that the Newmark method has $O(\Delta t^3)$ local errors. This statement is incorrect if the driving force is not continuous.

The *global error* at any time during an analysis is the total error accumulated by that time. It is more important than the local error of a single step. However, it is either very difficult

45

or impossible to calculate for anything other than unrealistically simple systems. A rule of thumb [24] is that the order of the global error is one order lower than the local error. This is often checked by a numerical example, which will be done in Section 3.5.3.

3.5.2 Additional considerations for sensitivity factors

The previous section presents an analysis of the errors associated with the Newmark method for the numerical integration of equations with discontinuous coefficients. It was assumed that the value of the RHS of the governing equation is known. However, an additional consideration is necessary for the calculation of sensitivity factors. Following the routine of figure 3-1, the displacement u is calculated first and used as input to the calculation of the sensitivity factor v_i. As can be seen in the example in Section 3.4, the RHS of the governing equation of the sensitivity factor is in general a function of the displacement. As there will be errors in the numerical solution for the displacement, the RHS will also contain errors.

The problem can be investigated using the same approach as in the previous section: take a single degree-of-freedom system, assume that the initial conditions at the start of a step are correct, and calculate exact and numerical solutions for the displacement and sensitivity factor at the end of the step. Consider a single degree-of-freedom system with the following governing equation of displacement

$$m\ddot{u}(t) + c\dot{u}(t) + r(u(t)) = f(t) \tag{3-45}$$

and, as in the previous section, a single time step of length Δt. The details of the restoring force relationship $r(u(t))$ are not important; however, it will be assumed that over the step it is piecewise linear with a change in tangent stiffness at a time instant $\eta\Delta t$ after the start of the step. For the first part of the time step, the tangent stiffness is k_1, and after $\eta\Delta t$, the tangent stiffness is k_4. The situation is illustrated in figure 3-11. As $f(t)$ is based on an earthquake ground motion, it will be assumed to be continuous over the step, varying linearly from f_1 to f_4.

The governing equation of the sensitivity factor v is

$$m\ddot{v}(t) + c\dot{v}(t) + \tilde{k}(t)v(t) = \tilde{f}(t) \tag{3-46}$$

where $\tilde{k} = k_1$ for the first part of the time step, and $\tilde{k} = k_4$ after $\eta\Delta t$. The exact form of the RHS $\tilde{f}(t)$ depends on the function r and the uncertain parameter, but based on the example of Section 3.4 it will be assumed that $\tilde{f}(t)$ is a linear function of $u(t)$.

The exact and numerical solutions to the problem proceed as follows:

46
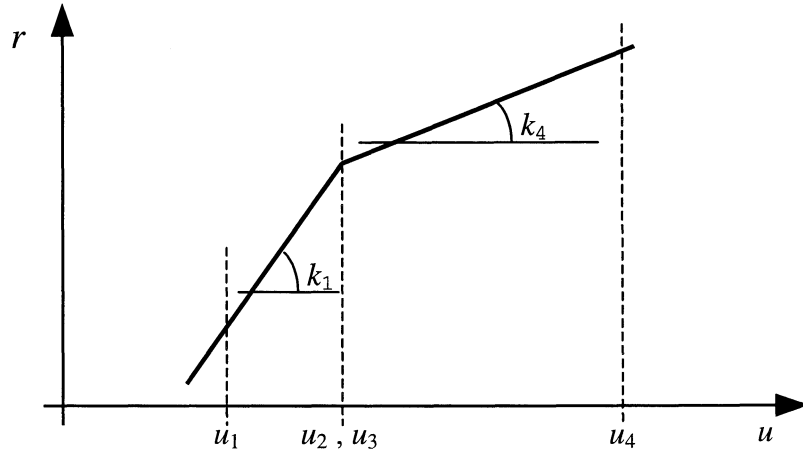
FIGURE 3-11 Restoring force r

1. Solve for the displacement. An exact solution can be found for u_2, u_3 and u_4, similar to that in Section 3.4. The numerical approach uses the Newmark method to calculate the displacement at the end of the step. In general this method has an $O(\Delta t^3)$ local error so will not give the exact value of u_4, but will give $u_4 + O(\Delta t^3)$.

2. Use the calculated displacement as input to the RHS of the governing equation of the sensitivity factor (equation 3-46). The exact solution will have the correct values for $\tilde{f}_1$, $\tilde{f}_2$ and $\tilde{f}_4$ calculated from u_2, u_3 and u_4. The numerical solution will only have $\tilde{f}_4 + O(\Delta t^3)$, calculated from $u_4 + O(\Delta t^3)$. The situation is illustrated in figure 3-12.

3. Calculate the exact and numerical solutions for the sensitivity factor at the end of the step. The exact solution is identical to that in the previous section (equation 3-43).

The numerical solution is given by

$$
\begin{aligned}
v_4 &= v_1 + \frac{\tilde{f}_4 + O(\Delta t^3) + \tilde{f}_1 - (k_4 + k_1)v_1 + \frac{4m}{\Delta t}\dot{v}_1}{k_4 + \frac{2}{\Delta t}c + \frac{4}{\Delta t^2}m} \\
&= v_1 + \frac{(\tilde{f}_4 + O(\Delta t^3) + \tilde{f}_1)\Delta t^2 - (k_4 + k_1)v_1\,\Delta t^2 + 4m\,\Delta t\,\dot{v}_1}{k_4\,\Delta t^2 + 2\,\Delta t\,c + 4m} \\
&= v_1 + \dot{v}_1\Delta t + \left[\frac{\tilde{f}_4 + \tilde{f}_1}{4m} - \frac{k_4 + k_1}{4m}v_1 - \frac{c}{2m}\dot{v}_1\right]\Delta t^2 + O(\Delta t^3)
\end{aligned}
\tag{3-47}
$$

which is equal to equation 3-39.

As the exact and numerical solutions are the same as in the previous section, the local error in the sensitivity factor is equal to equation 3-44 and the same conclusions as in the

47
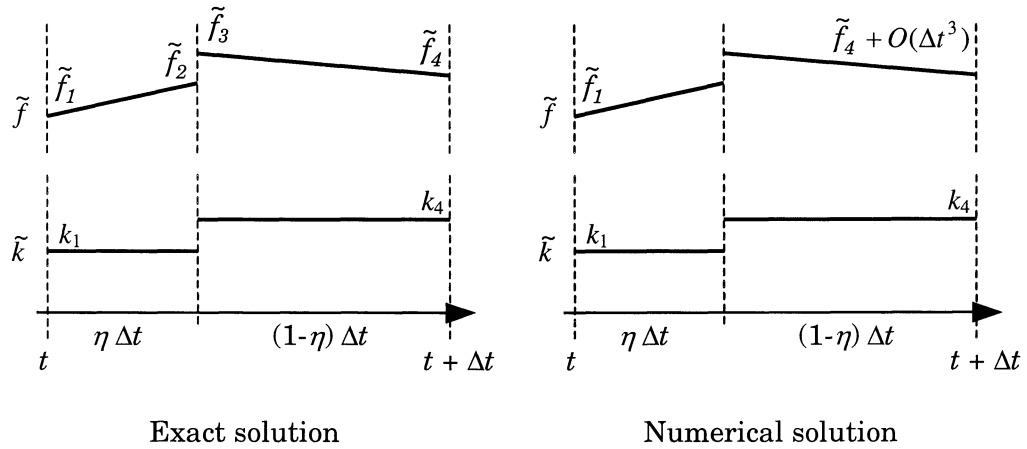
FIGURE 3-12 Single time step

previous section apply. The errors in the numerical solution for the sensitivity factor caused by using the calculated displacement as input are higher-order errors and do not affect the convergence of the solution. Consequently, it can be concluded that the local error in the sensitivity factor is $O(\Delta t^2)$. The next section uses an example to estimate the order of the global error.

3.5.3   Numerical example

The example of Section 3.4 was used to estimate the order of the global error. The problem was solved numerically using several different time steps and the magnitude of the error at different times determined by comparison with the exact analytical solution. Assuming that the global error at time t, $\epsilon(t)$, can be approximately expressed as $C(t)\Delta t^k$, then

$$\log \epsilon(t) \approx \log C(t) + k \log \Delta t \tag{3-48}$$

so the order of the error can be estimated from the gradient of a $\log \epsilon(t)$ versus $\log \Delta t$ graph [2]. These graphs have been plotted for the example of section 3.4 for both the solution for the displacement (figure 3-13) and the solution for the sensitivity factor (figure 3-14). The lines on the graphs are for several different values of t: $t = 0.1, 0.2, 0.3, \ldots, 1.4$. Lines with gradients of 1 and 2 have been drawn on the graphs for comparison.

For the displacement, it is clear from figure 3-13 that most of the lines have a gradient of approximately 2, indicating that the global errors are generally $O(\Delta t^2)$. This agrees with the rule of thumb for global errors, and with existing results for the Newmark method ([22],[70]). For the sensitivity factors, from figure 3-14 it appears that most of the lines have a gradient of approximately 1. The exception is the line for $t = 0.1$, which is before the first discontinuity
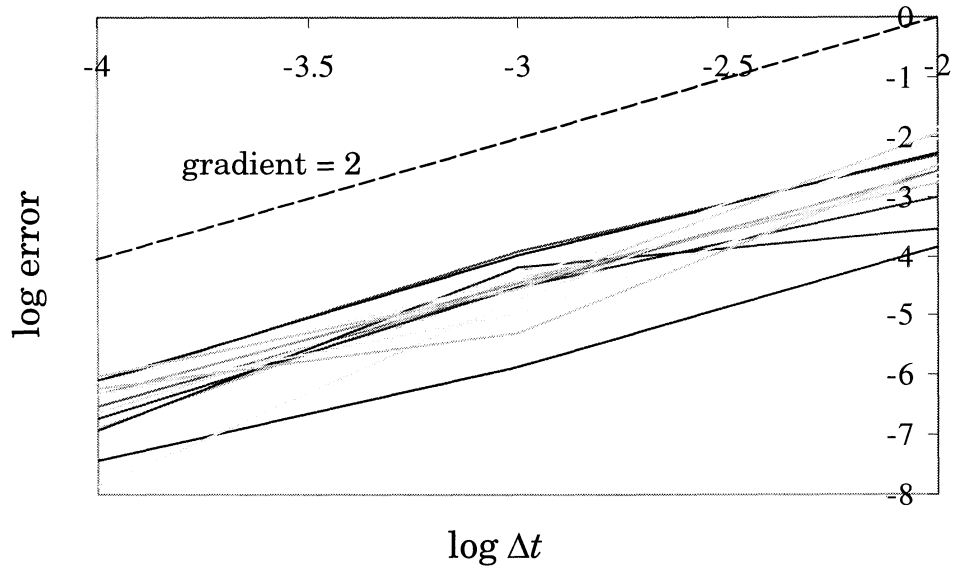
FIGURE 3-13 log error versus log Δt for displacement u
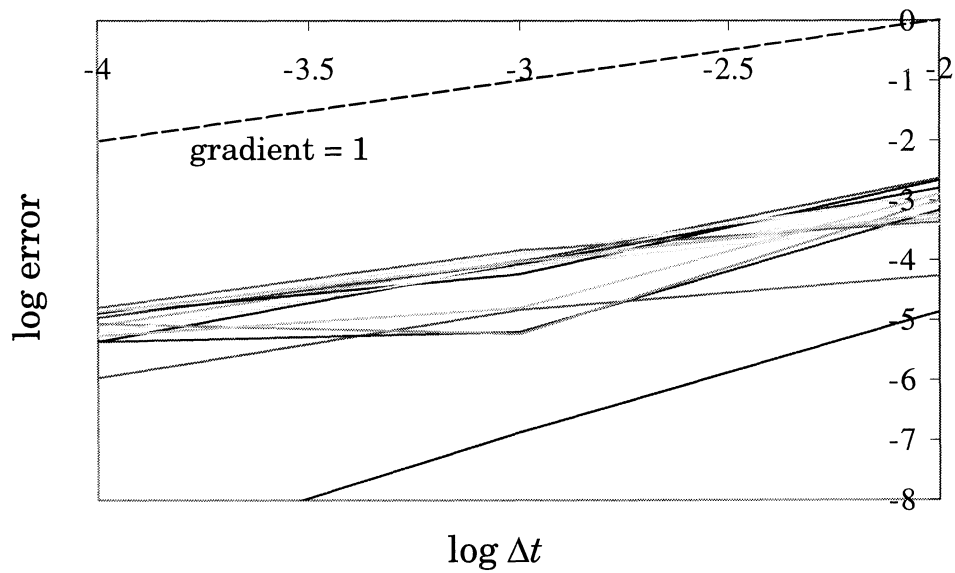
FIGURE 3-14 log error versus log Δt for sensitivity factor v

at $t = 0.182$. The figure indicates that the global error after the first discontinuity is $O(\Delta t)$, one order less than the local error.

3.5.4 Conclusions

Examples suggest that the solution for the sensitivity factor has errors that are one order less than the order of the errors in the displacement solution. The numerical solution for the sensitivity factor will thus converge as Δt is reduced, but will converge more slowly than the displacement solution. This certainly does not mean that the numerical solution for the sensitivity factor will be insufficiently accurate. All of the examples of sensitivity factors calculated in this thesis have been checked and found to be satisfactory. Sensitivity factors for the simple examples were checked against analytical solutions, while sensitivity factors for the more complex finite element models were checked against finite difference calculations with several different finite difference sizes to ensure accuracy. As indicated in section 3.1, the governing equation of the sensitivity factors is a linear differential equation. It is expected that a time step small enough for a nonlinear dynamic structural problem will be small enough to give a sufficiently accurate result for the sensitivity factor.

It may be possible to find more accurate methods for the numerical integration of the scale factor. However, the proposed method has the advantage that it also used to solve for the displacement, which leads to simpler implementation of sensitivity analysis and may also save computation time. For example, in equations 3-13 and 3-19 $\hat{k}$ and $\hat{\hat{k}}$ are identical in the absence of rate-dependent material models. This means that it is not necessary to calculate $\hat{\hat{k}}$ separately, which would probably be necessary if a different numerical integration method were used.

3.6 Multiple support excitations

In many applications, ranging from long-span bridges to piping systems in buildings, the assumption that the same input motion can be applied at all supports of the system is not valid. This section contains a formulation of the governing equations of the displacement and sensitivity factors for systems where multiple support excitations must be considered.

It is necessary to divide the degrees of freedom of the system into two groups: *supported* and *free*. A supported degree of freedom has a prescribed displacement: either a given time history of displacement for a degree of freedom that is subject to seismic excitation, or zero for a stationary degree of freedom. A free degree of freedom does not have a prescribed displacement, but the displacement must be calculated from analysis of the system subjected to the motion of the supported degrees of freedom.

Both the free and supported degrees of freedom of the system must be considered in the governing equation. However, it can be written in partitioned form where a subscript f is used for free degrees of freedom and s for supported degrees of freedom

$$\begin{bmatrix} \boldsymbol{m}_f & \boldsymbol{0} \\ \boldsymbol{0} & \boldsymbol{m}_s \end{bmatrix} \left\{ \begin{array}{c} \ddot{\boldsymbol{u}}_f(t, \boldsymbol{x}_0) \\ \ddot{\boldsymbol{u}}_s(t, \boldsymbol{x}_0) \end{array} \right\} + \begin{bmatrix} \boldsymbol{c}_f(\boldsymbol{x}_0) & \boldsymbol{c}_{fs}(\boldsymbol{x}_0) \\ \boldsymbol{c}_{sf}(\boldsymbol{x}_0) & \boldsymbol{c}_s(\boldsymbol{x}_0) \end{bmatrix} \left\{ \begin{array}{c} \dot{\boldsymbol{u}}_f(t, \boldsymbol{x}_0) \\ \dot{\boldsymbol{u}}_s(t, \boldsymbol{x}_0) \end{array} \right\}$$
$$+ \left\{ \begin{array}{c} \boldsymbol{r}_f(\boldsymbol{u}_f(t, \boldsymbol{x}_0), \boldsymbol{u}_s(t, \boldsymbol{x}_0), \dot{\boldsymbol{u}}_f(t, \boldsymbol{x}_0), \dot{\boldsymbol{u}}_s(t, \boldsymbol{x}_0), \boldsymbol{z}(t, \boldsymbol{x}_0), \boldsymbol{x}_0) \\ \boldsymbol{r}_s(\boldsymbol{u}_f(t, \boldsymbol{x}_0), \boldsymbol{u}_s(t, \boldsymbol{x}_0), \dot{\boldsymbol{u}}_f(t, \boldsymbol{x}_0), \dot{\boldsymbol{u}}_s(t, \boldsymbol{x}_0), \boldsymbol{z}(t, \boldsymbol{x}_0), \boldsymbol{x}_0) \end{array} \right\} = \left\{ \begin{array}{c} \boldsymbol{0} \\ \boldsymbol{f}_s(t, \boldsymbol{x}_0) \end{array} \right\} \qquad (3\text{-}49)$$

where $\boldsymbol{f}_s$ are the support reactions. The zero off-diagonal terms in the first matrix in equation 3-49 follow from the fact that the mass matrix is diagonal for lumped mass systems.

We are interested in displacement of the free degrees of freedom, $\boldsymbol{u}_f(t, \boldsymbol{x}_0)$. The governing equation is the first equation contained in equation 3-49

$$\boldsymbol{m}_f \ddot{\boldsymbol{u}}_f(t, \boldsymbol{x}_0) + \boldsymbol{c}_f(\boldsymbol{x}_0) \dot{\boldsymbol{u}}_f(t, \boldsymbol{x}_0) + \boldsymbol{c}_{fs}(\boldsymbol{x}_0) \dot{\boldsymbol{u}}_s(t, \boldsymbol{x}_0)$$
$$+ \boldsymbol{r}_f(\boldsymbol{u}_f(t, \boldsymbol{x}_0), \boldsymbol{u}_s(t, \boldsymbol{x}_0), \dot{\boldsymbol{u}}_f(t, \boldsymbol{x}_0), \dot{\boldsymbol{u}}_s(t, \boldsymbol{x}_0), \boldsymbol{z}(t, \boldsymbol{x}_0), \boldsymbol{x}_0) = \boldsymbol{0} \qquad (3\text{-}50)$$

The governing equation of the sensitivity factors of the free degrees of freedom, $\boldsymbol{v}_{f,i}(t)$, is obtained by differentiating equation 3-50 with respect to x_i and rearranging

$$\boldsymbol{m}_f \ddot{\boldsymbol{v}}_{f,i}(t) + \left[\boldsymbol{c}_f(\boldsymbol{x}_0) + \frac{\partial \boldsymbol{r}_f}{\partial \dot{\boldsymbol{u}}_f}(t, \boldsymbol{x}_0) \right] \dot{\boldsymbol{v}}_{f,i}(t) + \frac{\partial \boldsymbol{r}_f}{\partial \boldsymbol{u}_f}(t, \boldsymbol{x}_0) \boldsymbol{v}_{f,i}(t) =$$
$$- \frac{\partial \boldsymbol{c}_f(\boldsymbol{x}_0)}{\partial x_i} \dot{\boldsymbol{u}}_f(t, \boldsymbol{x}_0) - \frac{\partial \boldsymbol{c}_{fs}(\boldsymbol{x}_0)}{\partial x_i} \dot{\boldsymbol{u}}_s(t, \boldsymbol{x}_0) - \left[\boldsymbol{c}_{fs}(\boldsymbol{x}_0) + \frac{\partial \boldsymbol{r}_f}{\partial \dot{\boldsymbol{u}}_s}(t, \boldsymbol{x}_0) \right] \dot{\boldsymbol{v}}_{s,i}(t)$$
$$- \frac{\partial \boldsymbol{r}_f}{\partial \boldsymbol{u}_s}(t, \boldsymbol{x}_0) \boldsymbol{v}_{s,i}(t) - \left[\left. \frac{\partial \boldsymbol{r}_f}{\partial x_i} \right|_{\boldsymbol{u}_f, \boldsymbol{u}_s, \dot{\boldsymbol{u}}_f, \dot{\boldsymbol{u}}_s, \boldsymbol{z}} (t, \boldsymbol{x}_0) + \frac{\partial \boldsymbol{r}_f}{\partial \boldsymbol{z}}(t, \boldsymbol{x}_0) \frac{\partial \boldsymbol{z}}{\partial x_i}(t, \boldsymbol{x}_0) \right] \qquad (3\text{-}51)$$

where $\boldsymbol{v}_{f,i} = \dfrac{\partial \boldsymbol{u}_f}{\partial x_i}$ and $\boldsymbol{v}_{s,i} = \dfrac{\partial \boldsymbol{u}_s}{\partial x_i}$. If x_i is not a parameter of the input motion then $\boldsymbol{v}_{s,i} = \dot{\boldsymbol{v}}_{s,i} = \boldsymbol{0}$; otherwise $\boldsymbol{v}_{s,i}$ and $\dot{\boldsymbol{v}}_{s,i}$ must be given. Equation 3-51 is similar to equation 3-4 for a single support motion.

The formulation of a numerical solution proceeds in the same manner as for a single support motion. At a general time step t_j, equation 3-50 can be rewritten as

$$\boldsymbol{m}_f \ddot{\boldsymbol{u}}_f(t_j) + \boldsymbol{c}_f \dot{\boldsymbol{u}}_f(t_j) + \boldsymbol{c}_{fs} \dot{\boldsymbol{u}}_s(t_j) + \boldsymbol{r}_f(t_j) = \boldsymbol{0} \qquad (3\text{-}52)$$

The incremental form of the equation is

$$\boldsymbol{m}_f \Delta \ddot{\boldsymbol{u}}_f(t_j) + \boldsymbol{c}_f \Delta \dot{\boldsymbol{u}}_f(t_j) + \boldsymbol{c}_{fs} \Delta \dot{\boldsymbol{u}}_s(t_j) + \Delta \boldsymbol{r}_f(t_j) = \boldsymbol{0} \qquad (3\text{-}53)$$

51

For small time steps the following approximation can be made

$$\Delta \boldsymbol{r}_f(t_j) \approx \frac{\partial \boldsymbol{r}_f}{\partial \boldsymbol{u}_f}(t_j)\Delta \boldsymbol{u}_f(t_j) + \frac{\partial \boldsymbol{r}_f}{\partial \boldsymbol{u}_s}(t_j)\Delta \boldsymbol{u}_s(t_j) \tag{3-54}$$

The same steps are followed as in the single support motion case, ending in the following equation analogous to equation 3-13

$$\hat{\boldsymbol{k}}(t_j)\Delta \boldsymbol{u}_f(t_j) = \Delta \hat{\boldsymbol{f}}(t_j) \tag{3-55}$$

where $\hat{\boldsymbol{k}}(t_j)$ $=$ $\dfrac{\partial \boldsymbol{r}_f}{\partial \boldsymbol{u}_f}(t_j) + \dfrac{\gamma}{\beta\Delta t}\boldsymbol{c}_f + \dfrac{1}{\beta(\Delta t)^2}\boldsymbol{m}_f$

$\Delta \hat{\boldsymbol{f}}(t_j)$ $=$ $-\dfrac{\partial \boldsymbol{r}_f}{\partial \boldsymbol{u}_s}(t_j)\Delta \boldsymbol{u}_s(t_j) - \boldsymbol{c}_{fs}\Delta \dot{\boldsymbol{u}}_s(t_j) + \left[\dfrac{1}{\beta\Delta t}\boldsymbol{m}_f + \dfrac{\gamma}{\beta}\boldsymbol{c}_f\right]\dot{\boldsymbol{u}}_s(t_j)$

$+ \left[\dfrac{1}{2\beta}\boldsymbol{m}_f + \Delta t\left(\dfrac{\gamma}{2\beta} - 1\right)\boldsymbol{c}_f\right]\ddot{\boldsymbol{u}}_f(t_j)$

The numerical solution for the sensitivity factors is much the same as before, ending in the following, analogous to equation 3-19

$$\hat{\hat{\boldsymbol{k}}}(t_j)\Delta \boldsymbol{v}_{f,i}(t_j) = \Delta \hat{\hat{\boldsymbol{f}}}_i(t_j) \tag{3-56}$$

52

$$\text{where } \hat{\tilde{\boldsymbol{k}}}(t_j) \quad = \quad \frac{\partial \boldsymbol{r}_f}{\partial \boldsymbol{u}_f}(t_{j+1}) + \frac{\gamma}{\beta \Delta t}\tilde{\boldsymbol{c}}(t_{j+1}) + \frac{1}{\beta(\Delta t)^2}\boldsymbol{m}_f$$

$$\Delta \hat{\tilde{\boldsymbol{f}}}_i(t_j) \quad = \quad \Delta \tilde{\boldsymbol{f}}_i(t_j) - \Delta \tilde{\boldsymbol{c}}(t_j)\dot{\boldsymbol{v}}_{f,i}(t_j) - \Delta \tilde{\boldsymbol{k}}(t_j)\boldsymbol{v}_{f,i}(t_j)$$

$$+ \left[\frac{1}{\beta \Delta t}\boldsymbol{m}_f + \frac{\gamma}{\beta}\tilde{\boldsymbol{c}}(t_{j+1})\right]\dot{\boldsymbol{v}}_{f,i}(t_j)$$

$$+ \left[\frac{1}{2\beta}\boldsymbol{m}_f + \Delta t\left(\frac{\gamma}{2\beta} - 1\right)\tilde{\boldsymbol{c}}(t_{j+1})\right]\ddot{\boldsymbol{v}}_{f,i}(t_j)$$

$$\tilde{\boldsymbol{c}}(t_j) \quad = \quad \boldsymbol{c}_f + \frac{\partial \boldsymbol{r}_f}{\partial \dot{\boldsymbol{u}}_f}(t_j)$$

$$\tilde{\boldsymbol{k}}(t_j) \quad = \quad \frac{\partial \boldsymbol{r}_f}{\partial \boldsymbol{u}_f}(t_j)$$

$$\tilde{\boldsymbol{f}}_i(t_j) \quad = \quad -\frac{\partial \boldsymbol{c}_f}{\partial x_i}\dot{\boldsymbol{u}}_f(t_j) - \frac{\partial \boldsymbol{c}_{fs}}{\partial x_i}\dot{\boldsymbol{u}}_s(t_j)$$

$$- \left[\boldsymbol{c}_{fs} + \frac{\partial \boldsymbol{r}_f}{\partial \dot{\boldsymbol{u}}_s}(t_j)\right]\dot{\boldsymbol{v}}_{s,i}(t_j) - \frac{\partial \boldsymbol{r}_f}{\partial \boldsymbol{u}_s}(t_j)\boldsymbol{v}_{s,i}(t_j)$$

$$- \left[\left.\frac{\partial \boldsymbol{r}_f}{\partial x_i}\right|_{\boldsymbol{u}_f,\boldsymbol{u}_s,\dot{\boldsymbol{u}}_f,\dot{\boldsymbol{u}}_s,\boldsymbol{z}}(t_j) + \frac{\partial \boldsymbol{r}_f}{\partial \boldsymbol{z}}(t_j)\frac{\partial \boldsymbol{z}}{\partial x_i}(t_j)\right]$$

SECTION 4
APPLICATIONS OF SENSITIVITY FACTORS

4.1 Optimization

Among the most useful applications of the sensitivity factors are the calibration of the parameters of the structural model to match experimental data, or the selection of an optimal value of one of the parameters. Both tasks can be accomplished by nonlinear programming methods [38]. To formulate the problem, consider a scalar function of the the displacement of the structure, $g(\boldsymbol{u}(t, \boldsymbol{x}))$, called the objective function. We wish to find the value of $\boldsymbol{x}$ that minimizes the value of this function. This can be accomplished by a suitable nonlinear programming algorithm. Such algorithms are typically iterative, starting at a given point in $\boldsymbol{x}$-space and at each iteration taking a "step" in a direction such that the objective function is reduced. Different algorithms use different methods to select the direction and size of the "step". It is possible that a local rather than a global minimum will be found. The iterative nature of the algorithm means that $g(\boldsymbol{u}(t, \boldsymbol{x}))$ will have to be evaluated at several values of $\boldsymbol{x}$ before the minimum is found. Each evaluation requires a time-history analysis of the system, which may be time-consuming. The usefulness of the sensitivity factors is in calculating the gradients of g with respect to $\boldsymbol{x}$. These gradients allow more efficient nonlinear programming algorithms to be used, with a reduction in the number of evaluations of $g(\boldsymbol{u}(t, \boldsymbol{x}))$.

For an example of a typical objective function, consider the common problem of calibrating a simple computer model of a structure against either experimental data or data from a more accurate but also computationally intensive model. More specifically, the problem is to find values of the parameters of the simple model so that the calculated time history of displacement of a selected degree of freedom of the structure, say $u_j(t)$, $0 < t < \tau$, matches a given time history $\nu(t)$, $0 < t < \tau$. A commonly used objective function for this problem is the integral of the square of the difference between the two time histories:

$$g(\boldsymbol{u}(t, \boldsymbol{x})) = \int_0^{\tau} [u_j(t, \boldsymbol{x}) - \nu(t)]^2 \, dt \qquad (4\text{-}1)$$

Minimizing this objective function will tend to draw $\boldsymbol{u}(t, \boldsymbol{x})$ closer to $\nu(t)$ over the whole period under consideration.

The derivative of g is given by

$$\frac{\partial g(\boldsymbol{u}(t, \boldsymbol{x}))}{\partial x_i} = \int_0^{\tau} 2[u_j(t, \boldsymbol{x}) - \nu(t)] \, v_{j,i}(t) \, dt \qquad (4\text{-}2)$$

A second typical objective function is often found in seismic retrofit problems. The problem is to find the parameter values that minimize the peak absolute value of the displacement of

a critical degree of freedom. The objective function for this problem is

$$g\left(\boldsymbol{u}(t,\boldsymbol{x})\right) = \max_{t} |u_j(t,\boldsymbol{x})| \tag{4-3}$$

As explained in section 2, the sensitivity factor at the time of the peak can be used as the sensitivity of the peak, so the derivative is

$$\frac{\partial g\left(\boldsymbol{u}(t,\boldsymbol{x})\right)}{\partial x_i} = v_{j,i}(t^*)\text{sign}\left(u_j(t^*,\boldsymbol{x})\right) \tag{4-4}$$

where $t^* = \arg\max_t |u_j(t,\boldsymbol{x})|$, the time at which the maximum displacement occurs.

Many different nonlinear programming algorithms have been pre-programmed [42] [53] and are available for use, often simply as "black boxes" which take values of $\boldsymbol{x}$, g and $\dfrac{\partial g\left(\boldsymbol{u}(t,\boldsymbol{x})\right)}{\partial x_i}$ and return the values of $\boldsymbol{x}$ for the following iteration. These algorithms can be used with the software used to calculate the sensitivity factors. For example, MATLAB [42] uses the Broyden-Fletcher-Goldfarb-Shanno quasi-Newton method [38].

4.2   Approximate fragility curves

The sensitivity factors can also be used in probabilistic analysis to generate approximate fragility curves. Assume that the parameter vector is random. We will follow the convention that random quantities are written in uppercase letters, so the parameter vector will be denoted by $\boldsymbol{X}$. The mean of $\boldsymbol{X}$ is $\boldsymbol{\mu}_X$.

Consider a function $g\left(\boldsymbol{u}(t,\boldsymbol{X}),0<t<\tau\right)$ which defines the acceptable response of the system. Failure is assumed to occur if $g<0$. For example, the criterion that the maximum value of displacement in degree-of-freedom j should be less than u_{cr} can be expressed as

$$g\left(\boldsymbol{u}(t,\boldsymbol{X}),0<t<\tau\right) = u_{cr} - \max_{0<t<\tau} u_j(t,\boldsymbol{X}) \tag{4-5}$$

The set of values of $\boldsymbol{X}$ for which $g>0$ is frequently termed the "safe set" [40]. The boundary of the safe set is defined by $g=0$.

The fragility P_f is defined as the probability of failure,

$$P_f = P\left[g\left(\boldsymbol{u}(t,\boldsymbol{X}),0<t<\tau\right)<0\right]$$

56

It is generally not possible to find a closed form solution for the fragility, so approximate methods have to be used.

Monte Carlo simulation is one of the most commonly used methods for complex systems. Zhang and Der Kiureghian [69] use the first-order reliability method (FORM) [40]. However, both of these methods require many time-history analyses of the system, which may be time-consuming.

The sensitivity factors can be used to calculate approximate fragilities using the Monte Carlo or FORM methods with only one time-history analysis of the system. The approach is based on the first order Taylor expansion (equation 2-4) written about the mean

$$\boldsymbol{u}(t, \boldsymbol{X}) \approx \boldsymbol{u}(t, \boldsymbol{\mu}_X) + \boldsymbol{v}(t)\left(\boldsymbol{X} - \boldsymbol{\mu}_X\right) \tag{4-6}$$

As equation 4-6 is approximate, the resulting fragilities are approximate. The accuracy depends on the accuracy of equation 4-6. The methods are

- **First-order Monte Carlo simulation**: The required steps are listed below.

  1. Generate a sample $\boldsymbol{x}$ of $\boldsymbol{X}$.
  2. Calculate $\boldsymbol{u}(t_i, \boldsymbol{x}) \approx \boldsymbol{u}(t_i, \boldsymbol{\mu}_X) + \boldsymbol{v}(t_i)\left(\boldsymbol{x} - \boldsymbol{\mu}_X\right)$ for $i = 1, 2, 3, \ldots$ and check $g(\boldsymbol{u})$ after each step. It is not always necessary to consider every time step — the process can stop as soon as a failure is detected.
  3. If a failure is found, increase N_f, the number of failures, by 1.
  4. Repeat steps 1–3 a preselected number, N_s, times.
  5. The failure probability is approximately N_f/N_s.

- **First-order reliability method (FORM)**: The required steps are listed below.

  1. Transform $\boldsymbol{X}$ to standard Gaussian space by $\boldsymbol{Y} = f(\boldsymbol{X})$ where the elements of $\boldsymbol{Y}$ are uncorrelated standard Gaussian random variables. The form of the transformation f depends on the distribution of $\boldsymbol{X}$. If $\boldsymbol{X}$ is Gaussian then f can be determined from $\boldsymbol{X} = \boldsymbol{a}\boldsymbol{Y} + \boldsymbol{\mu}_X$ where matrix $\boldsymbol{a}$ can be calculated by a Cholesky factorization of the covariance matrix of $\boldsymbol{X}$.
  2. Set $\boldsymbol{u}(t_i, \boldsymbol{y}) \approx \boldsymbol{u}(t_i, \boldsymbol{\mu}_X) + \boldsymbol{v}(t_i)\left(f^{-1}(\boldsymbol{y}) - \boldsymbol{\mu}_X\right)$ and solve the constrained optimization problem:

     Minimize $\beta = \sqrt{\boldsymbol{y}^T \boldsymbol{y}}$ such that $g\left(\boldsymbol{u}(t, \boldsymbol{y}), 0 < t < \tau\right) = 0$
  3. The failure probability is approximately $1 - \Phi(\beta)$, where Φ is the standard Gaussian cumulative distribution function.

The optimization problem can be solved by one of the many nonlinear programming algorithms available. The Microsoft Excel Solver [23] also works well for this problem. The FORM method tends to be quicker than the first-order Monte Carlo method presented above, but is more approximate. However, as both methods presented here are based on equation 4-6 and are already approximate, this may not be a problem.

SECTION 5
GENERAL STRATEGY

Sections 5–7 describe the development of software for numerically calculating the sensitivity factors. The software is based on developments in Section 3. As explained in that section, the method used to calculate the displacement can be extended to calculate the sensitivity factors as the same time-stepping numerical integration method is used for both, derivatives of the restoring force are calculated in a similar manner to the restoring force itself, and results from the calculation of the displacement are used in the calculation of the sensitivity factors. It is thus sensible to use the same program for both sets of calculations. Two options are available: add sensitivity analysis capabilities to an existing program, or write an entirely new program. The following objectives should be considered when developing the software:

1. The program should allow the analysis of structures of a realistic size, like those described in Section 2.6.2.

2. A library of realistic material models is required. All models commonly used for steel and reinforced concrete structures should be included.

3. Various levels of detail of structural modeling should be possible.

4. The sensitivity analysis program should be able to be linked to other programs or routines that use the sensitivity factors in, for example, calibration.

5. The program will be used in education as well as research and analysis, so should illustrate the concepts of sensitivity analysis in a simple and clear manner.

It was felt that it would be difficult for a single program to satisfactorily meet all of the above objectives, so two programs were developed:

- **MATLAB:** An entire program to calculate both displacement and sensitivity factors was written using the MATLAB code [42]. The program was titled SABER (Sensitivity Analysis of Buildings subjected to Earthquake Records). SABER is intended for a relatively simple level of analysis and is user-friendly so that it can be used in education.

- **DIANA:** An existing finite element analysis program, DIANA [17], was adapted for sensitivity analysis. The existing program calculates the displacement and new subroutines were added to calculate the sensitivity factors. DIANA is intended for a more detailed level of analysis, such as that required for research purposes.

It must be emphasized that despite their differences, both programs follow the same basic procedure for calculating sensitivity factors as outlined in Section 3. The calculation sequence, equations used, and numerical integration method are the same for both. The only

major computational differences are in the types of element and material models available, and in the method used to calculate the element stiffness matrices and restoring forces. MATLAB uses stiffness elements with predefined stiffness matrices, while DIANA uses finite elements for which the stiffness matrices are obtained by numerical integration. Other practical differences between the programs are outlined below.

The MATLAB program has a graphical user interface and is the easier of the two to use. Several material models have been included, and others can be added through user-supplied subroutines. The program is intended to be the start of an evolving effort and further modules to allow, for example, cost-benefit analysis, can easily be added. It is intended to be used for a relatively simple, beam-element level of structural modeling, and would have limited accuracy and usefulness for more highly-detailed modeling.

DIANA allows much more detailed analysis, with a larger range of material models and element types. For example, plasticity and cracking material models and shell and plane stress element types are available. It may be used for accurate, detailed analyses against which a simpler MATLAB model can be calibrated. DIANA is generally more difficult and time-consuming to use than MATLAB.

Sections 6 and 7 cover the MATLAB and DIANA programs respectively. Each chapter contains a more detailed description of the program; an outline of the flow of calculations performed by the program; a description of the material models available; derivation of the sensitivity equations for each model; and an example to illustrate the use of the program.

The sensitivity equations derived depend on the material models used and are not specific to MATLAB or DIANA. They could in principle be used with any structural analysis code that uses the same material models.

SECTION 6
MATLAB IMPLEMENTATION

6.1 Introduction

MATLAB is a general purpose programming environment with particularly strong matrix analysis and graphics capabilities. It can be used to develop programs with graphical user interfaces so that the programs can be used without any knowledge of the underlying MATLAB code [41]. MATLAB also features SIMULINK, which allows analysis of general dynamic systems by means of graphical block diagrams [50]; however, SIMULINK was not used here as the graphical user interface approach is more traditional in structural analysis and may be more familiar to likely users of the program. The SABER program has been developed with such a graphical user interface as a relatively simple, easy to use and flexible program to illustrate sensitivity analysis [57]. SABER can be used to define the geometry and material properties of a structure and perform dynamic analysis to calculate displacement and sensitivity factors. Other modules to apply the sensitivity factors to problems like cost-benefit analysis can easily be added.

The program can be downloaded from *ceeserver.cee.cornell.edu/mdg12* in the form of p-files which run with MATLAB Version 5.3 or later.

There are two versions of SABER. The original version, SABER-2D, is limited to two dimensions and a single input motion at all supports and is intended for analysis of building frame systems; while the newer SABER-3D version allows three dimensions and multiple support motions and is intended for analysis of piping systems. The systems are defined in the traditional manner using nodes and elements. SABER is intended to be as flexible as possible so includes several different types of elements. The first version of SABER-2D includes linear and nonlinear truss and rotational spring elements, and a linear beam element. The first version of SABER-3D includes linear pipe elements, linear elbow elements, linear beam elements, dashpots and a rotational spring element for modeling nonlinear behavior of pipe elbows. The addition of further elements is also relatively simple, as the formulation of each element is contained in a separate subroutine. Additional subroutines can be written and used with the existing program.

Each element is connected to two nodes. For spring elements the two nodes should be coincident so that the element has zero length, while beam and truss elements are required to have non-zero length.

The program is designed for dynamic earthquake analysis. Masses, in the form of lumped nodal masses, are thus required. External forces such as static nodal or distributed loads cannot be included in the analysis. The damping is specified using the Rayleigh damping
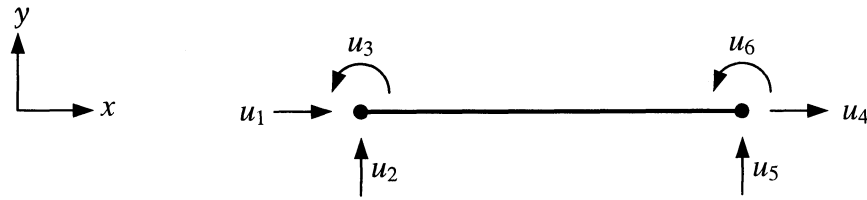
FIGURE 6-1 Typical element for SABER-2D

approach as a function of the mass and initial stiffness matrices:

$$C = aM + bK_0$$

The coefficients a and b are typically chosen to give reasonable damping ratios in the first two linear elastic modes of the structure. Damping due to dashpots in SABER-3D is also added to C.

6.2   Material models

Several quantities must be calculated before the numerical integration routine (equation 3-19) can be used to solve for the sensitivity factor v. Three of these, the tangent stiffness, the derivative of the restoring force with respect to the uncertain parameter, and the derivative of the vector of history-dependent variables with respect to the uncertain parameter, depend on the element and material model for the restoring force r.

This section contains descriptions of some representative elements: the linear frame and nonlinear truss elements used in SABER-2D, and the nonlinear rotational spring used in SABER-3D. The models and equations are formulated for individual elements, and may be combined into global quantities by the procedure of figure 3-2.

The general SABER elements are shown in figures 6-1 and 6-2. For SABER-2D, the general element is a two dimensional, six degree-of-freedom element; while for SABER-3D it is a three dimensional, twelve degree-of-freedom element. Many different types of element and material models may be defined based on these general elements. For example, a truss element is defined by providing stiffness in the axial direction only. The possibilities will be clearer after reviewing the elements in this section.
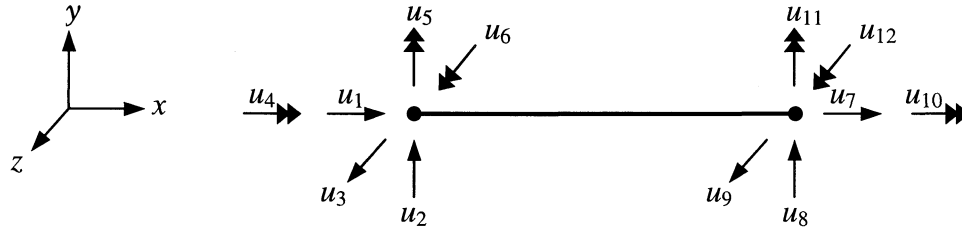
FIGURE 6-2 Typical element for SABER-3D

6.2.1 Linear elastic frame element (SABER-2D)

The linear elastic frame element is a commonly used element in structural analysis. The element properties that must be specified are the elastic modulus E, cross-sectional area A, and moment of inertia I. Any of these parameters can be considered to be uncertain. The element length l is fixed by the geometry of the structure and is thus considered to be deterministic according to the assumptions of section 2.6.

The restoring force at time t, $\boldsymbol{r}(t)$, is given by [43]:

$$
\boldsymbol{r}(t) =
\begin{bmatrix}
\frac{EA}{l} & 0 & 0 & -\frac{EA}{l} & 0 & 0 \\
0 & \frac{12EI}{l^3} & \frac{6EI}{l^2} & 0 & -\frac{12EI}{l^3} & \frac{6EI}{l^2} \\
0 & \frac{6EI}{l^2} & \frac{4EI}{l} & 0 & -\frac{6EI}{l^2} & \frac{2EI}{l} \\
-\frac{EA}{l} & 0 & 0 & \frac{EA}{l} & 0 & 0 \\
0 & -\frac{12EI}{l^3} & -\frac{6EI}{l^2} & 0 & \frac{12EI}{l^3} & -\frac{6EI}{l^2} \\
0 & \frac{6EI}{l^2} & \frac{2EI}{l} & 0 & -\frac{6EI}{l^2} & \frac{4EI}{l}
\end{bmatrix}
\begin{Bmatrix}
u_1(t) \\
u_2(t) \\
u_3(t) \\
u_4(t) \\
u_5(t) \\
u_6(t)
\end{Bmatrix}
\tag{6-1}
$$

6.2.2 Nonlinear truss element (SABER-2D)

A truss element has stiffness and restoring force in the axial direction only, so this element can be treated as a special case of the general element in figure 6-1 in which $r_2 = r_3 = r_5 = r_6 = 0$. The axial force-displacement relationship follows the elastic-plastic behaviour shown in figure 6-3. The yield surface for this uniaxial stress state consists of two parallel lines with gradient $\frac{\beta EA}{l}$, one on the positive r_1 side and one on the negative side. To simplify the equations, the change in length of the element, $u_1(t) - u_4(t)$, will be shortened to $\delta u(t)$. Element properties that must be specified are the elastic modulus E, cross-sectional area A, yield stress f_y and stiffness ratio β.

Although there are many different ways of mathematically formulating this element, in SABER it is done by considering three cases:

63
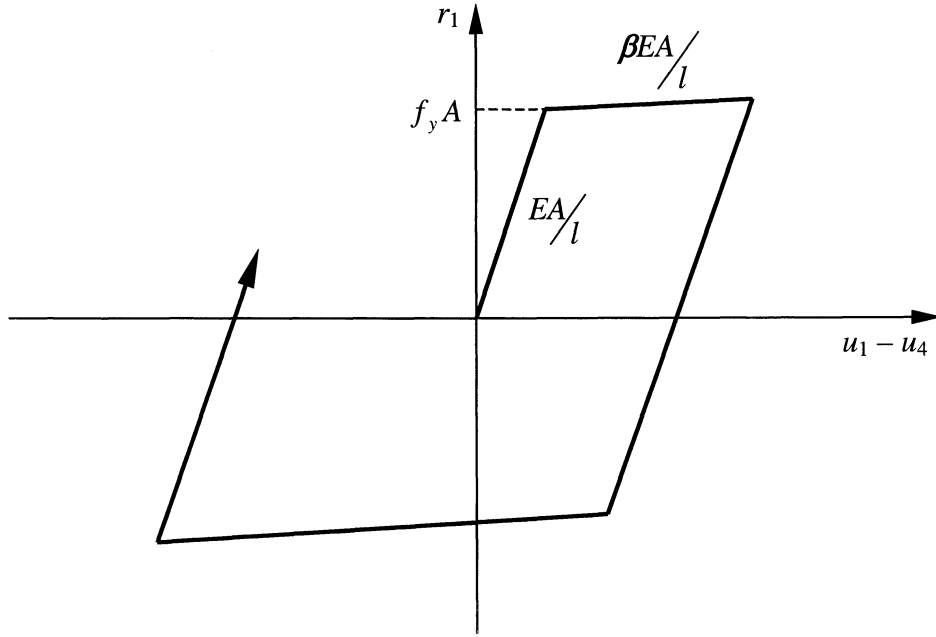
FIGURE 6-3 Axial force-displacement for nonlinear truss element

- Case 1 holds on the yield surface on the positive r_1 side, that is, if

$$z_2(t) + \frac{EA}{l}[\delta u(t) - z_1(t)] > Af_y + \beta \frac{EA}{l}\left[\delta u(t) - \frac{f_y l}{E}\right]$$

  where $z_1(t) = \delta u$ at last velocity sign change
  $ z_2(t) = r_1$ at last velocity sign change

- Case 2 holds on the yield surface on the negative r_1 side, that is, if

$$z_2(t) + \frac{EA}{l}[\delta u(t) - z_1(t)] < -Af_y + \beta \frac{EA}{l}\left[\delta u(t) + \frac{f_y l}{E}\right]$$

- Case 3 holds when inside the yield surface.

The restoring force is then:

$$r_1(t) = \begin{cases} Af_y + \beta\dfrac{EA}{l}\left[\delta u(t) - \dfrac{f_y l}{E}\right], & \text{Case 1} \\[2ex] -Af_y + \beta\dfrac{EA}{l}\left[\delta u(t) + \dfrac{f_y l}{E}\right], & \text{Case 2} \\[2ex] z_2(t) + \dfrac{EA}{l}[\delta u(t) - z_1(t)], & \text{Case 3} \end{cases} \tag{6-2}$$

$r_4(t)$ is always simply the negative of $r_1(t)$.

Equation 6-2 is valid for all t. However, when considering the equations for the history-dependent parameters z_1 and z_2, it is necessary to take account of the fact that the solution is found at series of discrete time steps. The notation t_j and t_{j+1} will be used for two general adjacent time steps.

If no sign change occurs at time t_j, that is, if $\text{sign}[\dot{u}_1(t_j) - \dot{u}_4(t_j)] = \text{sign}[\dot{u}_1(t_{j-1}) - \dot{u}_4(t_{j-1})]$, then

$$\begin{aligned} z_1(t_{j+1}) &= z_1(t_j) \\ z_2(t_{j+1}) &= z_2(t_j) \end{aligned} \tag{6-3}$$

where $z_1(t_0)$ and $z_2(t_0)$ are zero for zero initial conditions.

However, if $\text{sign}[\dot{u}_1(t_j) - \dot{u}_4(t_j)] \neq \text{sign}[\dot{u}_1(t_{j-1}) - \dot{u}_4(t_{j-1})]$ then

$$\begin{aligned} z_1(t_{j+1}) &= \delta u(t_j) \\ z_2(t_{j+1}) &= r_1(t_j) \end{aligned} \tag{6-4}$$

6.2.3 Nonlinear rotational spring element (SABER-3D)

This nonlinear rotational spring element is unique to SABER-3D. It is intended to represent the in-plane, nonlinear bending behavior of a pipe elbow, and is based on detailed finite element analyses. An example of one of the finite element models used to analyze an elbow is shown in figure 6-4. The model was subjected to a cyclic sawtooth load and moment-rotation curves plotted. Geometric and material nonlinearities were considered. The governing equations of the SABER element were obtained by fitting a suitable model to the moment-rotation curve.

A schematic drawing of the element is shown in figure 6-5. The element is actually a rotational spring at a point so nodes 1 and 2 should be co-incident; however, to determine the correct local axes it is useful to imagine the nodes a small distance apart. The model relates the restoring force and displacement in degrees of freedom 6 and 12 (figure 6-2), the rotations around the local z-axis, only. The element is assumed rigid in other directions so $u_1 = u_7$, $u_2 = u_8$, ..., $u_5 = u_{11}$. The local z-axis must be given by specifying a vector corresponding to the node 1 *closing* rotation direction using the right-hand rule. The local x and y axes are arbitrary.

The moment-rotation relationship of the model is shown in figure 6-6. The parameters of the model were determined from the finite element analyses. No attempt was made to relate

Model: ELBOWS
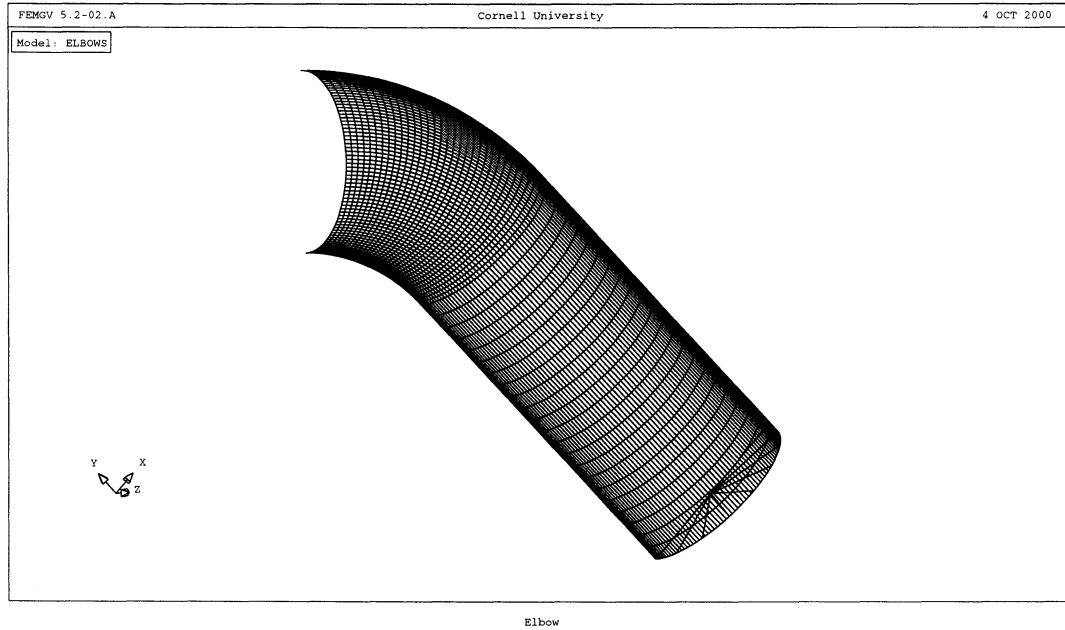
Elbow

FIGURE 6-4 DIANA finite element model of elbow
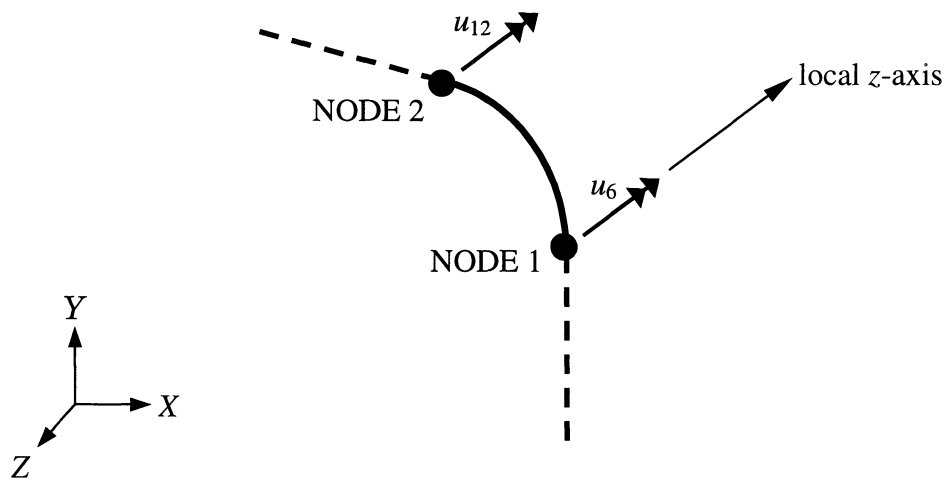
FIGURE 6-5 Schematic of element

66
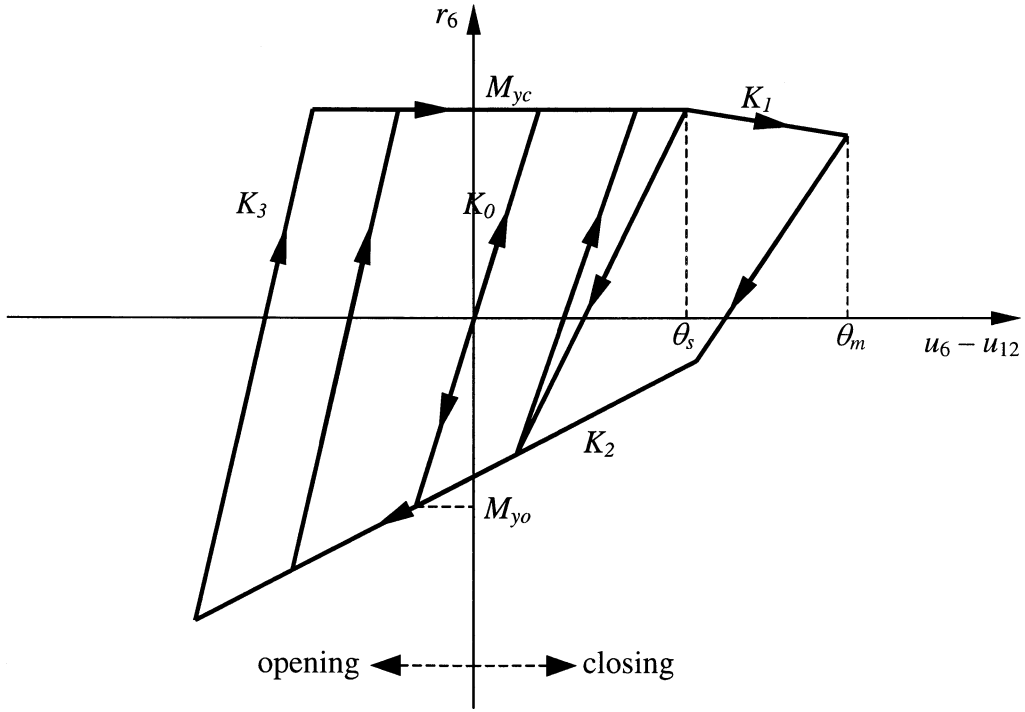
FIGURE 6-6 Moment-rotation for nonlinear elbow hinge element

the parameters to the elbow dimensions or the material properties. Parameters for three common steel elbows are listed in table 6-1. An example of the fit of the model to the finite element analysis output is shown in figure 6-7.

To simplify the governing equations, the rotation of the element, $u_6(t) - u_{12}(t)$ will be shortened to $\delta u(t)$. The model consists of 4 cases:

- Case 1 holds on the descending branch of the yield surface on the positive r_6 side, that is, if

$$z_2(t) + K(t)\left[\delta u(t) - z_1(t)\right] > M_{yc} + K_1\left[\delta u(t) - \theta_s\right] \text{ and } \delta u(t) > \theta_s$$

$$\text{where} \quad K(t) \quad = \quad \begin{cases} K_0 & \delta \dot{u}(t) \geq 0, z_1(t) \geq \frac{M_{yo}}{K_0} \\ K_3 & \delta \dot{u}(t) \geq 0, z_1(t) < \frac{M_{yo}}{K_0} \\ K_0 \left(\frac{M_{yc}}{K_0 z_3(t)}\right)^{\gamma} & \delta \dot{u}(t) < 0 \end{cases}$$

$$z_1(t) \quad = \quad \delta u \text{ at last velocity sign change}$$
$$z_2(t) \quad = \quad r_6 \text{ at last velocity sign change}$$
$$z_3(t) \quad = \quad \max\left[\max_{0 \leq \tau \leq t} \delta u(\tau), \frac{M_{yc}}{K_0}\right]$$

67

TABLE 6-1 Model parameters

Nominal diameter (in)	Outer diameter (in)	Thickness (in)	K_0 (k.in)	K_1 (k.in)	K_2 (k.in)	K_3 (k.in)	M_{yc} (k.in)	M_{yo} (k.in)	θ_s	γ
2	2.375	0.154	3846	-99	415	4421	13.2	-16.1	0.0114	0.164
6	6.625	0.280	36224	-1815	6193	54399	165.4	-188.5	0.0094	0.230
12	12.750	0.290	86231	-3281	23760	145065	438	-650	0.02	0.410

68
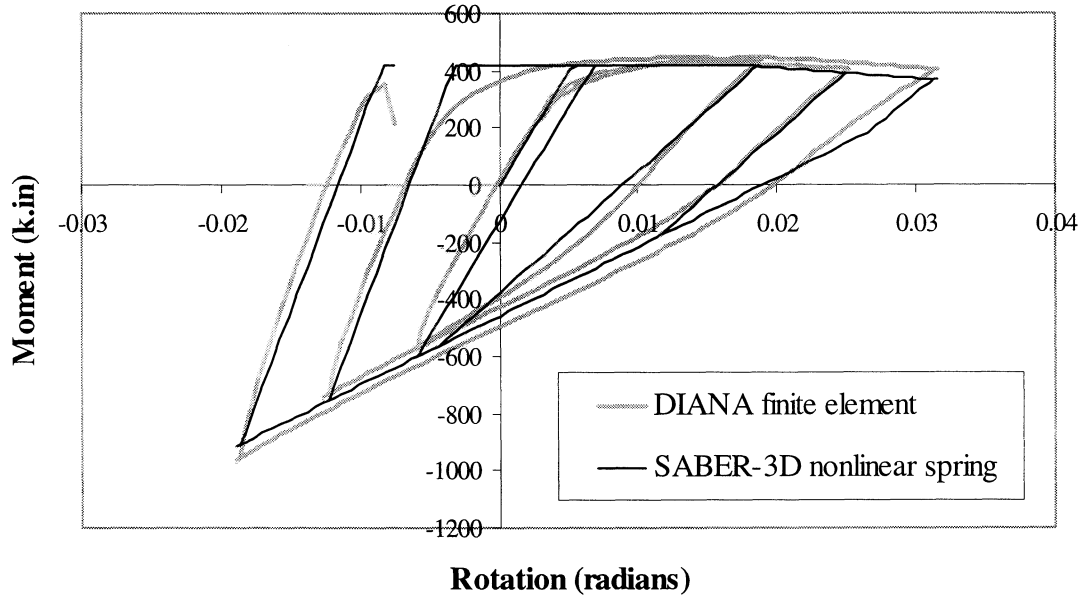
FIGURE 6-7 Comparison of moment versus rotation from DIANA and SABER-3D

- Case 2 holds on the yield surface on the negative r_6 side, that is, if

$$z_2(t) + K(t) \left[\delta u(t) - z_1(t) \right] < M_{yo} + K_2 \left[\delta u(t) - \frac{M_{yo}}{K_0} \right]$$

- Case 3 holds on the constant branch of the yield surface on the positive r_6 side, that is, if

$$z_2(t) + K(t) \left[\delta u(t) - z_1(t) \right] > M_{yc} \text{ and } \delta u(t) \leq \theta_s$$

- Case 4 holds when inside the yield surface. It has three subcases:
  Case 4a: $\delta \dot{u}(t) \geq 0, z_1(t) \geq \frac{M_{yo}}{K_0}$
  Case 4b: $\delta \dot{u}(t) \geq 0, z_1(t) < \frac{M_{yo}}{K_0}$
  Case 4c: $\delta \dot{u}(t) < 0$

The restoring force is then:

$$r_6(t) = \begin{cases} M_{yc} + K_1 \left[\delta u(t) - \theta_s \right], & \text{Case 1} \\[2mm] M_{yo} + K_2 \left[\delta u(t) - \dfrac{M_{yo}}{K_0} \right], & \text{Case 2} \\[2mm] M_{yc}, & \text{Case 3} \\[2mm] z_2(t) + K(t) \left[\delta u(t) - z_1(t) \right], & \text{Case 4} \end{cases} \tag{6-5}$$

69

$r_{12}(t)$ is always simply the negative of $r_6(t)$.

If no sign change occurs at time t_j, that is, if $\text{sign}[\dot{u}_6(t_j) - \dot{u}_{12}(t_j)] = \text{sign}[\dot{u}_6(t_{j-1}) - \dot{u}_{12}(t_{j-1})]$, then

$$
\begin{aligned}
z_1(t_{j+1}) &= z_1(t_j) \\
z_2(t_{j+1}) &= z_2(t_j)
\end{aligned}
\qquad (6\text{-}6)
$$

where $z_1(t_0)$ and $z_2(t_0)$ are zero for zero initial conditions.

However, if $\text{sign}[\dot{u}_6(t_j) - \dot{u}_{12}(t_j)] \neq \text{sign}[\dot{u}_6(t_{j-1}) - \dot{u}_{12}(t_{j-1})]$ then

$$
\begin{aligned}
z_1(t_{j+1}) &= \delta u(t_j) \\
z_2(t_{j+1}) &= r_6(t_j)
\end{aligned}
\qquad (6\text{-}7)
$$

The final history-dependent parameter is given by

$$
z_3(t_{j+1}) = \max\left[\delta u(t_j), z_3(t_j)\right]
\qquad (6\text{-}8)
$$

where $z_3(t_0) = \dfrac{M_{yc}}{K_0}$.

6.3 Sensitivity of material models

This section contains the equations used for calculating the quantities $\dfrac{\partial \boldsymbol{r}}{\partial \boldsymbol{u}}$, $\dfrac{\partial \boldsymbol{r}}{\partial x} + \dfrac{\partial \boldsymbol{r}}{\partial \boldsymbol{z}}\dfrac{\partial \boldsymbol{z}}{\partial x}$, and $\dfrac{\partial \boldsymbol{z}}{\partial x}$ needed to solve for the sensitivity factors for the linear frame, nonlinear truss and nonlinear rotational spring models in Section 6.2.

6.3.1 Linear elastic frame element

The tangent stiffness and partial derivatives with respect to uncertain parameters E, A and I can be calculated relatively simply for the linear elastic frame element. The tangent stiffness

is

$$\frac{\partial \boldsymbol{r}}{\partial \boldsymbol{u}}(t) = \begin{bmatrix} \frac{EA}{l} & 0 & 0 & -\frac{EA}{l} & 0 & 0 \\ 0 & \frac{12EI}{l^3} & \frac{6EI}{l^2} & 0 & -\frac{12EI}{l^3} & \frac{6EI}{l^2} \\ 0 & \frac{6EI}{l^2} & \frac{4EI}{l} & 0 & -\frac{6EI}{l^2} & \frac{2EI}{l} \\ -\frac{EA}{l} & 0 & 0 & \frac{EA}{l} & 0 & 0 \\ 0 & -\frac{12EI}{l^3} & -\frac{6EI}{l^2} & 0 & \frac{12EI}{l^3} & -\frac{6EI}{l^2} \\ 0 & \frac{6EI}{l^2} & \frac{2EI}{l} & 0 & -\frac{6EI}{l^2} & \frac{4EI}{l} \end{bmatrix} \tag{6-9}$$

- If the uncertain parameter x is the elastic modulus E then

$$\frac{\partial \boldsymbol{r}}{\partial x}(t) = \begin{bmatrix} \frac{A}{l} & 0 & 0 & -\frac{A}{l} & 0 & 0 \\ 0 & \frac{12I}{l^3} & \frac{6I}{l^2} & 0 & -\frac{12I}{l^3} & \frac{6I}{l^2} \\ 0 & \frac{6I}{l^2} & \frac{4I}{l} & 0 & -\frac{6I}{l^2} & \frac{2I}{l} \\ -\frac{A}{l} & 0 & 0 & \frac{A}{l} & 0 & 0 \\ 0 & -\frac{12I}{l^3} & -\frac{6I}{l^2} & 0 & \frac{12I}{l^3} & -\frac{6I}{l^2} \\ 0 & \frac{6I}{l^2} & \frac{2I}{l} & 0 & -\frac{6I}{l^2} & \frac{4I}{l} \end{bmatrix} \begin{Bmatrix} u_1(t) \\ u_2(t) \\ u_3(t) \\ u_4(t) \\ u_5(t) \\ u_6(t) \end{Bmatrix} \tag{6-10}$$

- If the uncertain parameter x is the cross-sectional area A then:

$$\frac{\partial \boldsymbol{r}}{\partial x}(t) = \begin{bmatrix} \frac{E}{l} & 0 & 0 & -\frac{E}{l} & 0 & 0 \\ 0 & 0 & 0 & 0 & 0 & 0 \\ 0 & 0 & 0 & 0 & 0 & 0 \\ -\frac{E}{l} & 0 & 0 & \frac{E}{l} & 0 & 0 \\ 0 & 0 & 0 & 0 & 0 & 0 \\ 0 & 0 & 0 & 0 & 0 & 0 \end{bmatrix} \begin{Bmatrix} u_1(t) \\ u_2(t) \\ u_3(t) \\ u_4(t) \\ u_5(t) \\ u_6(t) \end{Bmatrix} \tag{6-11}$$

- If the uncertain parameter x is the moment of inertia I then:

$$\frac{\partial \boldsymbol{r}}{\partial x}(t) = \begin{bmatrix} 0 & 0 & 0 & 0 & 0 & 0 \\ 0 & \frac{12E}{l^3} & \frac{6E}{l^2} & 0 & -\frac{12E}{l^3} & \frac{6E}{l^2} \\ 0 & \frac{6E}{l^2} & \frac{4E}{l} & 0 & -\frac{6E}{l^2} & \frac{2E}{l} \\ 0 & 0 & 0 & 0 & 0 & 0 \\ 0 & -\frac{12E}{l^3} & -\frac{6E}{l^2} & 0 & \frac{12E}{l^3} & -\frac{6E}{l^2} \\ 0 & \frac{6E}{l^2} & \frac{2E}{l} & 0 & -\frac{6E}{l^2} & \frac{4E}{l} \end{bmatrix} \begin{Bmatrix} u_1(t) \\ u_2(t) \\ u_3(t) \\ u_4(t) \\ u_5(t) \\ u_6(t) \end{Bmatrix} \tag{6-12}$$

As there are no history-dependent variables, $\dfrac{\partial \boldsymbol{r}}{\partial \boldsymbol{z}}$ and $\dfrac{\partial \boldsymbol{z}}{\partial x}$ can be taken as zero at all times.

71

6.3.2 Nonlinear truss element

The components of the tangent stiffness matrix $\dfrac{\partial \boldsymbol{r}}{\partial \boldsymbol{u}}$ for the nonlinear truss element are:

$$\frac{\partial r_1}{\partial u_1}(t) = \frac{\partial r_4}{\partial u_4}(t) = -\frac{\partial r_1}{\partial u_4}(t) = -\frac{\partial r_4}{\partial u_1}(t) = \begin{cases} \beta \dfrac{EA}{l}, & \text{Cases 1 and 2} \\[3mm] \dfrac{EA}{l}, & \text{Case 3} \end{cases} \tag{6-13}$$

- If the uncertain parameter x is the elastic modulus E then

$$\frac{\partial r_1}{\partial x}(t) + \frac{\partial r_1}{\partial z}(t)\frac{\partial z}{\partial x}(t) =$$

$$\begin{cases} \beta\dfrac{A}{l}\delta u(t), & \text{Cases 1 and 2} \\[4mm] \dfrac{A}{l}[\delta u(t) - z_1(t)] - \dfrac{EA}{l}\dfrac{\partial z_1}{\partial x}(t) + \dfrac{\partial z_2}{\partial x}(t), & \text{Case 3} \end{cases} \tag{6-14}$$

The derivative of $r_4(t)$ with respect to any parameter is always simply the negative of the derivative of r_1.

The equations for $\dfrac{\partial z_1}{\partial x}(t_{j+1})$ and $\dfrac{\partial z_2}{\partial x}(t_{j+1})$ depend on whether a velocity sign change occurs at time t_j. If no sign change occurs, that is, if $\text{sign}[\dot{u}_1(t_j) - \dot{u}_4(t_j)] = \text{sign}[\dot{u}_1(t_{j-1}) - \dot{u}_4(t_{j-1})]$, then $z_1(t_{j+1}) = z_1(t_j)$ and $z_2(t_{j+1}) = z_2(t_j)$ so

$$\frac{\partial z_1}{\partial x}(t_{j+1}) = \frac{\partial z_1}{\partial x}(t_j) \tag{6-15}$$

$$\frac{\partial z_2}{\partial x}(t_{j+1}) = \frac{\partial z_2}{\partial x}(t_j) \tag{6-16}$$

$\dfrac{\partial z_1}{\partial x}(t_0)$ and $\dfrac{\partial z_2}{\partial x}(t_0)$ are zero for zero initial conditions.

However, if $\text{sign}[\dot{u}_1(t_j) - \dot{u}_4(t_j)] \neq \text{sign}[\dot{u}_1(t_{j-1}) - \dot{u}_4(t_{j-1})]$ then $z_1(t_{j+1}) = \delta u(t_j)$ and $z_2(t_{j+1}) = r_1(t_j)$ so:

$$\frac{\partial z_1}{\partial x}(t_{j+1}) = v_1(t_j) - v_4(t_j) \tag{6-17}$$

$$
\frac{\partial z_2}{\partial x}(t_{j+1}) = \begin{cases} \beta\dfrac{A}{l}\delta u(t_j) + \beta\dfrac{EA}{l}[v_1(t_j) - v_4(t_j)], & \text{Cases 1 and 2} \\[2ex] \dfrac{A}{l}[\delta u(t_j) - z_1(t_j)] + \dfrac{EA}{l}[v_1(t_j) - v_4(t_j)] \\[2ex] \quad - \dfrac{EA}{l}\dfrac{\partial z_1}{\partial x}(t_j) + \dfrac{\partial z_2}{\partial x}(t_j), & \text{Case 3} \end{cases} \tag{6-18}
$$

- If the uncertain parameter x is the yield stress f_y then

$$
\frac{\partial r_1}{\partial x}(t) + \frac{\partial r_1}{\partial z}(t)\frac{\partial z}{\partial x}(t) = \begin{cases} \dfrac{1-\beta}{A}, & \text{Case 1} \\[2ex] -\dfrac{1-\beta}{A}, & \text{Case 2} \\[2ex] -\dfrac{EA}{l}\dfrac{\partial z_1}{\partial x}(t) + \dfrac{\partial z_2}{\partial x}(t), & \text{Case 3} \end{cases} \tag{6-19}
$$

If $\text{sign}[\dot{u}_1(t_j) - \dot{u}_4(t_j)] = \text{sign}[\dot{u}_1(t_{j-1}) - \dot{u}_4(t_{j-1})]$ then equations 6-15 and 6-16 hold,

otherwise

$$
\frac{\partial z_1}{\partial x}(t_{j+1}) = v_1(t_j) - v_4(t_j) \tag{6-20}
$$

$$
\frac{\partial z_2}{\partial x}(t_{j+1}) = \begin{cases} \dfrac{1-\beta}{A} + \beta\dfrac{EA}{l}[v_1(t_j) - v_4(t_j)], & \text{Case 1} \\[2ex] -\dfrac{1-\beta}{A} + \beta\dfrac{EA}{l}[v_1(t_j) - v_4(t_j)], & \text{Case 2} \\[2ex] \dfrac{EA}{l}[v_1(t_j) - v_4(t_j)] - \dfrac{EA}{l}\dfrac{\partial z_1}{\partial x}(t_j) + \dfrac{\partial z_2}{\partial x}(t_j), & \text{Case 3} \end{cases} \tag{6-21}
$$

- If the uncertain parameter x is the stiffness ratio β then

$$
\frac{\partial r_1}{\partial x}(t) + \frac{\partial r_1}{\partial z}(t)\frac{\partial z}{\partial x}(t) = \begin{cases} \dfrac{EA}{l}\delta u(t) - Af_y, & \text{Case 1} \\[2ex] \dfrac{EA}{l}\delta u(t) + Af_y, & \text{Case 2} \\[2ex] -\dfrac{EA}{l}\dfrac{\partial z_1}{\partial x}(t) + \dfrac{\partial z_2}{\partial x}(t), & \text{Case 3} \end{cases} \tag{6-22}
$$

If $\text{sign}[\dot{u}_1(t_j) - \dot{u}_4(t_j)] = \text{sign}[\dot{u}_1(t_{j-1}) - \dot{u}_4(t_{j-1})]$ then equations 6-15 and 6-16 hold,

73

otherwise

$$\frac{\partial z_1}{\partial x}(t_{j+1}) = v_1(t_j) - v_4(t_j)$$

$$\frac{\partial z_2}{\partial x}(t_{j+1}) =$$

$$\begin{cases} \frac{EA}{l}\delta u(t_j) - Af_y + \beta\frac{EA}{l}[v_1(t_j) - v_4(t_j)], & \text{Case 1} \\\\ \frac{EA}{l}\delta u(t_j) + Af_y + \beta\frac{EA}{l}[v_1(t_j) - v_4(t_j)], & \text{Case 2} \\\\ \frac{EA}{l}[v_1(t_j) - v_4(t_j)] - \frac{EA}{l}\frac{\partial z_1}{\partial x}(t_j) + \frac{\partial z_2}{\partial x}(t_j), & \text{Case 3} \end{cases} \qquad (6\text{-}23)$$

- If the uncertain parameter x is not a parameter of this element but is an input parameter, damping parameter or parameter of another element, then $\frac{\partial \boldsymbol{r}}{\partial x}$ will be zero but $\frac{\partial \boldsymbol{r}}{\partial \boldsymbol{z}}\frac{\partial \boldsymbol{z}}{\partial x}$ may be nonzero. This is a difference between nonlinear, history-dependent systems and non-history-dependent systems. In this case the equations are

$$\frac{\partial r_1}{\partial x}(t) + \frac{\partial r_1}{\partial z}(t)\frac{\partial \boldsymbol{z}}{\partial x}(t) = \begin{cases} 0, & \text{Cases 1 and 2} \\\\ -\frac{EA}{l}\frac{\partial z_1}{\partial x}(t) + \frac{\partial z_2}{\partial x}(t), & \text{Case 3} \end{cases} \qquad (6\text{-}24)$$

If $\text{sign}[\dot{u}_1(t_j) - \dot{u}_4(t_j)] = \text{sign}[\dot{u}_1(t_{j-1}) - \dot{u}_4(t_{j-1})]$ then equations 6-15 and 6-16 hold,

otherwise

$$\frac{\partial z_1}{\partial x}(t_{j+1}) = v_1(t_j) - v_4(t_j) \qquad (6\text{-}25)$$

$$\frac{\partial z_2}{\partial x}(t_{j+1}) = \begin{cases} \beta\frac{EA}{l}[v_1(t_j) - v_4(t_j)], & \text{Cases 1 and 2} \\\\ \frac{EA}{l}[v_1(t_j) - v_4(t_j)] - \frac{EA}{l}\frac{\partial z_1}{\partial x}(t_j) + \frac{\partial z_2}{\partial x}(t_j), & \text{Case 3} \end{cases} \qquad \begin{array}{c}(6\text{-}26)\end{array}$$

Notice how much larger the problem has become for the nonlinear element than for the linear element.

74

6.3.3   Nonlinear rotational spring element

The components of the tangent stiffness matrix $\dfrac{\partial \boldsymbol{r}}{\partial \boldsymbol{u}}$ for the nonlinear rotational spring element are:

$$\frac{\partial r_6}{\partial u_6}(t) = \frac{\partial r_{12}}{\partial u_{12}}(t) = -\frac{\partial r_6}{\partial u_{12}}(t) = -\frac{\partial r_{12}}{\partial u_6}(t) = \begin{cases} K_1, & \text{Case 1} \\[1.5ex] K_2, & \text{Case 2} \\[1.5ex] 0, & \text{Case 3} \\[1.5ex] K(t), & \text{Case 4} \end{cases} \tag{6-27}$$

- If the uncertain parameter x is the initial stiffness K_0 then

$$\frac{\partial r_6}{\partial x}(t) + \frac{\partial r_6}{\partial \boldsymbol{z}}(t)\frac{\partial \boldsymbol{z}}{\partial x}(t) =$$

$$\begin{cases} 0, & \text{Cases 1 and 3} \\[2ex] \dfrac{K_2 M_{yo}}{K_0^2}, & \text{Case 2} \\[2.5ex] [\delta u(t) - z_1(t)] - K_0\dfrac{\partial z_1}{\partial x}(t) + \dfrac{\partial z_2}{\partial x}(t), & \text{Case 4a} \\[2.5ex] -K_3\dfrac{\partial z_1}{\partial x}(t) + \dfrac{\partial z_2}{\partial x}(t), & \text{Case 4b} \\[2.5ex] [\delta u(t) - z_1(t)]\left(\dfrac{M_{yc}}{z_3(t)}\right)^\gamma (1 - \gamma)\, K_0^{-\gamma} - K(t)\dfrac{\partial z_1}{\partial x}(t) + \dfrac{\partial z_2}{\partial x}(t) \\[2.5ex] \qquad - [\delta u(t) - z_1(t)]\, K_0 \left(\dfrac{M_{yc}}{K_0}\right)^\gamma \gamma z_3(t)^{-\gamma-1}\dfrac{\partial z_3}{\partial x}(t), & \text{Case 4c} \end{cases} \tag{6-28}$$

The derivative of $r_{12}(t)$ with respect to any parameter is always simply the negative of the derivative of r_6.

The equations for $\dfrac{\partial z_1}{\partial x}(t_{j+1})$ and $\dfrac{\partial z_2}{\partial x}(t_{j+1})$ depend on whether a velocity sign change occurs at time t_j. If no sign change occurs, that is, if $\text{sign}[\dot{u}_6(t_j) - \dot{u}_{12}(t_j)] = \text{sign}[\dot{u}_6(t_{j-1}) -$

$\dot{u}_{12}(t_{j-1})]$, then $z_1(t_{j+1}) = z_1(t_j)$ and $z_2(t_{j+1}) = z_2(t_j)$ so

$$\frac{\partial z_1}{\partial x}(t_{j+1}) = \frac{\partial z_1}{\partial x}(t_j) \tag{6-29}$$

$$\frac{\partial z_2}{\partial x}(t_{j+1}) = \frac{\partial z_2}{\partial x}(t_j) \tag{6-30}$$

$\dfrac{\partial z_1}{\partial x}(t_0)$ and $\dfrac{\partial z_2}{\partial x}(t_0)$ are zero for zero initial conditions.

However, if $\text{sign}[\dot{u}_6(t_j) - \dot{u}_{12}(t_j)] \neq \text{sign}[\dot{u}_6(t_{j-1}) - \dot{u}_{12}(t_{j-1})]$ then $z_1(t_{j+1}) = \delta u(t_j)$ and $z_2(t_{j+1}) = r_6(t_j)$ so:

$$\frac{\partial z_1}{\partial x}(t_{j+1}) = v_6(t_j) - v_{12}(t_j) \tag{6-31}$$

$$\frac{\partial z_2}{\partial x}(t_{j+1}) = \begin{cases} K_1[v_6(t_j) - v_{12}(t_j)], & \text{Case 1} \\[2mm] \dfrac{K_2 M_{yo}}{K_0^2} + K_2[v_6(t_j) - v_{12}(t_j)], & \text{Case 2} \\[2mm] 0, & \text{Case 3} \\[2mm] [\delta u(t_j) - z_1(t_j)] + K_0[v_6(t_j) - v_{12}(t_j)] \\[1mm] \qquad - K_0 \dfrac{\partial z_1}{\partial x}(t_j) + \dfrac{\partial z_2}{\partial x}(t_j), & \text{Case 4a} \\[2mm] K_3[v_6(t_j) - v_{12}(t_j)] \\[1mm] \qquad - K_3 \dfrac{\partial z_1}{\partial x}(t_j) + \dfrac{\partial z_2}{\partial x}(t_j), & \text{Case 4b} \\[2mm] [\delta u(t_j) - z_1(t_j)] \left(\dfrac{M_{yc}}{z_3(t_j)}\right)^{\gamma} (1-\gamma) K_0^{-\gamma} \\[2mm] \qquad + K(t_j)[v_6(t_j) - v_{12}(t_j)] \\[2mm] \qquad - K(t_j) \dfrac{\partial z_1}{\partial x}(t_j) + \dfrac{\partial z_2}{\partial x}(t_j) \\[2mm] \qquad - [\delta u(t) - z_1(t)] K_0 \left(\dfrac{M_{yc}}{K_0}\right)^{\gamma} \\[2mm] \qquad \cdot \gamma z_3(t)^{-\gamma-1} \dfrac{\partial z_3}{\partial x}(t), & \text{Case 4c} \end{cases} \tag{6-32}$$

The equation for $\frac{\partial z_3}{\partial x}(t_{j+1})$ depends on whether a maximum closing displacement is reached at time t_j. If $u_6(t_j) - u_{12}(t_j) \leq z_3(t_j)$ then $z_3(t_{j+1}) = z_3(t_j)$ so

$$\frac{\partial z_3}{\partial x}(t_{j+1}) = \frac{\partial z_3}{\partial x}(t_j) \tag{6-33}$$

However, if $u_6(t_j) - u_{12}(t_j) > z_3(t_j)$ then $z_3(t_{j+1}) = u_6(t_j) - u_{12}(t_j)$ so

$$\frac{\partial z_3}{\partial x}(t_{j+1}) = v_6(t_j) - v_{12}(t_j) \tag{6-34}$$

- If the uncertain parameter x is the closing yield moment M_{yc} then

$$\frac{\partial r_6}{\partial x}(t) + \frac{\partial r_6}{\partial z}(t)\frac{\partial z}{\partial x}(t) =$$

$$\begin{cases}
1, & \text{Cases 1 and 3} \\[2ex]
0, & \text{Case 2} \\[2ex]
-K_0 \frac{\partial z_1}{\partial x}(t) + \frac{\partial z_2}{\partial x}(t), & \text{Case 4a} \\[2ex]
-K_3 \frac{\partial z_1}{\partial x}(t) + \frac{\partial z_2}{\partial x}(t), & \text{Case 4b} \\[2ex]
[\delta u(t) - z_1(t)] K_0^{1-\gamma} z_3(t)^{-\gamma} \gamma M_{yo}^{\gamma-1} - K(t)\frac{\partial z_1}{\partial x}(t) + \frac{\partial z_2}{\partial x}(t) \\[2ex]
\quad - [\delta u(t) - z_1(t)] K_0 \left(\frac{M_{yc}}{K_0}\right)^{\gamma} \gamma z_3(t)^{-\gamma-1}\frac{\partial z_3}{\partial x}(t), & \text{Case 4c}
\end{cases} \tag{6-35}$$

If $\text{sign}[\dot{u}_6(t_j) - \dot{u}_{12}(t_j)] = \text{sign}[\dot{u}_6(t_{j-1}) - \dot{u}_{12}(t_{j-1})]$ then equations 6-29 and 6-30 hold, otherwise

$$\frac{\partial z_1}{\partial x}(t_{j+1}) = v_6(t_j) - v_{12}(t_j) \tag{6-36}$$

$$\frac{\partial z_2}{\partial x}(t_{j+1}) = \begin{cases} 1 + K_1[v_6(t_j) - v_{12}(t_j)], & \text{Case 1} \\[2ex] K_2[v_6(t_j) - v_{12}(t_j)], & \text{Case 2} \\[2ex] 1, & \text{Case 3} \\[2ex] K_0[v_6(t_j) - v_{12}(t_j)] - K_0\dfrac{\partial z_1}{\partial x}(t_j) + \dfrac{\partial z_2}{\partial x}(t_j), & \text{Case 4a} \\[2ex] K_3[v_6(t_j) - v_{12}(t_j)] - K_3\dfrac{\partial z_1}{\partial x}(t_j) + \dfrac{\partial z_2}{\partial x}(t_j), & \text{Case 4b} \\[2ex] [\delta u(t_j) - z_1(t_j)] K_0^{1-\gamma} z_3(t_j)^{-\gamma} \gamma M_{yo}^{\gamma-1} \\[1ex] \quad + K(t_j)[v_6(t_j) - v_{12}(t_j)] \\[1ex] \quad - K(t_j)\dfrac{\partial z_1}{\partial x}(t_j) + \dfrac{\partial z_2}{\partial x}(t_j) \\[1ex] \quad - [\delta u(t_j) - z_1(t_j)] K_0 \left(\dfrac{M_{yc}}{K_0}\right)^{\gamma} \\[1ex] \quad \cdot \gamma z_3(t_j)^{-\gamma-1} \dfrac{\partial z_3}{\partial x}(t_j), & \text{Case 4c} \end{cases} \tag{6-37}$$

Equations 6-33 and 6-34 for $\dfrac{\partial z_3}{\partial x}(t_{j+1})$ apply.

- If the uncertain parameter x is not a parameter of this element then

$$\frac{\partial r_6}{\partial x}(t) + \frac{\partial r_6}{\partial \boldsymbol{z}}(t)\frac{\partial \boldsymbol{z}}{\partial x}(t) =$$

$$\begin{cases} 0, & \text{Cases 1, 2, 3} \\[2ex] -K_0\dfrac{\partial z_1}{\partial x}(t) + \dfrac{\partial z_2}{\partial x}(t), & \text{Case 4a} \\[2ex] -K_3\dfrac{\partial z_1}{\partial x}(t) + \dfrac{\partial z_2}{\partial x}(t), & \text{Case 4b} \\[2ex] -K(t)\dfrac{\partial z_1}{\partial x}(t) + \dfrac{\partial z_2}{\partial x}(t) \\[1ex] \quad - [\delta u(t) - z_1(t)] K_0 \left(\dfrac{M_{yc}}{K_0}\right)^{\gamma} \gamma z_3(t)^{-\gamma-1} \dfrac{\partial z_3}{\partial x}(t), & \text{Case 4c} \end{cases} \tag{6-38}$$

If $\text{sign}[\dot{u}_6(t_j) - \dot{u}_{12}(t_j)] = \text{sign}[\dot{u}_6(t_{j-1}) - \dot{u}_{12}(t_{j-1})]$ then equations 6-29 and 6-30 hold,

otherwise

$$\frac{\partial z_1}{\partial x}(t_{j+1}) = v_6(t_j) - v_{12}(t_j) \tag{6-39}$$

$$\frac{\partial z_2}{\partial x}(t_{j+1}) = \begin{cases} K_1[v_6(t_j) - v_{12}(t_j)], & \text{Case 1} \\[2ex] K_2[v_6(t_j) - v_{12}(t_j)], & \text{Case 2} \\[2ex] 0, & \text{Case 3} \\[2ex] K_0[v_6(t_j) - v_{12}(t_j)] - K_0\dfrac{\partial z_1}{\partial x}(t_j) + \dfrac{\partial z_2}{\partial x}(t_j), & \text{Case 4a} \\[2ex] K_3[v_6(t_j) - v_{12}(t_j)] - K_3\dfrac{\partial z_1}{\partial x}(t_j) + \dfrac{\partial z_2}{\partial x}(t_j), & \text{Case 4b} \\[2ex] K(t_j)[v_6(t_j) - v_{12}(t_j)] \\[1ex] \quad - K(t_j)\dfrac{\partial z_1}{\partial x}(t_j) + \dfrac{\partial z_2}{\partial x}(t_j) \\[1ex] \quad - [\delta u(t_j) - z_1(t_j)] \, K_0 \left(\dfrac{M_{yc}}{K_0}\right)^{\gamma} \\[1ex] \quad \cdot \gamma z_3(t_j)^{-\gamma-1}\dfrac{\partial z_3}{\partial x}(t_j), & \text{Case 4c} \end{cases} \tag{6-40}$$

Equations 6-33 and 6-34 for $\dfrac{\partial z_3}{\partial x}(t_{j+1})$ apply.

6.4 Calculation procedure

Figures 6-8 and 6-9 outline the algorithms in SABER-2D and SABER-3D. The differences between the two are not due to the difference in dimension, but to the multiple support excitations in the 3D version. The flowcharts show the equations used at a typical time step t_j. The flowcharts are based on equations developed in Section 3 and are included here for convenience.

It can be seen from the flowcharts that the element subroutines are called at various stages to calculate the restoring force $\boldsymbol{r}$ and the derivatives $\dfrac{\partial \boldsymbol{r}}{\partial \boldsymbol{u}}$, $\dfrac{\partial \boldsymbol{r}}{\partial x} + \dfrac{\partial \boldsymbol{r}}{\partial \boldsymbol{z}}\dfrac{\partial \boldsymbol{z}}{\partial x}$ and $\dfrac{\partial \boldsymbol{z}}{\partial x}$. These are calculated using the equations presented in Sections 6.2 and 6.3 and the procedure of figure 3-2.

First iteration: $k = 1$

$$\hat{\boldsymbol{k}}(t_j) = \frac{\partial \boldsymbol{r}}{\partial \boldsymbol{u}}(t_j) + \frac{\gamma}{\beta \Delta t}\boldsymbol{c} + \frac{1}{\beta(\Delta t)^2}\boldsymbol{m}$$

$$\Delta \hat{\boldsymbol{f}}(t_j) = \Delta \boldsymbol{f}(t_j) + \left[\frac{1}{\beta \Delta t}\boldsymbol{m} + \frac{\gamma}{\beta}\boldsymbol{c}\right]\dot{\boldsymbol{u}}(t_j) + \left[\frac{1}{2\beta}\boldsymbol{m} + \Delta t\left(\frac{\gamma}{2\beta} - 1\right)\boldsymbol{c}\right]\ddot{\boldsymbol{u}}(t_j)$$

$$\Delta \boldsymbol{R}^{(1)} = \Delta \hat{\boldsymbol{f}}(t_j)$$
$$\boldsymbol{u}^{(0)} = \boldsymbol{u}(t_j)$$

$$\Delta \boldsymbol{u}^{(1)} = \left[\hat{\boldsymbol{k}}(t_j)\right]^{-1}\Delta \boldsymbol{R}^{(1)}$$

$$\boldsymbol{u}^{(1)} = \boldsymbol{u}(t_j) + \Delta \boldsymbol{u}^{(1)}$$

Call subroutine to calculate $\boldsymbol{r}\left(\boldsymbol{u}^{(1)}\right)$
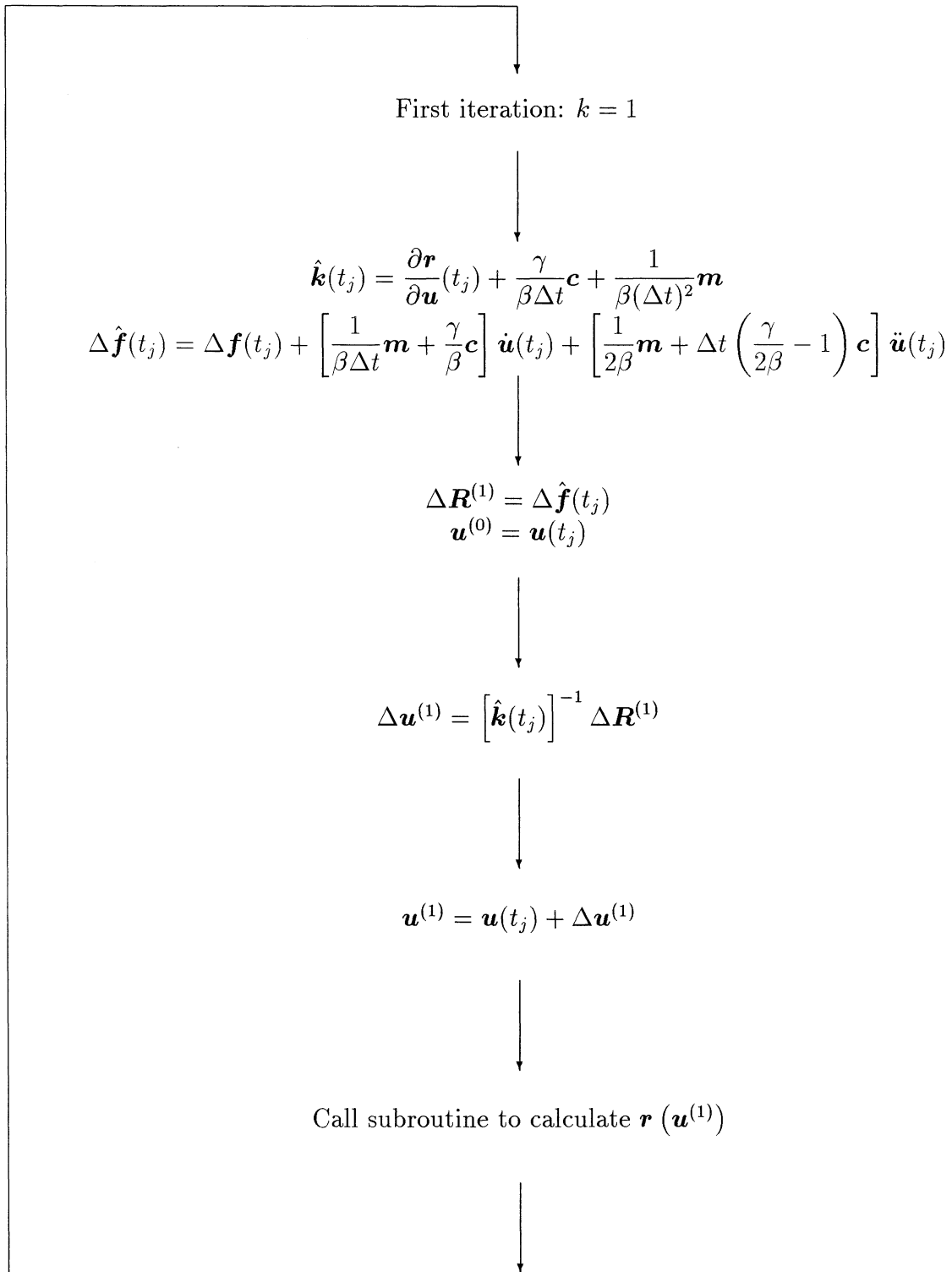
FIGURE 6-8 Flowchart of calculations at a typical time step t_j for SABER-2D

FIGURE 6-8 (Continued)

Calculate unbalanced force

$$\Delta \boldsymbol{R}^{(k+1)} = \Delta \boldsymbol{R}^{(k)} - \left[\boldsymbol{r}\left(\boldsymbol{u}^{(k)}\right) - \boldsymbol{r}\left(\boldsymbol{u}^{(k-1)}\right)\right] - \left[\hat{\boldsymbol{k}}(t_j) - \frac{\partial \boldsymbol{r}}{\partial \boldsymbol{u}}(t_j)\right] \Delta \boldsymbol{u}^{(k)}$$

Check unbalanced force $\Delta \boldsymbol{R}^{(k+1)}$ against tolerance

Tolerance not satisfied.
Iteration required: $k = k + 1$

Tolerance satisfied.
Solution for $\boldsymbol{u}(t_{j+1})$ found.

$$\Delta \boldsymbol{u}^{(k)} = \left[\hat{\boldsymbol{k}}(t_j)\right]^{-1} \Delta \boldsymbol{R}^{(k)}$$

$$\boldsymbol{u}^{(k)} = \boldsymbol{u}^{(k-1)} + \Delta \boldsymbol{u}^{(k)}$$

Call subroutine to calculate $\boldsymbol{r}\left(\boldsymbol{u}^{(k)}\right)$
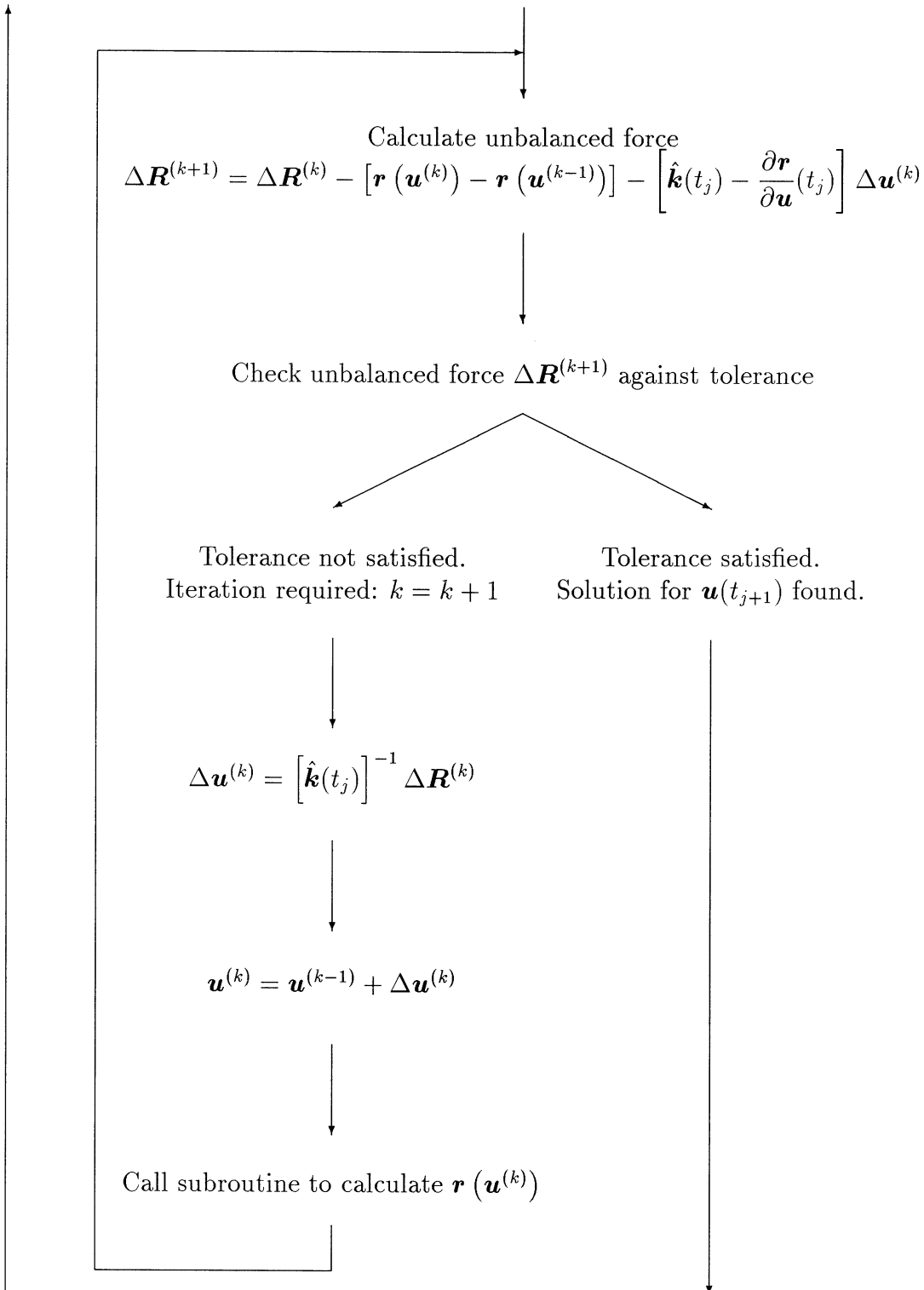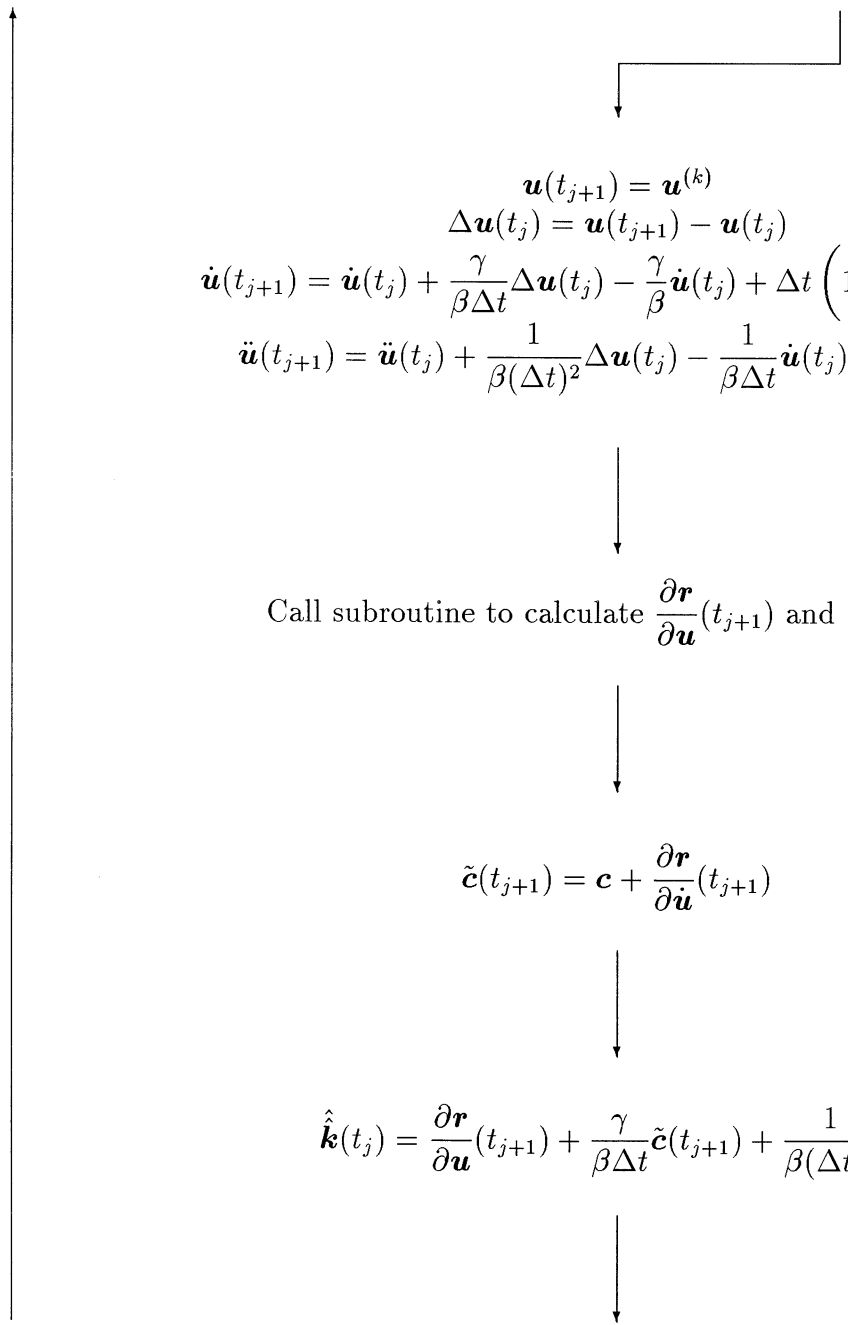
FIGURE 6-8 (Continued)

$$\boldsymbol{u}(t_{j+1}) = \boldsymbol{u}^{(k)}$$
$$\Delta\boldsymbol{u}(t_j) = \boldsymbol{u}(t_{j+1}) - \boldsymbol{u}(t_j)$$
$$\dot{\boldsymbol{u}}(t_{j+1}) = \dot{\boldsymbol{u}}(t_j) + \frac{\gamma}{\beta\Delta t}\Delta\boldsymbol{u}(t_j) - \frac{\gamma}{\beta}\dot{\boldsymbol{u}}(t_j) + \Delta t\left(1 - \frac{\gamma}{2\beta}\right)\ddot{\boldsymbol{u}}(t_j)$$
$$\ddot{\boldsymbol{u}}(t_{j+1}) = \ddot{\boldsymbol{u}}(t_j) + \frac{1}{\beta(\Delta t)^2}\Delta\boldsymbol{u}(t_j) - \frac{1}{\beta\Delta t}\dot{\boldsymbol{u}}(t_j) - \frac{1}{2\beta}\ddot{\boldsymbol{u}}(t_j)$$

Call subroutine to calculate $\dfrac{\partial\boldsymbol{r}}{\partial\boldsymbol{u}}(t_{j+1})$ and $\dfrac{\partial\boldsymbol{r}}{\partial\dot{\boldsymbol{u}}}(t_{j+1})$

$$\tilde{\boldsymbol{c}}(t_{j+1}) = \boldsymbol{c} + \frac{\partial\boldsymbol{r}}{\partial\dot{\boldsymbol{u}}}(t_{j+1})$$

$$\hat{\tilde{\boldsymbol{k}}}(t_j) = \frac{\partial\boldsymbol{r}}{\partial\boldsymbol{u}}(t_{j+1}) + \frac{\gamma}{\beta\Delta t}\tilde{\boldsymbol{c}}(t_{j+1}) + \frac{1}{\beta(\Delta t)^2}\boldsymbol{m}$$

FIGURE 6-8 (Continued)

First uncertain parameter: $i = 1$

Call subroutine to calculate $\dfrac{\partial \boldsymbol{r}}{\partial x_i}(t_{j+1})$ and $\dfrac{\partial \boldsymbol{r}}{\partial \boldsymbol{z}}(t_{j+1})\dfrac{\partial \boldsymbol{z}}{\partial x_i}(t_{j+1})$

$$\tilde{\boldsymbol{f}}_i(t_{j+1}) = \frac{\partial \boldsymbol{f}}{\partial x_i}(t_{j+1}) - \frac{\partial \boldsymbol{c}}{\partial x_i}\dot{\boldsymbol{u}}(t_{j+1}) - \frac{\partial \boldsymbol{r}}{\partial x_i}(t_{j+1}) - \frac{\partial \boldsymbol{r}}{\partial \boldsymbol{z}}(t_{j+1})\frac{\partial \boldsymbol{z}}{\partial x_i}(t_{j+1})$$

$$
\begin{aligned}
\Delta\hat{\tilde{\boldsymbol{f}}}_i(t_j) =\ & \tilde{\boldsymbol{f}}_i(t_{j+1}) - \tilde{\boldsymbol{f}}_i(t_j) - \Delta\tilde{\boldsymbol{c}}(t_j)\dot{\boldsymbol{v}}_i(t_j) - \Delta\tilde{\boldsymbol{k}}(t_j)\boldsymbol{v}_i(t_j) \\
& + \left[\frac{1}{\beta\Delta t}\boldsymbol{m} + \frac{\gamma}{\beta}\tilde{\boldsymbol{c}}(t_{j+1})\right]\dot{\boldsymbol{v}}_i(t_j) \\
& + \left[\frac{1}{2\beta}\boldsymbol{m} + \Delta t\left(\frac{\gamma}{2\beta} - 1\right)\tilde{\boldsymbol{c}}(t_{j+1})\right]\ddot{\boldsymbol{v}}_i(t_j)
\end{aligned}
$$

$i = i + 1$
Loop
through all
uncertain
parameters

$$\Delta\boldsymbol{v}_i(t_j) = \left[\hat{\tilde{\boldsymbol{k}}}(t_j)\right]^{-1}\Delta\hat{\tilde{\boldsymbol{f}}}_i(t_j)$$

$$\boldsymbol{v}_i(t_{j+1}) = \boldsymbol{v}_i(t_j) + \Delta\boldsymbol{v}_i(t_j)$$
$$\dot{\boldsymbol{v}}_i(t_{j+1}) = \dot{\boldsymbol{v}}_i(t_j) + \frac{\gamma}{\beta\Delta t}\Delta\boldsymbol{v}_i(t_j) - \frac{\gamma}{\beta}\dot{\boldsymbol{v}}_i(t_j) + \Delta t\left(1 - \frac{\gamma}{2\beta}\right)\ddot{\boldsymbol{v}}_i(t_j)$$
$$\ddot{\boldsymbol{v}}_i(t_{j+1}) = \ddot{\boldsymbol{v}}_i(t_j) + \frac{1}{\beta(\Delta t)^2}\Delta\boldsymbol{v}_i(t_j) - \frac{1}{\beta\Delta t}\dot{\boldsymbol{v}}_i(t_j) - \frac{1}{2\beta}\ddot{\boldsymbol{v}}_i(t_j)$$

Call subroutines to update $\boldsymbol{z}$, $\dfrac{\partial \boldsymbol{z}}{\partial x_1}$, $\dfrac{\partial \boldsymbol{z}}{\partial x_2}$, $\ldots$

Move on to next time step: $j = j + 1$

First iteration: $k = 1$

$$\hat{\boldsymbol{k}}(t_j) = \frac{\partial \boldsymbol{r}_f}{\partial \boldsymbol{u}_f}(t_j) + \frac{\gamma}{\beta \Delta t} \boldsymbol{c}_f + \frac{1}{\beta(\Delta t)^2} \boldsymbol{m}_f$$

$$\Delta \hat{\boldsymbol{f}}(t_j) = -\frac{\partial \boldsymbol{r}_f}{\partial \boldsymbol{u}_s}(t_j)\Delta \boldsymbol{u}_s(t_j) - \boldsymbol{c}_{fs}\Delta \dot{\boldsymbol{u}}_s(t_j) + \left[\frac{1}{\beta \Delta t} \boldsymbol{m}_f + \frac{\gamma}{\beta} \boldsymbol{c}_f \right] \dot{\boldsymbol{u}}_f(t_j)$$

$$+ \left[\frac{1}{2\beta} \boldsymbol{m}_f + \Delta t \left(\frac{\gamma}{2\beta} - 1 \right) \boldsymbol{c}_f \right] \ddot{\boldsymbol{u}}_f(t_j)$$

$$\Delta \boldsymbol{R}^{(1)} = \Delta \hat{\boldsymbol{f}}(t_j)$$
$$\boldsymbol{u}_f^{(0)} = \boldsymbol{u}_f(t_j)$$

$$\Delta \boldsymbol{u}_f^{(1)} = \left[\hat{\boldsymbol{k}}(t_j) \right]^{-1} \Delta \boldsymbol{R}^{(1)}$$

$$\boldsymbol{u}_f^{(1)} = \boldsymbol{u}_f(t_j) + \Delta \boldsymbol{u}_f^{(1)}$$

Call subroutine to calculate $\boldsymbol{r}_f \left(\boldsymbol{u}_f^{(1)} \right)$

FIGURE 6-9 Flowchart of calculations at a typical time step t_j for SABER-3D

FIGURE 6-9 (Continued)

Calculate unbalanced force

$$\Delta \boldsymbol{R}^{(2)} = \frac{\partial \boldsymbol{r}_f}{\partial \boldsymbol{u}_f}(t_j)\Delta \boldsymbol{u}_f^{(1)} + \frac{\partial \boldsymbol{r}_f}{\partial \boldsymbol{u}_s}(t_j)\Delta \boldsymbol{u}_s(t_j) - \left[\boldsymbol{r}_f\left(\boldsymbol{u}_f^{(1)} \right) - \boldsymbol{r}_f\left(\boldsymbol{u}_f^{(0)} \right) \right]$$

$$\Delta \boldsymbol{R}^{(k+1)} = \frac{\partial \boldsymbol{r}_f}{\partial \boldsymbol{u}_f}(t_j)\Delta \boldsymbol{u}_f^{(k)} - \left[\boldsymbol{r}_f\left(\boldsymbol{u}_f^{(k)} \right) - \boldsymbol{r}_f\left(\boldsymbol{u}_f^{(k-1)} \right) \right], \ k = 2, 3, 4, \ldots$$

Check unbalanced force $\Delta \boldsymbol{R}^{(k+1)}$ against tolerance

Tolerance not satisfied.   Tolerance satisfied.
Iteration required: $k = k + 1$ Solution for $\boldsymbol{u}_f(t_{j+1})$ found.

$$\Delta \boldsymbol{u}_f^{(k)} = \left[\hat{\boldsymbol{k}}(t_j) \right]^{-1} \Delta \boldsymbol{R}^{(k)}$$

$$\boldsymbol{u}_f^{(k)} = \boldsymbol{u}_f^{(k-1)} + \Delta \boldsymbol{u}_f^{(k)}$$

Call subroutine to calculate $\boldsymbol{r}_f\left(\boldsymbol{u}_f^{(k)} \right)$
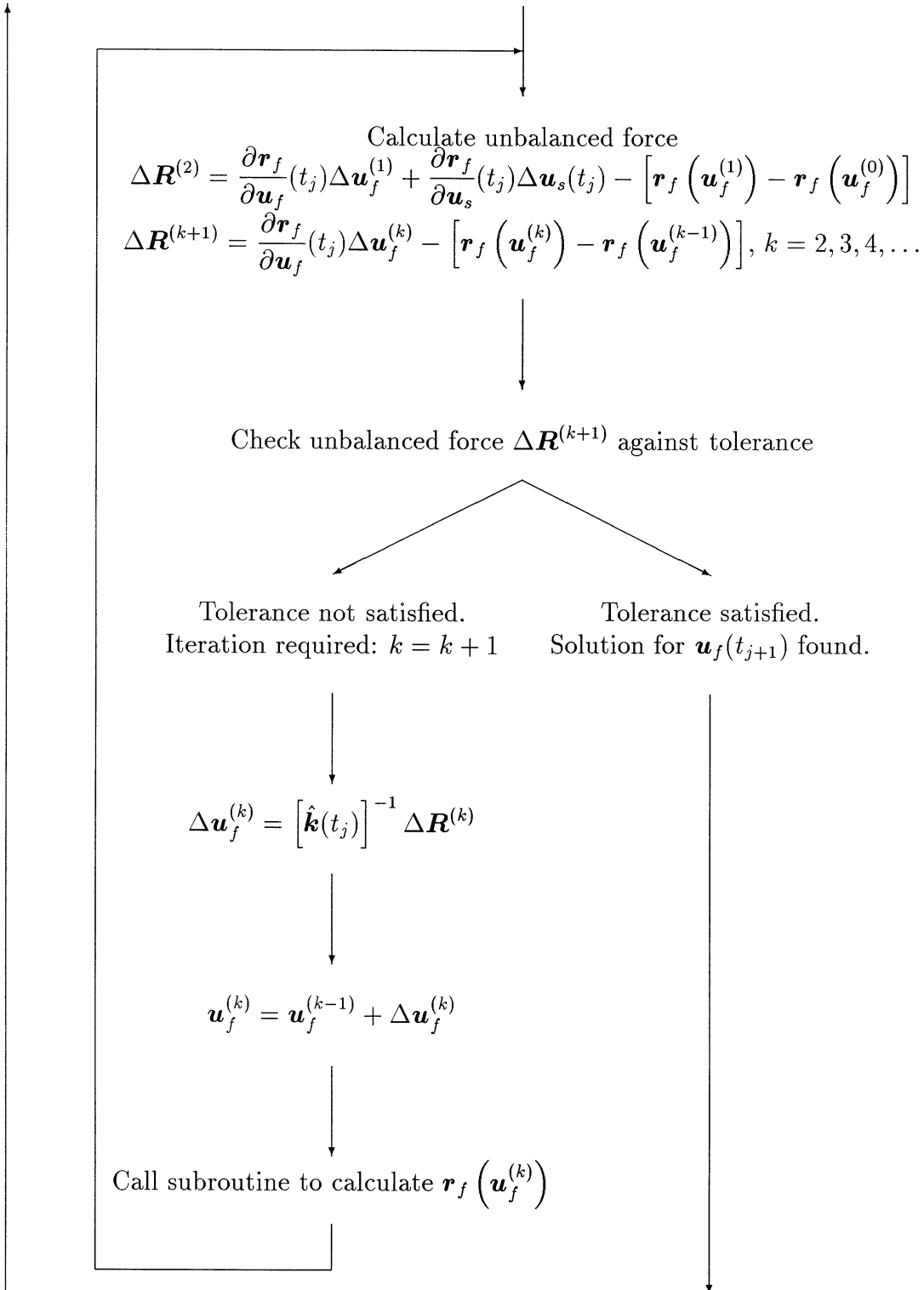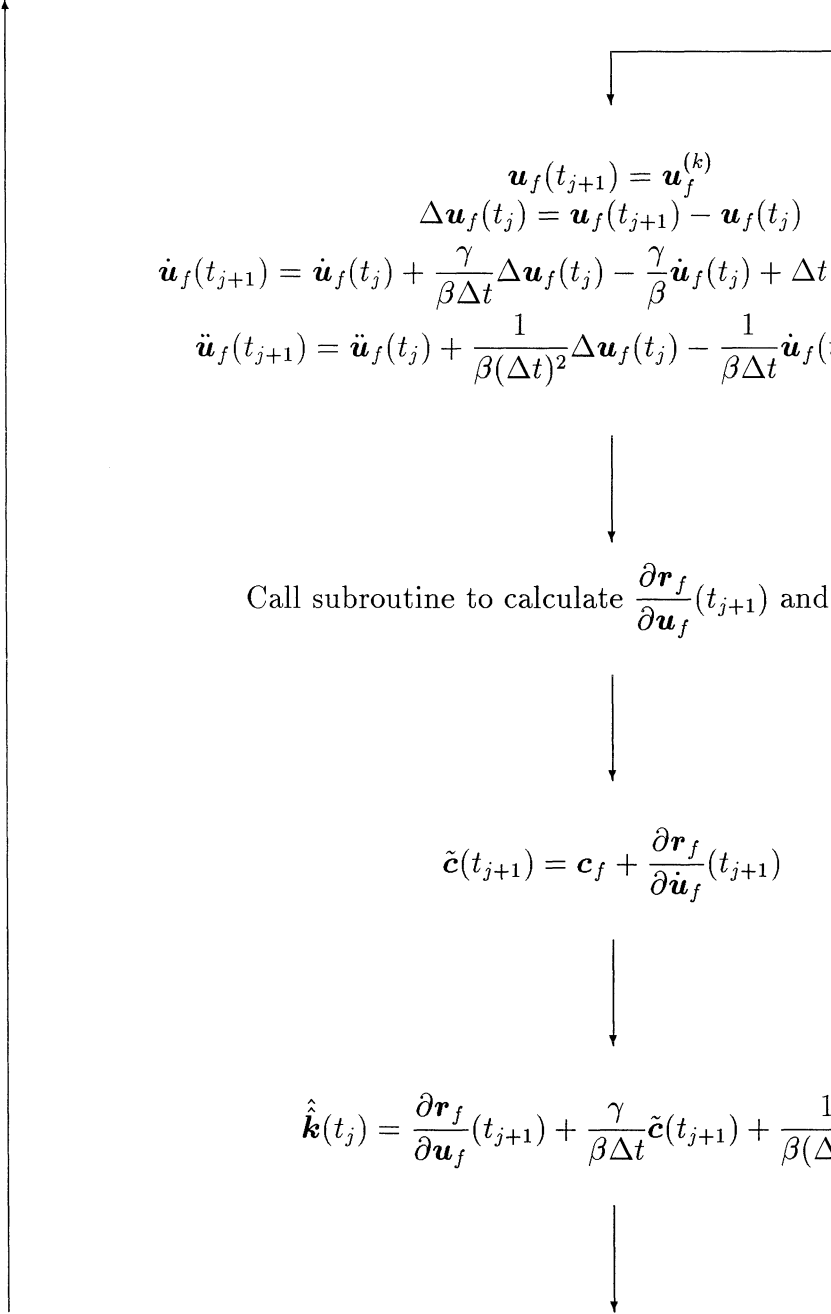
FIGURE 6-9 (Continued)

$$\boldsymbol{u}_f(t_{j+1}) = \boldsymbol{u}_f^{(k)}$$

$$\Delta \boldsymbol{u}_f(t_j) = \boldsymbol{u}_f(t_{j+1}) - \boldsymbol{u}_f(t_j)$$

$$\dot{\boldsymbol{u}}_f(t_{j+1}) = \dot{\boldsymbol{u}}_f(t_j) + \frac{\gamma}{\beta \Delta t} \Delta \boldsymbol{u}_f(t_j) - \frac{\gamma}{\beta} \dot{\boldsymbol{u}}_f(t_j) + \Delta t \left(1 - \frac{\gamma}{2\beta}\right) \ddot{\boldsymbol{u}}_f(t_j)$$
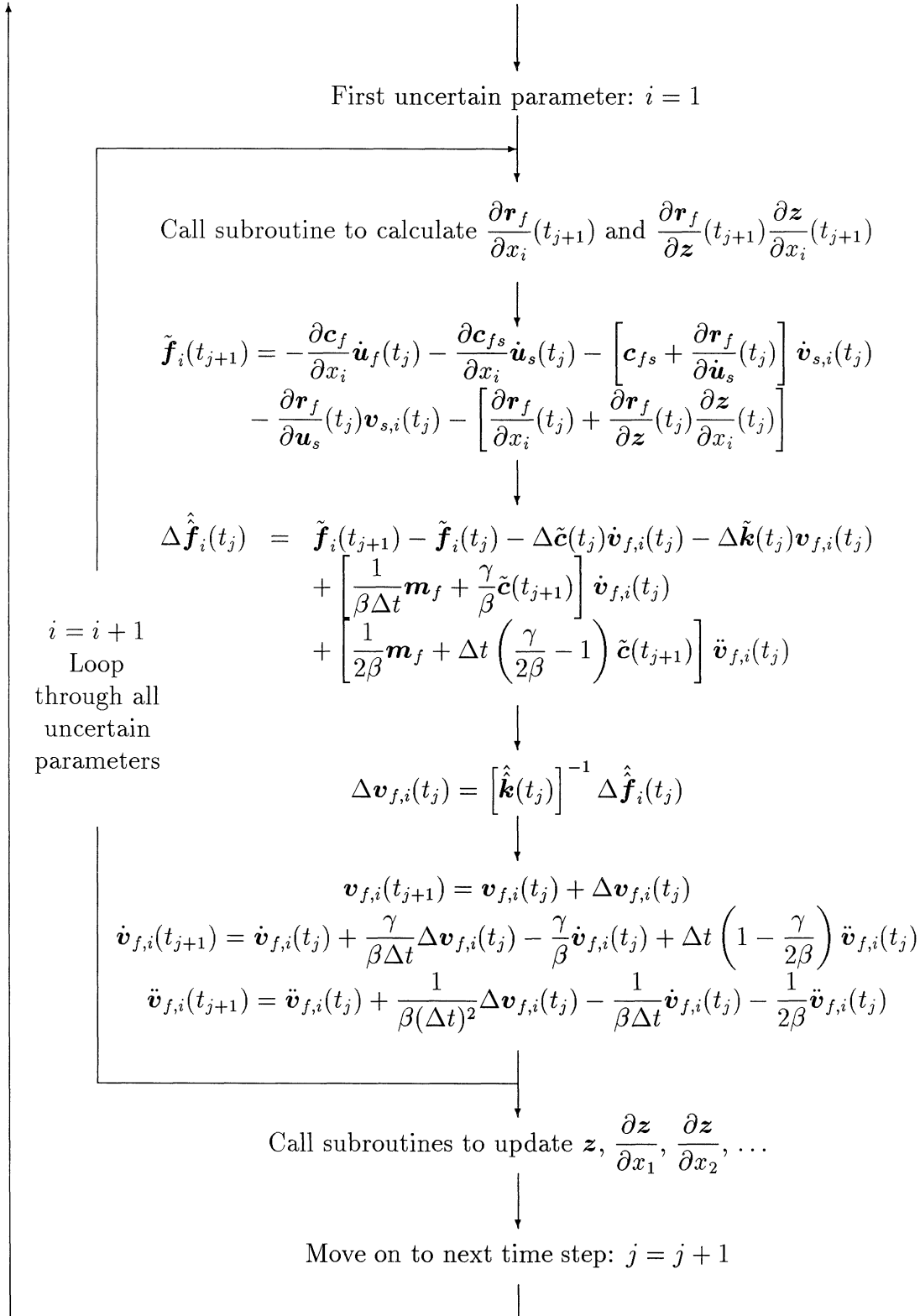
$$\ddot{\boldsymbol{u}}_f(t_{j+1}) = \ddot{\boldsymbol{u}}_f(t_j) + \frac{1}{\beta (\Delta t)^2} \Delta \boldsymbol{u}_f(t_j) - \frac{1}{\beta \Delta t} \dot{\boldsymbol{u}}_f(t_j) - \frac{1}{2\beta} \ddot{\boldsymbol{u}}_f(t_j)$$

Call subroutine to calculate $\dfrac{\partial \boldsymbol{r}_f}{\partial \boldsymbol{u}_f}(t_{j+1})$ and $\dfrac{\partial \boldsymbol{r}_f}{\partial \dot{\boldsymbol{u}}_f}(t_{j+1})$

$$\tilde{\boldsymbol{c}}(t_{j+1}) = \boldsymbol{c}_f + \frac{\partial \boldsymbol{r}_f}{\partial \dot{\boldsymbol{u}}_f}(t_{j+1})$$

$$\hat{\tilde{\boldsymbol{k}}}(t_j) = \frac{\partial \boldsymbol{r}_f}{\partial \boldsymbol{u}_f}(t_{j+1}) + \frac{\gamma}{\beta \Delta t} \tilde{\boldsymbol{c}}(t_{j+1}) + \frac{1}{\beta (\Delta t)^2} \boldsymbol{m}_f$$

FIGURE 6-9 (Continued)

First uncertain parameter: $i = 1$

Call subroutine to calculate $\dfrac{\partial \boldsymbol{r}_f}{\partial x_i}(t_{j+1})$ and $\dfrac{\partial \boldsymbol{r}_f}{\partial \boldsymbol{z}}(t_{j+1})\dfrac{\partial \boldsymbol{z}}{\partial x_i}(t_{j+1})$

$$\tilde{\boldsymbol{f}}_i(t_{j+1}) = -\frac{\partial \boldsymbol{c}_f}{\partial x_i}\dot{\boldsymbol{u}}_f(t_j) - \frac{\partial \boldsymbol{c}_{fs}}{\partial x_i}\dot{\boldsymbol{u}}_s(t_j) - \left[\boldsymbol{c}_{fs} + \frac{\partial \boldsymbol{r}_f}{\partial \dot{\boldsymbol{u}}_s}(t_j)\right]\dot{\boldsymbol{v}}_{s,i}(t_j)$$
$$- \frac{\partial \boldsymbol{r}_f}{\partial \boldsymbol{u}_s}(t_j)\boldsymbol{v}_{s,i}(t_j) - \left[\frac{\partial \boldsymbol{r}_f}{\partial x_i}(t_j) + \frac{\partial \boldsymbol{r}_f}{\partial \boldsymbol{z}}(t_j)\frac{\partial \boldsymbol{z}}{\partial x_i}(t_j)\right]$$

$$\Delta \hat{\tilde{\boldsymbol{f}}}_i(t_j) = \tilde{\boldsymbol{f}}_i(t_{j+1}) - \tilde{\boldsymbol{f}}_i(t_j) - \Delta\tilde{\boldsymbol{c}}(t_j)\dot{\boldsymbol{v}}_{f,i}(t_j) - \Delta\tilde{\boldsymbol{k}}(t_j)\boldsymbol{v}_{f,i}(t_j)$$
$$+ \left[\frac{1}{\beta\Delta t}\boldsymbol{m}_f + \frac{\gamma}{\beta}\tilde{\boldsymbol{c}}(t_{j+1})\right]\dot{\boldsymbol{v}}_{f,i}(t_j)$$
$$+ \left[\frac{1}{2\beta}\boldsymbol{m}_f + \Delta t\left(\frac{\gamma}{2\beta} - 1\right)\tilde{\boldsymbol{c}}(t_{j+1})\right]\ddot{\boldsymbol{v}}_{f,i}(t_j)$$

$$\Delta\boldsymbol{v}_{f,i}(t_j) = \left[\hat{\tilde{\boldsymbol{k}}}(t_j)\right]^{-1}\Delta\hat{\tilde{\boldsymbol{f}}}_i(t_j)$$

$$\boldsymbol{v}_{f,i}(t_{j+1}) = \boldsymbol{v}_{f,i}(t_j) + \Delta\boldsymbol{v}_{f,i}(t_j)$$
$$\dot{\boldsymbol{v}}_{f,i}(t_{j+1}) = \dot{\boldsymbol{v}}_{f,i}(t_j) + \frac{\gamma}{\beta\Delta t}\Delta\boldsymbol{v}_{f,i}(t_j) - \frac{\gamma}{\beta}\dot{\boldsymbol{v}}_{f,i}(t_j) + \Delta t\left(1 - \frac{\gamma}{2\beta}\right)\ddot{\boldsymbol{v}}_{f,i}(t_j)$$
$$\ddot{\boldsymbol{v}}_{f,i}(t_{j+1}) = \ddot{\boldsymbol{v}}_{f,i}(t_j) + \frac{1}{\beta(\Delta t)^2}\Delta\boldsymbol{v}_{f,i}(t_j) - \frac{1}{\beta\Delta t}\dot{\boldsymbol{v}}_{f,i}(t_j) - \frac{1}{2\beta}\ddot{\boldsymbol{v}}_{f,i}(t_j)$$

Call subroutines to update $\boldsymbol{z}, \dfrac{\partial \boldsymbol{z}}{\partial x_1}, \dfrac{\partial \boldsymbol{z}}{\partial x_2}, \ldots$

Move on to next time step: $j = j + 1$

6.5 Example

A simple example will be used to illustrate the use of SABER. As the entire program is new, the example is intended to illustrate all of the capabilities of the program so each step of the analysis will be shown: input of the structural model data, input of the dynamic analysis data such as the time step size, and calculation of the sensitivity factors. The example selected is a steel portal frame mounted on the shake table at the University at Buffalo (figure 6-10). The frame has been tested both bare and with dampers installed. A fair selection of experimental time history data is thus available and can be used to calibrate the models of the frame. The use of SABER-2D will be demonstrated by modeling a 1997 test subjecting the bare frame to the El Centro ground motion [14]. The SABER-3D program is very similar to SABER-2D; the major difference being the extra dimension available for the coordinates.

The displacement of the frame during the tests was small enough that linear behavior can be assumed. Linear beam elements are thus used to model the frame. Rotational spring elements are used to model the connection between the baseplate and the shake table, and the loosely attached concrete slab at the top is represented by a beam element with a low bending stiffness and a high axial stiffness (figure 6-11).

The geometric and material properties of the steel beam elements can be fairly accurately determined. However, the damping and the rotational stiffness of the connection between the baseplate and the shake table are more difficult to determine so we will consider them to be uncertain. To start, we will use estimated values for these parameters. For the rotational stiffness we select a value that makes the fundamental frequency of the frame the same as that observed in the experiments. This is the same approach that was followed at the University at Buffalo when modeling the frame using the ANSYS finite element program [14]. The damping used by SABER is Rayleigh damping and we will calculate the damping parameters to give damping ratios of 3.7% in the first two of the fourteen modes of the structure. This value of damping was found experimentally for the first mode.

To start the program, open MATLAB and type "saber" on the command line. This will open the graphical user interface, consisting of a main menu containing the commands required to run the program, and several graphics windows. One graphics window containing a plot of the structure is always open, and others will be opened as necessary to plot displacements, sensitivity factors or other results. The default MATLAB figure menu has deliberately been left on the graphics windows. Each figure's menu can be used to save the figure, zoom in or out, or manipulate the figure in other ways. The MATLAB command window will also remain open, but need not be used at all during the running of the program.

The main menu items are:

- **File:** save the structure or open an existing structure data file.
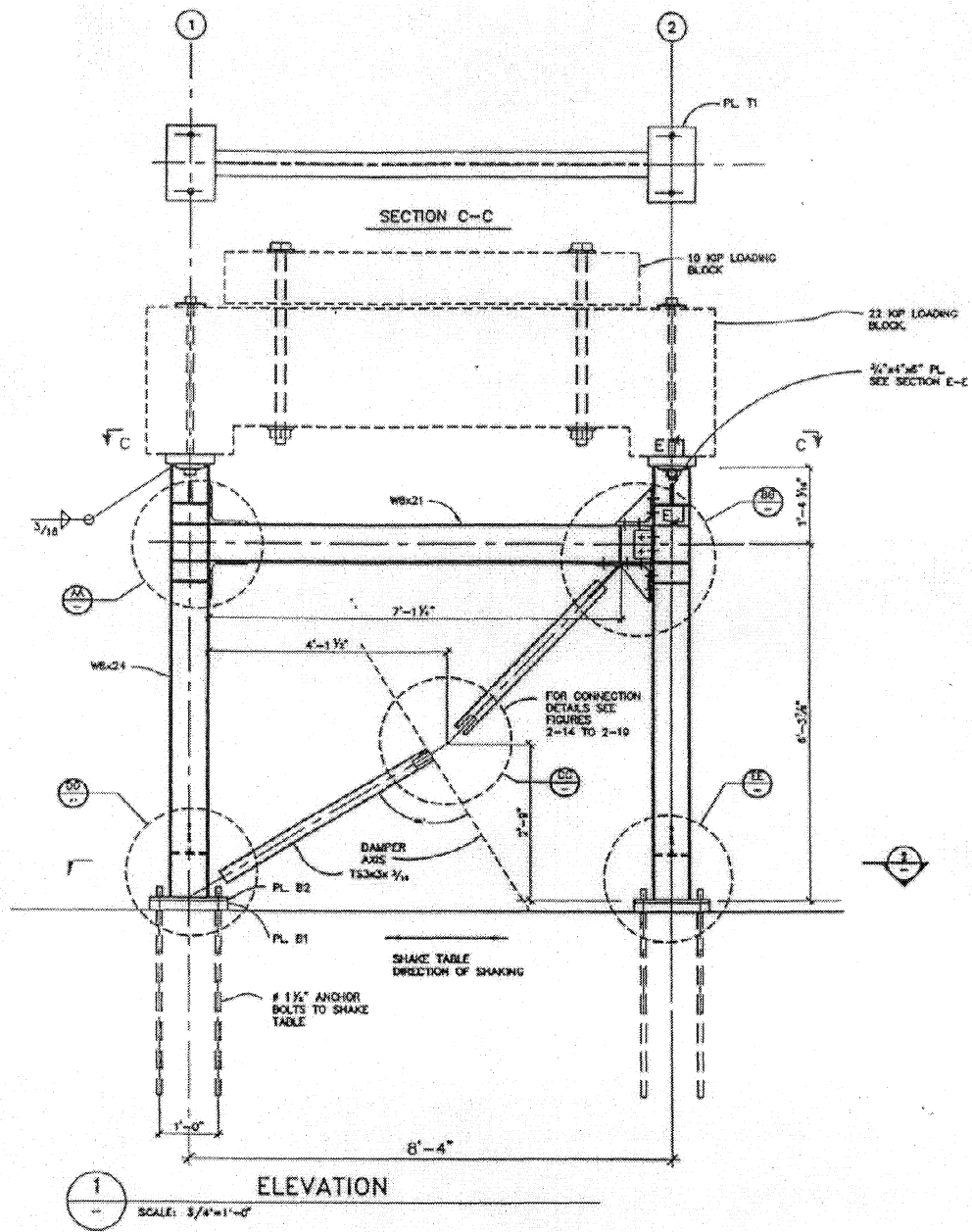
FIGURE 6-10 Buffalo test frame
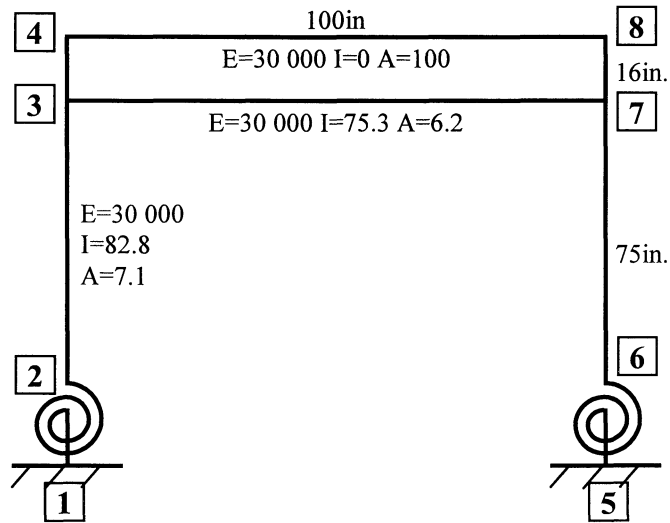
FIGURE 6-11 Buffalo test frame model

- **Edit structure:** input data or edit existing structure data.

- **Sensitivity analysis:** perform a dynamic analysis to calculate displacement and sensitivity factors.

- **Tools:** contains various tools or "wizards" to guide the user through using sensitivity factors for calibration, fragility curve generation, etc.

To enter the model data, we proceed through the "Edit structure" menu as follows:

- Coordinates: We call up the coordinate box and enter the values (figure 6-12).

- Elements: Call up the element box. Elements can be entered either by clicking on the nodes or by entering the node numbers in the element box. The element properties are contained in property sets, so three different sets will be required: one for the columns, one for the beam and one to model the concrete slab. We will use property sets 2, 3 and 4 for these beam elements, and property set 1 for the rotational spring elements. The element types and property set numbers are entered in the element data box (figure 6-13).

- Properties: Set 2 is used for the columns, and we enter the data in the property set box as shown in figure 6-14. Set 3 is used for the beam, so it is almost the same as set 2. The program indicates the data required by different element types.

  A property set cannot be used for more than one element type. For example, in this model property set 2 is used for one group of linear beam elements, and set 3

90

Nodal coordinates

	x	y
1	0	0
2	0	0
3	0	75
4	0	91
5	100	0
6	100	0
7	100	75
8	100	91
9		
10		

Submit

FIGURE 6-12 Coordinates data

Element data

Note: elements can also be defined by clicking on nodes

	Node 1	Node 2	Element type	Property set number
1	1	2	Linear rotational spring	1
2	5	6	Linear rotational spring	1
3	2	3	Linear elastic frame element	2
4	3	4	Linear elastic frame element	2
5	6	7	Linear elastic frame element	2
6	7	8	Linear elastic frame element	2
7	3	7	Linear elastic frame element	3
8	4	8	Linear elastic frame element	4
9			Linear elastic frame element	
10			Linear elastic frame element	

Submit

FIGURE 6-13 Element data

FIGURE 6-14 Property set data

for another group of less stiff linear beam elements. The program will give an error message if the user attempts to use property sets 2 or 3 for a different type of element such as a nonlinear beam element. The graphical user interface guides the user through correctly submitting the property set data.

- Supports: The rotational springs are fixed to the base, so nodes 1 and 5 are fixed in all degrees of freedom. Although not strictly necessary, the second nodes of the two rotational springs, nodes 2 and 6, can also be fixed against translation. Degrees of freedom are fixed by clicking on the appropriate boxes in the supports box (figure 6-15). Supports are indicated on the structure plot as red arrows in the direction of fixity.

- Nodal masses: Lumped nodal masses are entered on the masses box (figure 6-16). The non-zero masses appear on the structure plot as green asterisks.

- Damping: We calculate Rayleigh damping parameters a and b to give a damping ratio of 3.7% in the first two modes and enter the data accordingly (figure 6-17).

The model data is now complete and the structure is shown in the structure window (figure 6-18). We are now ready to proceed to a dynamic analysis to calculate the displacement and sensitivity factors for the nominal structure under the given ground motion. The necessary commands are found in the "Sensitivity analysis" menu item. First the uncertain parameters

Nodal supports

☐ Free   ☑ Fixed

	X-trans	Y-trans	Z-rotat
1	☑	☑	☑
2	☑	☑	☐
3	☐	☐	☐
4	☐	☐	☐
5	☑	☑	☑
6	☑	☑	☐
7	☐	☐	☐
8	☐	☐	☐

Submit

FIGURE 6-15 Support data

Nodal masses

1	0
2	0.00019
3	0.00045
4	0.02077
5	0
6	0.00019
7	0.00045
8	0.02077

Submit

FIGURE 6-16 Nodal mass data

FIGURE 6-17 Damping data

for which sensitivity factors are to be calculated are entered (figure 6-19). The rotational stiffness of the springs and the damping are uncertain, so we wish to calculate sensitivity factors for these parameters. Next the data file containing the acceleration time history of the shake table is selected. Finally the time step size to be used for analysis and the number of steps to be analyzed are entered and the analysis started (figure 6-20).

The displacements and sensitivity factors can be plotted when the analysis is complete. The x-direction displacement of node 3 gives the lateral drift of the frame and is an important degree of freedom of the structure. The displacement plot for this degree of freedom is shown in figure 6-21, and the sensitivity of the displacement to the rotational stiffness of the base spring is plotted in figure 6-22. To check the accuracy of SABER, a finite difference approximation of the sensitivity factor is also shown on figure 6-22. Differences between the two are shown on the same axes in figure 6-23. There is good agreement between the two curves. As the size of the finite difference is reduced further, the errors are reduced and the two curves become identical as shown in the part of the plot enlarged in figure 6-24. For a finite difference size of 1000 or less, the two sensitivity factor curves are indistinguishable. This confirms the accuracy of the sensitivity factors calculated by SABER. Further details of the use of these sensitivity factors for calibration and optimization will be found in Section 9.

94
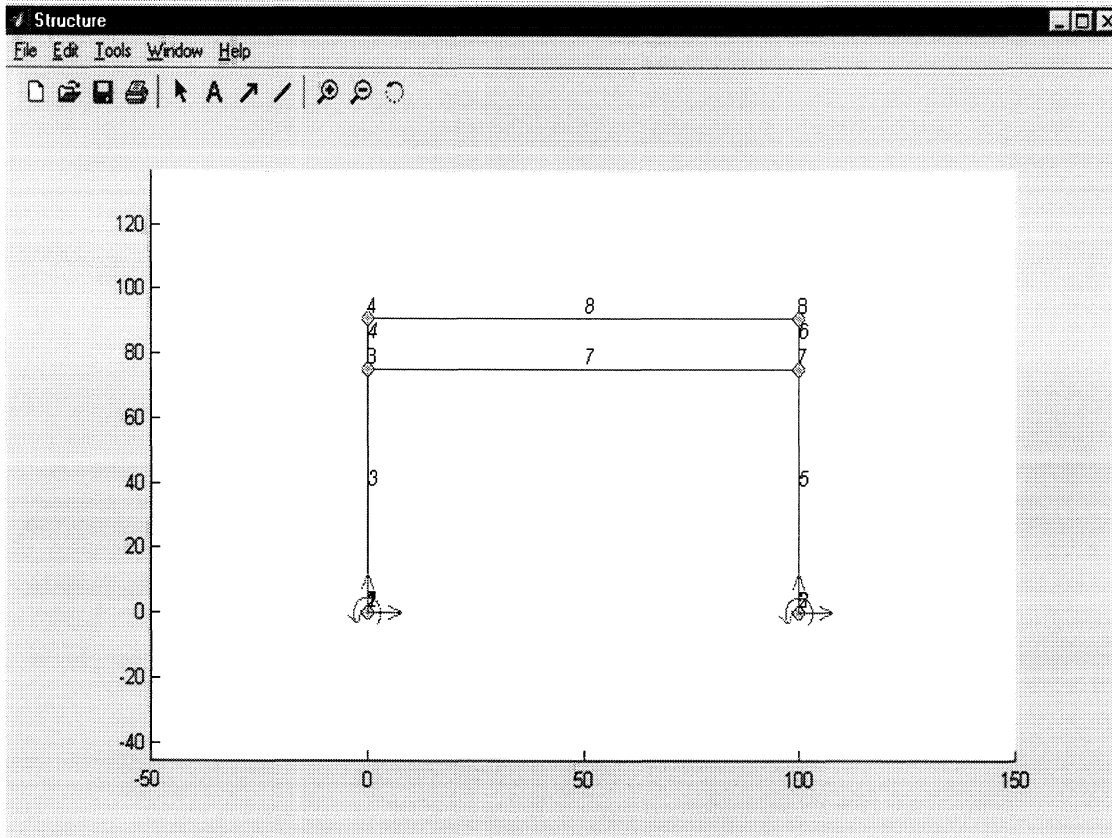
FIGURE 6-18 Structure window with completed structure

FIGURE 6-19 Uncertain parameters

FIGURE 6-20 Analysis parameters
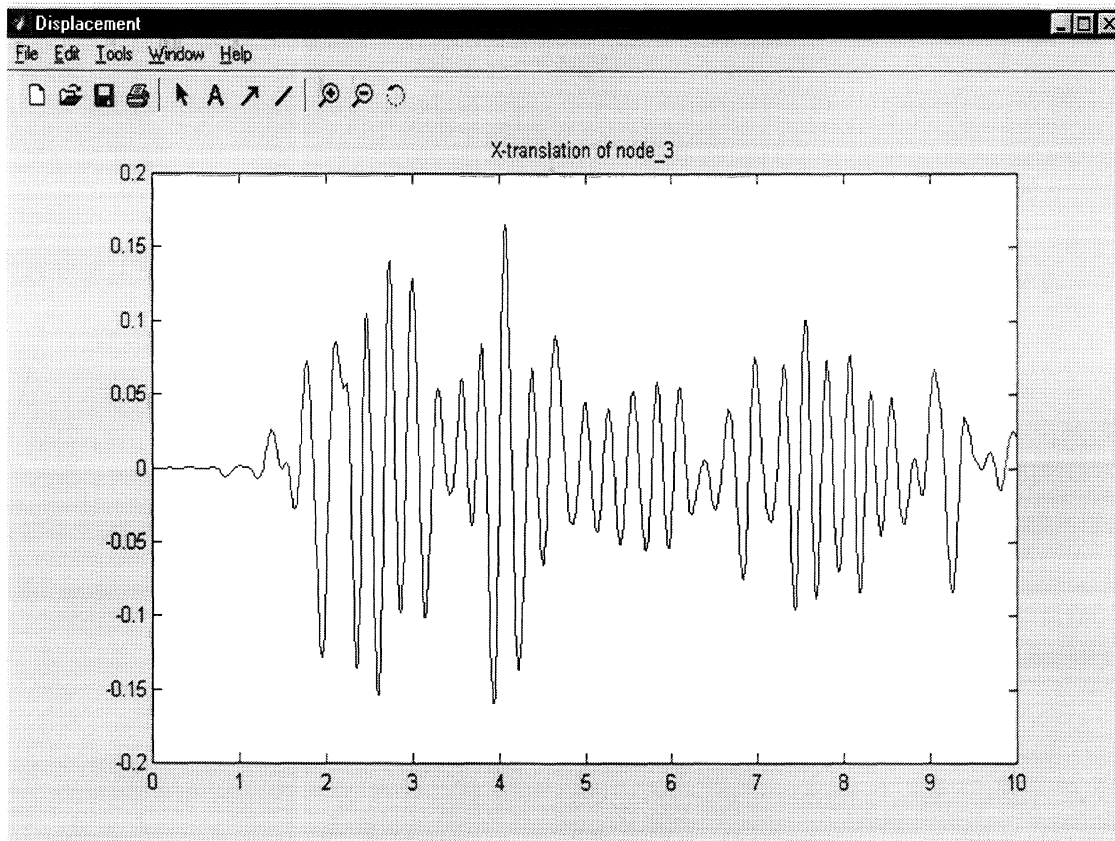
FIGURE 6-21 Displacement
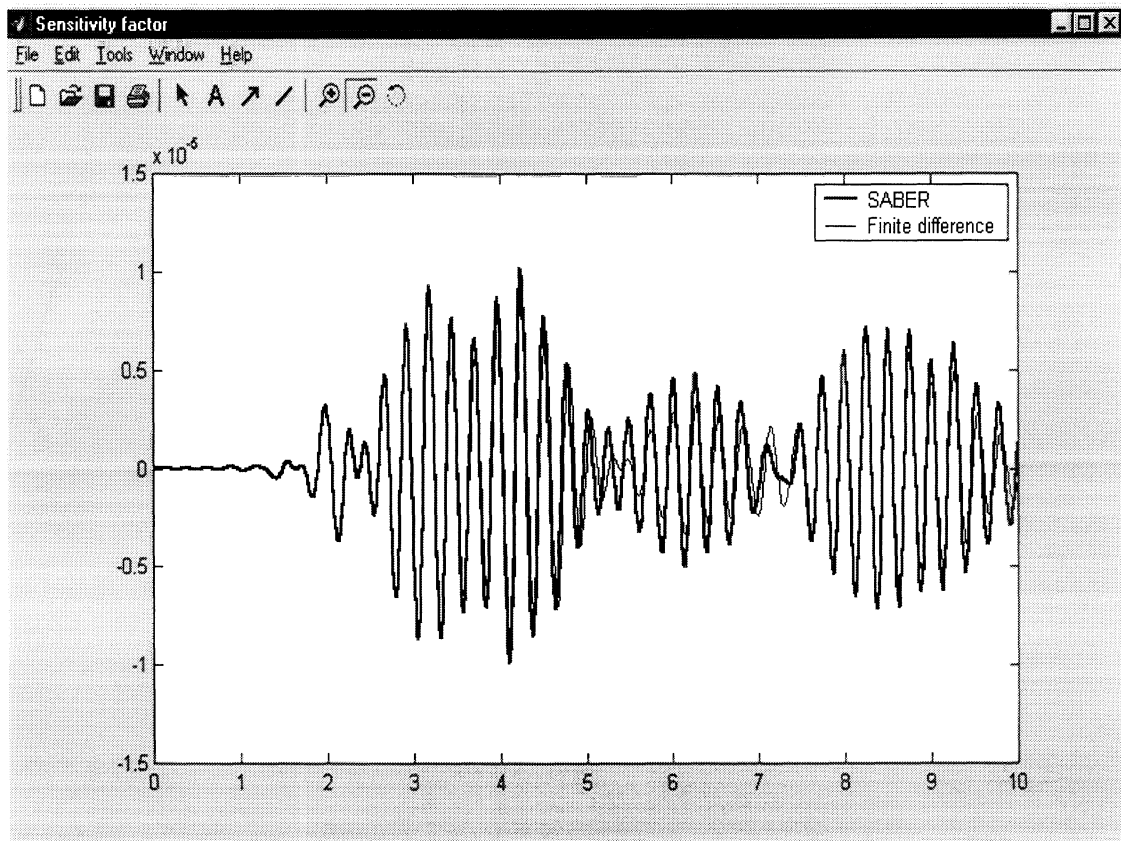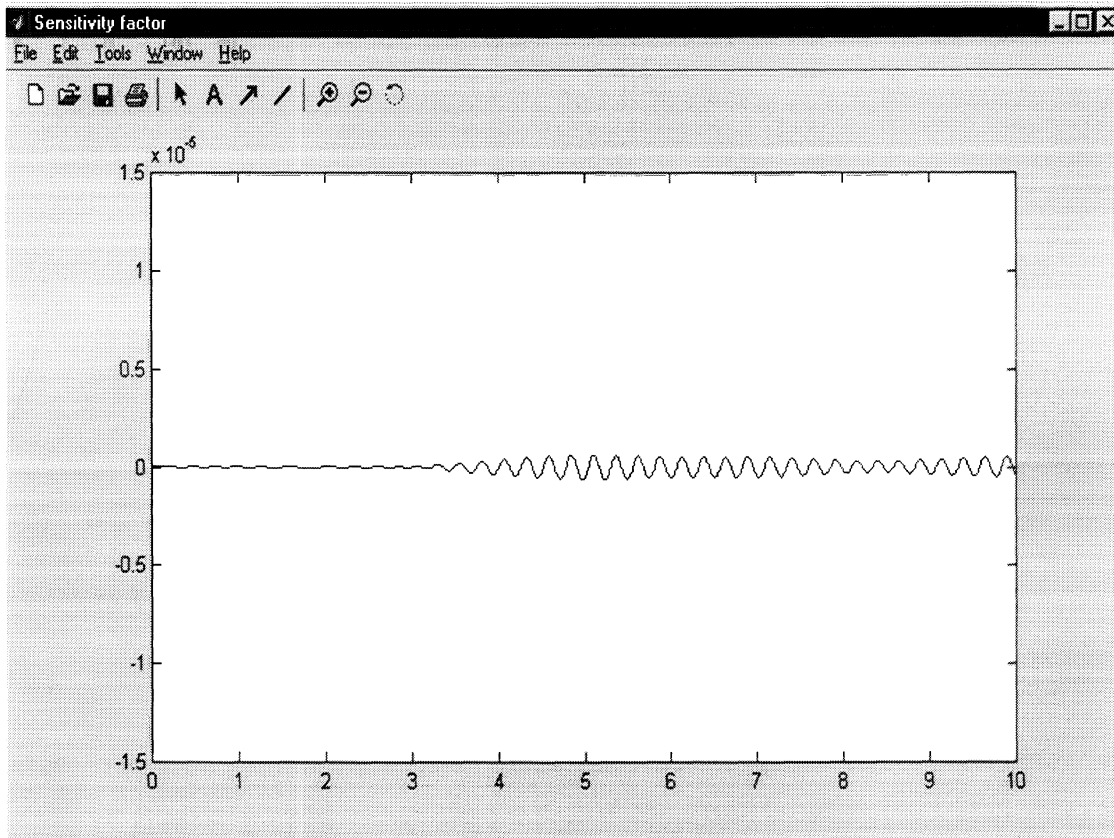
FIGURE 6-22 Sensitivity factor

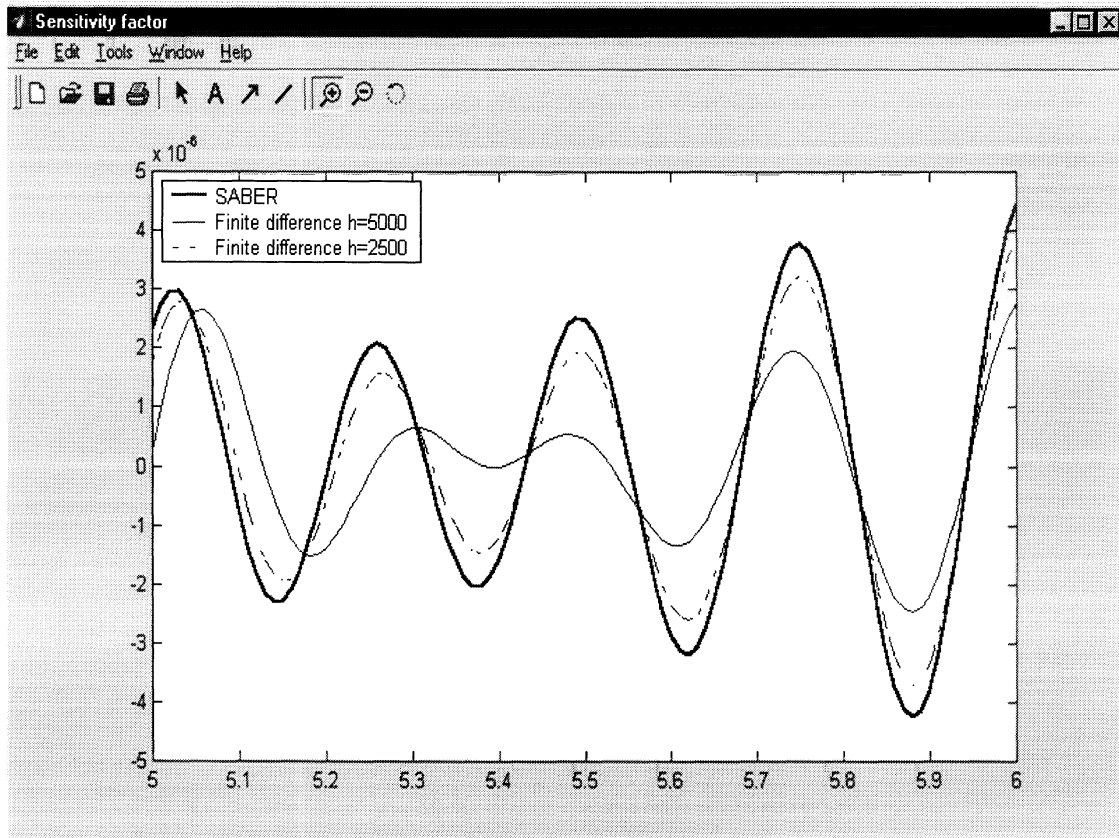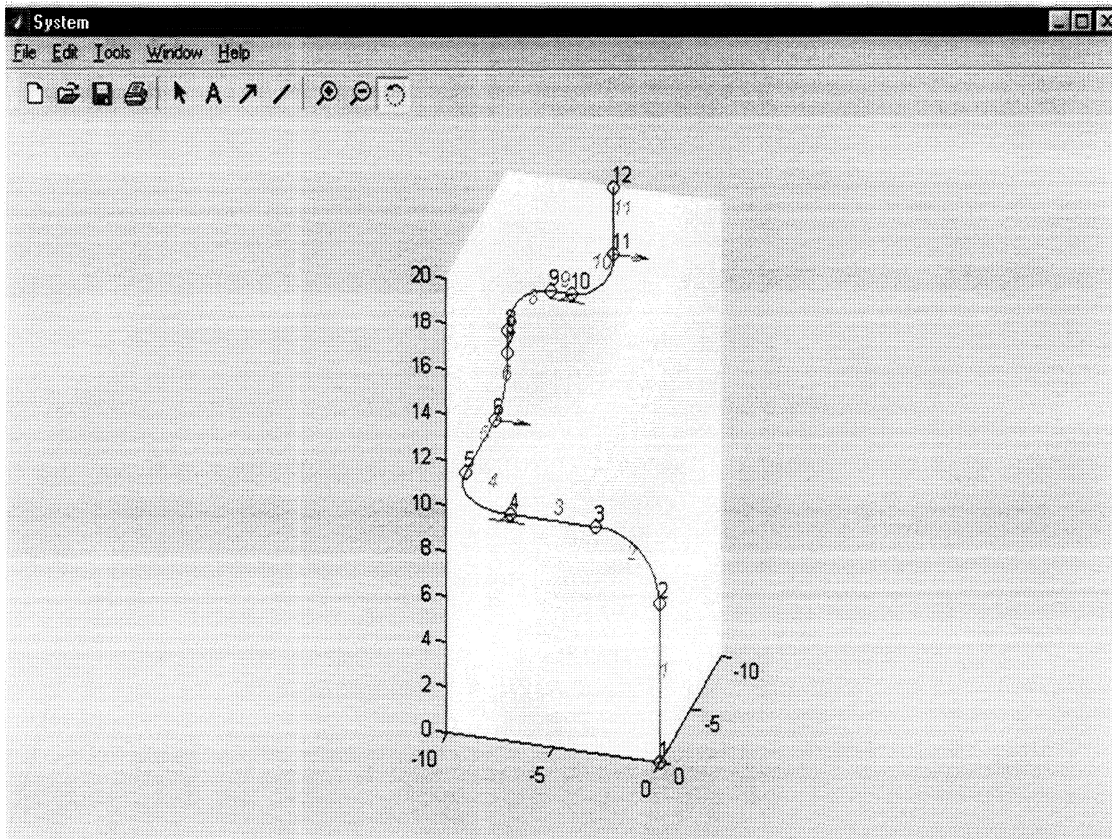FIGURE 6-23 Differences in sensitivity factor

FIGURE 6-24 Sensitivity factor

FIGURE 6-25 Piping system in SABER-3D

The use of the SABER-3D program is very similar to use of the SABER-2D program. Obviously, additional coordinates must be specified for the nodes and supports. The support excitations are specified in a text file, with one column for each excitation time history. The support conditions are then given by then either specifying the support as stationary, or specifying the column number corresponding to the support acceleration time history. An example of a piping system model in SABER-3D is shown in figure 6-25.

SECTION 7
DIANA IMPLEMENTATION

7.1 Introduction

DIANA (Displacement Analyzer) is a comprehensive finite element package developed at TNO Building and Construction Research in the Netherlands. A wide range of element types and material models is available for structural, geotechnical, and fluid flow analysis. DIANA is particularly well suited for structural analysis of reinforced concrete structures. It allows reinforcing bars to be defined inside the finite elements, and features good constitutive models for concrete; for example, the smeared cracking model. Pre- and post-processing can be done using the graphical user interfaces of FEMGEN and FEMVIEW [36], or using DIANA itself.

In addition to powerful finite element analysis capabilities, DIANA provides an environment in which the FORTRAN source code of the program can be modified to develop new features. The program is divided into several segments. The user can modify one segment and create a new, private version which can then be used with the other original segments. The advantages of this approach are that it is not necessary to recompile the whole program each time, and that other users can continue to use the original version of the segment. Each segment reads and writes data to a central data storage system known as the FILOS (File Organization System) file. The user can also store additional data on the FILOS file as required.

To implement sensitivity analysis in DIANA, many new subroutines had to be written for segments that form part of the linear static analysis (ls40) and nonlinear analysis (nl40) applications. The sensitivity analysis was implemented for the plasticity models used in analysis of realistic structures. It was also necessary to implement equations for sensitivity analysis for each element type that may be used and this was done for beam, plane stress, plane strain, shell and solid elements. Damping in DIANA is specified using the Rayleigh damping approach, and equations for calculating the sensitivity with respect to the damping parameters were also implemented.

The material models considered are described in Section 7.2 and equations for the sensitivity analysis are derived in Section 7.3. Section 7.4 describes the new subroutines added to DIANA and some special treatment required for certain elements. An example of the use of the program for sensitivity analysis is given in Section 7.5.

7.2 Material models

This section contains details of the material models in DIANA for which sensitivity analysis has been implemented. Recall from Section 3 that the material model determines the restoring force r as a function of displacement u, velocity $\dot{u}$, history-dependent variables z

103

and uncertain parameters $\boldsymbol{x}$. The function $\boldsymbol{r}(\boldsymbol{u}, \dot{\boldsymbol{u}}, \boldsymbol{z}, \boldsymbol{x})$ appears along with its derivatives in the governing equations for the displacement $\boldsymbol{u}$ and sensitivity factor $\boldsymbol{v}$ (equations 3-13 and 3-19).

In general for DIANA and other finite element packages, the global restoring force $\boldsymbol{r}$ is given by [15]

$$\boldsymbol{r} = \sum_i \boldsymbol{C}_i \int_{\Omega_i} \boldsymbol{B}_i \boldsymbol{\sigma}_i(\boldsymbol{u}, \dot{\boldsymbol{u}}, \boldsymbol{z}, \boldsymbol{x}) \, d\Omega \tag{7-1}$$

where the summation i is over all elements of the structure; Ω_i is the volume of element i; $\boldsymbol{C}_i$ converts from local to global coordinates; $\boldsymbol{B}_i$ depends on the geometry and shape function formulation of element i; and $\boldsymbol{\sigma}_i(\boldsymbol{u}, \dot{\boldsymbol{u}}, \boldsymbol{z}, \boldsymbol{x})$ is the stress in element i. The integration over the element volume is typically done numerically by considering a partition of the element, with part j of element i having volume $(\Delta\text{vol})_{ij}$. Each part has a representative integration point with $\boldsymbol{\sigma}_{ij}$ being the stress at the integration point in part j. The restoring force is then

$$\boldsymbol{r} = \sum_i \boldsymbol{C}_i \sum_j w_{ij} \boldsymbol{B}_{ij} \boldsymbol{\sigma}_{ij}(\boldsymbol{u}, \dot{\boldsymbol{u}}, \boldsymbol{z}, \boldsymbol{x})(\Delta\text{vol})_{ij} \tag{7-2}$$

where w_{ij} is a weighting factor depending on the element formulation and the integration method used.

In equation 7-2, the stresses $\boldsymbol{\sigma}_{ij}$ depend on the material model and must be evaluated at every step, while the other quantities depend only on the model geometry and the element formulation and remain constant throughout the analysis. The stresses are converted to forces $\boldsymbol{r}$ simply by multiplying by the relevant constants. The material models in the following sections are thus formulated in terms of stress $\boldsymbol{\sigma}$ rather than force $\boldsymbol{r}$.

To simplify the notation as much as possible, subscripts will be used for the time index. Two general adjacent time steps will written as t and $t + \Delta t$ for consistency with existing DIANA documentation.

The names of the material model parameters will be written as five or six letter words as this is how they must be entered in the DIANA input data file. For example, Young's modulus, commonly denoted by E, will be written as YOUNG.

7.2.1   Plasticity

Plasticity is a common nonlinear material model. In the existing DIANA plasticity formulation, the strain at an integration point is decomposed into an elastic part and an irreversible

104

or plastic part:

$$\varepsilon = \varepsilon^E + \varepsilon^P \tag{7-3}$$

where ε is the total strain; ε^E the elastic strain; and ε^P the plastic strain. The history dependence is taken into account by introducing an internal parameter κ which evolves with time according to a specified law. In a uniaxial stress situation κ is the plastic strain, but for more complex stress situations it does not have such a simple physical interpretation.

The general elastoplastic behavior is governed by the following assumptions:

- The elastic *stress–strain relationship*, which specifies the relationship between total stress and elastic strain:

$$\boldsymbol{\sigma} = \boldsymbol{D}\varepsilon^E \tag{7-4}$$

  where $\boldsymbol{D}$ is the elastic stress-strain matrix.

- The *yield function* $f(\boldsymbol{\sigma}, \kappa)$. If the value of the yield function is less than zero the stress state is elastic, while if it is equal to zero $\boldsymbol{\sigma}$ is on the yield surface and plastic flow occurs. The value of the yield function cannot exceed zero for rate-independent plasticity.

- The *flow rule*, which specifies the plastic strain rate as a function of the stress state

$$\dot{\varepsilon}^P = \dot{\lambda}\frac{\partial g(\boldsymbol{\sigma}, \kappa)}{\partial \boldsymbol{\sigma}} \tag{7-5}$$

  where $g(\boldsymbol{\sigma}, \kappa)$ is the plastic potential function.

- The *hardening hypothesis* which specifies the evolution of κ.

$$\frac{\partial \kappa}{\partial \lambda} = h \tag{7-6}$$

The above assumptions define the basic plasticity model. Different types of plasticity models such as von Mises and Tresca correspond to different f, g, and h functions.

The basic plasticity model above is implemented in DIANA in a form suitable for solution at discrete time steps. By applying the Euler backward algorithm [61], a set of equations governing the solution at two adjacent time steps is obtained. This set of equations must always be satisfied and is used by DIANA for plastic structural analysis.

105

If $\boldsymbol{\sigma}_{t+\Delta t}$ is on the yield surface, the equations are

$$\boldsymbol{\sigma}_{t+\Delta t} = \boldsymbol{D} \left[\boldsymbol{\varepsilon}_{t+\Delta t} - \boldsymbol{\varepsilon}^P_{t+\Delta t} \right] \tag{7-7}$$

$$\boldsymbol{\varepsilon}^P_{t+\Delta t} = \boldsymbol{\varepsilon}^P_t + \Delta\lambda \left[\frac{\partial g\left(\boldsymbol{\sigma},\kappa\right)}{\partial\boldsymbol{\sigma}} \right]_{t+\Delta t} \tag{7-8}$$

$$\kappa_{t+\Delta t} = \kappa_t + \Delta\lambda\, h \tag{7-9}$$

$$f\left(\boldsymbol{\sigma}_{t+\Delta t}, \kappa_{t+\Delta t}\right) = 0 \tag{7-10}$$

If $\boldsymbol{\sigma}_{t+\Delta t}$ is not on the yield surface, then the following equations are satisfied:

$$\boldsymbol{\sigma}_{t+\Delta t} = \boldsymbol{D} \left[\boldsymbol{\varepsilon}_{t+\Delta t} - \boldsymbol{\varepsilon}^P_{t+\Delta t} \right] \tag{7-11}$$

$$\boldsymbol{\varepsilon}^P_{t+\Delta t} = \boldsymbol{\varepsilon}^P_t \tag{7-12}$$

$$\kappa_{t+\Delta t} = \kappa_t \tag{7-13}$$

The value of $\boldsymbol{\sigma}_{t+\Delta t}$ obtained from equation 7-7 or 7-11 is then used in equation 7-2 to calculate the global restoring force $\boldsymbol{r}$.

7.2.1.1 von Mises

The von Mises material model considered has four parameters: elastic modulus YOUNG, Poisson's ratio POISON, yield stress YLDVAL and plastic modulus YOUNPL. The functions defining the model are

$$f\left(\boldsymbol{\sigma},\kappa\right) = g\left(\boldsymbol{\sigma},\kappa\right) = \sqrt{\tfrac{1}{2}\boldsymbol{\sigma}^T \boldsymbol{P}_{vm}\boldsymbol{\sigma}} - \bar{\sigma}\left(\kappa\right) \tag{7-14}$$

$$h = 1 \tag{7-15}$$

where $\bar{\sigma}(\cdot)$ is the uniaxial stress versus uniaxial plastic strain relationship derived from the uniaxial stress versus total strain relationship for the material (figure 7-1). $\boldsymbol{P}_{vm}$ is termed the projection matrix and is given by

$$
\boldsymbol{P}_{vm} = \begin{bmatrix} 2 & -1 & -1 & 0 & 0 & 0 \\ -1 & 2 & -1 & 0 & 0 & 0 \\ -1 & -1 & 2 & 0 & 0 & 0 \\ 0 & 0 & 0 & 6 & 0 & 0 \\ 0 & 0 & 0 & 0 & 6 & 0 \\ 0 & 0 & 0 & 0 & 0 & 6 \end{bmatrix} \tag{7-16}
$$

Based on this, the four governing equations for $\boldsymbol{\sigma}_{t+\Delta t}$ on the yield surface, analogous to equations 7-7–7-10, are

$$
\boldsymbol{\sigma}_{t+\Delta t} = \boldsymbol{D} \left[\boldsymbol{\varepsilon}_{t+\Delta t} - \boldsymbol{\varepsilon}^P_{t+\Delta t} \right] \tag{7-17}
$$

$$
\boldsymbol{\varepsilon}^P_{t+\Delta t} = \boldsymbol{\varepsilon}^P_t + \Delta\lambda \frac{\boldsymbol{P}_{vm}\, \boldsymbol{\sigma}_{t+\Delta t}}{2\bar{\sigma}\left(\kappa_{t+\Delta t}\right)} \tag{7-18}
$$

$$
\kappa_{t+\Delta t} = \kappa_t + \Delta\lambda \tag{7-19}
$$

$$
\sqrt{\tfrac{1}{2} \boldsymbol{\sigma}^T_{t+\Delta t} \boldsymbol{P}_{vm}\, \boldsymbol{\sigma}_{t+\Delta t}} - \bar{\sigma}\left(\kappa_{t+\Delta t}\right) = 0 \tag{7-20}
$$

For sensitivity analysis, only the simple uniaxial stress versus plastic strain relationship shown in figure 7-2 was considered. The equation is

$$
\bar{\sigma}(\kappa) = \texttt{YLDVAL} + \kappa \cdot \texttt{YOUNPL} \tag{7-21}
$$

7.2.1.2   Rankine/von Mises

The Rankine/von Mises model is a multi-yield surface plasticity model intended for brittle materials such as concrete [20]. It consists of a maximum principal stress or Rankine yield criterion in tension, along with the von Mises criterion in compression (figure 7-3). The model is formulated in DIANA for two-dimensional stress states so can only be used for plane stress, plane strain and axisymmetric elements. For plane strain and axisymmetric elements the Rankine criterion applies in the out-of-plane direction as well.
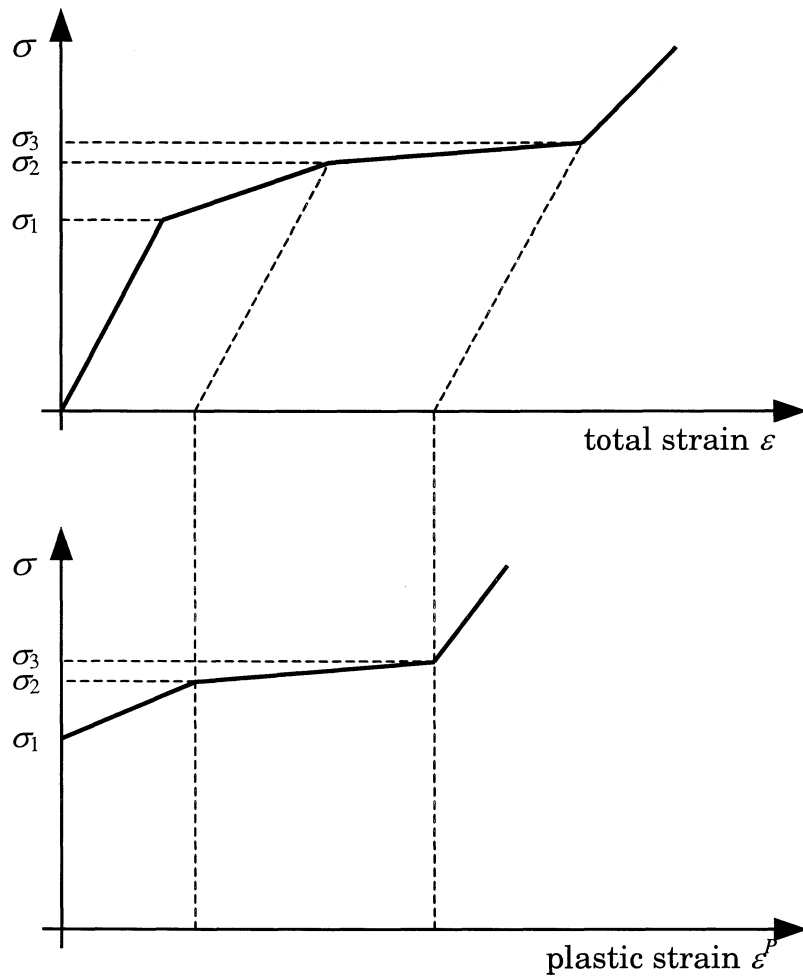
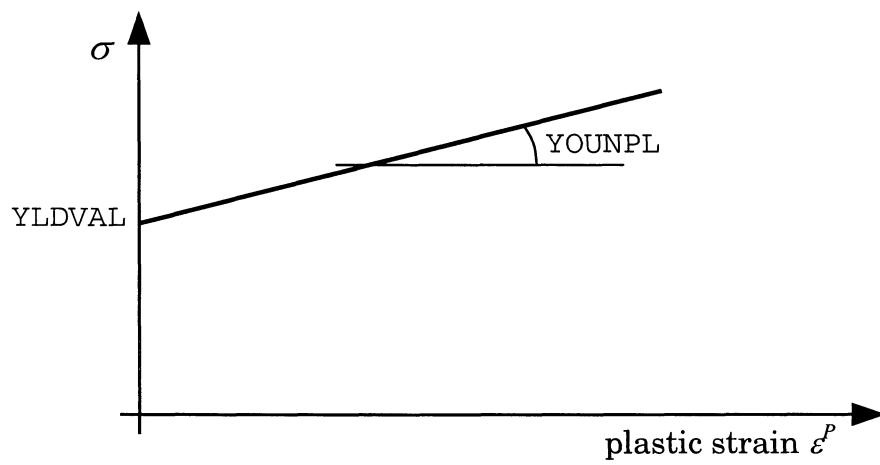**FIGURE 7-1** Uniaxial stress versus total strain and plastic strain

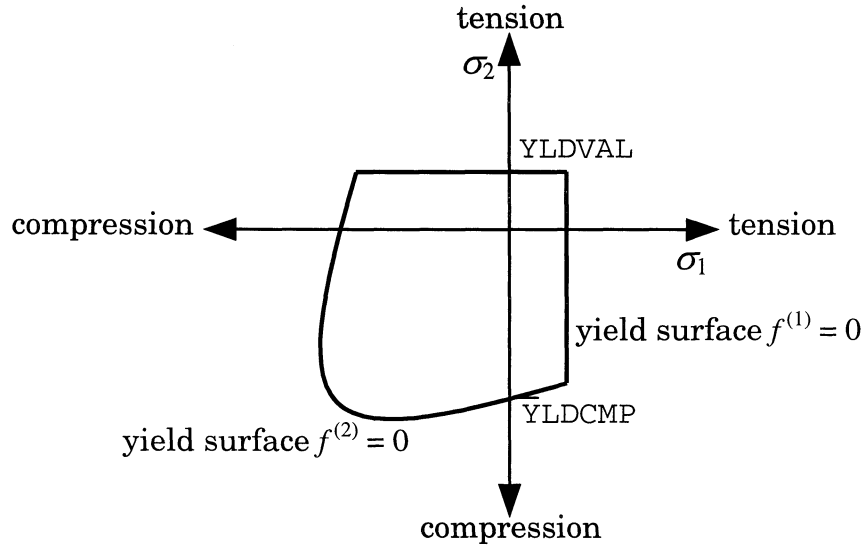**FIGURE 7-2** Uniaxial stress versus plastic strain relationship considered

108

FIGURE 7-3 Rankine/von Mises yield criteria

The sensitivity equations were also implemented for the pure Rankine plasticity model, which can be considered to be a special case of the Rankine/von Mises model in which the von Mises yield surface is never reached.

The Rankine/von Mises model considered is defined by six parameters: elastic modulus YOUNG, Poisson's ratio POISON, tensile yield stress YLDVAL, compressive yield stress YLDCMP, fracture energy HARVAL and plastic modulus CMPVAL.

As there are three yield criteria, there are three internal variables: $\kappa^{(1)}, \kappa^{(2)}$ and $\kappa^{(3)}$. The defining functions are

$$f^{(1)}\left(\boldsymbol{\sigma}, \kappa^{(1)}\right) = g^{(1)}\left(\boldsymbol{\sigma}, \kappa^{(1)}\right) = \sqrt{\tfrac{1}{2}\boldsymbol{\sigma}^T \boldsymbol{P}_r\, \boldsymbol{\sigma}} + \tfrac{1}{2}\boldsymbol{\pi}^{(1)T}\boldsymbol{\sigma} - \bar{\sigma}^{(1)}\left(\kappa^{(1)}\right) \tag{7-22}$$

$$f^{(2)}\left(\boldsymbol{\sigma}, \kappa^{(2)}\right) = g^{(2)}\left(\boldsymbol{\sigma}, \kappa^{(2)}\right) = \sqrt{\tfrac{1}{2}\boldsymbol{\sigma}^T \boldsymbol{P}_{vm}\, \boldsymbol{\sigma}} - \bar{\sigma}^{(2)}\left(\kappa^{(2)}\right) \tag{7-23}$$

$$f^{(3)}\left(\boldsymbol{\sigma}, \kappa^{(3)}\right) = g^{(3)}\left(\boldsymbol{\sigma}, \kappa^{(3)}\right) = \boldsymbol{\pi}^{(3)T}\boldsymbol{\sigma} - \bar{\sigma}^{(3)}\left(\kappa^{(3)}\right) \tag{7-24}$$

$$h^{(1)} = h^{(2)} = h^{(3)} = 1 \tag{7-25}$$

Equation 7-24 applies to plane strain and axisymmetric elements only.

In the above, $\bar{\sigma}^{(i)}\left(\kappa^{(i)}\right)$, $i = 1, 2, 3, \ldots$ are the uniaxial stress versus uniaxial plastic strain relationships (figure 7-1). $\boldsymbol{P}_{vm}$ is the von Mises projection matrix of equation 7-16. The Rankine projection matrix $\boldsymbol{P}_r$ is given by

$$\boldsymbol{P}_r = \begin{bmatrix} \frac{1}{2} & -\frac{1}{2} & 0 & 0 & 0 & 0 \\ -\frac{1}{2} & \frac{1}{2} & 0 & 0 & 0 & 0 \\ 0 & 0 & 0 & 0 & 0 & 0 \\ 0 & 0 & 0 & 2 & 0 & 0 \\ 0 & 0 & 0 & 0 & 0 & 0 \\ 0 & 0 & 0 & 0 & 0 & 0 \end{bmatrix} \tag{7-26}$$

and the projection vectors by

$$\boldsymbol{\pi}^{(1)} = \left\{ \begin{array}{c} 1 \\ 1 \\ 0 \\ 0 \\ 0 \\ 0 \end{array} \right\} \tag{7-27}$$

$$\boldsymbol{\pi}^{(3)} = \left\{ \begin{array}{c} 0 \\ 0 \\ 1 \\ 0 \\ 0 \\ 0 \end{array} \right\} \tag{7-28}$$

With three yield surfaces, each of which may be either active or inactive, eight different cases are possible. However, the governing equations analogous to equations 7-7–7-13 can be summarized as follows for all eight cases

$$\boldsymbol{\sigma}_{t+\Delta t} = \boldsymbol{D} \left[\boldsymbol{\varepsilon}_{t+\Delta t} - \boldsymbol{\varepsilon}^P_{t+\Delta t} \right] \tag{7-29}$$

$$\boldsymbol{\varepsilon}^P_{t+\Delta t} = \boldsymbol{\varepsilon}^P_t + \Delta\lambda^{(1)} \left[\frac{\boldsymbol{P}_r\,\boldsymbol{\sigma}_{t+\Delta t}}{\sqrt{2\boldsymbol{\sigma}^T_{t+\Delta t}\boldsymbol{P}_r\boldsymbol{\sigma}_{t+\Delta t}}} + \tfrac{1}{2}\boldsymbol{\pi}^{(1)} \right]$$
$$+ \Delta\lambda^{(2)} \frac{\boldsymbol{P}_{vm}\,\boldsymbol{\sigma}_{t+\Delta t}}{\sqrt{2\boldsymbol{\sigma}^T_{t+\Delta t}\boldsymbol{P}_{vm}\boldsymbol{\sigma}_{t+\Delta t}}} + \Delta\lambda^{(3)}\boldsymbol{\pi}^{(3)} \tag{7-30}$$
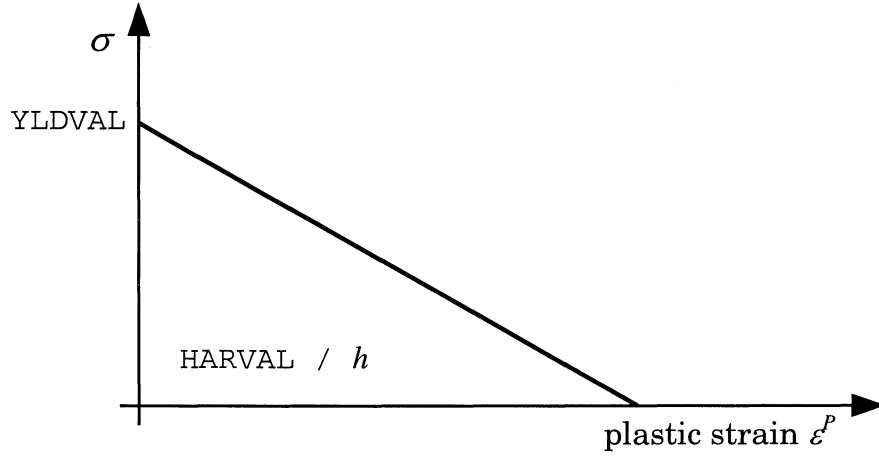
FIGURE 7-4 Uniaxial stress versus plastic strain relationship for Rankine

$$\kappa^{(i)}_{t+\Delta t} = \kappa^{(i)}_t + \Delta\lambda^{(i)}, \qquad i = 1, 2, 3 \tag{7-31}$$

$$\Delta\lambda^{(i)} = 0 \text{ if yield surface } f^{(i)} \text{ is not active}, \qquad i = 1, 2, 3 \tag{7-32}$$

$$\sqrt{\tfrac{1}{2}\boldsymbol{\sigma}^T_{t+\Delta t}\boldsymbol{P}_r\,\boldsymbol{\sigma}_{t+\Delta t}} + \tfrac{1}{2}\boldsymbol{\pi}^{(1)T}\boldsymbol{\sigma}_{t+\Delta t} - \bar{\sigma}^{(1)}\left(\kappa^{(1)}_{t+\Delta t}\right) = 0 \text{ if yield surface } f^{(1)} \text{ is active} \tag{7-33}$$

$$\sqrt{\tfrac{1}{2}\boldsymbol{\sigma}^T_{t+\Delta t}\boldsymbol{P}_{vm}\,\boldsymbol{\sigma}_{t+\Delta t}} - \bar{\sigma}^{(2)}\left(\kappa^{(2)}_{t+\Delta t}\right) = 0 \text{ if yield surface } f^{(2)} \text{ is active} \tag{7-34}$$

$$\boldsymbol{\pi}^{(3)T}\boldsymbol{\sigma}_{t+\Delta t} - \bar{\sigma}^{(3)}\left(\kappa^{(3)}_{t+\Delta t}\right) = 0 \text{ if yield surface } f^{(3)} \text{ is active} \tag{7-35}$$

For the sensitivity analysis, the simple uniaxial stress versus plastic strain relationships shown in figures 7-4 and 7-5 were considered. The relationship for the Rankine yield criterion is based on linear softening where HARVAL is the fracture energy, usually written G_f, and h is the "crack bandwidth". DIANA assumes a value for h related to the square root of the area of the element. The relationship for the von Mises yield criterion is linear hardening as in the previous section. It will be assumed that CMPVAL is nonzero.

The equations are

$$\bar{\sigma}^{(1)}\left(\kappa^{(1)}\right) = \text{YLDVAL} - \frac{h(\text{YLDVAL})^2}{2(\text{HARVAL})} \cdot \kappa^{(1)} \tag{7-36}$$

111
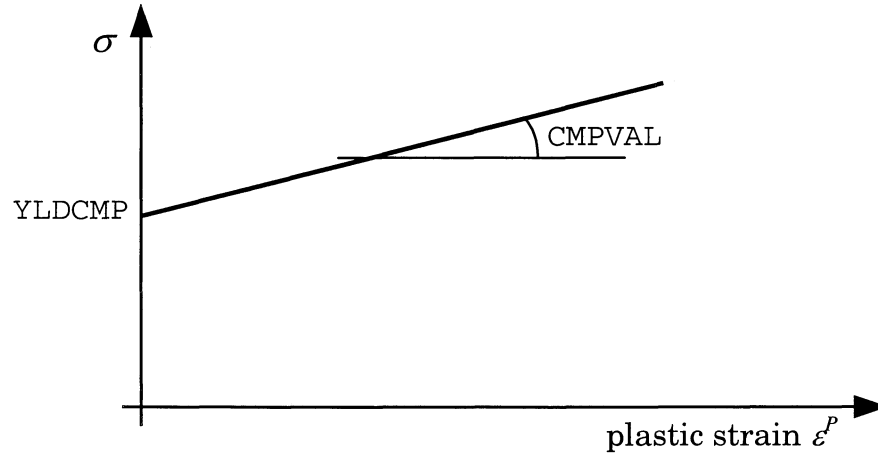
FIGURE 7-5 Uniaxial stress versus plastic strain relationship for von Mises

$$\bar{\sigma}^{(2)}\left(\kappa^{(2)}\right) = \texttt{YLDCMP} + \texttt{CMPVAL} \cdot \kappa^{(2)} \tag{7-37}$$

$$\bar{\sigma}^{(3)}\left(\kappa^{(3)}\right) = \texttt{YLDVAL} - \frac{h(\texttt{YLDVAL})^2}{2(\texttt{HARVAL})} \cdot \kappa^{(3)} \tag{7-38}$$

7.3   Sensitivity analysis for material models

This section contains derivation of the equations used for calculating the quantities $\left.\dfrac{\partial \boldsymbol{r}}{\partial x}\right|_{\boldsymbol{u},\dot{\boldsymbol{u}},\boldsymbol{z}} +$ $\dfrac{\partial \boldsymbol{r}}{\partial \boldsymbol{z}}\dfrac{\partial \boldsymbol{z}}{\partial x}$ and $\dfrac{\partial \boldsymbol{z}}{\partial x}$ needed to solve for the sensitivity factors for all of the material models in section 7.2. The tangent stiffness $\dfrac{\partial \boldsymbol{r}}{\partial \boldsymbol{u}}$ is already calculated and used by DIANA so it will not be covered here.

As in equation 7-2, $\boldsymbol{r}$ is given by

$$\boldsymbol{r} = \sum_i \boldsymbol{C}_i \sum_j w_{ij} \boldsymbol{B}_{ij} \boldsymbol{\sigma}_{ij}(\boldsymbol{u}, \dot{\boldsymbol{u}}, \boldsymbol{z}, \boldsymbol{x})(\Delta\text{vol})_{ij} \tag{7-39}$$

It should be noted that w_{ij}, $\boldsymbol{C}_i$, $\boldsymbol{B}_{ij}$ and the volume are independent of x and $\boldsymbol{z}$. This means that

$$\left.\frac{\partial \boldsymbol{r}}{\partial x}\right|_{\boldsymbol{u},\dot{\boldsymbol{u}},\boldsymbol{z}} + \frac{\partial \boldsymbol{r}}{\partial \boldsymbol{z}}\frac{\partial \boldsymbol{z}}{\partial x} = \sum_i \boldsymbol{C}_i \sum_j w_{ij} \boldsymbol{B}_{ij} \left[\left.\frac{\partial \boldsymbol{\sigma}_{ij}}{\partial x}\right|_{\boldsymbol{u},\dot{\boldsymbol{u}},\boldsymbol{z}} + \frac{\partial \boldsymbol{\sigma}_{ij}}{\partial \boldsymbol{z}}\frac{\partial \boldsymbol{z}}{\partial x}\right](\Delta\text{vol})_{ij} \tag{7-40}$$

112

It is thus possible to find $\left.\dfrac{\partial \boldsymbol{r}}{\partial x}\right|_{\boldsymbol{u},\dot{\boldsymbol{u}},\boldsymbol{z}} + \dfrac{\partial \boldsymbol{r}}{\partial \boldsymbol{z}}\dfrac{\partial \boldsymbol{z}}{\partial x}$ by first finding $\left.\dfrac{\partial \boldsymbol{\sigma}}{\partial x}\right|_{\boldsymbol{u},\dot{\boldsymbol{u}},\boldsymbol{z}} + \dfrac{\partial \boldsymbol{\sigma}}{\partial \boldsymbol{z}}\dfrac{\partial \boldsymbol{z}}{\partial x}$ and then multiplying it by the necessary constants. This approach will be followed in the following sections.

7.3.1 Plasticity

Equations 7-7–7-13 can be used to derive equations for the quantities needed to solve for the sensitivity factor. Differentiating equations 7-7–7-10 with respect to the uncertain parameter x:

$$\frac{\partial \boldsymbol{\sigma}_{t+\Delta t}}{\partial x} = \frac{\partial \boldsymbol{D}}{\partial x}\left[\boldsymbol{\varepsilon}_{t+\Delta t} - \boldsymbol{\varepsilon}^P_{t+\Delta t}\right] + \boldsymbol{D}\left[\frac{\partial \boldsymbol{\varepsilon}_{t+\Delta t}}{\partial x} - \frac{\partial \boldsymbol{\varepsilon}^P_{t+\Delta t}}{\partial x}\right] \tag{7-41}$$

$$\begin{aligned}
\frac{\partial \boldsymbol{\varepsilon}^P_{t+\Delta t}}{\partial x} =\ & \frac{\partial \boldsymbol{\varepsilon}^P_t}{\partial x} + \frac{\partial \Delta\lambda}{\partial x} \cdot \left[\frac{\partial g\left(\boldsymbol{\sigma},\kappa\right)}{\partial \boldsymbol{\sigma}}\right]_{t+\Delta t} \\
& + \Delta\lambda \left[\frac{\partial^2 g\left(\boldsymbol{\sigma},\kappa\right)}{\partial \boldsymbol{\sigma}^2}\right]_{t+\Delta t} \cdot \frac{\partial \boldsymbol{\sigma}_{t+\Delta t}}{\partial x} \\
& + \Delta\lambda \left[\frac{\partial^2 g\left(\boldsymbol{\sigma},\kappa\right)}{\partial \boldsymbol{\sigma}\,\partial\kappa}\right]_{t+\Delta t} \cdot \frac{\partial \kappa_{t+\Delta t}}{\partial x} \\
& + \Delta\lambda \left[\frac{\partial}{\partial x}\frac{\partial g\left(\boldsymbol{\sigma},\kappa\right)}{\partial \boldsymbol{\sigma}}\right]_{t+\Delta t}
\end{aligned} \tag{7-42}$$

$$\frac{\partial \kappa_{t+\Delta t}}{\partial x} = \frac{\partial \kappa_t}{\partial x} + \frac{\partial \Delta\lambda}{\partial x}h + \Delta\lambda\frac{\partial h}{\partial x} \tag{7-43}$$

$$\left[\frac{\partial f\left(\boldsymbol{\sigma},\kappa\right)}{\partial \boldsymbol{\sigma}}\right]_{t+\Delta t} \cdot \frac{\partial \boldsymbol{\sigma}_{t+\Delta t}}{\partial x} + \left[\frac{\partial f\left(\boldsymbol{\sigma},\kappa\right)}{\partial \kappa}\right]_{t+\Delta t} \cdot \frac{\partial \kappa_{t+\Delta t}}{\partial x} + \left[\frac{\partial f\left(\boldsymbol{\sigma},\kappa\right)}{\partial x}\right]_{t+\Delta t} = 0 \tag{7-44}$$

The above equations contain derivatives with respect to vector quantities, which need to be defined for clarity. If

$$\boldsymbol{\sigma} = \left\{\begin{array}{c} \sigma_1 \\ \sigma_2 \\ \sigma_3 \\ \vdots \\ \sigma_n \end{array}\right\} \tag{7-45}$$

113

then the derivatives are defined as

$$\frac{\partial g\left(\boldsymbol{\sigma},\kappa\right)}{\partial \boldsymbol{\sigma}} = \left\{ \begin{array}{c} \dfrac{\partial g\left(\boldsymbol{\sigma},\kappa\right)}{\partial \sigma_1} \\[6pt] \dfrac{\partial g\left(\boldsymbol{\sigma},\kappa\right)}{\partial \sigma_2} \\[6pt] \dfrac{\partial g\left(\boldsymbol{\sigma},\kappa\right)}{\partial \sigma_3} \\[6pt] \vdots \\[6pt] \dfrac{\partial g\left(\boldsymbol{\sigma},\kappa\right)}{\partial \sigma_n} \end{array} \right\} \tag{7-46}$$

$$\frac{\partial^2 g\left(\boldsymbol{\sigma},\kappa\right)}{\partial \boldsymbol{\sigma}^2} = \left[\begin{array}{cccc} \dfrac{\partial^2 g\left(\boldsymbol{\sigma},\kappa\right)}{\partial \sigma_1^2} & \dfrac{\partial^2 g\left(\boldsymbol{\sigma},\kappa\right)}{\partial \sigma_1 \partial \sigma_2} & \cdots & \dfrac{\partial^2 g\left(\boldsymbol{\sigma},\kappa\right)}{\partial \sigma_1 \partial \sigma_n} \\[6pt] \dfrac{\partial^2 g\left(\boldsymbol{\sigma},\kappa\right)}{\partial \sigma_2 \partial \sigma_1} & \dfrac{\partial^2 g\left(\boldsymbol{\sigma},\kappa\right)}{\partial \sigma_2^2} & \cdots & \dfrac{\partial^2 g\left(\boldsymbol{\sigma},\kappa\right)}{\partial \sigma_2 \partial \sigma_n} \\[6pt] \vdots & & \ddots & \\[6pt] \dfrac{\partial^2 g\left(\boldsymbol{\sigma},\kappa\right)}{\partial \sigma_n \partial \sigma_1} & & & \dfrac{\partial^2 g\left(\boldsymbol{\sigma},\kappa\right)}{\partial \sigma_n^2} \end{array} \right] \tag{7-47}$$

$$\frac{\partial^2 g\left(\boldsymbol{\sigma},\kappa\right)}{\partial \boldsymbol{\sigma} \partial \kappa} = \left\{ \begin{array}{c} \dfrac{\partial^2 g\left(\boldsymbol{\sigma},\kappa\right)}{\partial \sigma_1 \partial \kappa} \\[6pt] \dfrac{\partial^2 g\left(\boldsymbol{\sigma},\kappa\right)}{\partial \sigma_2 \partial \kappa} \\[6pt] \dfrac{\partial^2 g\left(\boldsymbol{\sigma},\kappa\right)}{\partial \sigma_3 \partial \kappa} \\[6pt] \vdots \\[6pt] \dfrac{\partial^2 g\left(\boldsymbol{\sigma},\kappa\right)}{\partial \sigma_n \partial \kappa} \end{array} \right\} \tag{7-48}$$

In equations 7-41–7-44, $\dfrac{\partial \boldsymbol{D}}{\partial x}$, $\left[\dfrac{\partial g\left(\boldsymbol{\sigma},\kappa\right)}{\partial \boldsymbol{\sigma}}\right]_{t+\Delta t}$, $\left[\dfrac{\partial^2 g\left(\boldsymbol{\sigma},\kappa\right)}{\partial \boldsymbol{\sigma}^2}\right]_{t+\Delta t}$, $\left[\dfrac{\partial^2 g\left(\boldsymbol{\sigma},\kappa\right)}{\partial \boldsymbol{\sigma}\, \partial \kappa}\right]_{t+\Delta t}$, $\left[\dfrac{\partial}{\partial x}\dfrac{\partial g\left(\boldsymbol{\sigma},\kappa\right)}{\partial \boldsymbol{\sigma}}\right]_{t+\Delta t}$, $\dfrac{\partial h}{\partial x}$, $\left[\dfrac{\partial f\left(\boldsymbol{\sigma},\kappa\right)}{\partial \boldsymbol{\sigma}}\right]_{t+\Delta t}$, $\left[\dfrac{\partial f\left(\boldsymbol{\sigma},\kappa\right)}{\partial \kappa}\right]_{t+\Delta t}$ and $\left[\dfrac{\partial f\left(\boldsymbol{\sigma},\kappa\right)}{\partial x}\right]_{t+\Delta t}$ depend on the plasticity model used and the uncertain parameter and can be determined relatively simply once $\boldsymbol{\sigma}_{t+\Delta t}$ and $\kappa_{t+\Delta t}$ are known. There are then $2n+2$ remaining unknowns: $\dfrac{\partial \boldsymbol{\sigma}_{t+\Delta t}}{\partial x}$,

$\dfrac{\partial \varepsilon^P_{t+\Delta t}}{\partial x}$, $\dfrac{\partial \Delta \lambda}{\partial x}$ and $\dfrac{\partial \kappa_{t+\Delta t}}{\partial x}$. Equations 7-41–7-44 form a set of $2n+2$ linear equations so the unknowns can be uniquely determined.

The two quantities that are needed to solve for the sensitivity factors are $\dfrac{\partial r}{\partial x}\Big|_{u,\dot{u},z} + \dfrac{\partial r}{\partial z}\dfrac{\partial z}{\partial x}$ and $\dfrac{\partial z}{\partial x}$; or equivalently, as explained in the introduction to Section 7.3, $\dfrac{\partial \sigma}{\partial x}\Big|_{u,\dot{u},z} + \dfrac{\partial \sigma}{\partial z}\dfrac{\partial z}{\partial x}$ and $\dfrac{\partial z}{\partial x}$. As explained in Section 3, the first of these two quantities is the partial derivative of σ with respect to x with displacement u held fixed, and the second is the derivative of the vector of history-dependent variables. Holding the displacement fixed means that the strain ε is also fixed, so the required partial derivative can be found by (1) rearranging equations 7-41–7-44 to find a solution for $\dfrac{\partial \sigma}{\partial x}$ and (2) setting $\dfrac{\partial \varepsilon}{\partial x}$ to zero. This will be done in the following sections for the plasticity models of Section 7.2.1.

The resulting equation will be in terms of the known quantities and $\dfrac{\partial \varepsilon^P_t}{\partial x}$ and $\dfrac{\partial \kappa_t}{\partial x}$, the derivatives of the history-dependent variables. Equations for calculating these derivatives are also required, and can be derived from equations 7-41–7-44. As in the flowchart of figure 3-1, $\dfrac{\partial \varepsilon^P_{t+\Delta t}}{\partial x}$ and $\dfrac{\partial \kappa_{t+\Delta t}}{\partial x}$ will be calculated at the end of each time step and then used in the equation for $\dfrac{\partial \sigma}{\partial x}$ at the following time step. The values used at the first step will depend on the initial conditions.

If $\sigma_{t+\Delta t}$ is not on the yield surface, the equations become simpler. Differentiating equations 7-11–7-13 with respect to x

$$\frac{\partial \sigma_{t+\Delta t}}{\partial x} = \frac{\partial D}{\partial x}\left[\varepsilon_{t+\Delta t} - \varepsilon^P_{t+\Delta t}\right] + D\left[\frac{\partial \varepsilon_{t+\Delta t}}{\partial x} - \frac{\partial \varepsilon^P_{t+\Delta t}}{\partial x}\right] \tag{7-49}$$

$$\frac{\partial \varepsilon^P_{t+\Delta t}}{\partial x} = \frac{\partial \varepsilon^P_t}{\partial x} \tag{7-50}$$

$$\frac{\partial \kappa_{t+\Delta t}}{\partial x} = \frac{\partial \kappa_t}{\partial x} \tag{7-51}$$

In this case, setting $\dfrac{\partial \varepsilon_{t+\Delta t}}{\partial x}$ to zero in equation 7-49 gives the equation for $\dfrac{\partial \sigma}{\partial x}\Big|_{u,\dot{u},z} + \dfrac{\partial \sigma}{\partial z}\dfrac{\partial z}{\partial x}$ directly and equations 7-50 and 7-51 give $\dfrac{\partial \varepsilon^P_{t+\Delta t}}{\partial x}$ and $\dfrac{\partial \kappa_{t+\Delta t}}{\partial x}$ without any further manipulation. Then solution for this case is straightforward and need not be examined in any more detail for the different plasticity models.

115

7.3.1.1 von Mises

Differentiating equations 7-17–7-20 with respect to a general x

$$\frac{\partial \boldsymbol{\sigma}_{t+\Delta t}}{\partial x} = \frac{\partial \boldsymbol{D}}{\partial x}\left[\boldsymbol{\varepsilon}_{t+\Delta t} - \boldsymbol{\varepsilon}_{t+\Delta t}^{P}\right] + \boldsymbol{D}\left[\frac{\partial \boldsymbol{\varepsilon}_{t+\Delta t}}{\partial x} - \frac{\partial \boldsymbol{\varepsilon}_{t+\Delta t}^{P}}{\partial x}\right] \tag{7-52}$$

$$
\begin{aligned}
\frac{\partial \boldsymbol{\varepsilon}_{t+\Delta t}^{P}}{\partial x} &= \frac{\partial \boldsymbol{\varepsilon}_{t}^{P}}{\partial x} + \frac{\partial \Delta\lambda}{\partial x}\cdot\frac{\boldsymbol{P}_{vm}\,\boldsymbol{\sigma}_{t+\Delta t}}{2\bar{\sigma}\left(\kappa_{t+\Delta t}\right)} \\
&\quad + \Delta\lambda\frac{\boldsymbol{P}_{vm}}{2\bar{\sigma}\left(\kappa_{t+\Delta t}\right)}\cdot\frac{\partial \boldsymbol{\sigma}_{t+\Delta t}}{\partial x} \\
&\quad - \Delta\lambda\frac{\boldsymbol{P}_{vm}\,\boldsymbol{\sigma}_{t+\Delta t}}{2\left[\bar{\sigma}\left(\kappa_{t+\Delta t}\right)\right]^{2}}\cdot\left[\frac{\partial\bar{\sigma}}{\partial\kappa}\right]_{t+\Delta t}\cdot\frac{\partial \kappa_{t+\Delta t}}{\partial x} \\
&\quad - \Delta\lambda\frac{\boldsymbol{P}_{vm}\,\boldsymbol{\sigma}_{t+\Delta t}}{2\left[\bar{\sigma}\left(\kappa_{t+\Delta t}\right)\right]^{2}}\cdot\frac{\partial\bar{\sigma}\left(\kappa_{t+\Delta t}\right)}{\partial x}
\end{aligned} \tag{7-53}
$$

$$\frac{\partial \kappa_{t+\Delta t}}{\partial x} = \frac{\partial \kappa_{t}}{\partial x} + \frac{\partial \Delta\lambda}{\partial x} \tag{7-54}$$

$$\frac{\boldsymbol{\sigma}_{t+\Delta t}^{T}\boldsymbol{P}_{vm}}{\sqrt{2\,\boldsymbol{\sigma}_{t+\Delta t}^{T}\boldsymbol{P}_{vm}\,\boldsymbol{\sigma}_{t+\Delta t}}}\cdot\frac{\partial \boldsymbol{\sigma}_{t+\Delta t}}{\partial x} - \left[\frac{\partial\bar{\sigma}}{\partial\kappa}\right]_{t+\Delta t}\cdot\frac{\partial \kappa_{t+\Delta t}}{\partial x} - \frac{\partial\bar{\sigma}\left(\kappa_{t+\Delta t}\right)}{\partial x} = 0 \tag{7-55}$$

Substituting equation 7-20 into equation 7-55 and rearranging

$$\frac{\boldsymbol{\sigma}_{t+\Delta t}^{T}\boldsymbol{P}_{vm}}{2\bar{\sigma}\left(\kappa_{t+\Delta t}\right)}\cdot\frac{\partial \boldsymbol{\sigma}_{t+\Delta t}}{\partial x} = \left[\frac{\partial\bar{\sigma}}{\partial\kappa}\right]_{t+\Delta t}\cdot\frac{\partial \kappa_{t+\Delta t}}{\partial x} + \frac{\partial\bar{\sigma}\left(\kappa_{t+\Delta t}\right)}{\partial x} \tag{7-56}$$

Pre-multiplying equation 7-53 by $\boldsymbol{\sigma}_{t+\Delta t}^{T}$

$$
\begin{aligned}
\boldsymbol{\sigma}_{t+\Delta t}^{T}\cdot\frac{\partial \boldsymbol{\varepsilon}_{t+\Delta t}^{P}}{\partial x} &= \boldsymbol{\sigma}_{t+\Delta t}^{T}\cdot\frac{\partial \boldsymbol{\varepsilon}_{t}^{P}}{\partial x} + \frac{\partial \Delta\lambda}{\partial x}\cdot\frac{\boldsymbol{\sigma}_{t+\Delta t}^{T}\boldsymbol{P}_{vm}\,\boldsymbol{\sigma}_{t+\Delta t}}{2\bar{\sigma}\left(\kappa_{t+\Delta t}\right)} \\
&\quad + \Delta\lambda\frac{\boldsymbol{\sigma}_{t+\Delta t}^{T}\boldsymbol{P}_{vm}}{2\bar{\sigma}\left(\kappa_{t+\Delta t}\right)}\cdot\frac{\partial \boldsymbol{\sigma}_{t+\Delta t}}{\partial x} \\
&\quad - \Delta\lambda\frac{\boldsymbol{\sigma}_{t+\Delta t}^{T}\boldsymbol{P}_{vm}\,\boldsymbol{\sigma}_{t+\Delta t}}{2\left[\bar{\sigma}\left(\kappa_{t+\Delta t}\right)\right]^{2}}\cdot\left[\frac{\partial\bar{\sigma}}{\partial\kappa}\right]_{t+\Delta t}\cdot\frac{\partial \kappa_{t+\Delta t}}{\partial x}
\end{aligned}
$$

116

$$- \Delta\lambda \frac{\boldsymbol{\sigma}_{t+\Delta t}^{T} \boldsymbol{P}_{vm}\, \boldsymbol{\sigma}_{t+\Delta t}}{2\left[\bar{\sigma}\left(\kappa_{t+\Delta t}\right)\right]^{2}} \cdot \frac{\partial \bar{\sigma}\left(\kappa_{t+\Delta t}\right)}{\partial x}$$

$$= \boldsymbol{\sigma}_{t+\Delta t}^{T} \cdot \frac{\partial \boldsymbol{\varepsilon}_{t}^{P}}{\partial x} + \frac{\partial \Delta\lambda}{\partial x} \cdot \bar{\sigma}\left(\kappa_{t+\Delta t}\right)$$

$$+ \Delta\lambda \left\{ \left[\frac{\partial \bar{\sigma}}{\partial \kappa}\right]_{t+\Delta t} \cdot \frac{\partial \kappa_{t+\Delta t}}{\partial x} + \frac{\partial \bar{\sigma}\left(\kappa_{t+\Delta t}\right)}{\partial x} \right\}$$

$$- \Delta\lambda \left[\frac{\partial \bar{\sigma}}{\partial \kappa}\right]_{t+\Delta t} \cdot \frac{\partial \kappa_{t+\Delta t}}{\partial x}$$

$$- \Delta\lambda \frac{\partial \bar{\sigma}\left(\kappa_{t+\Delta t}\right)}{\partial x}$$

$$= \boldsymbol{\sigma}_{t+\Delta t}^{T} \cdot \frac{\partial \boldsymbol{\varepsilon}_{t}^{P}}{\partial x} + \frac{\partial \Delta\lambda}{\partial x} \cdot \bar{\sigma}\left(\kappa_{t+\Delta t}\right) \qquad (7\text{-}57)$$

therefore

$$\frac{\partial \Delta\lambda}{\partial x} = \frac{\boldsymbol{\sigma}_{t+\Delta t}^{T}}{\bar{\sigma}\left(\kappa_{t+\Delta t}\right)} \left[\frac{\partial \boldsymbol{\varepsilon}_{t+\Delta t}^{P}}{\partial x} - \frac{\partial \boldsymbol{\varepsilon}_{t}^{P}}{\partial x}\right] \qquad (7\text{-}58)$$

Substituting 7-54 and 7-58 into 7-53

$$\frac{\partial \boldsymbol{\varepsilon}_{t+\Delta t}^{P}}{\partial x} = \frac{\partial \boldsymbol{\varepsilon}_{t}^{P}}{\partial x}$$

$$+ \frac{\boldsymbol{\sigma}_{t+\Delta t}^{T}}{\bar{\sigma}\left(\kappa_{t+\Delta t}\right)} \left[\frac{\partial \boldsymbol{\varepsilon}_{t+\Delta t}^{P}}{\partial x} - \frac{\partial \boldsymbol{\varepsilon}_{t}^{P}}{\partial x}\right] \frac{\boldsymbol{P}_{vm}\, \boldsymbol{\sigma}_{t+\Delta t}}{2\bar{\sigma}\left(\kappa_{t+\Delta t}\right)}$$

$$+ \Delta\lambda \frac{\boldsymbol{P}_{vm}}{2\bar{\sigma}\left(\kappa_{t+\Delta t}\right)} \cdot \frac{\partial \boldsymbol{\sigma}_{t+\Delta t}}{\partial x}$$

$$- \Delta\lambda \frac{\boldsymbol{P}_{vm}\, \boldsymbol{\sigma}_{t+\Delta t}}{2\left[\bar{\sigma}\left(\kappa_{t+\Delta t}\right)\right]^{2}} \cdot \left[\frac{\partial \bar{\sigma}}{\partial \kappa}\right]_{t+\Delta t} \cdot \left[\frac{\partial \kappa_{t}}{\partial x} + \frac{\boldsymbol{\sigma}_{t+\Delta t}^{T}}{\bar{\sigma}\left(\kappa_{t+\Delta t}\right)} \left(\frac{\partial \boldsymbol{\varepsilon}_{t+\Delta t}^{P}}{\partial x} - \frac{\partial \boldsymbol{\varepsilon}_{t}^{P}}{\partial x}\right)\right]$$

$$- \Delta\lambda \frac{\boldsymbol{P}_{vm}\, \boldsymbol{\sigma}_{t+\Delta t}}{2\left[\bar{\sigma}\left(\kappa_{t+\Delta t}\right)\right]^{2}} \cdot \frac{\partial \bar{\sigma}\left(\kappa_{t+\Delta t}\right)}{\partial x}$$

$$= \frac{\partial \boldsymbol{\varepsilon}_{t}^{P}}{\partial x}$$

$$+ \frac{\boldsymbol{P}_{vm}\, \boldsymbol{\sigma}_{t+\Delta t}\, \boldsymbol{\sigma}_{t+\Delta t}^{T}}{2\left[\bar{\sigma}\left(\kappa_{t+\Delta t}\right)\right]^{2}} \cdot \left[\frac{\partial \boldsymbol{\varepsilon}_{t+\Delta t}^{P}}{\partial x} - \frac{\partial \boldsymbol{\varepsilon}_{t}^{P}}{\partial x}\right]$$

$$+ \Delta\lambda \frac{\boldsymbol{P}_{vm}}{2\bar{\sigma}\left(\kappa_{t+\Delta t}\right)} \cdot \frac{\partial \boldsymbol{\sigma}_{t+\Delta t}}{\partial x}$$

$$- \Delta\lambda \frac{\boldsymbol{P}_{vm}\, \boldsymbol{\sigma}_{t+\Delta t}}{2\left[\bar{\sigma}\left(\kappa_{t+\Delta t}\right)\right]^{2}} \cdot \left[\left[\frac{\partial \bar{\sigma}}{\partial \kappa}\right]_{t+\Delta t} \frac{\partial \kappa_{t}}{\partial x} + \frac{\partial \bar{\sigma}\left(\kappa_{t+\Delta t}\right)}{\partial x}\right]$$

117

$$- \Delta\lambda \frac{\boldsymbol{P}_{vm}\,\boldsymbol{\sigma}_{t+\Delta t}\,\boldsymbol{\sigma}_{t+\Delta t}^{T}}{2\left[\bar{\sigma}\left(\kappa_{t+\Delta t}\right)\right]^{3}}\cdot\left[\frac{\partial\bar{\sigma}}{\partial\kappa}\right]_{t+\Delta t}\cdot\left[\frac{\partial\varepsilon_{t+\Delta t}^{P}}{\partial x}-\frac{\partial\varepsilon_{t}^{P}}{\partial x}\right] \tag{7-59}$$

Rearranging equation 7-59

$$\left[\boldsymbol{I}-\frac{\boldsymbol{P}_{vm}\,\boldsymbol{\sigma}_{t+\Delta t}\,\boldsymbol{\sigma}_{t+\Delta t}^{T}}{2\left[\bar{\sigma}\left(\kappa_{t+\Delta t}\right)\right]^{2}}\left(1-\frac{\Delta\lambda}{\bar{\sigma}\left(\kappa_{t+\Delta t}\right)}\cdot\left[\frac{\partial\bar{\sigma}}{\partial\kappa}\right]_{t+\Delta t}\right)\right]\frac{\partial\varepsilon_{t+\Delta t}^{P}}{\partial x}$$

$$=\left[\boldsymbol{I}-\frac{\boldsymbol{P}_{vm}\,\boldsymbol{\sigma}_{t+\Delta t}\,\boldsymbol{\sigma}_{t+\Delta t}^{T}}{2\left[\bar{\sigma}\left(\kappa_{t+\Delta t}\right)\right]^{2}}\left(1-\frac{\Delta\lambda}{\bar{\sigma}\left(\kappa_{t+\Delta t}\right)}\cdot\left[\frac{\partial\bar{\sigma}}{\partial\kappa}\right]_{t+\Delta t}\right)\right]\frac{\partial\varepsilon_{t}^{P}}{\partial x}$$

$$+\Delta\lambda\frac{\boldsymbol{P}_{vm}}{2\bar{\sigma}\left(\kappa_{t+\Delta t}\right)}\cdot\frac{\partial\boldsymbol{\sigma}_{t+\Delta t}}{\partial x}$$

$$-\Delta\lambda\frac{\boldsymbol{P}_{vm}\,\boldsymbol{\sigma}_{t+\Delta t}}{2\left[\bar{\sigma}\left(\kappa_{t+\Delta t}\right)\right]^{2}}\left[\left[\frac{\partial\bar{\sigma}}{\partial\kappa}\right]_{t+\Delta t}\frac{\partial\kappa_{t}}{\partial x}+\frac{\partial\bar{\sigma}\left(\kappa_{t+\Delta t}\right)}{\partial x}\right] \tag{7-60}$$

where $\boldsymbol{I}$ is the identity matrix. From equation 7-60

$$\frac{\partial\varepsilon_{t+\Delta t}^{P}}{\partial x}=\frac{\partial\varepsilon_{t}^{P}}{\partial x}$$

$$+\left[\boldsymbol{I}-\frac{\boldsymbol{P}_{vm}\,\boldsymbol{\sigma}_{t+\Delta t}\,\boldsymbol{\sigma}_{t+\Delta t}^{T}}{2\left[\bar{\sigma}\left(\kappa_{t+\Delta t}\right)\right]^{2}}\left(1-\frac{\Delta\lambda}{\bar{\sigma}\left(\kappa_{t+\Delta t}\right)}\cdot\left[\frac{\partial\bar{\sigma}}{\partial\kappa}\right]_{t+\Delta t}\right)\right]^{-1}$$

$$\cdot\left\{\Delta\lambda\frac{\boldsymbol{P}_{vm}}{2\bar{\sigma}\left(\kappa_{t+\Delta t}\right)}\cdot\frac{\partial\boldsymbol{\sigma}_{t+\Delta t}}{\partial x}\right.$$

$$\left.-\Delta\lambda\frac{\boldsymbol{P}_{vm}\,\boldsymbol{\sigma}_{t+\Delta t}}{2\left[\bar{\sigma}\left(\kappa_{t+\Delta t}\right)\right]^{2}}\left[\left[\frac{\partial\bar{\sigma}}{\partial\kappa}\right]_{t+\Delta t}\frac{\partial\kappa_{t}}{\partial x}+\frac{\partial\bar{\sigma}\left(\kappa_{t+\Delta t}\right)}{\partial x}\right]\right\} \tag{7-61}$$

Substitute 7-61 into 7-52

$$\frac{\partial\boldsymbol{\sigma}_{t+\Delta t}}{\partial x}=\frac{\partial\boldsymbol{D}}{\partial x}\left[\varepsilon_{t+\Delta t}-\varepsilon_{t+\Delta t}^{P}\right]$$

$$+\boldsymbol{D}\left\{\frac{\partial\varepsilon_{t+\Delta t}}{\partial x}-\frac{\partial\varepsilon_{t}^{P}}{\partial x}\right.$$

$$-\left[\boldsymbol{I}-\frac{\boldsymbol{P}_{vm}\,\boldsymbol{\sigma}_{t+\Delta t}\,\boldsymbol{\sigma}_{t+\Delta t}^{T}}{2\left[\bar{\sigma}\left(\kappa_{t+\Delta t}\right)\right]^{2}}\left(1-\frac{\Delta\lambda}{\bar{\sigma}\left(\kappa_{t+\Delta t}\right)}\cdot\left[\frac{\partial\bar{\sigma}}{\partial\kappa}\right]_{t+\Delta t}\right)\right]^{-1}$$

$$\cdot\left[\Delta\lambda\frac{\boldsymbol{P}_{vm}}{2\bar{\sigma}\left(\kappa_{t+\Delta t}\right)}\cdot\frac{\partial\boldsymbol{\sigma}_{t+\Delta t}}{\partial x}\right.$$

$$\left.\left.-\Delta\lambda\frac{\boldsymbol{P}_{vm}\,\boldsymbol{\sigma}_{t+\Delta t}}{2\left[\bar{\sigma}\left(\kappa_{t+\Delta t}\right)\right]^{2}}\left(\left[\frac{\partial\bar{\sigma}}{\partial\kappa}\right]_{t+\Delta t}\cdot\frac{\partial\kappa_{t}}{\partial x}+\frac{\partial\bar{\sigma}\left(\kappa_{t+\Delta t}\right)}{\partial x}\right)\right]\right\} \tag{7-62}$$

118

Rearranging equation 7-62

$$
\left\{ \boldsymbol{I} + \boldsymbol{D} \left[\boldsymbol{I} - \frac{\boldsymbol{P}_{vm}\,\boldsymbol{\sigma}_{t+\Delta t}\,\boldsymbol{\sigma}_{t+\Delta t}^{T}}{2\left[\bar{\sigma}\left(\kappa_{t+\Delta t}\right)\right]^{2}} \left(1 - \frac{\Delta\lambda}{\bar{\sigma}\left(\kappa_{t+\Delta t}\right)} \cdot \left[\frac{\partial\bar{\sigma}}{\partial\kappa}\right]_{t+\Delta t} \right) \right]^{-1} \frac{\Delta\lambda\boldsymbol{P}_{vm}}{2\bar{\sigma}\left(\kappa_{t+\Delta t}\right)} \right\} \frac{\partial\,\boldsymbol{\sigma}_{t+\Delta t}}{\partial x}
$$

$$
= \frac{\partial \boldsymbol{D}}{\partial x} \left[\boldsymbol{\varepsilon}_{t+\Delta t} - \boldsymbol{\varepsilon}_{t+\Delta t}^{P} \right]
$$

$$
+ \boldsymbol{D} \left\{ \frac{\partial \boldsymbol{\varepsilon}_{t+\Delta t}}{\partial x} - \frac{\partial\,\boldsymbol{\varepsilon}_{t}^{P}}{\partial x} \right.
$$

$$
+ \left[\boldsymbol{I} - \frac{\boldsymbol{P}_{vm}\,\boldsymbol{\sigma}_{t+\Delta t}\,\boldsymbol{\sigma}_{t+\Delta t}^{T}}{2\left[\bar{\sigma}\left(\kappa_{t+\Delta t}\right)\right]^{2}} \left(1 - \frac{\Delta\lambda}{\bar{\sigma}\left(\kappa_{t+\Delta t}\right)} \cdot \left[\frac{\partial\bar{\sigma}}{\partial\kappa}\right]_{t+\Delta t} \right) \right]^{-1}
$$

$$
\left. \cdot \Delta\lambda \frac{\boldsymbol{P}_{vm}\,\boldsymbol{\sigma}_{t+\Delta t}}{2\left[\bar{\sigma}\left(\kappa_{t+\Delta t}\right)\right]^{2}} \left[\left[\frac{\partial\bar{\sigma}}{\partial\kappa}\right]_{t+\Delta t} \frac{\partial\,\kappa_{t}}{\partial x} + \frac{\partial\bar{\sigma}\left(\kappa_{t+\Delta t}\right)}{\partial x} \right] \right\}
$$

(7-63)

therefore

$$
\frac{\partial\,\boldsymbol{\sigma}_{t+\Delta t}}{\partial x} = \left\{ \boldsymbol{I} + \boldsymbol{D} \left[\boldsymbol{I} - \frac{\boldsymbol{P}_{vm}\,\boldsymbol{\sigma}_{t+\Delta t}\,\boldsymbol{\sigma}_{t+\Delta t}^{T}}{2\left[\bar{\sigma}\left(\kappa_{t+\Delta t}\right)\right]^{2}} \left(1 - \frac{\Delta\lambda}{\bar{\sigma}\left(\kappa_{t+\Delta t}\right)} \cdot \left[\frac{\partial\bar{\sigma}}{\partial\kappa}\right]_{t+\Delta t} \right) \right]^{-1} \right.
$$

$$
\left. \frac{\Delta\lambda\boldsymbol{P}_{vm}}{2\bar{\sigma}\left(\kappa_{t+\Delta t}\right)} \right\}^{-1} \cdot \left\{ \frac{\partial \boldsymbol{D}}{\partial x} \left[\boldsymbol{\varepsilon}_{t+\Delta t} - \boldsymbol{\varepsilon}_{t+\Delta t}^{P} \right] \right.
$$

$$
+ \boldsymbol{D} \left\{ \frac{\partial\,\boldsymbol{\varepsilon}_{t+\Delta t}}{\partial x} - \frac{\partial\,\boldsymbol{\varepsilon}_{t}^{P}}{\partial x} \right.
$$

$$
+ \left[\boldsymbol{I} - \frac{\boldsymbol{P}_{vm}\,\boldsymbol{\sigma}_{t+\Delta t}\,\boldsymbol{\sigma}_{t+\Delta t}^{T}}{2\left[\bar{\sigma}\left(\kappa_{t+\Delta t}\right)\right]^{2}} \left(1 - \frac{\Delta\lambda}{\bar{\sigma}\left(\kappa_{t+\Delta t}\right)} \cdot \left[\frac{\partial\bar{\sigma}}{\partial\kappa}\right]_{t+\Delta t} \right) \right]^{-1}
$$

$$
\left. \left. \cdot \Delta\lambda \frac{\boldsymbol{P}_{vm}\,\boldsymbol{\sigma}_{t+\Delta t}}{2\left[\bar{\sigma}\left(\kappa_{t+\Delta t}\right)\right]^{2}} \left[\left[\frac{\partial\bar{\sigma}}{\partial\kappa}\right]_{t+\Delta t} \frac{\partial\,\kappa_{t}}{\partial x} + \frac{\partial\bar{\sigma}\left(\kappa_{t+\Delta t}\right)}{\partial x} \right] \right\} \right\}
$$

(7-64)

Setting $\dfrac{\partial \boldsymbol{\varepsilon}_{t+\Delta t}}{\partial x}$ to zero on the right hand side of equation 7-64 results in an equation for the quantity required

$$
\left. \frac{\partial \boldsymbol{\sigma}_{t+\Delta t}}{\partial x} \right|_{\boldsymbol{u},\dot{\boldsymbol{u}},\boldsymbol{z}} + \frac{\partial \boldsymbol{\sigma}_{t+\Delta t}}{\partial \boldsymbol{z}_{t+\Delta t}} \frac{\partial \boldsymbol{z}_{t+\Delta t}}{\partial x} =
$$

$$
\left\{ \boldsymbol{I} + \boldsymbol{D} \left[\boldsymbol{I} - \frac{\boldsymbol{P}_{vm}\, \boldsymbol{\sigma}_{t+\Delta t}\, \boldsymbol{\sigma}_{t+\Delta t}^{T}}{2\left[\bar{\sigma}\left(\kappa_{t+\Delta t}\right)\right]^{2}} \left(1 - \frac{\Delta\lambda}{\bar{\sigma}\left(\kappa_{t+\Delta t}\right)} \cdot \left[\frac{\partial \bar{\sigma}}{\partial \kappa}\right]_{t+\Delta t} \right) \right]^{-1} \frac{\Delta\lambda \boldsymbol{P}_{vm}}{2\bar{\sigma}\left(\kappa_{t+\Delta t}\right)} \right\}^{-1}
$$

$$
\cdot \left\{ \frac{\partial \boldsymbol{D}}{\partial x} \left[\boldsymbol{\varepsilon}_{t+\Delta t} - \boldsymbol{\varepsilon}_{t+\Delta t}^{P} \right] + \boldsymbol{D} \left\{ -\frac{\partial \boldsymbol{\varepsilon}_{t}^{P}}{\partial x} \right. \right. \tag{7-65}
$$

$$
+ \left[\boldsymbol{I} - \frac{\boldsymbol{P}_{vm}\, \boldsymbol{\sigma}_{t+\Delta t}\, \boldsymbol{\sigma}_{t+\Delta t}^{T}}{2\left[\bar{\sigma}\left(\kappa_{t+\Delta t}\right)\right]^{2}} \left(1 - \frac{\Delta\lambda}{\bar{\sigma}\left(\kappa_{t+\Delta t}\right)} \cdot \left[\frac{\partial \bar{\sigma}}{\partial \kappa}\right]_{t+\Delta t} \right) \right]^{-1}
$$

$$
\left. \left. \cdot \Delta\lambda \frac{\boldsymbol{P}_{vm}\, \boldsymbol{\sigma}_{t+\Delta t}}{2\left[\bar{\sigma}\left(\kappa_{t+\Delta t}\right)\right]^{2}} \left[\left[\frac{\partial \bar{\sigma}}{\partial \kappa}\right]_{t+\Delta t} \frac{\partial \kappa_{t}}{\partial x} + \frac{\partial \bar{\sigma}\left(\kappa_{t+\Delta t}\right)}{\partial x} \right] \right\} \right\}
$$

The terms on the right hand side of equation 7-65 can easily be calculated and are given below.

- If the uncertain parameter x is the elastic modulus YOUNG or Poisson's ratio POISON then $\dfrac{\partial \boldsymbol{D}}{\partial x}$ is nonzero, but depends on the element formulation. It is typically not difficult to find. In this case $\dfrac{\partial \bar{\sigma}\left(\kappa_{t+\Delta t}\right)}{\partial x}$ is zero.

- If the uncertain parameter x is the yield stress YLDVAL then $\dfrac{\partial \boldsymbol{D}}{\partial x}$ is zero and $\dfrac{\partial \bar{\sigma}\left(\kappa_{t+\Delta t}\right)}{\partial x}$ is 1.

- If the uncertain parameter x is the plastic modulus YOUNPL then $\dfrac{\partial \boldsymbol{D}}{\partial x}$ is zero and $\dfrac{\partial \bar{\sigma}\left(\kappa_{t+\Delta t}\right)}{\partial x}$ is $\kappa_{t+\Delta t}$.

- If the uncertain parameter x is not a parameter of this element then $\dfrac{\partial \boldsymbol{D}}{\partial x}$ and $\dfrac{\partial \bar{\sigma}\left(\kappa_{t+\Delta t}\right)}{\partial x}$ are zero.

Finally, from equation 7-21 it is clear that $\left[\dfrac{\partial \bar{\sigma}}{\partial \kappa}\right]_{t+\Delta t}$ is YOUNPL.

The history-dependent variables are $\boldsymbol{\varepsilon}^{P}$ and κ. To find an equation for $\dfrac{\partial \boldsymbol{\varepsilon}_{t+\Delta t}^{P}}{\partial x}$, substitute equation 7-52 into equation 7-60:

$$\left[\boldsymbol{I} - \frac{\boldsymbol{P}_{vm}\,\boldsymbol{\sigma}_{t+\Delta t}\,\boldsymbol{\sigma}_{t+\Delta t}^T}{2\left[\bar{\sigma}\left(\kappa_{t+\Delta t}\right)\right]^2}\left(1 - \frac{\Delta\lambda}{\bar{\sigma}\left(\kappa_{t+\Delta t}\right)}\cdot\left[\frac{\partial\bar{\sigma}}{\partial\kappa}\right]_{t+\Delta t}\right)\right]\frac{\partial\boldsymbol{\varepsilon}_{t+\Delta t}^P}{\partial x}$$

$$= \left[\boldsymbol{I} - \frac{\boldsymbol{P}_{vm}\,\boldsymbol{\sigma}_{t+\Delta t}\,\boldsymbol{\sigma}_{t+\Delta t}^T}{2\left[\bar{\sigma}\left(\kappa_{t+\Delta t}\right)\right]^2}\left(1 - \frac{\Delta\lambda}{\bar{\sigma}\left(\kappa_{t+\Delta t}\right)}\cdot\left[\frac{\partial\bar{\sigma}}{\partial\kappa}\right]_{t+\Delta t}\right)\right]\frac{\partial\boldsymbol{\varepsilon}_t^P}{\partial x}$$

$$+ \Delta\lambda\frac{\boldsymbol{P}_{vm}}{2\bar{\sigma}\left(\kappa_{t+\Delta t}\right)}\left[\frac{\partial\boldsymbol{D}}{\partial x}\left(\boldsymbol{\varepsilon}_{t+\Delta t} - \boldsymbol{\varepsilon}_{t+\Delta t}^P\right) + \boldsymbol{D}\left(\frac{\partial\boldsymbol{\varepsilon}_{t+\Delta t}}{\partial x} - \frac{\partial\boldsymbol{\varepsilon}_{t+\Delta t}^P}{\partial x}\right)\right]$$

$$- \Delta\lambda\frac{\boldsymbol{P}_{vm}\,\boldsymbol{\sigma}_{t+\Delta t}}{2\left[\bar{\sigma}\left(\kappa_{t+\Delta t}\right)\right]^2}\left[\left[\frac{\partial\bar{\sigma}}{\partial\kappa}\right]_{t+\Delta t}\frac{\partial\kappa_t}{\partial x} + \frac{\partial\bar{\sigma}\left(\kappa_{t+\Delta t}\right)}{\partial x}\right] \qquad (7\text{-}66)$$

Rearranging equation 7-66 to calculate $\dfrac{\partial\boldsymbol{\varepsilon}_{t+\Delta t}^P}{\partial x}$

$$\frac{\partial\boldsymbol{\varepsilon}_{t+\Delta t}^P}{\partial x} = \left[\boldsymbol{I} - \frac{\boldsymbol{P}_{vm}\,\boldsymbol{\sigma}_{t+\Delta t}\,\boldsymbol{\sigma}_{t+\Delta t}^T}{2\left[\bar{\sigma}\left(\kappa_{t+\Delta t}\right)\right]^2}\left(1 - \frac{\Delta\lambda}{\bar{\sigma}\left(\kappa_{t+\Delta t}\right)}\cdot\left[\frac{\partial\bar{\sigma}}{\partial\kappa}\right]_{t+\Delta t}\right) + \frac{\Delta\lambda\boldsymbol{P}_{vm}\boldsymbol{D}}{2\bar{\sigma}\left(\kappa_{t+\Delta t}\right)}\right]^{-1}$$

$$\cdot\left\{\left[\boldsymbol{I} - \frac{\boldsymbol{P}_{vm}\,\boldsymbol{\sigma}_{t+\Delta t}\,\boldsymbol{\sigma}_{t+\Delta t}^T}{2\left[\bar{\sigma}\left(\kappa_{t+\Delta t}\right)\right]^2}\left(1 - \frac{\Delta\lambda}{\bar{\sigma}\left(\kappa_{t+\Delta t}\right)}\cdot\left[\frac{\partial\bar{\sigma}}{\partial\kappa}\right]_{t+\Delta t}\right)\right]\frac{\partial\boldsymbol{\varepsilon}_t^P}{\partial x}\right.$$

$$+ \Delta\lambda\frac{\boldsymbol{P}_{vm}}{2\bar{\sigma}\left(\kappa_{t+\Delta t}\right)}\left[\frac{\partial\boldsymbol{D}}{\partial x}\left(\boldsymbol{\varepsilon}_{t+\Delta t} - \boldsymbol{\varepsilon}_{t+\Delta t}^P\right) + \boldsymbol{D}\frac{\partial\boldsymbol{\varepsilon}_{t+\Delta t}}{\partial x}\right]$$

$$\left.- \Delta\lambda\frac{\boldsymbol{P}_{vm}\,\boldsymbol{\sigma}_{t+\Delta t}}{2\left[\bar{\sigma}\left(\kappa_{t+\Delta t}\right)\right]^2}\left[\left[\frac{\partial\bar{\sigma}}{\partial\kappa}\right]_{t+\Delta t}\frac{\partial\kappa_t}{\partial x} + \frac{\partial\bar{\sigma}\left(\kappa_{t+\Delta t}\right)}{\partial x}\right]\right\} \qquad (7\text{-}67)$$

Once $\dfrac{\partial\boldsymbol{\varepsilon}_{t+\Delta t}^P}{\partial x}$ is found, $\dfrac{\partial\kappa_{t+\Delta t}}{\partial x}$ can be calculated from

$$\frac{\partial\kappa_{t+\Delta t}}{\partial x} = \frac{\partial\kappa_t}{\partial x} + \frac{\boldsymbol{\sigma}_{t+\Delta t}^T}{\bar{\sigma}\left(\kappa_{t+\Delta t}\right)}\left[\frac{\partial\boldsymbol{\varepsilon}_{t+\Delta t}^P}{\partial x} - \frac{\partial\boldsymbol{\varepsilon}_t^P}{\partial x}\right] \qquad (7\text{-}68)$$

7.3.1.2   Rankine/von Mises

As there are eight possible cases depending on which yield surfaces are active, eight different derivations should be done. However, as each derivation is similar, only a representative one

121

will be done and results for all eight cases will be summarized at the end. As a representative case, we will assume that all three yield surfaces are active.

Differentiating equations 7-29–7-35 with respect to a general x for this case

$$\frac{\partial \boldsymbol{\sigma}_{t+\Delta t}}{\partial x} = \frac{\partial \boldsymbol{D}}{\partial x} \left[\boldsymbol{\varepsilon}_{t+\Delta t} - \boldsymbol{\varepsilon}^P_{t+\Delta t} \right] + \boldsymbol{D} \left[\frac{\partial \boldsymbol{\varepsilon}_{t+\Delta t}}{\partial x} - \frac{\partial \boldsymbol{\varepsilon}^P_{t+\Delta t}}{\partial x} \right] \tag{7-69}$$

$$
\begin{aligned}
\frac{\partial \boldsymbol{\varepsilon}^P_{t+\Delta t}}{\partial x} &= \frac{\partial \boldsymbol{\varepsilon}^P_t}{\partial x} + \frac{\partial \Delta \lambda^{(1)}}{\partial x} \left[\frac{\boldsymbol{P}_r \boldsymbol{\sigma}_{t+\Delta t}}{\sqrt{2\boldsymbol{\sigma}^T_{t+\Delta t} \boldsymbol{P}_r \boldsymbol{\sigma}_{t+\Delta t}}} + \tfrac{1}{2}\boldsymbol{\pi}^{(1)} \right] \\
&\quad + \Delta \lambda^{(1)} \left[\frac{\boldsymbol{P}_r}{\sqrt{2\boldsymbol{\sigma}^T_{t+\Delta t}\boldsymbol{P}_r \boldsymbol{\sigma}_{t+\Delta t}}} - \frac{2\boldsymbol{P}_r \boldsymbol{\sigma}_{t+\Delta t}\boldsymbol{\sigma}^T_{t+\Delta t}\boldsymbol{P}_r}{(2\boldsymbol{\sigma}^T_{t+\Delta t}\boldsymbol{P}_r \boldsymbol{\sigma}_{t+\Delta t})^{\frac{3}{2}}} \right] \frac{\partial \boldsymbol{\sigma}_{t+\Delta t}}{\partial x} \\
&\quad + \frac{\partial \Delta \lambda^{(2)}}{\partial x} \cdot \frac{\boldsymbol{P}_{vm} \boldsymbol{\sigma}_{t+\Delta t}}{\sqrt{2\boldsymbol{\sigma}^T_{t+\Delta t}\boldsymbol{P}_{vm}\boldsymbol{\sigma}_{t+\Delta t}}} \\
&\quad + \Delta \lambda^{(2)} \left[\frac{\boldsymbol{P}_{vm}}{\sqrt{2\boldsymbol{\sigma}^T_{t+\Delta t}\boldsymbol{P}_{vm}\boldsymbol{\sigma}_{t+\Delta t}}} - \frac{2\boldsymbol{P}_{vm}\boldsymbol{\sigma}_{t+\Delta t}\boldsymbol{\sigma}^T_{t+\Delta t}\boldsymbol{P}_{vm}}{(2\boldsymbol{\sigma}^T_{t+\Delta t}\boldsymbol{P}_{vm}\boldsymbol{\sigma}_{t+\Delta t})^{\frac{3}{2}}} \right] \frac{\partial \boldsymbol{\sigma}_{t+\Delta t}}{\partial x} \\
&\quad + \frac{\partial \Delta \lambda^{(3)}}{\partial x} \boldsymbol{\pi}^{(3)}
\end{aligned}
\tag{7-70}
$$

$$\frac{\partial \kappa^{(i)}_{t+\Delta t}}{\partial x} = \frac{\partial \kappa^{(i)}_t}{\partial x} + \frac{\partial \Delta \lambda^{(i)}}{\partial x}, \qquad i = 1,2,3 \tag{7-71}$$

$$
\begin{aligned}
\frac{\boldsymbol{\sigma}^T_{t+\Delta t}\boldsymbol{P}_r}{\sqrt{2\boldsymbol{\sigma}^T_{t+\Delta t}\boldsymbol{P}_r \boldsymbol{\sigma}_{t+\Delta t}}} \cdot \frac{\partial \boldsymbol{\sigma}_{t+\Delta t}}{\partial x} &+ \tfrac{1}{2}\boldsymbol{\pi}^{(1)T} \cdot \frac{\partial \boldsymbol{\sigma}_{t+\Delta t}}{\partial x} - \left(\frac{\partial \bar{\sigma}^{(1)}}{\partial \kappa^{(1)}} \right)_{t+\Delta t} \cdot \frac{\partial \kappa^{(1)}_{t+\Delta t}}{\partial x} \\
&\quad - \frac{\partial \bar{\sigma}^{(1)} \left(\kappa^{(1)}_{t+\Delta t} \right)}{\partial x} = 0
\end{aligned}
\tag{7-72}
$$

$$\frac{\boldsymbol{\sigma}^T_{t+\Delta t}\boldsymbol{P}_{vm}}{\sqrt{2\boldsymbol{\sigma}^T_{t+\Delta t}\boldsymbol{P}_{vm}\boldsymbol{\sigma}_{t+\Delta t}}} \cdot \frac{\partial \boldsymbol{\sigma}_{t+\Delta t}}{\partial x} - \left(\frac{\partial \bar{\sigma}^{(2)}}{\partial \kappa^{(2)}} \right)_{t+\Delta t} \cdot \frac{\partial \kappa^{(2)}_{t+\Delta t}}{\partial x} - \frac{\partial \bar{\sigma}^{(2)} \left(\kappa^{(2)}_{t+\Delta t} \right)}{\partial x} = 0 \tag{7-73}$$

122

$$\boldsymbol{\pi}^{(3)T} \cdot \frac{\partial \boldsymbol{\sigma}_{t+\Delta t}}{\partial x} - \left(\frac{\partial \bar{\sigma}^{(3)}}{\partial \kappa^{(3)}}\right)_{t+\Delta t} \cdot \frac{\partial \kappa^{(3)}_{t+\Delta t}}{\partial x} - \frac{\partial \bar{\sigma}^{(3)}\left(\kappa^{(3)}_{t+\Delta t}\right)}{\partial x} = 0 \tag{7-74}$$

Rearranging equations 7-72–7-74

$$\frac{\partial \kappa^{(1)}_{t+\Delta t}}{\partial x} = \left(\frac{\partial \bar{\sigma}^{(1)}}{\partial \kappa^{(1)}}\right)^{-1}_{t+\Delta t} \left[\left(\frac{\boldsymbol{\sigma}^T_{t+\Delta t} \boldsymbol{P}_r}{\sqrt{2\boldsymbol{\sigma}^T_{t+\Delta t} \boldsymbol{P}_r \boldsymbol{\sigma}_{t+\Delta t}}} + \tfrac{1}{2}\boldsymbol{\pi}^{(1)T} \right) \frac{\partial \boldsymbol{\sigma}_{t+\Delta t}}{\partial x} - \frac{\partial \bar{\sigma}^{(1)}\left(\kappa^{(1)}_{t+\Delta t}\right)}{\partial x} \right] \tag{7-75}$$

$$\frac{\partial \kappa^{(2)}_{t+\Delta t}}{\partial x} = \left(\frac{\partial \bar{\sigma}^{(2)}}{\partial \kappa^{(2)}}\right)^{-1}_{t+\Delta t} \left[\frac{\boldsymbol{\sigma}^T_{t+\Delta t} \boldsymbol{P}_{vm}}{\sqrt{2\boldsymbol{\sigma}^T_{t+\Delta t} \boldsymbol{P}_{vm} \boldsymbol{\sigma}_{t+\Delta t}}} \cdot \frac{\partial \boldsymbol{\sigma}_{t+\Delta t}}{\partial x} - \frac{\partial \bar{\sigma}^{(2)}\left(\kappa^{(2)}_{t+\Delta t}\right)}{\partial x} \right] \tag{7-76}$$

$$\frac{\partial \kappa^{(3)}_{t+\Delta t}}{\partial x} = \left(\frac{\partial \bar{\sigma}^{(3)}}{\partial \kappa^{(3)}}\right)^{-1}_{t+\Delta t} \left[\boldsymbol{\pi}^{(3)T} \cdot \frac{\partial \boldsymbol{\sigma}_{t+\Delta t}}{\partial x} - \frac{\partial \bar{\sigma}^{(3)}\left(\kappa^{(3)}_{t+\Delta t}\right)}{\partial x} \right] \tag{7-77}$$

Substitute equations 7-75–7-77 into equation 7-70

$$
\begin{aligned}
\frac{\partial \boldsymbol{\varepsilon}^P_{t+\Delta t}}{\partial x} = {}& \frac{\partial \boldsymbol{\varepsilon}^P_t}{\partial x} \\
& + \left\{ \left(\frac{\partial \bar{\sigma}^{(1)}}{\partial \kappa^{(1)}}\right)^{-1}_{t+\Delta t} \left[\left(\frac{\boldsymbol{\sigma}^T_{t+\Delta t} \boldsymbol{P}_r}{\sqrt{2\boldsymbol{\sigma}^T_{t+\Delta t} \boldsymbol{P}_r \boldsymbol{\sigma}_{t+\Delta t}}} + \tfrac{1}{2}\boldsymbol{\pi}^{(1)T} \right) \frac{\partial \boldsymbol{\sigma}_{t+\Delta t}}{\partial x} \right. \right. \\
& \left. \left. - \frac{\partial \bar{\sigma}^{(1)}\left(\kappa^{(1)}_{t+\Delta t}\right)}{\partial x} \right] - \frac{\partial \kappa^{(1)}_t}{\partial x} \right\} \left\{ \frac{\boldsymbol{P}_r \boldsymbol{\sigma}_{t+\Delta t}}{\sqrt{2\boldsymbol{\sigma}^T_{t+\Delta t} \boldsymbol{P}_r \boldsymbol{\sigma}_{t+\Delta t}}} + \tfrac{1}{2}\boldsymbol{\pi}^{(1)} \right\} \\
& + \Delta\lambda^{(1)} \left[\frac{\boldsymbol{P}_r}{\sqrt{2\boldsymbol{\sigma}^T_{t+\Delta t} \boldsymbol{P}_r \boldsymbol{\sigma}_{t+\Delta t}}} - \frac{2\boldsymbol{P}_r \boldsymbol{\sigma}_{t+\Delta t} \boldsymbol{\sigma}^T_{t+\Delta t} \boldsymbol{P}_r}{(2\boldsymbol{\sigma}^T_{t+\Delta t} \boldsymbol{P}_r \boldsymbol{\sigma}_{t+\Delta t})^{\frac{3}{2}}} \right] \frac{\partial \boldsymbol{\sigma}_{t+\Delta t}}{\partial x} \\
& + \left\{ \left(\frac{\partial \bar{\sigma}^{(2)}}{\partial \kappa^{(2)}}\right)^{-1}_{t+\Delta t} \left[\frac{\boldsymbol{\sigma}^T_{t+\Delta t} \boldsymbol{P}_{vm}}{\sqrt{2\boldsymbol{\sigma}^T_{t+\Delta t} \boldsymbol{P}_{vm} \boldsymbol{\sigma}_{t+\Delta t}}} \cdot \frac{\partial \boldsymbol{\sigma}_{t+\Delta t}}{\partial x} \right. \right. \\
& \left. \left. - \frac{\partial \bar{\sigma}^{(2)}\left(\kappa^{(2)}_{t+\Delta t}\right)}{\partial x} \right] - \frac{\partial \kappa^{(2)}_t}{\partial x} \right\} \frac{\boldsymbol{P}_{vm} \boldsymbol{\sigma}_{t+\Delta t}}{\sqrt{2\boldsymbol{\sigma}^T_{t+\Delta t} \boldsymbol{P}_{vm} \boldsymbol{\sigma}_{t+\Delta t}}}
\end{aligned}
$$

$$
+ \Delta\lambda^{(2)} \left[\frac{\boldsymbol{P}_{vm}}{\sqrt{2\boldsymbol{\sigma}_{t+\Delta t}^T \boldsymbol{P}_{vm} \boldsymbol{\sigma}_{t+\Delta t}}} - \frac{2\boldsymbol{P}_{vm}\boldsymbol{\sigma}_{t+\Delta t}\boldsymbol{\sigma}_{t+\Delta t}^T \boldsymbol{P}_{vm}}{\left(2\boldsymbol{\sigma}_{t+\Delta t}^T \boldsymbol{P}_{vm} \boldsymbol{\sigma}_{t+\Delta t}\right)^{\frac{3}{2}}} \right] \frac{\partial\,\boldsymbol{\sigma}_{t+\Delta t}}{\partial x}
$$

$$
+ \left\{ \left(\frac{\partial\bar{\sigma}^{(3)}}{\partial\kappa^{(3)}}\right)_{t+\Delta t}^{-1} \left[\boldsymbol{\pi}^{(3)T} \cdot \frac{\partial\,\boldsymbol{\sigma}_{t+\Delta t}}{\partial x} - \frac{\partial\bar{\sigma}^{(3)}\left(\kappa_{t+\Delta t}^{(3)}\right)}{\partial x} \right] - \frac{\partial\kappa_t^{(3)}}{\partial x} \right\} \boldsymbol{\pi}^{(3)}
$$

$$
= \frac{\partial\,\boldsymbol{\varepsilon}_t^P}{\partial x}
$$

$$
+ \left\{ \left(\frac{\partial\bar{\sigma}^{(1)}}{\partial\kappa^{(1)}}\right)_{t+\Delta t}^{-1} \left[\frac{\boldsymbol{P}_r\boldsymbol{\sigma}_{t+\Delta t}}{\sqrt{2\boldsymbol{\sigma}_{t+\Delta t}^T \boldsymbol{P}_r \boldsymbol{\sigma}_{t+\Delta t}}} + \tfrac{1}{2}\boldsymbol{\pi}^{(1)} \right] \left[\frac{\boldsymbol{\sigma}_{t+\Delta t}^T \boldsymbol{P}_r}{\sqrt{2\boldsymbol{\sigma}_{t+\Delta t}^T \boldsymbol{P}_r \boldsymbol{\sigma}_{t+\Delta t}}} \right. \right.
$$

$$
\left. + \tfrac{1}{2}\boldsymbol{\pi}^{(1)T} \right] + \Delta\lambda^{(1)} \left[\frac{\boldsymbol{P}_r}{\sqrt{2\boldsymbol{\sigma}_{t+\Delta t}^T \boldsymbol{P}_r \boldsymbol{\sigma}_{t+\Delta t}}} - \frac{2\boldsymbol{P}_r\boldsymbol{\sigma}_{t+\Delta t}\boldsymbol{\sigma}_{t+\Delta t}^T \boldsymbol{P}_r}{\left(2\boldsymbol{\sigma}_{t+\Delta t}^T \boldsymbol{P}_r \boldsymbol{\sigma}_{t+\Delta t}\right)^{\frac{3}{2}}} \right]
$$

$$
+ \left(\frac{\partial\bar{\sigma}^{(2)}}{\partial\kappa^{(2)}}\right)_{t+\Delta t}^{-1} \cdot \frac{\boldsymbol{P}_{vm}\boldsymbol{\sigma}_{t+\Delta t}}{\sqrt{2\boldsymbol{\sigma}_{t+\Delta t}^T \boldsymbol{P}_{vm} \boldsymbol{\sigma}_{t+\Delta t}}} \cdot \frac{\boldsymbol{\sigma}_{t+\Delta t}^T \boldsymbol{P}_{vm}}{\sqrt{2\boldsymbol{\sigma}_{t+\Delta t}^T \boldsymbol{P}_{vm} \boldsymbol{\sigma}_{t+\Delta t}}}
$$

$$
+ \Delta\lambda^{(2)} \left[\frac{\boldsymbol{P}_{vm}}{\sqrt{2\boldsymbol{\sigma}_{t+\Delta t}^T \boldsymbol{P}_{vm} \boldsymbol{\sigma}_{t+\Delta t}}} - \frac{2\boldsymbol{P}_{vm}\boldsymbol{\sigma}_{t+\Delta t}\boldsymbol{\sigma}_{t+\Delta t}^T \boldsymbol{P}_{vm}}{\left(2\boldsymbol{\sigma}_{t+\Delta t}^T \boldsymbol{P}_{vm} \boldsymbol{\sigma}_{t+\Delta t}\right)^{\frac{3}{2}}} \right]
$$

$$
+ \left(\frac{\partial\bar{\sigma}^{(3)}}{\partial\kappa^{(3)}}\right)_{t+\Delta t}^{-1} \boldsymbol{\pi}^{(3)}\boldsymbol{\pi}^{(3)T} \right\} \frac{\partial\,\boldsymbol{\sigma}_{t+\Delta t}}{\partial x}
$$

$$
- \left[\left(\frac{\partial\bar{\sigma}^{(1)}}{\partial\kappa^{(1)}}\right)_{t+\Delta t}^{-1} \frac{\partial\bar{\sigma}^{(1)}\left(\kappa_{t+\Delta t}^{(1)}\right)}{\partial x} + \frac{\partial\kappa_t^{(1)}}{\partial x} \right]
$$

$$
\cdot \left[\frac{\boldsymbol{P}_r\boldsymbol{\sigma}_{t+\Delta t}}{\sqrt{2\boldsymbol{\sigma}_{t+\Delta t}^T \boldsymbol{P}_r \boldsymbol{\sigma}_{t+\Delta t}}} + \tfrac{1}{2}\boldsymbol{\pi}^{(1)} \right]
$$

$$
- \left[\left(\frac{\partial\bar{\sigma}^{(2)}}{\partial\kappa^{(2)}}\right)_{t+\Delta t}^{-1} \frac{\partial\bar{\sigma}^{(2)}\left(\kappa_{t+\Delta t}^{(2)}\right)}{\partial x} + \frac{\partial\kappa_t^{(2)}}{\partial x} \right] \frac{\boldsymbol{P}_{vm}}{\sqrt{2\boldsymbol{\sigma}_{t+\Delta t}^T \boldsymbol{P}_{vm} \boldsymbol{\sigma}_{t+\Delta t}}}
$$

$$
- \left[\left(\frac{\partial\bar{\sigma}^{(3)}}{\partial\kappa^{(3)}}\right)_{t+\Delta t}^{-1} \frac{\partial\bar{\sigma}^{(3)}\left(\kappa_{t+\Delta t}^{(3)}\right)}{\partial x} + \frac{\partial\kappa_t^{(3)}}{\partial x} \right] \boldsymbol{\pi}^{(3)} \tag{7-78}
$$

124

Substitute equation 7-78 into equation 7-69

$$
\begin{aligned}
\frac{\partial \boldsymbol{\sigma}_{t+\Delta t}}{\partial x} \;=\;& \frac{\partial \boldsymbol{D}}{\partial x}\left[\boldsymbol{\varepsilon}_{t+\Delta t}-\boldsymbol{\varepsilon}_{t+\Delta t}^{P}\right]+\boldsymbol{D}\left\{\frac{\partial \boldsymbol{\varepsilon}_{t+\Delta t}}{\partial x}-\frac{\partial \boldsymbol{\varepsilon}_{t}^{P}}{\partial x}\right\} \\[2mm]
& -\boldsymbol{D}\left\{\left(\frac{\partial \bar{\sigma}^{(1)}}{\partial \kappa^{(1)}}\right)_{t+\Delta t}^{-1}\left[\frac{\boldsymbol{P}_{r}\boldsymbol{\sigma}_{t+\Delta t}}{\sqrt{2\boldsymbol{\sigma}_{t+\Delta t}^{T}\boldsymbol{P}_{r}\boldsymbol{\sigma}_{t+\Delta t}}}+\tfrac{1}{2}\boldsymbol{\pi}^{(1)}\right]\right. \\[2mm]
& \cdot\left[\frac{\boldsymbol{\sigma}_{t+\Delta t}^{T}\boldsymbol{P}_{r}}{\sqrt{2\boldsymbol{\sigma}_{t+\Delta t}^{T}\boldsymbol{P}_{r}\boldsymbol{\sigma}_{t+\Delta t}}}+\tfrac{1}{2}\boldsymbol{\pi}^{(1)T}\right] \\[2mm]
& +\Delta\lambda^{(1)}\left[\frac{\boldsymbol{P}_{r}}{\sqrt{2\boldsymbol{\sigma}_{t+\Delta t}^{T}\boldsymbol{P}_{r}\boldsymbol{\sigma}_{t+\Delta t}}}-\frac{2\boldsymbol{P}_{r}\boldsymbol{\sigma}_{t+\Delta t}\boldsymbol{\sigma}_{t+\Delta t}^{T}\boldsymbol{P}_{r}}{(2\boldsymbol{\sigma}_{t+\Delta t}^{T}\boldsymbol{P}_{r}\boldsymbol{\sigma}_{t+\Delta t})^{\frac{3}{2}}}\right] \\[2mm]
& +\left(\frac{\partial \bar{\sigma}^{(2)}}{\partial \kappa^{(2)}}\right)_{t+\Delta t}^{-1}\cdot\frac{\boldsymbol{P}_{vm}\boldsymbol{\sigma}_{t+\Delta t}}{\sqrt{2\boldsymbol{\sigma}_{t+\Delta t}^{T}\boldsymbol{P}_{vm}\boldsymbol{\sigma}_{t+\Delta t}}}\cdot\frac{\boldsymbol{\sigma}_{t+\Delta t}^{T}\boldsymbol{P}_{vm}}{\sqrt{2\boldsymbol{\sigma}_{t+\Delta t}^{T}\boldsymbol{P}_{vm}\boldsymbol{\sigma}_{t+\Delta t}}} \\[2mm]
& +\Delta\lambda^{(2)}\left[\frac{\boldsymbol{P}_{vm}}{\sqrt{2\boldsymbol{\sigma}_{t+\Delta t}^{T}\boldsymbol{P}_{vm}\boldsymbol{\sigma}_{t+\Delta t}}}-\frac{2\boldsymbol{P}_{vm}\boldsymbol{\sigma}_{t+\Delta t}\boldsymbol{\sigma}_{t+\Delta t}^{T}\boldsymbol{P}_{vm}}{(2\boldsymbol{\sigma}_{t+\Delta t}^{T}\boldsymbol{P}_{vm}\boldsymbol{\sigma}_{t+\Delta t})^{\frac{3}{2}}}\right] \\[2mm]
& \left.+\left(\frac{\partial \bar{\sigma}^{(3)}}{\partial \kappa^{(3)}}\right)_{t+\Delta t}^{-1}\boldsymbol{\pi}^{(3)}\boldsymbol{\pi}^{(3)T}\right\}\frac{\partial \boldsymbol{\sigma}_{t+\Delta t}}{\partial x} \\[2mm]
& +\boldsymbol{D}\left[\left(\frac{\partial \bar{\sigma}^{(1)}}{\partial \kappa^{(1)}}\right)_{t+\Delta t}^{-1}\frac{\partial \bar{\sigma}^{(1)}\left(\kappa_{t+\Delta t}^{(1)}\right)}{\partial x}+\frac{\partial \kappa_{t}^{(1)}}{\partial x}\right] \\[2mm]
& \cdot\left[\frac{\boldsymbol{P}_{r}\boldsymbol{\sigma}_{t+\Delta t}}{\sqrt{2\boldsymbol{\sigma}_{t+\Delta t}^{T}\boldsymbol{P}_{r}\boldsymbol{\sigma}_{t+\Delta t}}}+\tfrac{1}{2}\boldsymbol{\pi}^{(1)}\right] \\[2mm]
& +\boldsymbol{D}\left[\left(\frac{\partial \bar{\sigma}^{(2)}}{\partial \kappa^{(2)}}\right)_{t+\Delta t}^{-1}\frac{\partial \bar{\sigma}^{(2)}\left(\kappa_{t+\Delta t}^{(2)}\right)}{\partial x}+\frac{\partial \kappa_{t}^{(2)}}{\partial x}\right]\frac{\boldsymbol{P}_{vm}}{\sqrt{2\boldsymbol{\sigma}_{t+\Delta t}^{T}\boldsymbol{P}_{vm}\boldsymbol{\sigma}_{t+\Delta t}}} \\[2mm]
& +\boldsymbol{D}\left[\left(\frac{\partial \bar{\sigma}^{(3)}}{\partial \kappa^{(3)}}\right)_{t+\Delta t}^{-1}\frac{\partial \bar{\sigma}^{(3)}\left(\kappa_{t+\Delta t}^{(3)}\right)}{\partial x}+\frac{\partial \kappa_{t}^{(3)}}{\partial x}\right]\boldsymbol{\pi}^{(3)} \qquad\text{(7-79)}
\end{aligned}
$$

125

Rearranging equation 7-79

$$
\frac{\partial \boldsymbol{\sigma}_{t+\Delta t}}{\partial x} = \left\{ \boldsymbol{I} + \boldsymbol{D} \left[\left(\frac{\partial \bar{\sigma}^{(1)}}{\partial \kappa^{(1)}} \right)^{-1}_{t+\Delta t} \left(\frac{\boldsymbol{P}_r \boldsymbol{\sigma}_{t+\Delta t}}{\sqrt{2\boldsymbol{\sigma}^T_{t+\Delta t} \boldsymbol{P}_r \boldsymbol{\sigma}_{t+\Delta t}}} + \tfrac{1}{2}\boldsymbol{\pi}^{(1)} \right) \right. \right.
$$

$$
\cdot \left(\frac{\boldsymbol{\sigma}^T_{t+\Delta t} \boldsymbol{P}_r}{\sqrt{2\boldsymbol{\sigma}^T_{t+\Delta t} \boldsymbol{P}_r \boldsymbol{\sigma}_{t+\Delta t}}} + \tfrac{1}{2}\boldsymbol{\pi}^{(1)T} \right)
$$

$$
+ \Delta\lambda^{(1)} \left(\frac{\boldsymbol{P}_r}{\sqrt{2\boldsymbol{\sigma}^T_{t+\Delta t} \boldsymbol{P}_r \boldsymbol{\sigma}_{t+\Delta t}}} - \frac{2\boldsymbol{P}_r \boldsymbol{\sigma}_{t+\Delta t} \boldsymbol{\sigma}^T_{t+\Delta t} \boldsymbol{P}_r}{(2\boldsymbol{\sigma}^T_{t+\Delta t} \boldsymbol{P}_r \boldsymbol{\sigma}_{t+\Delta t})^{\frac{3}{2}}} \right)
$$

$$
+ \left(\frac{\partial \bar{\sigma}^{(2)}}{\partial \kappa^{(2)}} \right)^{-1}_{t+\Delta t} \cdot \frac{\boldsymbol{P}_{vm} \boldsymbol{\sigma}_{t+\Delta t}}{\sqrt{2\boldsymbol{\sigma}^T_{t+\Delta t} \boldsymbol{P}_{vm} \boldsymbol{\sigma}_{t+\Delta t}}} \cdot \frac{\boldsymbol{\sigma}^T_{t+\Delta t} \boldsymbol{P}_{vm}}{\sqrt{2\boldsymbol{\sigma}^T_{t+\Delta t} \boldsymbol{P}_{vm} \boldsymbol{\sigma}_{t+\Delta t}}}
$$

$$
+ \Delta\lambda^{(2)} \left(\frac{\boldsymbol{P}_{vm}}{\sqrt{2\boldsymbol{\sigma}^T_{t+\Delta t} \boldsymbol{P}_{vm} \boldsymbol{\sigma}_{t+\Delta t}}} - \frac{2\boldsymbol{P}_{vm} \boldsymbol{\sigma}_{t+\Delta t} \boldsymbol{\sigma}^T_{t+\Delta t} \boldsymbol{P}_{vm}}{(2\boldsymbol{\sigma}^T_{t+\Delta t} \boldsymbol{P}_{vm} \boldsymbol{\sigma}_{t+\Delta t})^{\frac{3}{2}}} \right)
$$

$$
\left. \left. + \left(\frac{\partial \bar{\sigma}^{(3)}}{\partial \kappa^{(3)}} \right)^{-1}_{t+\Delta t} \boldsymbol{\pi}^{(3)} \boldsymbol{\pi}^{(3)T} \right] \right\}^{-1}
$$

$$
\cdot \left\{ \frac{\partial \boldsymbol{D}}{\partial x} \left[\boldsymbol{\varepsilon}_{t+\Delta t} - \boldsymbol{\varepsilon}^P_{t+\Delta t} \right] + \boldsymbol{D} \left[\frac{\partial \boldsymbol{\varepsilon}_{t+\Delta t}}{\partial x} - \frac{\partial \boldsymbol{\varepsilon}^P_t}{\partial x} \right] \right.
$$

$$
+ \boldsymbol{D} \left[\left(\frac{\partial \bar{\sigma}^{(1)}}{\partial \kappa^{(1)}} \right)^{-1}_{t+\Delta t} \frac{\partial \bar{\sigma}^{(1)} \left(\kappa^{(1)}_{t+\Delta t} \right)}{\partial x} + \frac{\partial \kappa^{(1)}_t}{\partial x} \right]
$$

$$
\cdot \left[\frac{\boldsymbol{P}_r \boldsymbol{\sigma}_{t+\Delta t}}{\sqrt{2\boldsymbol{\sigma}^T_{t+\Delta t} \boldsymbol{P}_r \boldsymbol{\sigma}_{t+\Delta t}}} + \tfrac{1}{2}\boldsymbol{\pi}^{(1)} \right]
$$

$$
+ \boldsymbol{D} \left[\left(\frac{\partial \bar{\sigma}^{(2)}}{\partial \kappa^{(2)}} \right)^{-1}_{t+\Delta t} \frac{\partial \bar{\sigma}^{(2)} \left(\kappa^{(2)}_{t+\Delta t} \right)}{\partial x} + \frac{\partial \kappa^{(2)}_t}{\partial x} \right] \frac{\boldsymbol{P}_{vm}}{\sqrt{2\boldsymbol{\sigma}^T_{t+\Delta t} \boldsymbol{P}_{vm} \boldsymbol{\sigma}_{t+\Delta t}}}
$$

$$
\left. + \boldsymbol{D} \left[\left(\frac{\partial \bar{\sigma}^{(3)}}{\partial \kappa^{(3)}} \right)^{-1}_{t+\Delta t} \frac{\partial \bar{\sigma}^{(3)} \left(\kappa^{(3)}_{t+\Delta t} \right)}{\partial x} + \frac{\partial \kappa^{(3)}_t}{\partial x} \right] \boldsymbol{\pi}^{(3)} \right\} \tag{7-80}
$$

Setting $\dfrac{\partial \boldsymbol{\varepsilon}_{t+\Delta t}}{\partial x}$ to zero on the right hand side of equation 7-80 results in an equation for the

quantity required

$$\left.\frac{\partial \boldsymbol{\sigma}_{t+\Delta t}}{\partial x}\right|_{\boldsymbol{u},\dot{\boldsymbol{u}},\boldsymbol{z}} + \frac{\partial \boldsymbol{\sigma}_{t+\Delta t}}{\partial \boldsymbol{z}_{t+\Delta t}}\frac{\partial \boldsymbol{z}_{t+\Delta t}}{\partial x} =$$

$$\left\{ \boldsymbol{I} + \boldsymbol{D}\left[\left(\frac{\partial \bar{\sigma}^{(1)}}{\partial \kappa^{(1)}}\right)^{-1}_{t+\Delta t} \left(\frac{\boldsymbol{P}_r \boldsymbol{\sigma}_{t+\Delta t}}{\sqrt{2\boldsymbol{\sigma}_{t+\Delta t}^T \boldsymbol{P}_r \boldsymbol{\sigma}_{t+\Delta t}}} + \tfrac{1}{2}\boldsymbol{\pi}^{(1)} \right) \right.\right.$$

$$\cdot \left(\frac{\boldsymbol{\sigma}_{t+\Delta t}^T \boldsymbol{P}_r}{\sqrt{2\boldsymbol{\sigma}_{t+\Delta t}^T \boldsymbol{P}_r \boldsymbol{\sigma}_{t+\Delta t}}} + \tfrac{1}{2}\boldsymbol{\pi}^{(1)T} \right)$$

$$+ \Delta\lambda^{(1)} \left(\frac{\boldsymbol{P}_r}{\sqrt{2\boldsymbol{\sigma}_{t+\Delta t}^T \boldsymbol{P}_r \boldsymbol{\sigma}_{t+\Delta t}}} - \frac{2\boldsymbol{P}_r \boldsymbol{\sigma}_{t+\Delta t} \boldsymbol{\sigma}_{t+\Delta t}^T \boldsymbol{P}_r}{(2\boldsymbol{\sigma}_{t+\Delta t}^T \boldsymbol{P}_r \boldsymbol{\sigma}_{t+\Delta t})^{\frac{3}{2}}} \right)$$

$$+ \left(\frac{\partial \bar{\sigma}^{(2)}}{\partial \kappa^{(2)}}\right)^{-1}_{t+\Delta t} \cdot \frac{\boldsymbol{P}_{vm} \boldsymbol{\sigma}_{t+\Delta t}}{\sqrt{2\boldsymbol{\sigma}_{t+\Delta t}^T \boldsymbol{P}_{vm} \boldsymbol{\sigma}_{t+\Delta t}}} \cdot \frac{\boldsymbol{\sigma}_{t+\Delta t}^T \boldsymbol{P}_{vm}}{\sqrt{2\boldsymbol{\sigma}_{t+\Delta t}^T \boldsymbol{P}_{vm} \boldsymbol{\sigma}_{t+\Delta t}}}$$

$$+ \Delta\lambda^{(2)} \left(\frac{\boldsymbol{P}_{vm}}{\sqrt{2\boldsymbol{\sigma}_{t+\Delta t}^T \boldsymbol{P}_{vm} \boldsymbol{\sigma}_{t+\Delta t}}} - \frac{2\boldsymbol{P}_{vm} \boldsymbol{\sigma}_{t+\Delta t} \boldsymbol{\sigma}_{t+\Delta t}^T \boldsymbol{P}_{vm}}{(2\boldsymbol{\sigma}_{t+\Delta t}^T \boldsymbol{P}_{vm} \boldsymbol{\sigma}_{t+\Delta t})^{\frac{3}{2}}} \right) \tag{7-81}$$

$$\left.\left. + \left(\frac{\partial \bar{\sigma}^{(3)}}{\partial \kappa^{(3)}}\right)^{-1}_{t+\Delta t} \boldsymbol{\pi}^{(3)} \boldsymbol{\pi}^{(3)T} \right] \right\}^{-1}$$

$$\cdot \left\{ \frac{\partial \boldsymbol{D}}{\partial x}\left[\boldsymbol{\varepsilon}_{t+\Delta t} - \boldsymbol{\varepsilon}_{t+\Delta t}^P \right] + \boldsymbol{D}\left[-\frac{\partial \boldsymbol{\varepsilon}_t^P}{\partial x} \right] \right.$$

$$+ \boldsymbol{D}\left[\left(\frac{\partial \bar{\sigma}^{(1)}}{\partial \kappa^{(1)}}\right)^{-1}_{t+\Delta t} \frac{\partial \bar{\sigma}^{(1)}\left(\kappa_{t+\Delta t}^{(1)}\right)}{\partial x} + \frac{\partial \kappa_t^{(1)}}{\partial x} \right]$$

$$\cdot \left[\frac{\boldsymbol{P}_r \boldsymbol{\sigma}_{t+\Delta t}}{\sqrt{2\boldsymbol{\sigma}_{t+\Delta t}^T \boldsymbol{P}_r \boldsymbol{\sigma}_{t+\Delta t}}} + \tfrac{1}{2}\boldsymbol{\pi}^{(1)} \right]$$

$$+ \boldsymbol{D}\left[\left(\frac{\partial \bar{\sigma}^{(2)}}{\partial \kappa^{(2)}}\right)^{-1}_{t+\Delta t} \frac{\partial \bar{\sigma}^{(2)}\left(\kappa_{t+\Delta t}^{(2)}\right)}{\partial x} + \frac{\partial \kappa_t^{(2)}}{\partial x} \right] \frac{\boldsymbol{P}_{vm}}{\sqrt{2\boldsymbol{\sigma}_{t+\Delta t}^T \boldsymbol{P}_{vm} \boldsymbol{\sigma}_{t+\Delta t}}}$$

$$\left. + \boldsymbol{D}\left[\left(\frac{\partial \bar{\sigma}^{(3)}}{\partial \kappa^{(3)}}\right)^{-1}_{t+\Delta t} \frac{\partial \bar{\sigma}^{(3)}\left(\kappa_{t+\Delta t}^{(3)}\right)}{\partial x} + \frac{\partial \kappa_t^{(3)}}{\partial x} \right] \boldsymbol{\pi}^{(3)} \right\}$$

The terms on the right hand side of equation 7-81 can easily be calculated from equations 7-36–7-38 and are given below.

- If the uncertain parameter x is the elastic modulus YOUNG or Poisson's ratio POISON then $\dfrac{\partial \boldsymbol{D}}{\partial x}$ is nonzero, but depends on the element formulation. It is typically not

127

difficult to find. In this case $\dfrac{\partial \bar{\sigma}^{(i)}\left(\kappa^{(i)}_{t+\Delta t}\right)}{\partial x}$ is zero for all i.

- If the uncertain parameter x is the tensile yield stress `YLDVAL` then $\dfrac{\partial \boldsymbol{D}}{\partial x}$ is zero and

$$
\frac{\partial \bar{\sigma}^{(i)}\left(\kappa^{(i)}_{t+\Delta t}\right)}{\partial x} = \begin{cases} 1 - \dfrac{h(\texttt{YLDVAL})}{\texttt{HARVAL}}\kappa^{(i)}_{t+\Delta t}, & i = 1,3 \\ 0, & i = 2 \end{cases} \tag{7-82}
$$

- If the uncertain parameter x is the compressive yield stress `YLDCMP` then $\dfrac{\partial \boldsymbol{D}}{\partial x}$ is zero and

$$
\frac{\partial \bar{\sigma}^{(i)}\left(\kappa^{(i)}_{t+\Delta t}\right)}{\partial x} = \begin{cases} 0, & i = 1,3 \\ 1, & i = 2 \end{cases} \tag{7-83}
$$

- If the uncertain parameter x is the fracture energy `HARVAL` then $\dfrac{\partial \boldsymbol{D}}{\partial x}$ is zero and

$$
\frac{\partial \bar{\sigma}^{(i)}\left(\kappa^{(i)}_{t+\Delta t}\right)}{\partial x} = \begin{cases} \dfrac{h(\texttt{YLDVAL})^2}{2(\texttt{HARVAL})^2}\kappa^{(i)}_{t+\Delta t}, & i = 1,3 \\ 0, & i = 2 \end{cases} \tag{7-84}
$$

- If the uncertain parameter x is the plastic modulus `CMPVAL` then $\dfrac{\partial \boldsymbol{D}}{\partial x}$ is zero and

$$
\frac{\partial \bar{\sigma}^{(i)}\left(\kappa^{(i)}_{t+\Delta t}\right)}{\partial x} = \begin{cases} 0, & i = 1,3 \\ \kappa^{(i)}_{t+\Delta t}, & i = 2 \end{cases} \tag{7-85}
$$

- If the uncertain parameter x is not a parameter of this element then $\dfrac{\partial \boldsymbol{D}}{\partial x}$ and $\dfrac{\partial \bar{\sigma}^{(i)}\left(\kappa^{(i)}_{t+\Delta t}\right)}{\partial x}, i = 1,2,3$ are zero.

Finally, from equations 7-36–7-38 it is also clear that

$$
\left(\frac{\partial \bar{\sigma}^{(i)}}{\partial \kappa^{(i)}}\right)_{t+\Delta t} = \begin{cases} -\dfrac{h(\texttt{YLDVAL})^2}{2(\texttt{HARVAL})}, & i = 1,3 \\ \texttt{CMPVAL}, & i = 2 \end{cases} \tag{7-86}
$$

128

The history-dependent variables are $\boldsymbol{\varepsilon}^P$ and κ. To find an equation for $\dfrac{\partial\, \boldsymbol{\varepsilon}^P_{t+\Delta t}}{\partial x}$, substitute equation 7-69 into equation 7-78

$$
\begin{aligned}
\frac{\partial\, \boldsymbol{\varepsilon}^P_{t+\Delta t}}{\partial x} \;=\;& \frac{\partial\, \boldsymbol{\varepsilon}^P_t}{\partial x} \\[4pt]
&+ \left\{ \left(\frac{\partial \bar{\sigma}^{(1)}}{\partial \kappa^{(1)}}\right)^{-1}_{t+\Delta t} \left[\frac{\boldsymbol{P}_r \boldsymbol{\sigma}_{t+\Delta t}}{\sqrt{2\boldsymbol{\sigma}^T_{t+\Delta t}\boldsymbol{P}_r \boldsymbol{\sigma}_{t+\Delta t}}} + \tfrac{1}{2}\boldsymbol{\pi}^{(1)} \right] \right. \\[4pt]
&\quad\cdot \left[\frac{\boldsymbol{\sigma}^T_{t+\Delta t}\boldsymbol{P}_r}{\sqrt{2\boldsymbol{\sigma}^T_{t+\Delta t}\boldsymbol{P}_r \boldsymbol{\sigma}_{t+\Delta t}}} + \tfrac{1}{2}\boldsymbol{\pi}^{(1)T} \right] \\[4pt]
&\quad + \Delta\lambda^{(1)} \left[\frac{\boldsymbol{P}_r}{\sqrt{2\boldsymbol{\sigma}^T_{t+\Delta t}\boldsymbol{P}_r \boldsymbol{\sigma}_{t+\Delta t}}} - \frac{2\boldsymbol{P}_r \boldsymbol{\sigma}_{t+\Delta t}\boldsymbol{\sigma}^T_{t+\Delta t}\boldsymbol{P}_r}{(2\boldsymbol{\sigma}^T_{t+\Delta t}\boldsymbol{P}_r \boldsymbol{\sigma}_{t+\Delta t})^{\frac{3}{2}}} \right] \\[4pt]
&\quad + \left(\frac{\partial \bar{\sigma}^{(2)}}{\partial \kappa^{(2)}}\right)^{-1}_{t+\Delta t} \cdot \frac{\boldsymbol{P}_{vm} \boldsymbol{\sigma}_{t+\Delta t}}{\sqrt{2\boldsymbol{\sigma}^T_{t+\Delta t}\boldsymbol{P}_{vm} \boldsymbol{\sigma}_{t+\Delta t}}} \cdot \frac{\boldsymbol{\sigma}^T_{t+\Delta t}\boldsymbol{P}_{vm}}{\sqrt{2\boldsymbol{\sigma}^T_{t+\Delta t}\boldsymbol{P}_{vm} \boldsymbol{\sigma}_{t+\Delta t}}} \\[4pt]
&\quad + \Delta\lambda^{(2)} \left[\frac{\boldsymbol{P}_{vm}}{\sqrt{2\boldsymbol{\sigma}^T_{t+\Delta t}\boldsymbol{P}_{vm} \boldsymbol{\sigma}_{t+\Delta t}}} - \frac{2\boldsymbol{P}_{vm} \boldsymbol{\sigma}_{t+\Delta t}\boldsymbol{\sigma}^T_{t+\Delta t}\boldsymbol{P}_{vm}}{(2\boldsymbol{\sigma}^T_{t+\Delta t}\boldsymbol{P}_{vm} \boldsymbol{\sigma}_{t+\Delta t})^{\frac{3}{2}}} \right] \\[4pt]
&\quad \left. + \left(\frac{\partial \bar{\sigma}^{(3)}}{\partial \kappa^{(3)}}\right)^{-1}_{t+\Delta t} \boldsymbol{\pi}^{(3)}\boldsymbol{\pi}^{(3)T} \right\} \left\{ \frac{\partial \boldsymbol{D}}{\partial x}\left[\boldsymbol{\varepsilon}_{t+\Delta t} - \boldsymbol{\varepsilon}^P_{t+\Delta t}\right] \right. \\[4pt]
&\quad \left. + \boldsymbol{D}\left[\frac{\partial\, \boldsymbol{\varepsilon}_{t+\Delta t}}{\partial x} - \frac{\partial\, \boldsymbol{\varepsilon}^P_{t+\Delta t}}{\partial x}\right] \right\} \\[4pt]
&- \left[\left(\frac{\partial \bar{\sigma}^{(1)}}{\partial \kappa^{(1)}}\right)^{-1}_{t+\Delta t} \frac{\partial \bar{\sigma}^{(1)}\left(\kappa^{(1)}_{t+\Delta t}\right)}{\partial x} + \frac{\partial \kappa^{(1)}_t}{\partial x} \right] \left[\frac{\boldsymbol{P}_r \boldsymbol{\sigma}_{t+\Delta t}}{\sqrt{2\boldsymbol{\sigma}^T_{t+\Delta t}\boldsymbol{P}_r \boldsymbol{\sigma}_{t+\Delta t}}} + \tfrac{1}{2}\boldsymbol{\pi}^{(1)} \right] \\[4pt]
&- \left[\left(\frac{\partial \bar{\sigma}^{(2)}}{\partial \kappa^{(2)}}\right)^{-1}_{t+\Delta t} \frac{\partial \bar{\sigma}^{(2)}\left(\kappa^{(2)}_{t+\Delta t}\right)}{\partial x} + \frac{\partial \kappa^{(2)}_t}{\partial x} \right] \frac{\boldsymbol{P}_{vm}}{\sqrt{2\boldsymbol{\sigma}^T_{t+\Delta t}\boldsymbol{P}_{vm} \boldsymbol{\sigma}_{t+\Delta t}}} \\[4pt]
&- \left[\left(\frac{\partial \bar{\sigma}^{(3)}}{\partial \kappa^{(3)}}\right)^{-1}_{t+\Delta t} \frac{\partial \bar{\sigma}^{(3)}\left(\kappa^{(3)}_{t+\Delta t}\right)}{\partial x} + \frac{\partial \kappa^{(3)}_t}{\partial x} \right] \boldsymbol{\pi}^{(3)}
\end{aligned}
\tag{7-87}
$$

Rearranging equation 7-87

$$
\begin{aligned}
\frac{\partial\, \boldsymbol{\varepsilon}_{t+\Delta t}^{P}}{\partial x} \;=\; & \left\{ \boldsymbol{I} + \left[\left(\frac{\partial \bar{\sigma}^{(1)}}{\partial \kappa^{(1)}}\right)^{-1}_{t+\Delta t} \left(\frac{\boldsymbol{P}_r \boldsymbol{\sigma}_{t+\Delta t}}{\sqrt{2\boldsymbol{\sigma}_{t+\Delta t}^T \boldsymbol{P}_r \boldsymbol{\sigma}_{t+\Delta t}}} + \tfrac{1}{2}\boldsymbol{\pi}^{(1)}\right) \right. \right. \\[2mm]
& \left(\frac{\boldsymbol{\sigma}_{t+\Delta t}^T \boldsymbol{P}_r}{\sqrt{2\boldsymbol{\sigma}_{t+\Delta t}^T \boldsymbol{P}_r \boldsymbol{\sigma}_{t+\Delta t}}} + \tfrac{1}{2}\boldsymbol{\pi}^{(1)T}\right) \\[2mm]
& + \Delta\lambda^{(1)} \left(\frac{\boldsymbol{P}_r}{\sqrt{2\boldsymbol{\sigma}_{t+\Delta t}^T \boldsymbol{P}_r \boldsymbol{\sigma}_{t+\Delta t}}} - \frac{2\boldsymbol{P}_r \boldsymbol{\sigma}_{t+\Delta t}\boldsymbol{\sigma}_{t+\Delta t}^T \boldsymbol{P}_r}{\left(2\boldsymbol{\sigma}_{t+\Delta t}^T \boldsymbol{P}_r \boldsymbol{\sigma}_{t+\Delta t}\right)^{\frac{3}{2}}}\right) \\[2mm]
& + \left(\frac{\partial \bar{\sigma}^{(2)}}{\partial \kappa^{(2)}}\right)^{-1}_{t+\Delta t} \cdot \frac{\boldsymbol{P}_{vm} \boldsymbol{\sigma}_{t+\Delta t}}{\sqrt{2\boldsymbol{\sigma}_{t+\Delta t}^T \boldsymbol{P}_{vm} \boldsymbol{\sigma}_{t+\Delta t}}} \cdot \frac{\boldsymbol{\sigma}_{t+\Delta t}^T \boldsymbol{P}_{vm}}{\sqrt{2\boldsymbol{\sigma}_{t+\Delta t}^T \boldsymbol{P}_{vm} \boldsymbol{\sigma}_{t+\Delta t}}} \\[2mm]
& + \Delta\lambda^{(2)} \left(\frac{\boldsymbol{P}_{vm}}{\sqrt{2\boldsymbol{\sigma}_{t+\Delta t}^T \boldsymbol{P}_{vm} \boldsymbol{\sigma}_{t+\Delta t}}} - \frac{2\boldsymbol{P}_{vm} \boldsymbol{\sigma}_{t+\Delta t}\boldsymbol{\sigma}_{t+\Delta t}^T \boldsymbol{P}_{vm}}{\left(2\boldsymbol{\sigma}_{t+\Delta t}^T \boldsymbol{P}_{vm} \boldsymbol{\sigma}_{t+\Delta t}\right)^{\frac{3}{2}}}\right) \\[2mm]
& \left. \left. + \left(\frac{\partial \bar{\sigma}^{(3)}}{\partial \kappa^{(3)}}\right)^{-1}_{t+\Delta t} \boldsymbol{\pi}^{(3)}\boldsymbol{\pi}^{(3)T} \right] \boldsymbol{D} \right\}^{-1} \\[2mm]
& \cdot \left\{ \frac{\partial\, \boldsymbol{\varepsilon}_{t}^{P}}{\partial x} + \left[\left(\frac{\partial \bar{\sigma}^{(1)}}{\partial \kappa^{(1)}}\right)^{-1}_{t+\Delta t} \left(\frac{\boldsymbol{P}_r \boldsymbol{\sigma}_{t+\Delta t}}{\sqrt{2\boldsymbol{\sigma}_{t+\Delta t}^T \boldsymbol{P}_r \boldsymbol{\sigma}_{t+\Delta t}}} + \tfrac{1}{2}\boldsymbol{\pi}^{(1)}\right) \right. \right. \\[2mm]
& \cdot \left(\frac{\boldsymbol{\sigma}_{t+\Delta t}^T \boldsymbol{P}_r}{\sqrt{2\boldsymbol{\sigma}_{t+\Delta t}^T \boldsymbol{P}_r \boldsymbol{\sigma}_{t+\Delta t}}} + \tfrac{1}{2}\boldsymbol{\pi}^{(1)T}\right) \\[2mm]
& + \Delta\lambda^{(1)} \left(\frac{\boldsymbol{P}_r}{\sqrt{2\boldsymbol{\sigma}_{t+\Delta t}^T \boldsymbol{P}_r \boldsymbol{\sigma}_{t+\Delta t}}} - \frac{2\boldsymbol{P}_r \boldsymbol{\sigma}_{t+\Delta t}\boldsymbol{\sigma}_{t+\Delta t}^T \boldsymbol{P}_r}{\left(2\boldsymbol{\sigma}_{t+\Delta t}^T \boldsymbol{P}_r \boldsymbol{\sigma}_{t+\Delta t}\right)^{\frac{3}{2}}}\right) \\[2mm]
& + \left(\frac{\partial \bar{\sigma}^{(2)}}{\partial \kappa^{(2)}}\right)^{-1}_{t+\Delta t} \cdot \frac{\boldsymbol{P}_{vm} \boldsymbol{\sigma}_{t+\Delta t}}{\sqrt{2\boldsymbol{\sigma}_{t+\Delta t}^T \boldsymbol{P}_{vm} \boldsymbol{\sigma}_{t+\Delta t}}} \cdot \frac{\boldsymbol{\sigma}_{t+\Delta t}^T \boldsymbol{P}_{vm}}{\sqrt{2\boldsymbol{\sigma}_{t+\Delta t}^T \boldsymbol{P}_{vm} \boldsymbol{\sigma}_{t+\Delta t}}} \\[2mm]
& + \Delta\lambda^{(2)} \left(\frac{\boldsymbol{P}_{vm}}{\sqrt{2\boldsymbol{\sigma}_{t+\Delta t}^T \boldsymbol{P}_{vm} \boldsymbol{\sigma}_{t+\Delta t}}} - \frac{2\boldsymbol{P}_{vm} \boldsymbol{\sigma}_{t+\Delta t}\boldsymbol{\sigma}_{t+\Delta t}^T \boldsymbol{P}_{vm}}{\left(2\boldsymbol{\sigma}_{t+\Delta t}^T \boldsymbol{P}_{vm} \boldsymbol{\sigma}_{t+\Delta t}\right)^{\frac{3}{2}}}\right) \\[2mm]
& \left. + \left(\frac{\partial \bar{\sigma}^{(3)}}{\partial \kappa^{(3)}}\right)^{-1}_{t+\Delta t} \boldsymbol{\pi}^{(3)}\boldsymbol{\pi}^{(3)T} \right] \\[2mm]
& \cdot \left[\frac{\partial \boldsymbol{D}}{\partial x}\left(\boldsymbol{\varepsilon}_{t+\Delta t} - \boldsymbol{\varepsilon}_{t+\Delta t}^{P}\right) + \boldsymbol{D}\frac{\partial\, \boldsymbol{\varepsilon}_{t+\Delta t}}{\partial x} \right]
\end{aligned}
$$

$$- \left[\left(\frac{\partial \bar{\sigma}^{(1)}}{\partial \kappa^{(1)}} \right)_{t+\Delta t}^{-1} \frac{\partial \bar{\sigma}^{(1)} \left(\kappa^{(1)}_{t+\Delta t} \right)}{\partial x} + \frac{\partial \kappa^{(1)}_t}{\partial x} \right] \left[\frac{P_r \sigma_{t+\Delta t}}{\sqrt{2 \sigma^T_{t+\Delta t} P_r \sigma_{t+\Delta t}}} + \tfrac{1}{2} \pi^{(1)} \right]$$

$$- \left[\left(\frac{\partial \bar{\sigma}^{(2)}}{\partial \kappa^{(2)}} \right)_{t+\Delta t}^{-1} \frac{\partial \bar{\sigma}^{(2)} \left(\kappa^{(2)}_{t+\Delta t} \right)}{\partial x} + \frac{\partial \kappa^{(2)}_t}{\partial x} \right] \frac{P_{vm}}{\sqrt{2 \sigma^T_{t+\Delta t} P_{vm} \sigma_{t+\Delta t}}}$$

$$- \left[\left(\frac{\partial \bar{\sigma}^{(3)}}{\partial \kappa^{(3)}} \right)_{t+\Delta t}^{-1} \frac{\partial \bar{\sigma}^{(3)} \left(\kappa^{(3)}_{t+\Delta t} \right)}{\partial x} + \frac{\partial \kappa^{(3)}_t}{\partial x} \right] \pi^{(3)} \Bigg\} \tag{7-88}$$

Once $\dfrac{\partial \varepsilon^P_{t+\Delta t}}{\partial x}$ is found, $\dfrac{\partial \kappa^{(i)}_{t+\Delta t}}{\partial x}$ can be calculated from

$$
\begin{aligned}
\frac{\partial \kappa^{(1)}_{t+\Delta t}}{\partial x} &= \left(\frac{\partial \bar{\sigma}^{(1)}}{\partial \kappa^{(1)}} \right)_{t+\Delta t}^{-1} \Bigg\{ \left[\frac{\sigma^T_{t+\Delta t} P_r}{\sqrt{2 \sigma^T_{t+\Delta t} P_r \sigma_{t+\Delta t}}} + \tfrac{1}{2} \pi^{(1)T} \right] \\
&\qquad \cdot \left[\frac{\partial D}{\partial x} \left(\varepsilon_{t+\Delta t} - \varepsilon^P_{t+\Delta t} \right) + D \left(\frac{\partial \varepsilon_{t+\Delta t}}{\partial x} - \frac{\partial \varepsilon^P_{t+\Delta t}}{\partial x} \right) \right] \\
&\qquad - \frac{\partial \bar{\sigma}^{(1)} \left(\kappa^{(1)}_{t+\Delta t} \right)}{\partial x} \Bigg\}
\end{aligned}
\tag{7-89}
$$

$$
\begin{aligned}
\frac{\partial \kappa^{(2)}_{t+\Delta t}}{\partial x} &= \left(\frac{\partial \bar{\sigma}^{(2)}}{\partial \kappa^{(2)}} \right)_{t+\Delta t}^{-1} \Bigg\{ \frac{\sigma^T_{t+\Delta t} P_{vm}}{\sqrt{2 \sigma^T_{t+\Delta t} P_{vm} \sigma_{t+\Delta t}}} \\
&\qquad \cdot \left[\frac{\partial D}{\partial x} \left(\varepsilon_{t+\Delta t} - \varepsilon^P_{t+\Delta t} \right) + D \left(\frac{\partial \varepsilon_{t+\Delta t}}{\partial x} - \frac{\partial \varepsilon^P_{t+\Delta t}}{\partial x} \right) \right] \\
&\qquad - \frac{\partial \bar{\sigma}^{(2)} \left(\kappa^{(2)}_{t+\Delta t} \right)}{\partial x} \Bigg\}
\end{aligned}
\tag{7-90}
$$

$$
\begin{aligned}
\frac{\partial \kappa^{(3)}_{t+\Delta t}}{\partial x} &= \left(\frac{\partial \bar{\sigma}^{(3)}}{\partial \kappa^{(3)}} \right)_{t+\Delta t}^{-1} \Big\{ \pi^{(3)T} \\
&\qquad \cdot \left[\frac{\partial D}{\partial x} \left(\varepsilon_{t+\Delta t} - \varepsilon^P_{t+\Delta t} \right) + D \left(\frac{\partial \varepsilon_{t+\Delta t}}{\partial x} - \frac{\partial \varepsilon^P_{t+\Delta t}}{\partial x} \right) \right]
\end{aligned}
$$

$$
\left.\quad - \frac{\partial \bar{\sigma}^{(3)}\left(\kappa^{(3)}_{t+\Delta t}\right)}{\partial x} \right\}
\tag{7-91}
$$

The above derivations were for the case with all three yield surfaces active. It can be shown that the relevant equations for all of the eight cases can be summarized by

$$
\left. \frac{\partial \boldsymbol{\sigma}_{t+\Delta t}}{\partial x} \right|_{\boldsymbol{u},\dot{\boldsymbol{u}},\boldsymbol{z}} + \frac{\partial \boldsymbol{\sigma}_{t+\Delta t}}{\partial \boldsymbol{z}_{t+\Delta t}} \frac{\partial \boldsymbol{z}_{t+\Delta t}}{\partial x} = \left\{ \boldsymbol{I} + \boldsymbol{D}\left[\boldsymbol{L}^{(1)}_{t+\Delta t} + \boldsymbol{L}^{(2)}_{t+\Delta t} + \boldsymbol{L}^{(3)}_{t+\Delta t} \right] \right\}^{-1}
$$
$$
\cdot \left\{ \frac{\partial \boldsymbol{D}}{\partial x}\left[\boldsymbol{\varepsilon}_{t+\Delta t} - \boldsymbol{\varepsilon}^{P}_{t+\Delta t} \right] + \boldsymbol{D}\left[-\frac{\partial \boldsymbol{\varepsilon}^{P}_{t}}{\partial x} \right] \right.
$$
$$
\left. + \boldsymbol{D}\left[\boldsymbol{R}^{(1)}_{t+\Delta t} + \boldsymbol{R}^{(2)}_{t+\Delta t} + \boldsymbol{R}^{(3)}_{t+\Delta t} \right] \right\}
\tag{7-92}
$$

$$
\frac{\partial \boldsymbol{\varepsilon}^{P}_{t+\Delta t}}{\partial x} = \left\{ \boldsymbol{I} + \left[\boldsymbol{L}^{(1)}_{t+\Delta t} + \boldsymbol{L}^{(2)}_{t+\Delta t} + \boldsymbol{L}^{(3)}_{t+\Delta t} \right]\boldsymbol{D} \right\}^{-1}
$$
$$
\cdot \left\{ \frac{\partial \boldsymbol{\varepsilon}^{P}_{t}}{\partial x} + \left[\boldsymbol{L}^{(1)}_{t+\Delta t} + \boldsymbol{L}^{(2)}_{t+\Delta t} + \boldsymbol{L}^{(3)}_{t+\Delta t} \right] \right.
$$
$$
\cdot \left[\frac{\partial \boldsymbol{D}}{\partial x}\left(\boldsymbol{\varepsilon}_{t+\Delta t} - \boldsymbol{\varepsilon}^{P}_{t+\Delta t} \right) + \boldsymbol{D}\frac{\partial \boldsymbol{\varepsilon}_{t+\Delta t}}{\partial x} \right]
$$
$$
\left. - \boldsymbol{R}^{(1)}_{t+\Delta t} - \boldsymbol{R}^{(2)}_{t+\Delta t} - \boldsymbol{R}^{(3)}_{t+\Delta t} \right\}
\tag{7-93}
$$

where

$$
\boldsymbol{L}^{(1)}_{t+\Delta t} = \begin{cases} \left(\dfrac{\partial \bar{\sigma}^{(1)}}{\partial \kappa^{(1)}} \right)^{-1}_{t+\Delta t} \left(\dfrac{\boldsymbol{P}_{r}\boldsymbol{\sigma}_{t+\Delta t}}{\sqrt{2\boldsymbol{\sigma}^{T}_{t+\Delta t}\boldsymbol{P}_{r}\boldsymbol{\sigma}_{t+\Delta t}}} + \tfrac{1}{2}\boldsymbol{\pi}^{(1)} \right) \\[3ex] \qquad \cdot \left(\dfrac{\boldsymbol{\sigma}^{T}_{t+\Delta t}\boldsymbol{P}_{r}}{\sqrt{2\boldsymbol{\sigma}^{T}_{t+\Delta t}\boldsymbol{P}_{r}\boldsymbol{\sigma}_{t+\Delta t}}} + \tfrac{1}{2}\boldsymbol{\pi}^{(1)\,T} \right) \\[3ex] \quad + \Delta\lambda^{(1)} \left(\dfrac{\boldsymbol{P}_{r}}{\sqrt{2\boldsymbol{\sigma}^{T}_{t+\Delta t}\boldsymbol{P}_{r}\boldsymbol{\sigma}_{t+\Delta t}}} \right. \\[3ex] \qquad\quad \left. - \dfrac{2\boldsymbol{P}_{r}\boldsymbol{\sigma}_{t+\Delta t}\boldsymbol{\sigma}^{T}_{t+\Delta t}\boldsymbol{P}_{r}}{[2\boldsymbol{\sigma}^{T}_{t+\Delta t}\boldsymbol{P}_{r}\boldsymbol{\sigma}_{t+\Delta t}]^{\frac{3}{2}}} \right), \quad f^{(1)} \text{ active} \\[4ex] \boldsymbol{0}_{L}, \qquad\qquad\qquad\qquad\qquad f^{(1)} \text{ not active} \end{cases}
\tag{7-94}
$$

132

where $\mathbf{0}_L$ is a square matrix of zeros,

$$
\boldsymbol{L}^{(2)}_{t+\Delta t} = \begin{cases}
\left(\dfrac{\partial \bar{\sigma}^{(2)}}{\partial \kappa^{(2)}}\right)^{-1}_{t+\Delta t} \cdot \dfrac{\boldsymbol{P}_{vm}\boldsymbol{\sigma}_{t+\Delta t}}{\sqrt{2\boldsymbol{\sigma}^T_{t+\Delta t}\boldsymbol{P}_{vm}\boldsymbol{\sigma}_{t+\Delta t}}} \\[4mm]
\quad \cdot \dfrac{\boldsymbol{\sigma}^T_{t+\Delta t}\boldsymbol{P}_{vm}}{\sqrt{2\boldsymbol{\sigma}^T_{t+\Delta t}\boldsymbol{P}_{vm}\boldsymbol{\sigma}_{t+\Delta t}}} \\[4mm]
\quad + \Delta\lambda^{(2)} \left(\dfrac{\boldsymbol{P}_{vm}}{\sqrt{2\boldsymbol{\sigma}^T_{t+\Delta t}\boldsymbol{P}_{vm}\boldsymbol{\sigma}_{t+\Delta t}}} \right. \\[4mm]
\quad \left. - \dfrac{2\boldsymbol{P}_{vm}\boldsymbol{\sigma}_{t+\Delta t}\boldsymbol{\sigma}^T_{t+\Delta t}\boldsymbol{P}_{vm}}{[2\boldsymbol{\sigma}^T_{t+\Delta t}\boldsymbol{P}_{vm}\boldsymbol{\sigma}_{t+\Delta t}]^{\frac{3}{2}}} \right), \quad f^{(2)} \text{ active} \\[6mm]
\mathbf{0}_L, \qquad\qquad\qquad\qquad\qquad\quad f^{(2)} \text{ not active}
\end{cases}
\tag{7-95}
$$

$$
\boldsymbol{L}^{(3)}_{t+\Delta t} = \begin{cases}
\left(\dfrac{\partial \bar{\sigma}^{(3)}}{\partial \kappa^{(3)}}\right)^{-1}_{t+\Delta t} \boldsymbol{\pi}^{(3)}\boldsymbol{\pi}^{(3)\,T}, & f^{(3)} \text{ active} \\[4mm]
\mathbf{0}_L, & f^{(3)} \text{ not active}
\end{cases}
\tag{7-96}
$$

$$
\boldsymbol{R}^{(1)}_{t+\Delta t} = \begin{cases}
\left[\left(\dfrac{\partial \bar{\sigma}^{(1)}}{\partial \kappa^{(1)}}\right)^{-1}_{t+\Delta t} \dfrac{\partial \bar{\sigma}^{(1)}\left(\kappa^{(1)}_{t+\Delta t}\right)}{\partial x} + \dfrac{\partial \kappa^{(1)}_t}{\partial x} \right] \\[4mm]
\quad \cdot \left[\dfrac{\boldsymbol{P}_r\boldsymbol{\sigma}_{t+\Delta t}}{\sqrt{2\boldsymbol{\sigma}^T_{t+\Delta t}\boldsymbol{P}_r\boldsymbol{\sigma}_{t+\Delta t}}} + \tfrac{1}{2}\boldsymbol{\pi}^{(1)} \right], \quad f^{(1)} \text{ active} \\[6mm]
\mathbf{0}_R, \qquad\qquad\qquad\qquad\qquad\qquad\quad f^{(1)} \text{ not active}
\end{cases}
\tag{7-97}
$$

where $\mathbf{0}_R$ is a column vector of zeros,

$$
\boldsymbol{R}^{(2)}_{t+\Delta t} = \begin{cases}
\left[\left(\dfrac{\partial \bar{\sigma}^{(2)}}{\partial \kappa^{(2)}}\right)^{-1}_{t+\Delta t} \dfrac{\partial \bar{\sigma}^{(2)}\left(\kappa^{(2)}_{t+\Delta t}\right)}{\partial x} + \dfrac{\partial \kappa^{(2)}_t}{\partial x} \right] \\[4mm]
\quad \cdot \dfrac{\boldsymbol{P}_{vm}}{\sqrt{2\boldsymbol{\sigma}^T_{t+\Delta t}\boldsymbol{P}_{vm}\boldsymbol{\sigma}_{t+\Delta t}}}, \quad f^{(2)} \text{ active} \\[6mm]
\mathbf{0}_R, \qquad\qquad\qquad\qquad\quad f^{(2)} \text{ not active}
\end{cases}
\tag{7-98}
$$

$$R_{t+\Delta t}^{(3)} = \begin{cases} \left[\left(\dfrac{\partial \bar{\sigma}^{(3)}}{\partial \kappa^{(3)}} \right)_{t+\Delta t}^{-1} \dfrac{\partial \bar{\sigma}^{(3)} \left(\kappa_{t+\Delta t}^{(3)} \right)}{\partial x} + \dfrac{\partial \kappa_t^{(3)}}{\partial x} \right] \boldsymbol{\pi}^{(3)}, & f^{(3)} \text{ active} \\[4mm] \mathbf{0}_R, & f^{(3)} \text{ not active} \end{cases} \qquad (7\text{-}99)$$

and equations 7-89 if $f^{(1)}$ is active, 7-90 if $f^{(2)}$ is active, and 7-91 if $f^{(3)}$ is active.

7.4 Calculation procedure

7.4.1 Added subroutines

To implement the sensitivity analysis equations from Section 3 and Section 7.3 in DIANA, a number of the existing subroutines had to be modified. Many new subroutines were also added. This section is a record of all of the subroutines that were modified or added for sensitivity analysis. These are the subroutines that must be copied and compiled to add sensitivity analysis capabilities to an existing version of DIANA.

Subroutines for sensitivity analysis calculations that have to be performed at each time step are called from existing subroutine DOSTEP, which is a high level subroutine in application n140 that controls the analysis at each step. In its original form, DOSTEP calls other subroutines to calculate the tangent stiffness, solve for the incremental displacement, calculate the new restoring force, check equilibrium, and iterate if necessary. This is the first step of the flowchart of figure 3-1 and as it is part of the original DIANA program it will not be dealt with here. A command was added in DOSTEP to call new subroutines to perform the remaining steps of the flowchart. The new subroutines are shown in figures 7-6, 7-7 and 7-8. The loops have been shown on the flowcharts in these figures as they are sometimes useful. For example, subroutine FORCE2 contains a loop through all of the elements in the structure. The subroutines after FORCE2 are thus called once for each element. Similar considerations apply for the other loops indicated.

Subroutines to calculate $\left. \dfrac{\partial \boldsymbol{r}}{\partial x} \right|_{\boldsymbol{u}, \dot{\boldsymbol{u}}, \boldsymbol{z}} + \dfrac{\partial \boldsymbol{r}}{\partial \boldsymbol{z}} \dfrac{\partial \boldsymbol{z}}{\partial x}$ are shown in figure 7-6. The element-by-element method used based on figure 3-2 is similar to that used to calculate restoring force $\boldsymbol{r}$. The most sensible procedure was thus to copy the routines used to calculate $\boldsymbol{r}$, rename them, and edit them where necessary. The subroutines were renamed by replacing the last letter of each name with a "2". The functions of each of the subroutines are summarized below.

- XQELE2: Open FILOS files, allocate arrays; call FORCE2; store $\dfrac{\partial \boldsymbol{r}}{\partial x} + \dfrac{\partial \boldsymbol{r}}{\partial \boldsymbol{z}} \dfrac{\partial \boldsymbol{z}}{\partial x}$.

- `FORCE2`: Convert displacement $\boldsymbol{u}$ to local coordinates for each element; call `YNSWI2`; convert element $\dfrac{\partial \boldsymbol{r}}{\partial x} + \dfrac{\partial \boldsymbol{r}}{\partial z}\dfrac{\partial z}{\partial x}$ to global coordinates and add to global $\dfrac{\partial \boldsymbol{r}}{\partial x} + \dfrac{\partial \boldsymbol{r}}{\partial z}\dfrac{\partial z}{\partial x}$.

- `YNSWI2`: "Switch" file to call subroutine corresponding to element type.

- `YNBEN2`: Beam elements only. Convert $\boldsymbol{u}$ to strain $\boldsymbol{\varepsilon}$ for each integration point; call `IFIP2`; convert $\dfrac{\partial \boldsymbol{\sigma}}{\partial x} + \dfrac{\partial \boldsymbol{\sigma}}{\partial z}\dfrac{\partial z}{\partial x}$ to $\dfrac{\partial \boldsymbol{r}}{\partial x} + \dfrac{\partial \boldsymbol{r}}{\partial z}\dfrac{\partial z}{\partial x}$ for each integration point, and add to total $\dfrac{\partial \boldsymbol{r}}{\partial x} + \dfrac{\partial \boldsymbol{r}}{\partial z}\dfrac{\partial z}{\partial x}$ for element.

- `YNNI2`: Plane stress, plane strain, solid and shell elements. Convert $\boldsymbol{u}$ to strain $\boldsymbol{\varepsilon}$ for each integration point; call `IFIP2`; convert $\dfrac{\partial \boldsymbol{\sigma}}{\partial x} + \dfrac{\partial \boldsymbol{\sigma}}{\partial z}\dfrac{\partial z}{\partial x}$ to $\dfrac{\partial \boldsymbol{r}}{\partial x} + \dfrac{\partial \boldsymbol{r}}{\partial z}\dfrac{\partial z}{\partial x}$ for each integration point, and add to total $\dfrac{\partial \boldsymbol{r}}{\partial x} + \dfrac{\partial \boldsymbol{r}}{\partial z}\dfrac{\partial z}{\partial x}$ for element.

- `IFEL2`: Read element data such as $\boldsymbol{D}$ and $\dfrac{\partial \boldsymbol{D}}{\partial x}$ from FILOS file.

- `IFIP2`: Call subroutine corresponding to material model.

- `YLD2`: No function, kept for consistency only.

- `PLSW2`: "Switch" file to call subroutine corresponding to plasticity model.

- `MIPL2`: Calculate $\dfrac{\partial \boldsymbol{\sigma}}{\partial x} + \dfrac{\partial \boldsymbol{\sigma}}{\partial z}\dfrac{\partial z}{\partial x}$ for von Mises plasticity.

- `RAPL2`: Calculate $\dfrac{\partial \boldsymbol{\sigma}}{\partial x} + \dfrac{\partial \boldsymbol{\sigma}}{\partial z}\dfrac{\partial z}{\partial x}$ for Rankine plasticity.

- `RVPL2`: Calculate $\dfrac{\partial \boldsymbol{\sigma}}{\partial x} + \dfrac{\partial \boldsymbol{\sigma}}{\partial z}\dfrac{\partial z}{\partial x}$ for Rankine/von Mises plasticity.

Once $\dfrac{\partial \boldsymbol{r}}{\partial x} + \dfrac{\partial \boldsymbol{r}}{\partial z}\dfrac{\partial z}{\partial x}$ has been found the next step is to solve for $\boldsymbol{v}$. Several completely new subroutines were written for this purpose. The routines compile the left and right-hand sides of equation 3-19 and then use the existing solver in DIANA to solve for the sensitivity factor. Routines for calculating $\dfrac{\partial \boldsymbol{c}}{\partial x}$ are also included in figure 7-7. The functions of each of the subroutines are summarized below.

- `SENSIT`: Open FILOS files, allocate arrays used in calculating $\boldsymbol{v}$, $\dot{\boldsymbol{v}}$ and $\ddot{\boldsymbol{v}}$; call `GNSYDA`, `SOSYEQ` and `UPSYDA`; and store $\boldsymbol{v}$.

- `GNSYDA`: Open FILOS files, allocate arrays used in calculating right-hand side of equation 3-19; call `GNXELM`.

- `GNXELM`: Call `FBRD`, `FBRDA` or `FBRDB`; calculate right-hand side of equation 3-19.
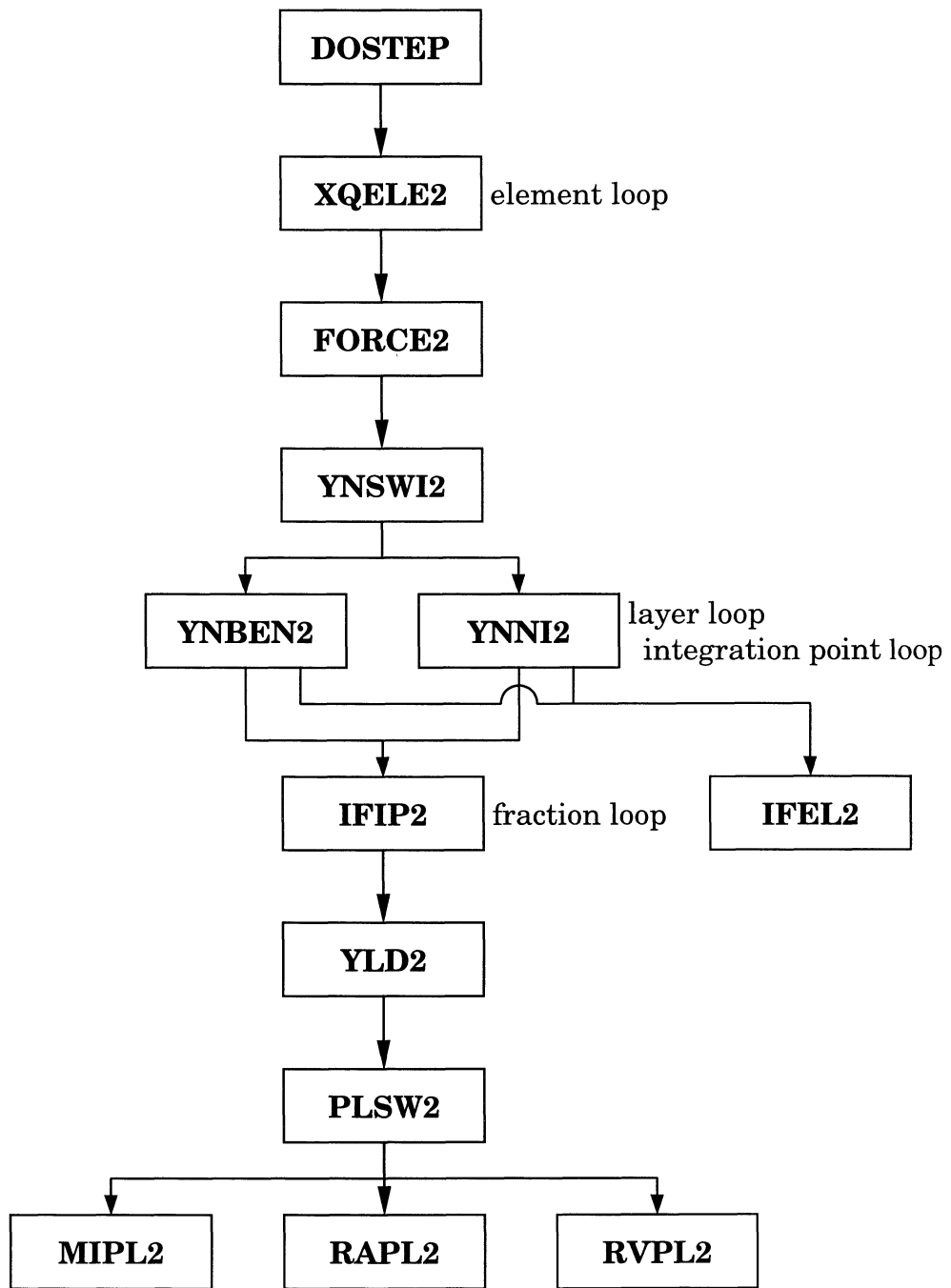
FIGURE 7-6 Subroutines to calculate $\left.\dfrac{\partial \boldsymbol{r}}{\partial x}\right|_{\boldsymbol{u},\dot{\boldsymbol{u}},\boldsymbol{z}} + \dfrac{\partial \boldsymbol{r}}{\partial \boldsymbol{z}}\dfrac{\partial \boldsymbol{z}}{\partial x}$
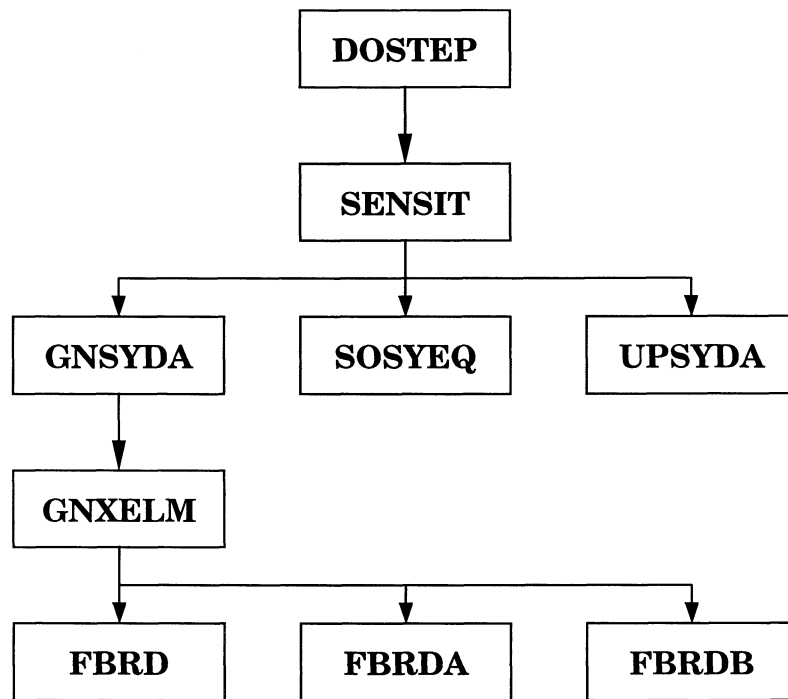
FIGURE 7-7 Subroutines to calculate $\dfrac{\partial c}{\partial x}$ and v

- FBRD: Calculate $\dfrac{\partial c}{\partial x}\dot{u}$ for general x.

- FBRDA: Calculate $\dfrac{\partial c}{\partial x}\dot{u}$ where x is the coefficient of the mass matrix in Rayleigh damping.

- FBRDB: Calculate $\dfrac{\partial c}{\partial x}\dot{u}$ where x is the coefficient of the initial stiffness matrix in Rayleigh damping.

- SOSYEQ: Solve for Δv.

- UPSYDA: Update v, $\dot{v}$ and $\ddot{v}$.

Subroutines for calculating $\dfrac{\partial z}{\partial x}$ (figure 7-8) are obtained in the same manner as those for calculating $\dfrac{\partial r}{\partial x}$. The subroutines for calculating r are copied, renamed by replacing the last letter of each name with a "3", and edited where necessary. The functions of each of the subroutines are summarized below.

- XQELE3: Open FILOS files, allocate arrays.

137

- FORCE3: Convert sensitivity factor v to local coordinates for each element.

- YNSWI3: "Switch" file to call subroutine corresponding to element type.

- YNBEN3: Beam elements only. Convert v to $\frac{\partial \varepsilon}{\partial x}$ for each integration point.

- YNNI3: Plane stress, plane strain, solid and shell elements. Convert v to $\frac{\partial \varepsilon}{\partial x}$ for each integration point.

- IFIP3: Call subroutine corresponding to material type.

- YLD3: No function, kept for consistency only.

- PLSW3: "Switch" file to call subroutine corresponding to plasticity model.

- MIPL3: Calculate and store $\frac{\partial z}{\partial x}$ for von Mises plasticity.

- RAPL3: Calculate and store $\frac{\partial z}{\partial x}$ for Rankine plasticity.

- RVPL3: Calculate and store $\frac{\partial z}{\partial x}$ for Rankine/von Mises plasticity.

Several calculations need only be performed once during an analysis, so subroutines to perform these calculations were added to the linear static analysis application ls40 and are called only at the start. The linear stress–strain matrices D of each integration point are calculated and stored at this stage, and read again during the dynamic analysis. The derivatives of these matrices, $\frac{\partial D}{\partial x}$, are needed to calculate the sensitivity factors, and it is sensible to calculate these derivatives directly after calculating D. The subroutines used were copied from those used to find D, renamed and edited where necessary (figure 7-9). Subroutine ELDATA in ls40 calls the subroutines for the calculation of D, so commands were added to it to call the new subroutines to calculate $\frac{\partial D}{\partial x}$.

- DLSWI2: "Switch" file to call subroutine corresponding to element type.

- DLBEN2, DLCLB2, DLME2, DLSH2, DLSHF2: No function, kept for consistency only.

- DLPEA2, DLSO2, ISBEN2, ISCLB2, ISME2, ISSH2, ISSHF2: Store $\frac{\partial D}{\partial x}$.

- MATAX2, MATSO2, MATSL2, MATSF2: Call CSOL2, assemble $\frac{\partial D}{\partial x}$ matrix from individual elements.

- MATME2: No function, kept for consistency only.

138
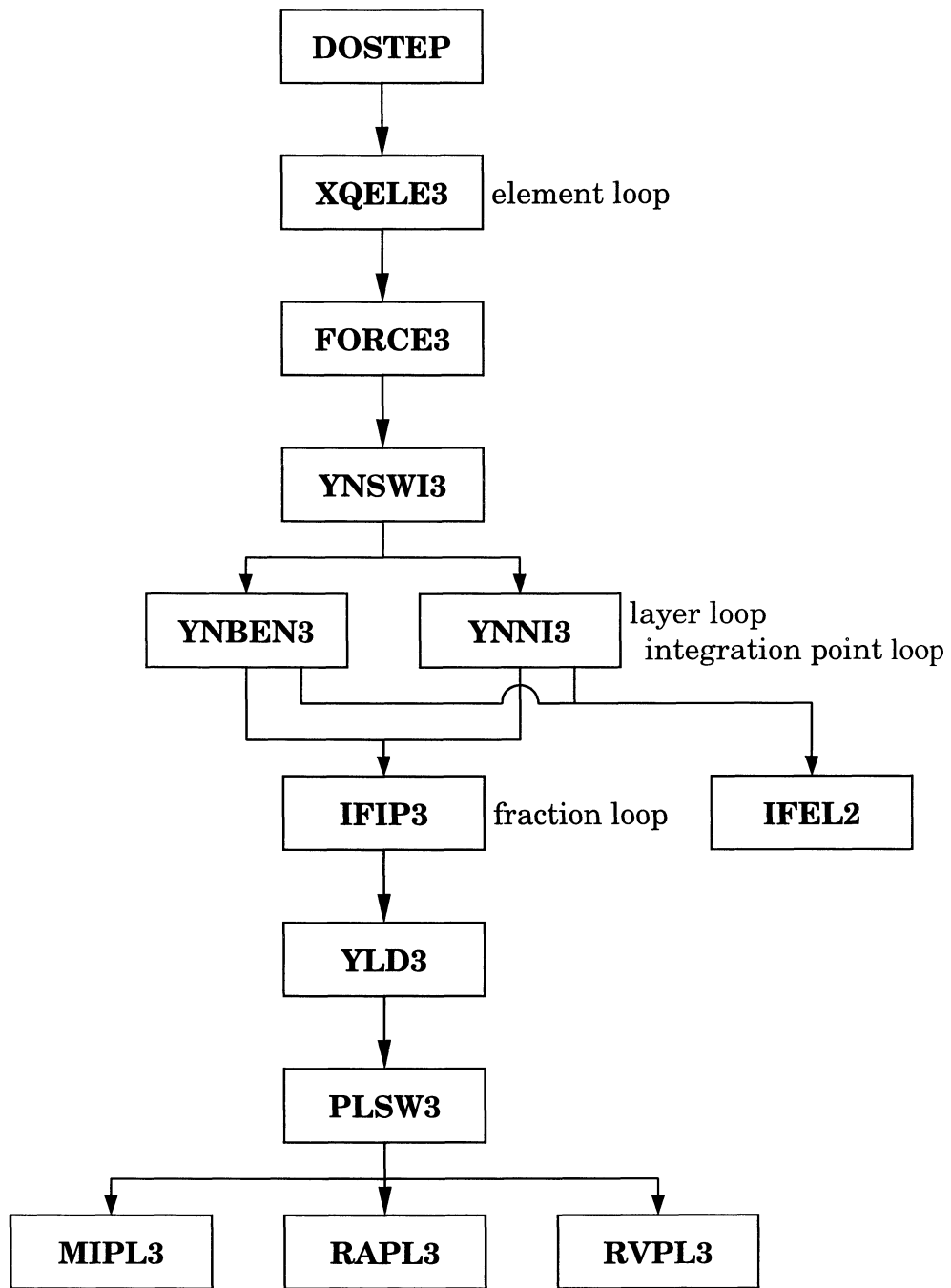
FIGURE 7-8 Subroutines to calculate $\dfrac{\partial z}{\partial x}$

139

- `CSOL2, CSHL2`: Calculate elements of $\frac{\partial \boldsymbol{D}}{\partial x}$.

- `MATCL2, SEME2`: Calculate $\frac{\partial \boldsymbol{D}}{\partial x}$.

As DIANA uses Rayleigh damping, the damping is in general a function of the stiffness. If the unknown parameter x is a stiffness parameter the damping becomes a function of x so it is necessary to calculate $\frac{\partial \boldsymbol{c}}{\partial x}$. The subroutines used for this were adapted from those used to calculate $\boldsymbol{c}$ and are shown in figure 7-10. They are called at the beginning of the analysis in application `ls40` by subroutine `XQELMA`, which calls subroutines to calculate element mass, damping and stiffness matrices.

- `OVSTM2`: Open FILOS files, allocate arrays.

- `ELSTI2`: Convert derivative of element stiffness matrix to local coordinates; store.

- `KLSWI2`: "Switch" file to call subroutine corresponding to element type.

- `KLBEN2`: Beam elements only. Calculate derivative of element stiffness matrix.

- `KLNI2`: Plane stress, plane strain, solid and shell elements. Calculate derivative of element stiffness matrix.

- `OVELD2`: Open FILOS files, allocate arrays.

- `ELDAM2`: Convert derivative of element damping matrix to local coordinates; store.

- `DASWI2`: "Switch" file to call subroutine corresponding to element type.

- `DAME2`: Plane stress, plane strain and solid elements. Calculate derivative of element damping matrix.

- `DAZOL2`: Beam and shell elements. Calculate derivative of element damping matrix.

7.4.2 Special procedures for beam, plane stress and shell elements

Some types of finite elements have, by definition, zero normal stress in certain directions. For example, plane stress and shell elements have zero stress perpendicular to the plane of the element, while beam elements have zero stress in the two directions perpendicular to the axis of the element. This can be accomplished computationally by omitting the zero stress components from the stress vector. However, this approach has two disadvantages. Firstly, different stress computation subroutines are needed for each element type. Secondly, the material modeling approach known as the fraction model [7] cannot be used. The fraction
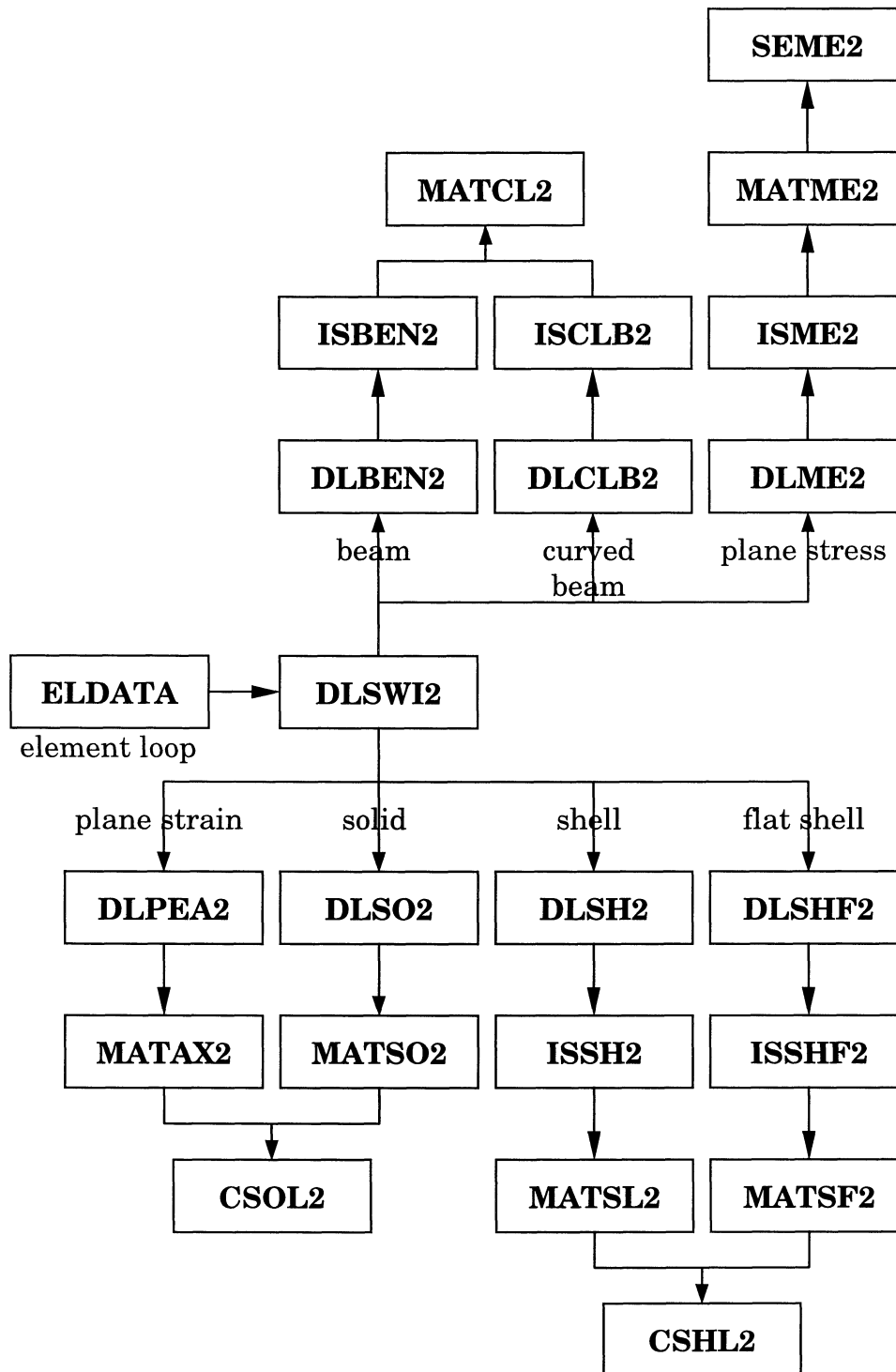
FIGURE 7-9 Subroutines to calculate $\dfrac{\partial D}{\partial x}$
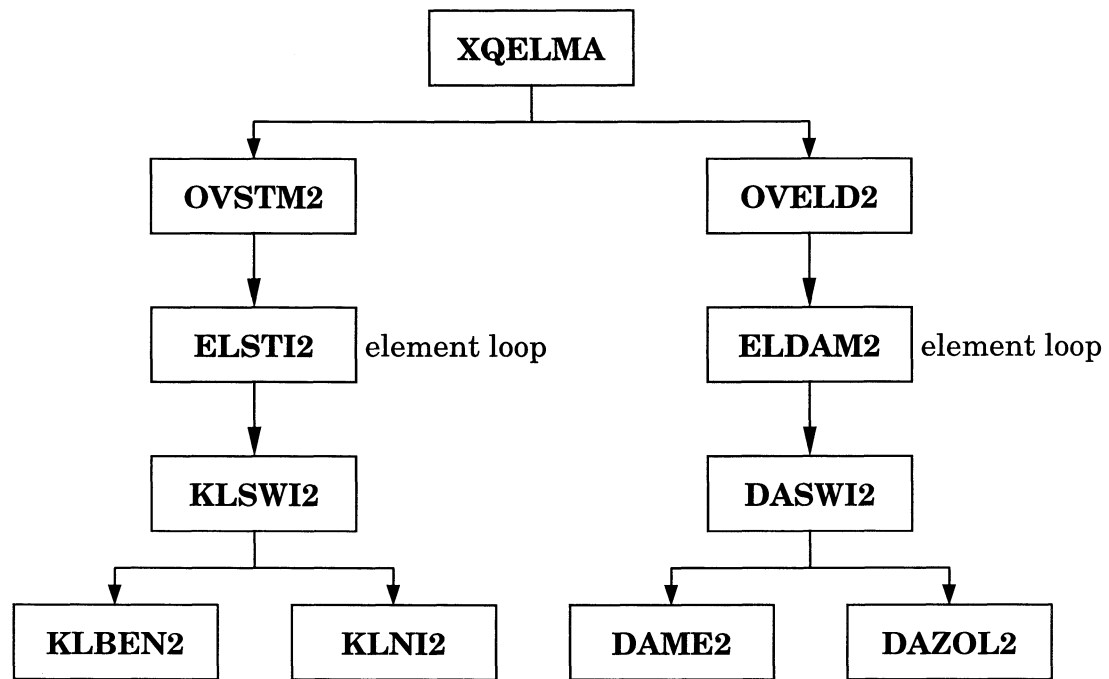
FIGURE 7-10 Subroutines to calculate $\dfrac{\partial c}{\partial x}$

model allows the use of several different material models in parallel in an element. Each material model has the same displacement, but the restoring force from each is weighted such that the sum of the weights is unity. The weighted sum of the restoring forces is used as the restoring force for the element. The fraction model requires only that the weighted sum of the normal stress components of the various models in an element are zero, not that each individual model component is zero.

In DIANA, a different approach is used to ensure that the normal stresses are zero. The approach considers both an *expanded* stress space in which only the zero shear stresses are omitted, and a *condensed* stress space in which all of the zero stress components are omitted. An algorithm is used to expand strains and compress stresses in such a way that the zero normal stress criterion is enforced [16]. The dimensions of the expanded and condensed stress spaces are 3 and 1 respectively for beams, 4 and 3 for plane stress elements, and 6 and 5 for shell elements.

The concept may be clearer after considering the calculation of the restoring force from the displacement at a typical iteration, shown in figure 7-11(a). A superscript C is used to indicate the condensed form of a quantity. First, the displacement is used to calculate the strain in the condensed space, $\varepsilon^C_{t+\Delta t}$, from the strain-displacement relationship for the element. The strain is then expanded to $\varepsilon_{t+\Delta t}$ and the relevant material model applied to find the stress $\boldsymbol{\sigma}_{t+\Delta t}$. This stress is then condensed to $\boldsymbol{\sigma}^C_{t+\Delta t}$ and used to find the restoring force $\boldsymbol{r}$ by equation 7-2.

142

Element level | Integration point level

condensed space | expanded space

displacement u → strain $\boldsymbol{\varepsilon}^C$ → [expand] → strain $\boldsymbol{\varepsilon}$

[apply material model]

force r ← stress $\boldsymbol{\sigma}^C$ ← [condense] ← stress $\boldsymbol{\sigma}$

(a)

$\boldsymbol{\varepsilon}, \boldsymbol{\varepsilon}^P, \boldsymbol{\sigma}, \partial\boldsymbol{\varepsilon}^P/\partial x$
from FILOS file

[apply equation]

$$\left.\frac{\partial r}{\partial x}\right|_{u,\dot{u},z} + \frac{\partial r}{\partial z}\frac{\partial z}{\partial x} \longleftarrow \left.\frac{\partial \boldsymbol{\sigma}^C}{\partial x}\right|_{u,\dot{u},z} + \frac{\partial \boldsymbol{\sigma}^C}{\partial z}\frac{\partial z}{\partial x} \longleftarrow [\text{condense}] \longleftarrow \left.\frac{\partial \boldsymbol{\sigma}}{\partial x}\right|_{u,\dot{u},z} + \frac{\partial \boldsymbol{\sigma}}{\partial z}\frac{\partial z}{\partial x}$$

(b)

$v \longrightarrow \dfrac{\partial \boldsymbol{\varepsilon}^C}{\partial x} \longrightarrow$ [apply updated equation]

save $\dfrac{\partial \boldsymbol{\varepsilon}^P}{\partial x}$ on FILOS file

(c)
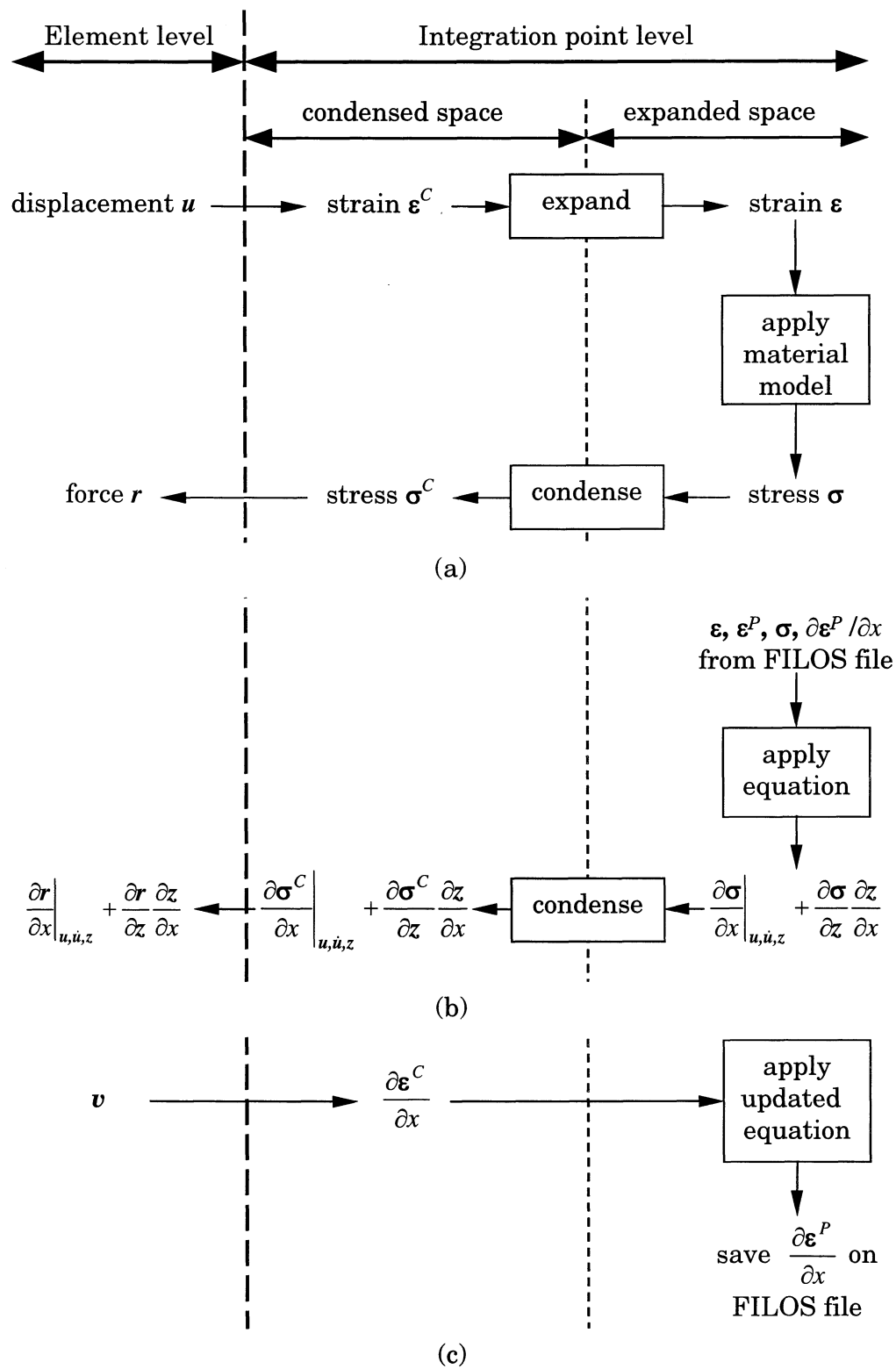
FIGURE 7-11 Calculation procedure

143

All material model calculations are done in the expanded space, and variables such as the plastic strain $\boldsymbol{\varepsilon}^P$ are stored in the expanded form. It is thus easier to apply the equations to calculate derivatives in the expanded space. Two different derivative quantities must be calculated at each time step. The first quantity, calculated in step 2 of figure 3-1, is $\left.\dfrac{\partial \boldsymbol{r}}{\partial x}\right|_{\boldsymbol{u},\dot{\boldsymbol{u}},\boldsymbol{z}} +$ $\dfrac{\partial \boldsymbol{r}}{\partial \boldsymbol{z}}\dfrac{\partial \boldsymbol{z}}{\partial x}$ and is calculated using equations 7-65 or 7-92, and 7-40. The procedure is shown in figure 7-11(b). The vectors $\boldsymbol{\sigma}_{t+\Delta t}$, $\boldsymbol{\varepsilon}_{t+\Delta t}$, $\boldsymbol{\varepsilon}^P_{t+\Delta t}$ and $\dfrac{\partial \boldsymbol{\varepsilon}^P_t}{\partial x}$ are read from the FILOS file and the relevant equation is applied to calculate $\left.\dfrac{\partial \boldsymbol{\sigma}_{t+\Delta t}}{\partial x}\right|_{\boldsymbol{u},\dot{\boldsymbol{u}},\boldsymbol{z}} + \dfrac{\partial \boldsymbol{\sigma}_{t+\Delta t}}{\partial \boldsymbol{z}_{t+\Delta t}}\dfrac{\partial \boldsymbol{z}_{t+\Delta t}}{\partial x}$. The condensation algorithm is then applied to calculate the condensed form $\left.\dfrac{\partial \boldsymbol{\sigma}^C_{t+\Delta t}}{\partial x}\right|_{\boldsymbol{u},\dot{\boldsymbol{u}},\boldsymbol{z}} + \dfrac{\partial \boldsymbol{\sigma}^C_{t+\Delta t}}{\partial \boldsymbol{z}_{t+\Delta t}}\dfrac{\partial \boldsymbol{z}_{t+\Delta t}}{\partial x}$ which is then converted to $\left.\dfrac{\partial \boldsymbol{r}_{t+\Delta t}}{\partial x}\right|_{\boldsymbol{u},\dot{\boldsymbol{u}},\boldsymbol{z}} + \dfrac{\partial \boldsymbol{r}_{t+\Delta t}}{\partial \boldsymbol{z}_{t+\Delta t}}\dfrac{\partial \boldsymbol{z}_{t+\Delta t}}{\partial x}$ by equation 7-40. The only point to note here is that the algorithm parameters used in condensing $\left.\dfrac{\partial \boldsymbol{\sigma}_{t+\Delta t}}{\partial x}\right|_{\boldsymbol{u},\dot{\boldsymbol{u}},\boldsymbol{z}} + \dfrac{\partial \boldsymbol{\sigma}_{t+\Delta t}}{\partial \boldsymbol{z}_{t+\Delta t}}\dfrac{\partial \boldsymbol{z}_{t+\Delta t}}{\partial x}$ must be the same as those used in condensing $\boldsymbol{\sigma}_{t+\Delta t}$. This presents no problem as the parameters can be saved on the FILOS file and reused.

The second derivative quantity calculated at each time step presents a greater challenge. It is $\dfrac{\partial \boldsymbol{z}}{\partial x}$, the derivative of the history-dependent parameters, calculated in step 4 of figure 3-1. For the material models in Section 7.2, the history-dependent parameters are $\boldsymbol{\varepsilon}^P$ and κ for the von Mises model, or $\boldsymbol{\varepsilon}^P$ and $\kappa^{(i)}, i = 1, 2, 3$ for the Rankine/von Mises model. The derivatives are calculated using equations 7-67 and 7-68, or 7-93, 7-89, 7-90 and 7-91 for the von Mises and Rankine/von Mises models respectively. A problem arises as the equations contain the derivative of the total strain, $\dfrac{\partial \boldsymbol{\varepsilon}_{t+\Delta t}}{\partial x}$. For most elements, this is calculated directly from the derivative of the displacement $\boldsymbol{v}_{t+\Delta t}$. However, for beam, plane stress and shell elements, only the condensed form $\dfrac{\partial \boldsymbol{\varepsilon}^C_{t+\Delta t}}{\partial x}$ can be obtained directly from $\boldsymbol{v}_{t+\Delta t}$. The expanded form depends on $\dfrac{\partial \boldsymbol{\varepsilon}^P_{t+\Delta t}}{\partial x}$, which is what we are trying to calculate. It is thus not possible to apply equations 7-67 and 7-93 directly. The problem can be overcome by expressing the expanded total strain in terms of the condensed total strain and the expanded plastic strain

$$\boldsymbol{\varepsilon}_{t+\Delta t} = \boldsymbol{I}^C \boldsymbol{\varepsilon}^C_{t+\Delta t} + \boldsymbol{I}^P \boldsymbol{\varepsilon}^P_{t+\Delta t} \tag{7-100}$$

where $\boldsymbol{I}^C$ and $\boldsymbol{I}^P$ are matrices that depend on the element type. They are given at the end of this section. Differentiating equation 7-100 with respect to x gives

$$\dfrac{\partial \boldsymbol{\varepsilon}_{t+\Delta t}}{\partial x} = \dfrac{\partial \boldsymbol{I}^C}{\partial x}\boldsymbol{\varepsilon}^C_{t+\Delta t} + \boldsymbol{I}^C \dfrac{\partial \boldsymbol{\varepsilon}^C_{t+\Delta t}}{\partial x} + \dfrac{\partial \boldsymbol{I}^P}{\partial x}\boldsymbol{\varepsilon}^P_{t+\Delta t} + \boldsymbol{I}^P \dfrac{\partial \boldsymbol{\varepsilon}^P_{t+\Delta t}}{\partial x} \tag{7-101}$$

144

which can be substituted into equations 7-67 and 7-93. The equations are then rearranged to give

$$
\begin{aligned}
\frac{\partial \boldsymbol{\varepsilon}^P_{t+\Delta t}}{\partial x} \;=\; & \left[\boldsymbol{I} - \frac{\boldsymbol{P}\,\boldsymbol{\sigma}_{t+\Delta t}\,\boldsymbol{\sigma}^T_{t+\Delta t}}{2\left[\bar{\sigma}\left(\kappa_{t+\Delta t}\right)\right]^2} \left(1 - \frac{\Delta\lambda}{\bar{\sigma}\left(\kappa_{t+\Delta t}\right)} \cdot \left[\frac{\partial \bar{\sigma}}{\partial \kappa}\right]_{t+\Delta t}\right) \right. \\
& \left. + \frac{\Delta\lambda \boldsymbol{P} \boldsymbol{D}}{2\bar{\sigma}\left(\kappa_{t+\Delta t}\right)}\left(\boldsymbol{I} - \boldsymbol{I}^P\right) \right]^{-1} \\
& \cdot \left\{ \left[\boldsymbol{I} - \frac{\boldsymbol{P}\,\boldsymbol{\sigma}_{t+\Delta t}\,\boldsymbol{\sigma}^T_{t+\Delta t}}{2\left[\bar{\sigma}\left(\kappa_{t+\Delta t}\right)\right]^2}\left(1 - \frac{\Delta\lambda}{\bar{\sigma}\left(\kappa_{t+\Delta t}\right)}\cdot\left[\frac{\partial\bar{\sigma}}{\partial\kappa}\right]_{t+\Delta t}\right)\right] \frac{\partial\boldsymbol{\varepsilon}^P_t}{\partial x} \right. \\
& + \Delta\lambda \frac{\boldsymbol{P}}{2\bar{\sigma}\left(\kappa_{t+\Delta t}\right)}\left[\frac{\partial \boldsymbol{D}}{\partial x}\left(\boldsymbol{\varepsilon}_{t+\Delta t} - \boldsymbol{\varepsilon}^P_{t+\Delta t}\right)\right. \\
& \left. + \boldsymbol{D}\left(\frac{\partial \boldsymbol{I}^C}{\partial x}\boldsymbol{\varepsilon}^C_{t+\Delta t} + \boldsymbol{I}^C \frac{\partial \boldsymbol{\varepsilon}^C_{t+\Delta t}}{\partial x} + \frac{\partial \boldsymbol{I}^P}{\partial x}\boldsymbol{\varepsilon}^P_{t+\Delta t}\right)\right] \\
& \left. - \Delta\lambda \frac{\boldsymbol{P}\,\boldsymbol{\sigma}_{t+\Delta t}}{2\left[\bar{\sigma}\left(\kappa_{t+\Delta t}\right)\right]^2}\left[\left[\frac{\partial\bar{\sigma}}{\partial\kappa}\right]_{t+\Delta t}\frac{\partial \kappa_t}{\partial x} + \frac{\partial\bar{\sigma}\left(\kappa_{t+\Delta t}\right)}{\partial x}\right]\right\}
\end{aligned}
\tag{7-102}
$$

which is used instead of equation 7-67, and

$$
\begin{aligned}
\frac{\partial \boldsymbol{\varepsilon}^P_{t+\Delta t}}{\partial x} \;=\; & \left\{\boldsymbol{I} + \left[\boldsymbol{L}^{(1)}_{t+\Delta t} + \boldsymbol{L}^{(2)}_{t+\Delta t} + \boldsymbol{L}^{(3)}_{t+\Delta t}\right]\boldsymbol{D}\left[\boldsymbol{I} - \boldsymbol{I}^P\right]\right\}^{-1} \\
& \cdot \left\{ \frac{\partial \boldsymbol{\varepsilon}^P_t}{\partial x} + \left[\boldsymbol{L}^{(1)}_{t+\Delta t} + \boldsymbol{L}^{(2)}_{t+\Delta t} + \boldsymbol{L}^{(3)}_{t+\Delta t}\right]\right. \\
& \cdot \left[\frac{\partial \boldsymbol{D}}{\partial x}\left(\boldsymbol{\varepsilon}_{t+\Delta t} - \boldsymbol{\varepsilon}^P_{t+\Delta t}\right)\right. \\
& \left. + \boldsymbol{D}\left(\frac{\partial \boldsymbol{I}^C}{\partial x}\boldsymbol{\varepsilon}^C_{t+\Delta t} + \boldsymbol{I}^C\frac{\partial \boldsymbol{\varepsilon}^C_{t+\Delta t}}{\partial x} + \frac{\partial \boldsymbol{I}^P}{\partial x}\boldsymbol{\varepsilon}^P_{t+\Delta t}\right)\right] \\
& \left. - \boldsymbol{R}^{(1)}_{t+\Delta t} - \boldsymbol{R}^{(2)}_{t+\Delta t} - \boldsymbol{R}^{(3)}_{t+\Delta t}\right\}
\end{aligned}
\tag{7-103}
$$

which is used instead of equation 7-93. This procedure omits the expansion algorithm and is shown in figure 7-11(c).

The $\boldsymbol{I}^C$ and $\boldsymbol{I}^P$ matrices are

$$
\boldsymbol{I}^C_{\text{beam}} \;=\; \begin{bmatrix} 1 \\ -\texttt{POISON} \\ -\texttt{POISON} \end{bmatrix}
\tag{7-104}
$$

145

$$\boldsymbol{I}^P_{\text{beam}} = \begin{bmatrix} 0 & 0 & 0 \\ \text{POISON} & 1 & 0 \\ \text{POISON} & 0 & 1 \end{bmatrix} \tag{7-105}$$

$$\boldsymbol{I}^C_{\text{plane stress}} = \begin{bmatrix} 1 & 0 & 0 \\ 0 & 1 & 0 \\ \frac{-\text{POISON}}{1-\text{POISON}} & \frac{-\text{POISON}}{1-\text{POISON}} & 0 \\ 0 & 0 & 1 \end{bmatrix} \tag{7-106}$$

$$\boldsymbol{I}^P_{\text{plane stress}} = \begin{bmatrix} 0 & 0 & 0 & 0 \\ 0 & 0 & 0 & 0 \\ \frac{\text{POISON}}{1-\text{POISON}} & \frac{\text{POISON}}{1-\text{POISON}} & 1 & 0 \\ 0 & 0 & 0 & 0 \end{bmatrix} \tag{7-107}$$

$$\boldsymbol{I}^C_{\text{shell}} = \begin{bmatrix} 1 & 0 & 0 & 0 & 0 \\ 0 & 1 & 0 & 0 & 0 \\ \frac{-\text{POISON}}{1-\text{POISON}} & \frac{-\text{POISON}}{1-\text{POISON}} & 0 & 0 & 0 \\ 0 & 0 & 1 & 0 & 0 \\ 0 & 0 & 0 & 1 & 0 \\ 0 & 0 & 0 & 0 & 1 \end{bmatrix} \tag{7-108}$$

$$\boldsymbol{I}^P_{\text{shell}} = \begin{bmatrix} 0 & 0 & 0 & 0 & 0 & 0 \\ 0 & 0 & 0 & 0 & 0 & 0 \\ \frac{\text{POISON}}{1-\text{POISON}} & \frac{\text{POISON}}{1-\text{POISON}} & 1 & 0 & 0 & 0 \\ 0 & 0 & 0 & 0 & 0 & 0 \\ 0 & 0 & 0 & 0 & 0 & 0 \\ 0 & 0 & 0 & 0 & 0 & 0 \end{bmatrix} \tag{7-109}$$

7.5 Example

The steel portal frame at the University at Buffalo, used in Section 6.5 to illustrate the MATLAB program, will also be used here to illustrate the use of DIANA. However, as DIANA is an existing program, the emphasis here will be entirely on the additional input data required for calculating the sensitivity factors. Details of selecting and generating the data for the structural model itself can be found elsewhere [17]. This section will thus be most useful to users who already have some knowledge of DIANA; however, it will also give other users an impression of the capabilities of the program for sensitivity analysis.

Using DIANA, a more detailed model of the Buffalo frame than than the MATLAB model of Section 6.5 can be constructed. The frame will be modeled using shell elements to represent the flanges and webs of the beam and columns (figure 7-12). The elements are the four-noded curved shell elements labeled `Q20SH` in DIANA. The columns will be assumed to be fixed to the shake table to avoid additional complexity; however, spring elements could be used for a more detailed analysis.
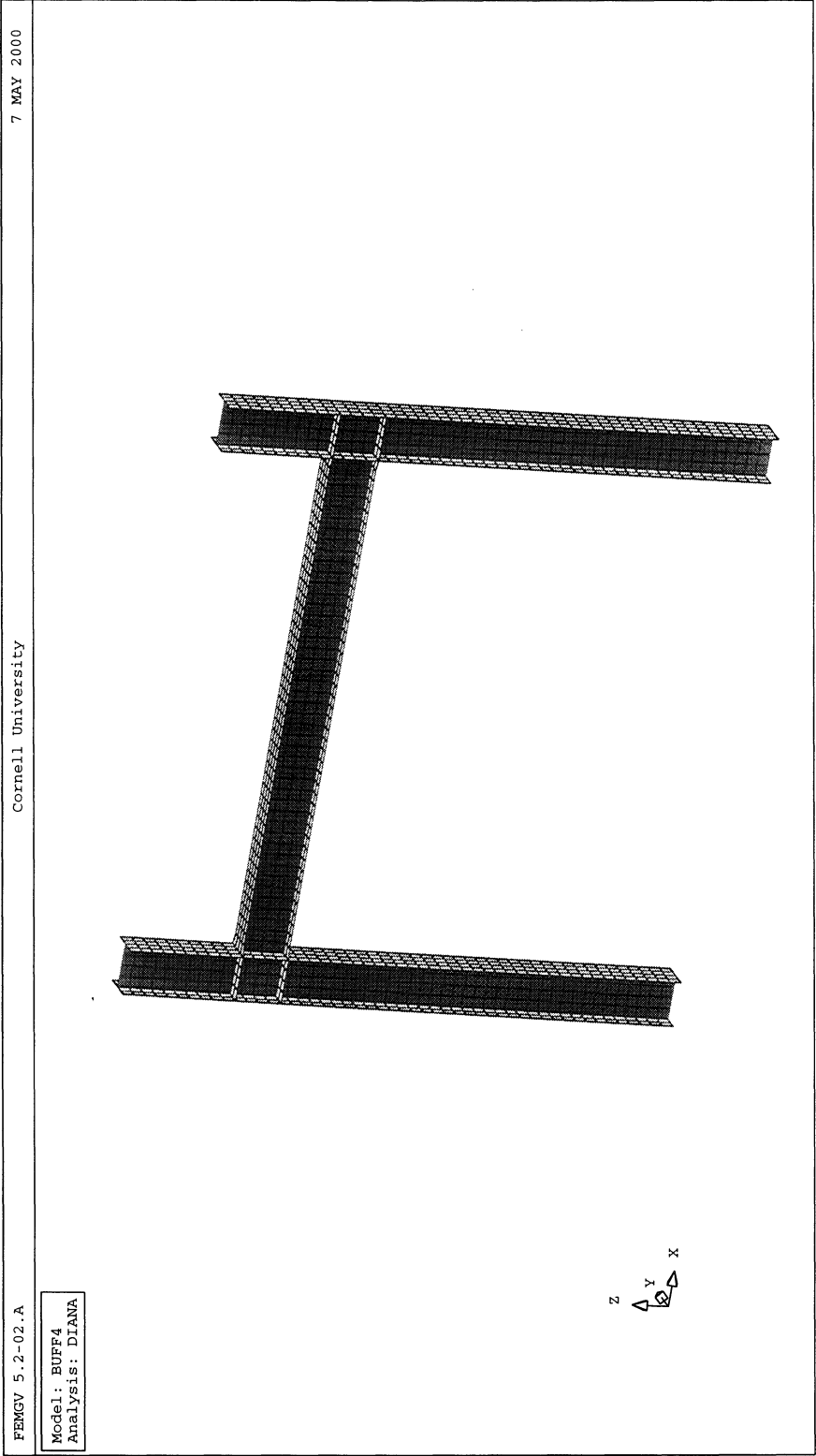
FIGURE 7-12 DIANA model of Buffalo frame

```
MATERI
 / 1-1816 / 1
DATA
 / 1-1816 / 1

  .
  .
  .

'DATA'
  1   SENVAR   YOUNG
```

FIGURE 7-13 Additional input in .dat file

The first additional input data required for the sensitivity analysis is the five or six letter
name of the uncertain parameter, which must be specified in the model data (.dat) file
(figure 7-13). The parameter is specified in the DATA table under property SENVAR. If the
uncertain parameter is a material parameter it is assumed to apply to material 1, while if the
uncertain parameter is a damping parameter it applies to all of the materials. The different
parameters that can be considered uncertain are detailed for the different material models
in Section 7.2. For this example of the Buffalo frame, the Young's modulus is uncertain so
YOUNG is entered.

Once the uncertain parameter is specified, several new commands must be added to the
analysis command (.com) file (figure 7-14). First, commands must be added to call the
special sensitivity analysis applications (ls40mc, ci33mc, nl40mc and wr30mc) rather than
the standard DIANA applications. These commands take different forms for the different
applications and are illustrated in figure 7-14. Next, a command must be added to actually
perform the sensitivity analysis. This is done by inserting option sensit in the initia
command block of module *NONLIN. If this line is removed, a normal analysis without cal-
culation of sensitivity factors will be performed. Finally, commands specifying the type of
output required must be added to the *NONLIN and/or *POST modules. The calculated sen-
sitivity factors can be written to a text file by the output tabula command, or to a file for
the graphical postprocessor FEMVIEW by the output femvie command. In either case,
the output can be manipulated like regular displacement output by using select and other
commands.

The DIANA analysis was then run using the standard diana command. The input motion
was scaled up to ensure nonlinear behavior. The resulting horizontal displacement of a node
at the intersection of the beam and column is plotted in figure 7-15. Sensitivity factors
were calculated with respect to the Young's modulus YOUNG (figure 7-16) and the yield stress
YLDVAL (figure 7-17) of the elements. The sensitivity factor with respect to the yield stress
is zero while the elements remain elastic.

The accuracy of the calculated sensitivity factors were then checked by the finite difference
method. Results are shown in figures 7-18 and 7-19. As the size of the finite difference is

148

```
*LINSTA
 !segmen ls40mc

 ⋮

*NONLIN/ci33mc
 segmen *applic nonlin/nl40mc
 initia
  analys physic dynami
   use
    newmar
   end use
   option sensit
 end initia

 ⋮

 output tabula sensit file="sensit"
  displa sensit
 end output

 ⋮

*POST/ci30mc
 segmen write/wr30mc
 output femvie sensit binary file="sensit"
  displa sensit
 end output
```

FIGURE 7-14 Additional input in `.com` **file**
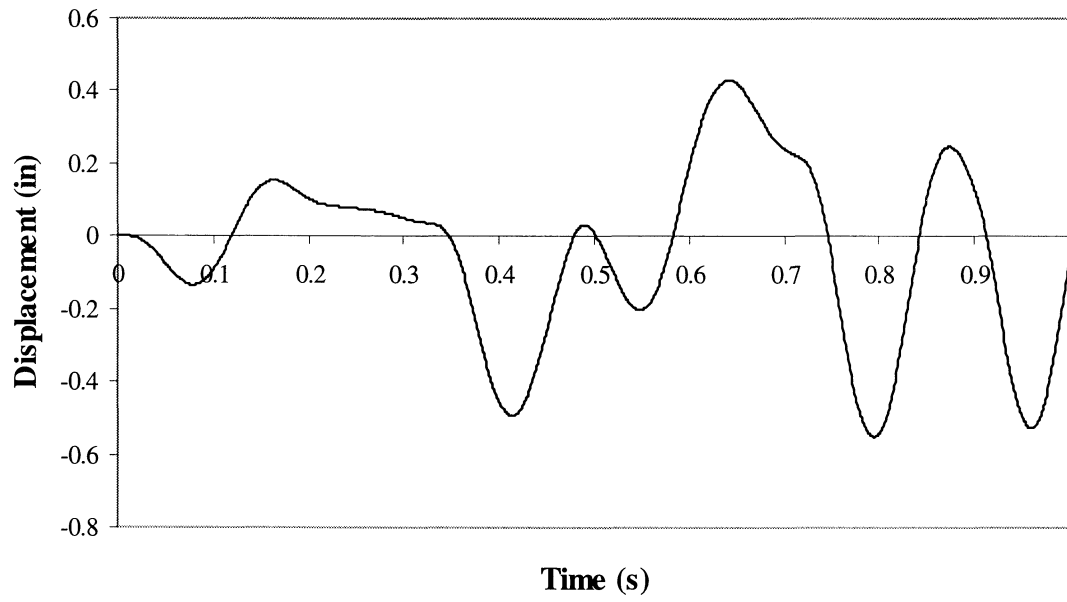
FIGURE 7-15 Displacement
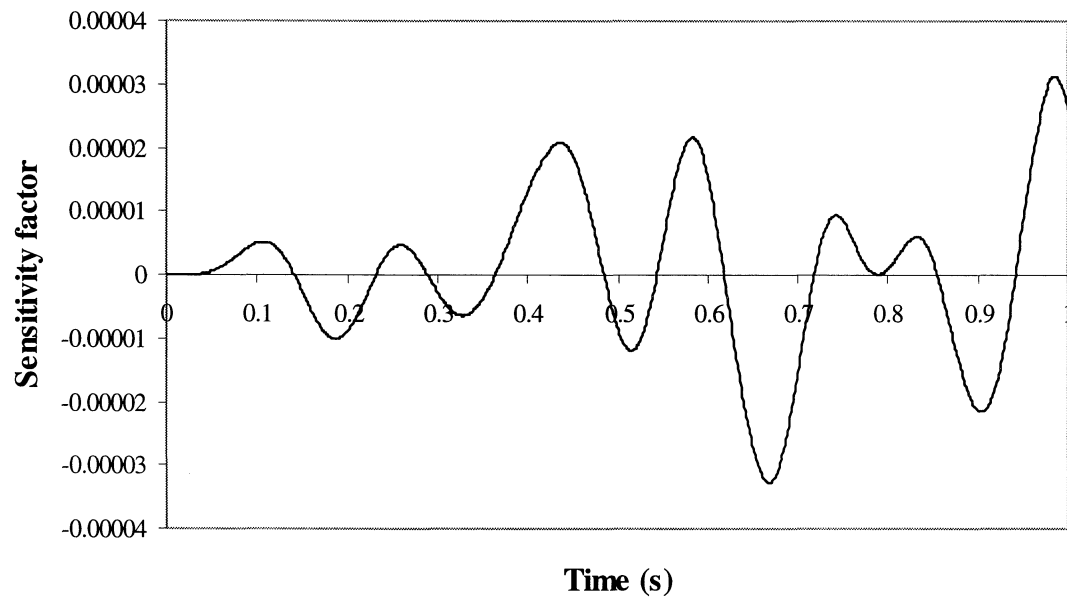
FIGURE 7-16 Sensitivity factor with respect to Young's modulus

150
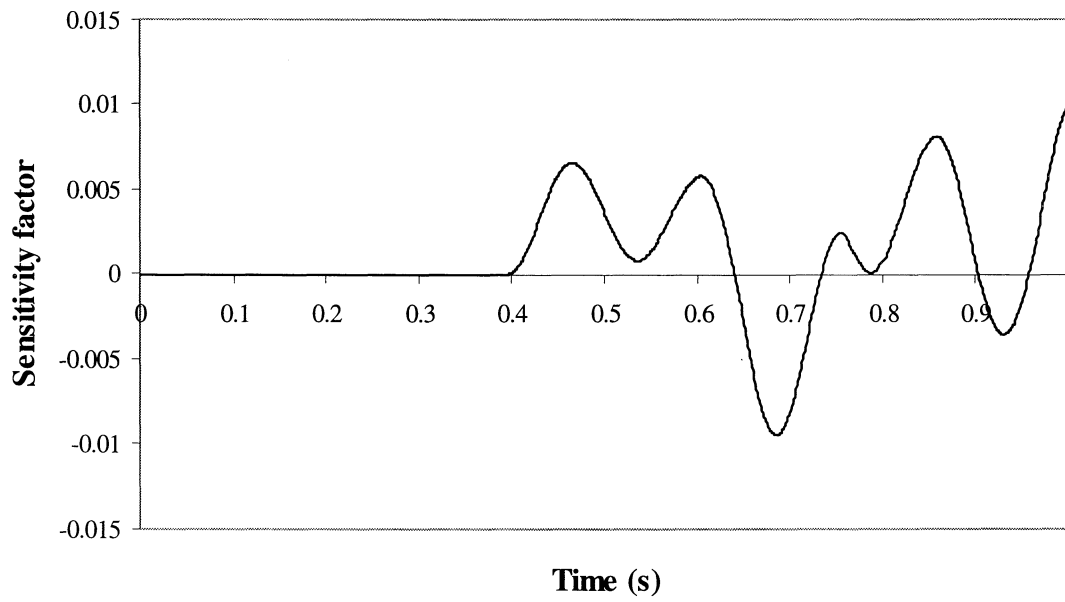
FIGURE 7-17 Sensitivity factor with respect to yield stress

reduced, the calculated and finite difference curves become closer. For a finite difference of 1000 or less in figure 7-18, and 1 or less in figure 7-19, the curves are indistinguishable. This confirms the accuracy of the sensitivity factors calculated by DIANA. Further details of the use of these sensitivity factors for calibration and optimization will be found in Section 9.

For some applications it is useful to plot the sensitivity factors on the structure in the same manner as stresses or strains. This can be done using the FEMVIEW program. Figure 7-20 shows an example of the sensitivity factors for the entire structure at a certain time instant.
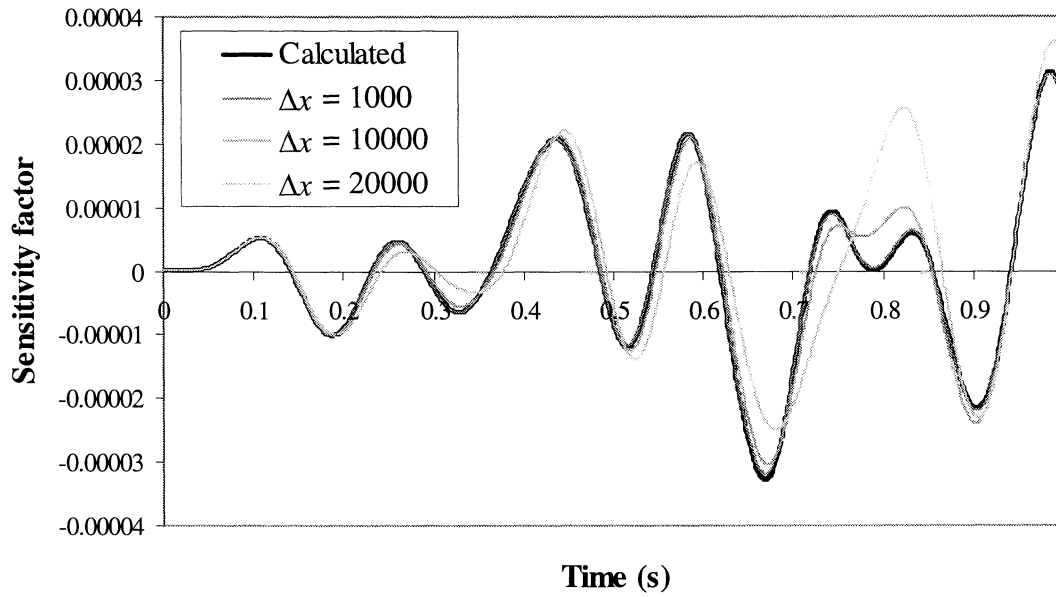
FIGURE 7-18 Sensitivity factor with respect to Young's modulus
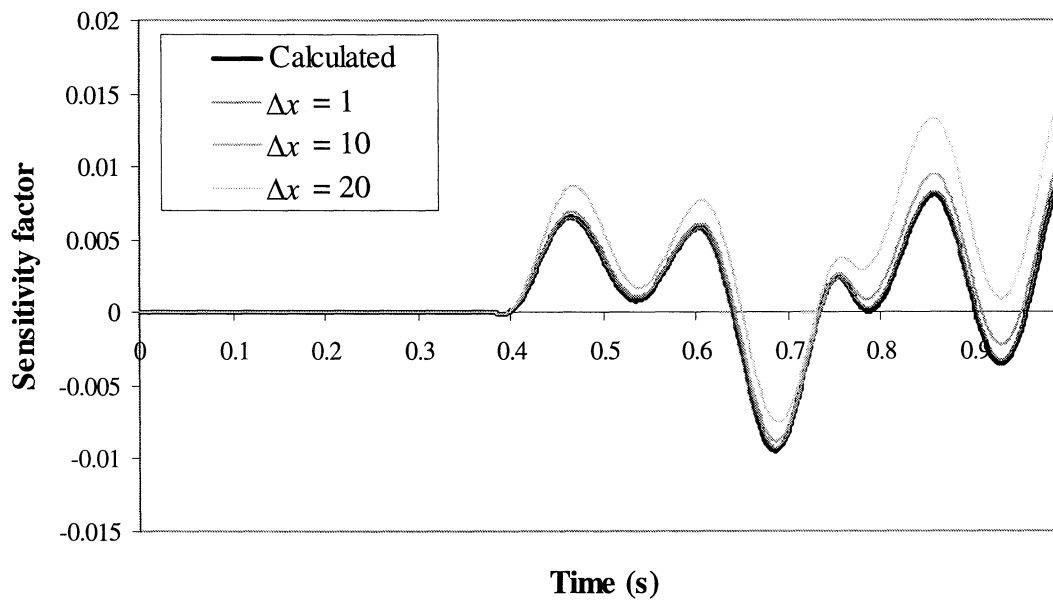
FIGURE 7-19 Sensitivity factor with respect to yield stress

152
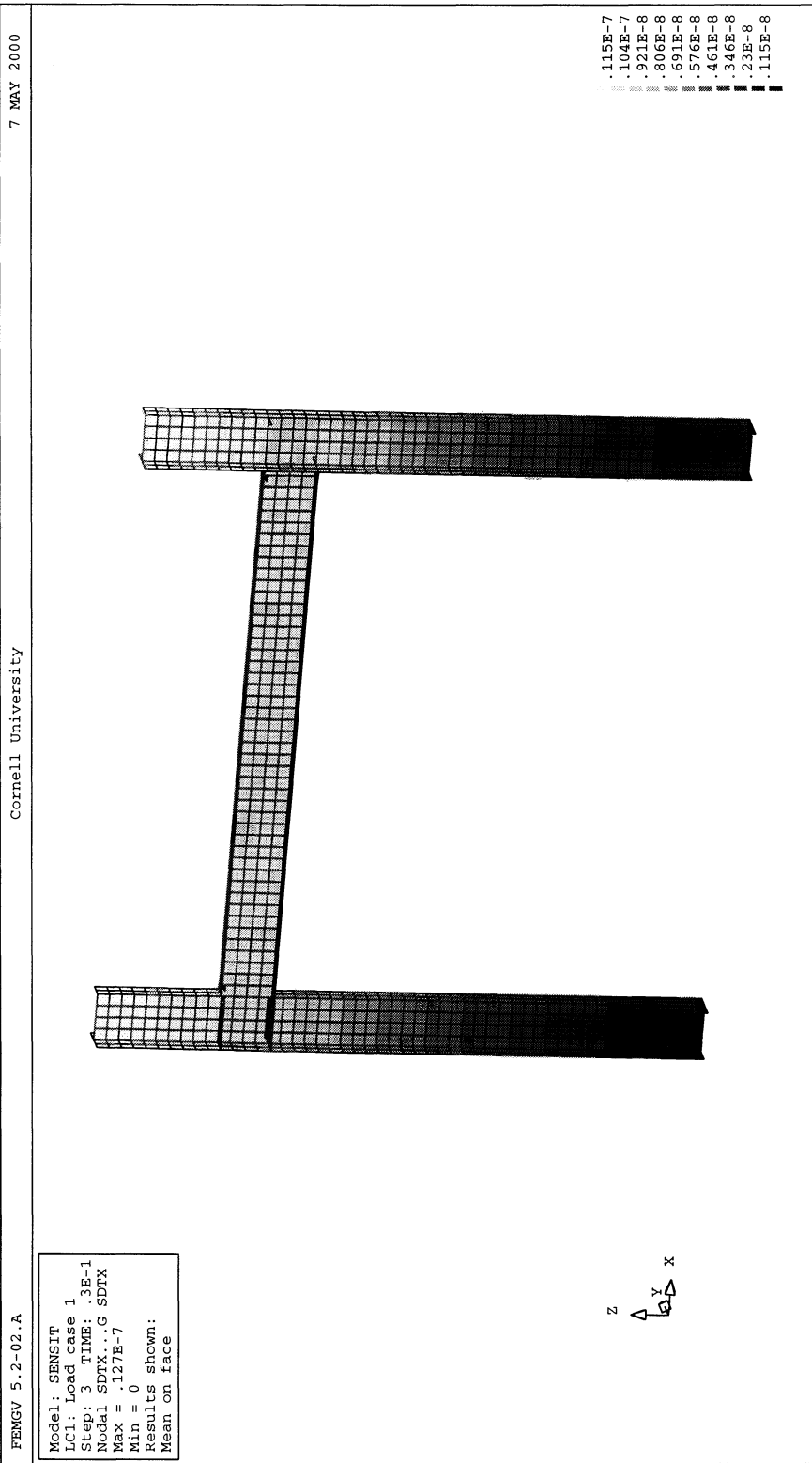
FIGURE 7-20 Sensitivity factors

153

SECTION 8
COMPARISON OF MATLAB AND DIANA OUTPUTS

After consideration of the MATLAB and DIANA programs to calculate sensitivity factors described in Sections 6 and 7, the following question naturally arises: is it meaningful or even possible to compare the outputs from the two programs for the same problem?

In general, due to differences in the material model formulation, element formulation, tolerance calculation, and many other factors, it is difficult to compare the results calculated by two different computer programs for a nonlinear problem. For example, it should not be expected that the two programs will necessarily give very similar displacement results. The MATLAB and DIANA programs are good examples of two programs with different modeling approaches, material models and element types and will probably not give identical results. Consider, for example, the simple nonlinear elastic-plastic oscillator of Section 3.4. The oscillator was analyzed for 10 seconds of the Taft ground motion (figure 8-1) using both MATLAB (SABER-2D) and DIANA. In MATLAB, the oscillator was modeled by the nonlinear truss element of Section 6.2.2 (figure 8-2). In DIANA, a two-dimensional beam element with von Mises plasticity and a stress–strain curve selected to match figure 3-3 was used (figure 8-3). The calculated displacements are shown in figure 8-4. Due to the differences mentioned before, the displacements are different. If the displacements are different, the sensitivity factors will also be different. The sensitivity factors with respect to the yield strength f_y calculated by the two programs are shown in figure 8-5. As expected, the sensitivity factors are of a similar order of magnitude but are not identical. Sensitivity factors with respect to other parameters show the same trend.

It must be emphasized that it is not the case that one program has given "correct" results and the other "incorrect" results. The sensitivity factors calculated by each program were checked by finite differences, and each one is correct for its corresponding displacement. The displacements are different due to the different formulation of the models used. Each program could be calibrated against experimental results to improve its accuracy. There is no reason for the displacements and sensitivity factors to be identical.

The only problems for which identical displacements and sensitivity factors should be expected are simple linear problems. To illustrate this, the plastic behavior of the oscillator was dropped and the resulting linear elastic oscillator analyzed under the same Taft ground motion as before. The resulting displacements and sensitivity factors are identical for both programs, as shown in figures 8-6 and 8-7.

In conclusion, comparing the results for MATLAB and DIANA is not really meaningful for nonlinear problems. The sensitivity factors calculated by each are correct, but should not be expected to be identical. Each program has a different modeling approach, resulting in different displacements and sensitivity factors. The different modeling approaches were in fact selected intentionally, to allow different levels of modeling detail in accordance with the required capabilities listed in Section 5.
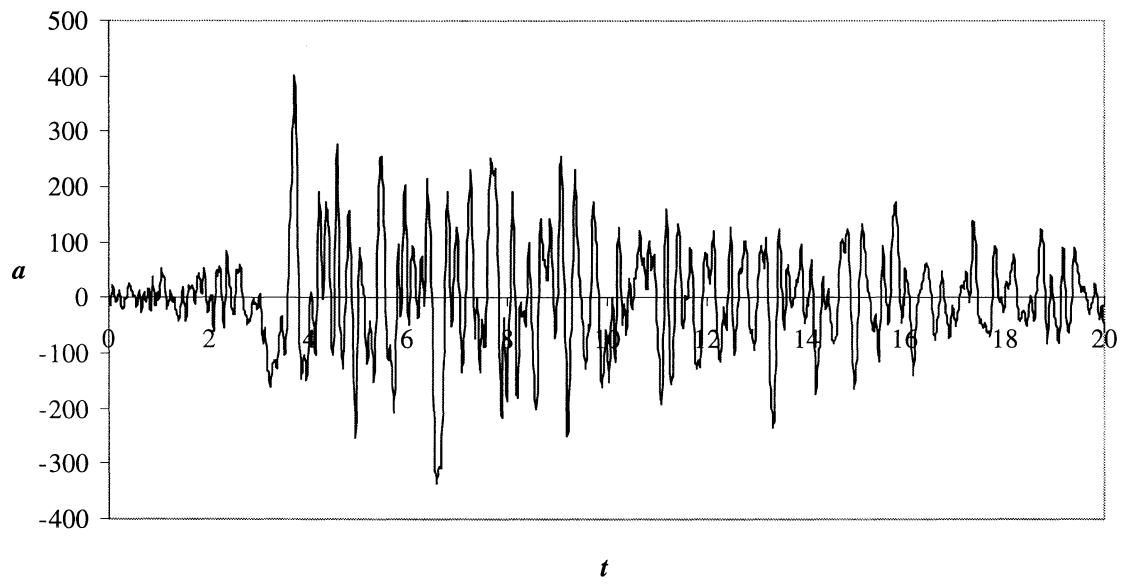
FIGURE 8-1 Taft ground motion
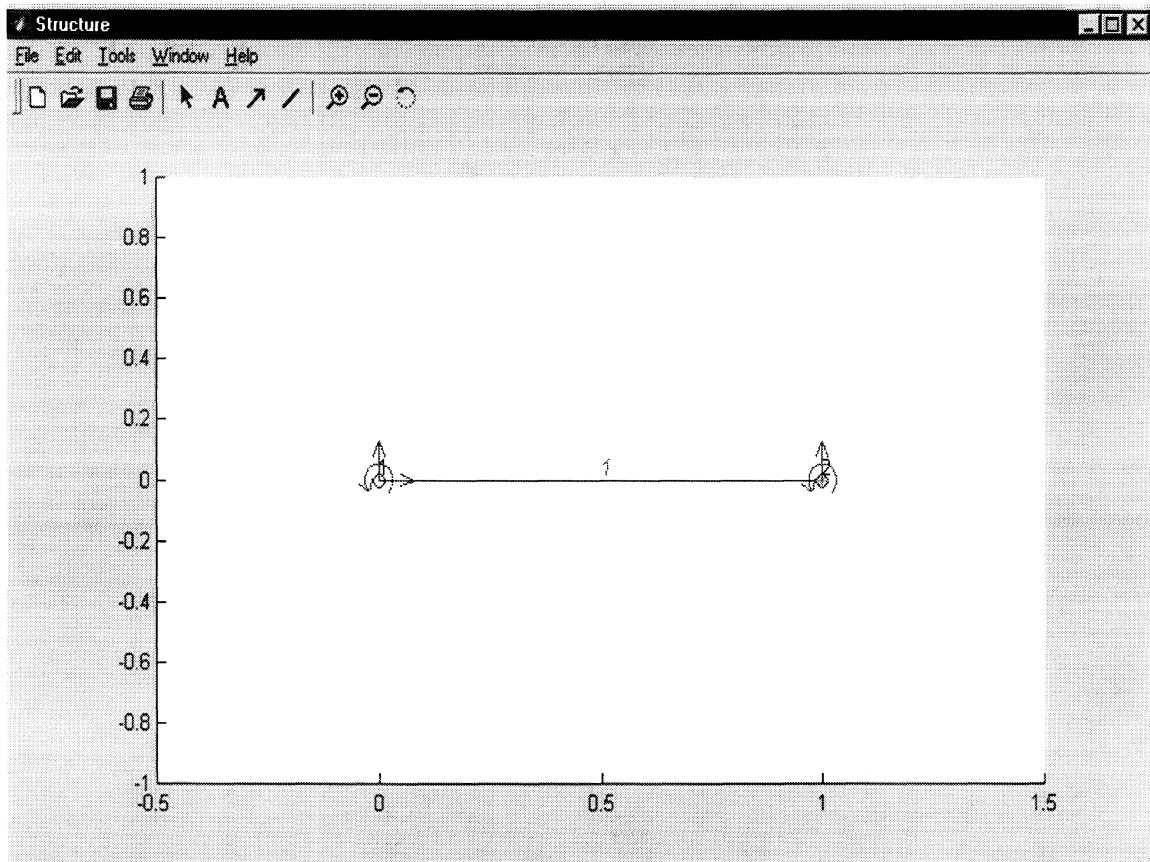
FIGURE 8-2 MATLAB model

156
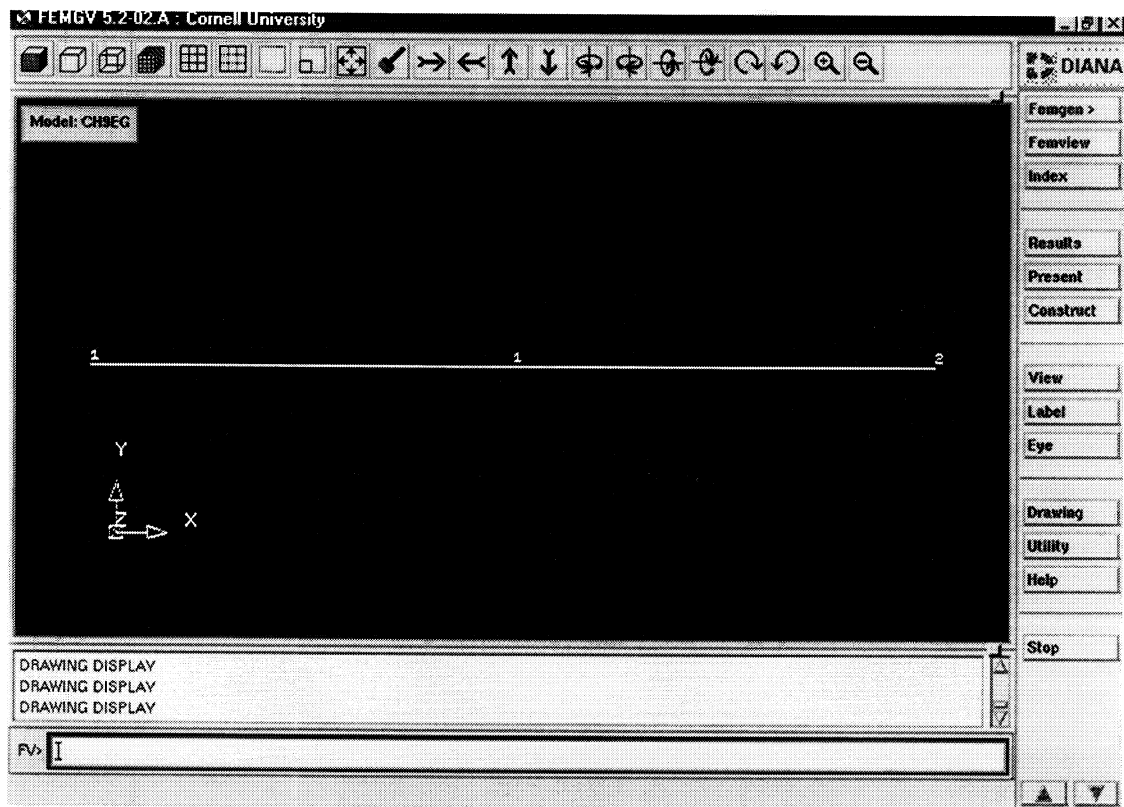
FIGURE 8-3 DIANA model
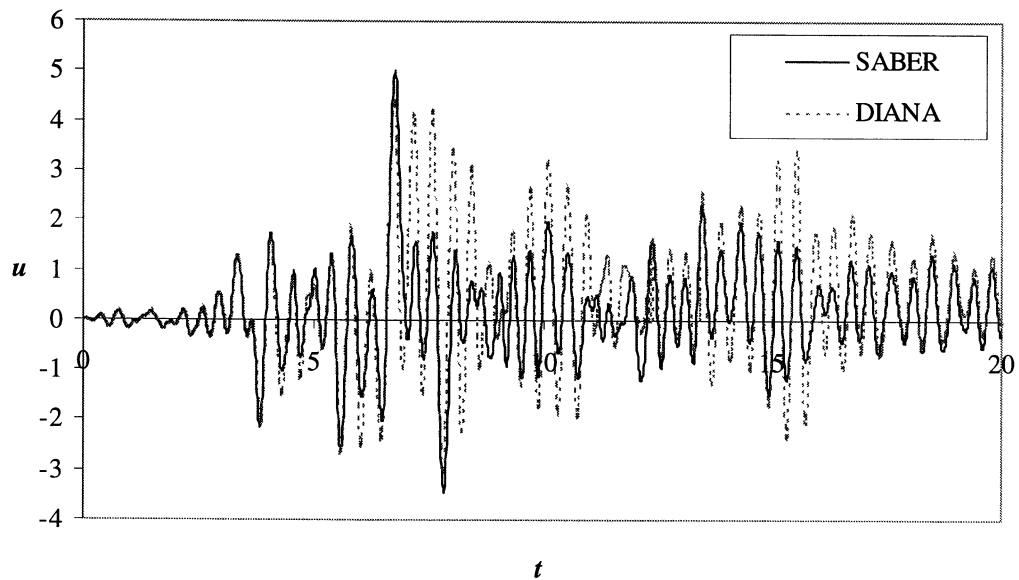
FIGURE 8-4 Displacement of nonlinear oscillator
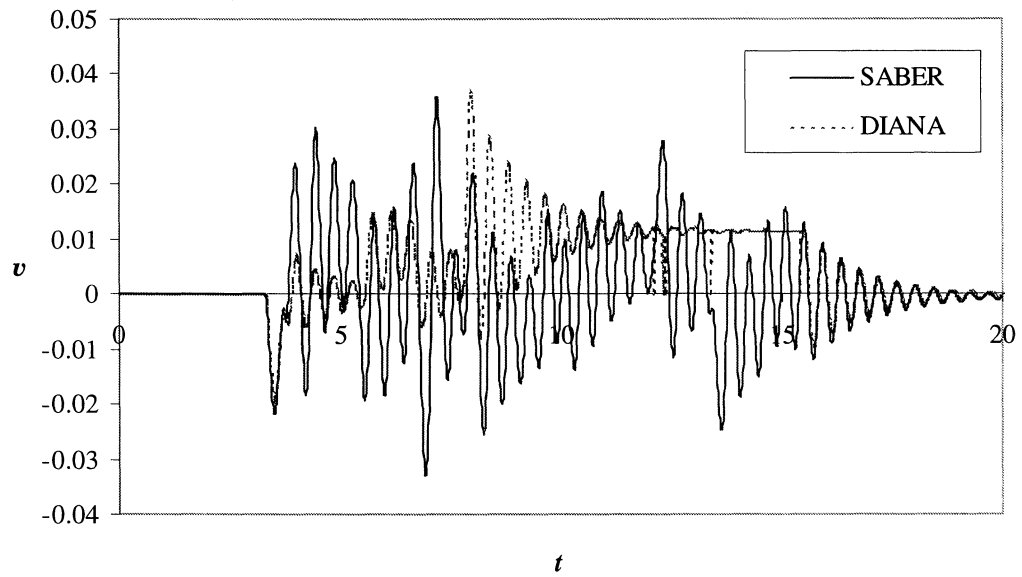
FIGURE 8-5 Sensitivity factors with respect to yield stress for nonlinear oscillator
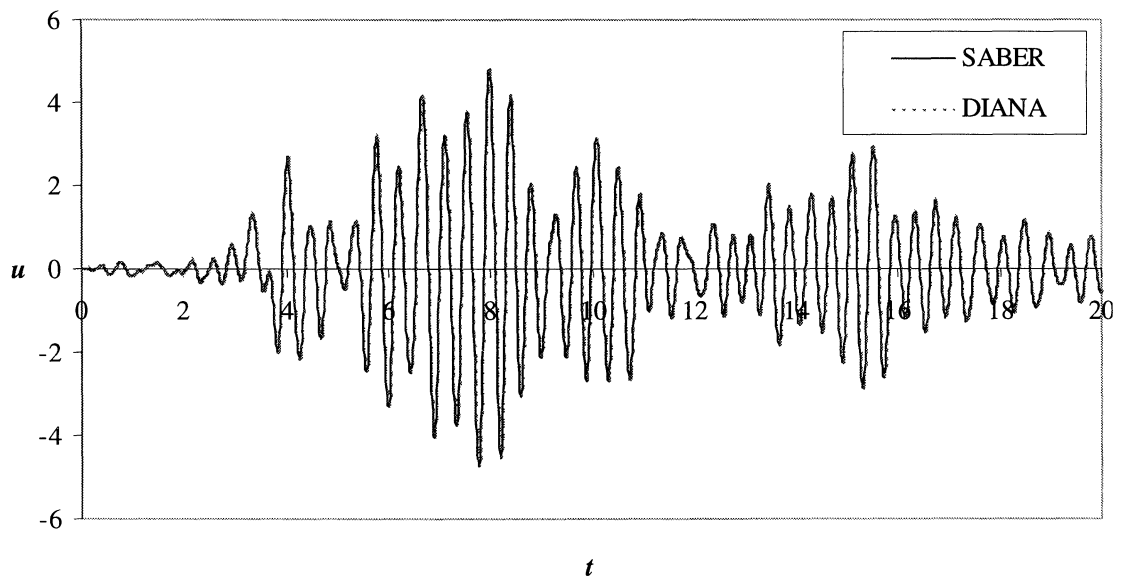
FIGURE 8-6 Displacement of linear oscillator

158
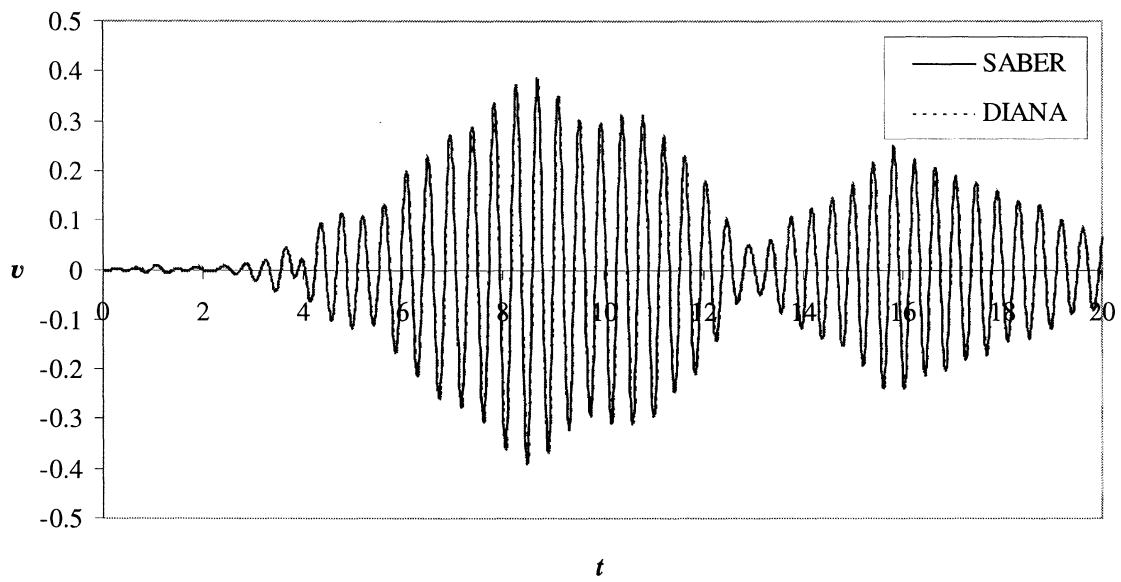
FIGURE 8-7 Sensitivity factors with respect to stiffness for linear oscillator

SECTION 9
DEMONSTRATION PROJECT

9.1 Introduction

This section describes a demonstration project to illustrate the use of the sensitivity factors in the analysis and design of a real building. The example chosen is a hospital in Buffalo. Both primary and secondary systems in the hospital will be considered: the primary system is the hospital structure itself, while the secondary system is the piping system that supplies water for fire suppression. Although both systems are based on real, existing systems, simplifications and assumptions will be made either where necessary to illustrate the use of the sensitivity factors without excessive complication, or where insufficient data is available. The work is not intended to be applied to the real structure, but only as a demonstration of the use of the sensitivity factors for the identification of critical parameters, selection of design and retrofit strategies, and generation of approximate fragility curves.

In analysis of secondary systems it is frequently assumed that "cascade" analysis applies. This assumption is made here. The characteristic of a cascade analysis is that there is no feedback from the secondary to the primary system. The primary system is analyzed without considering the secondary system, and the results used as input to the analysis of the secondary system. The assumption is valid if the primary system is substantially heavier and more stiff than the secondary system, which is clearly true for a structural frame primary system and non-structural piping secondary system.

9.2 Ground motion

As insufficient real earthquake records exist for the Buffalo area, artificial motions are used as the input ground motions to the primary system. The ground motions are realizations of a Gaussian stochastic process with the amplitude modulated through time by an envelope function. The power spectral density $g(\omega)$ of the process is based on the specific barrier model for simulating earthquake ground motion [51]. The parameters of the model are the magnitude M and distance r of the earthquake event causing the motion, and the average soil shear wave velocity to a depth of 30 m at the site, V_{30}. The values selected are $M = 6$, $r = 50$ km and $V_{30} = 255$ m.s^{-1}. This magnitude-distance pair has a return period of 10000 years at the site (based on data in [21]). The average shear wave velocity is for a typical soil.

The resulting power spectral density is shown in figure 9-1. The magnitude, distance and average shear wave velocity are typically highly uncertain, and are considered in the sensitivity analysis in the following sections. The effects of changes in the parameter values on the power spectral density are shown in figures 9-2–9-4.

The ground motion is generated from the power spectral density by equation 2-15 multiplied

161
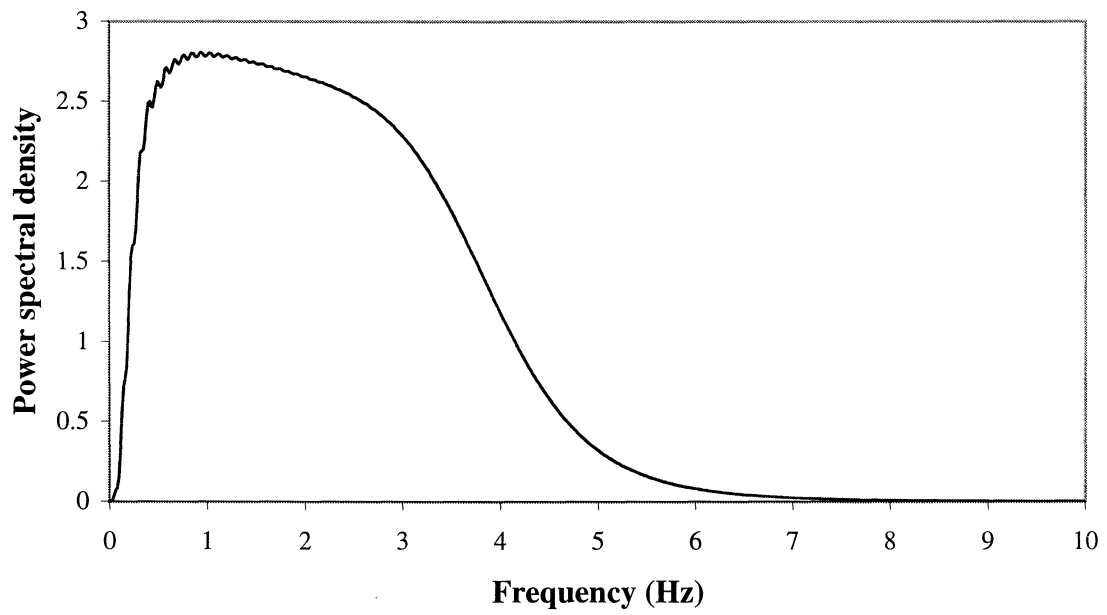
FIGURE 9-1 Power spectral density
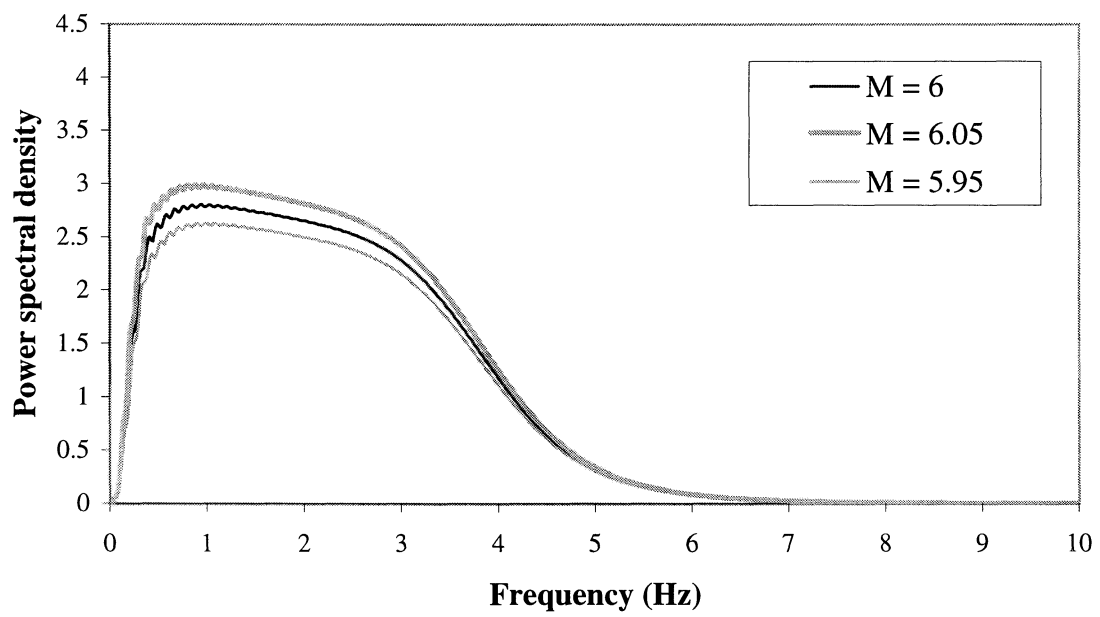
FIGURE 9-2 Effect on power spectral density of changes in magnitude M
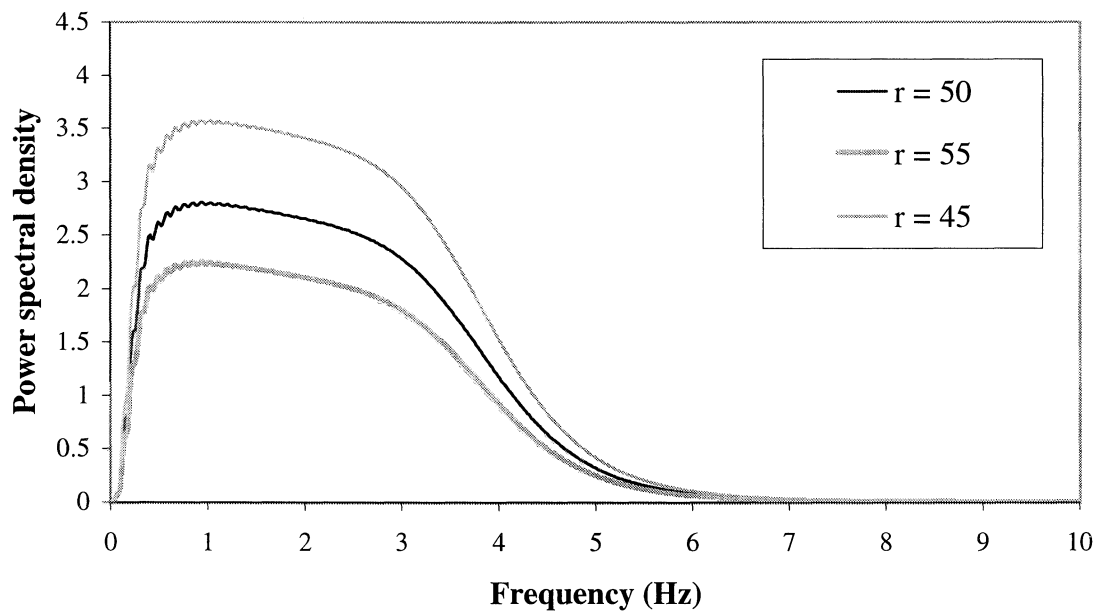
FIGURE 9-3 Effect on power spectral density of changes in distance r
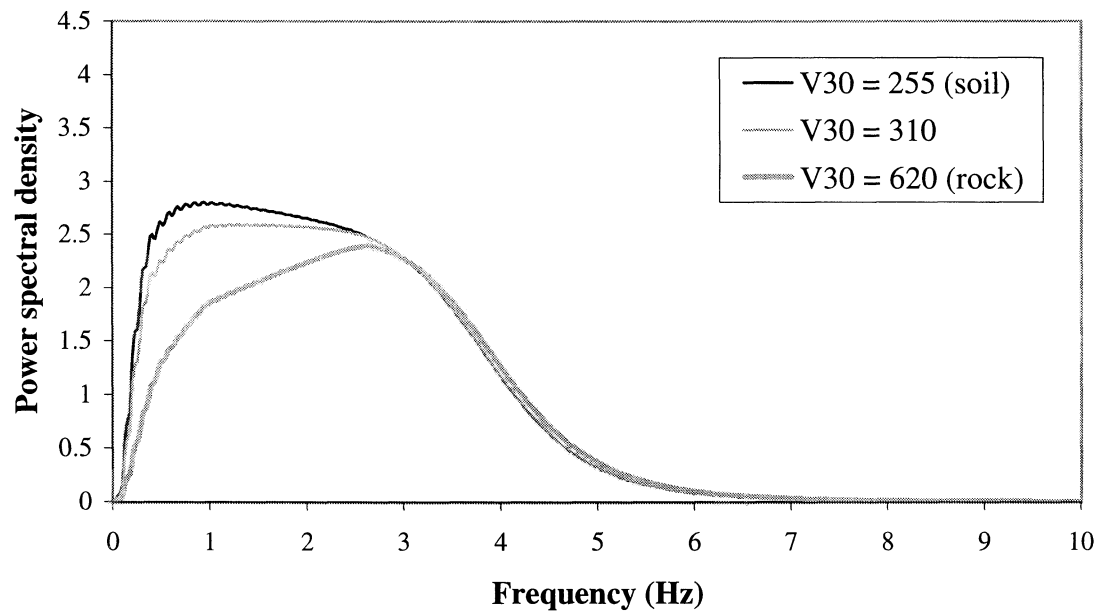
FIGURE 9-4 Effect on power spectral density of changes in average shear wave velocity V_{30}
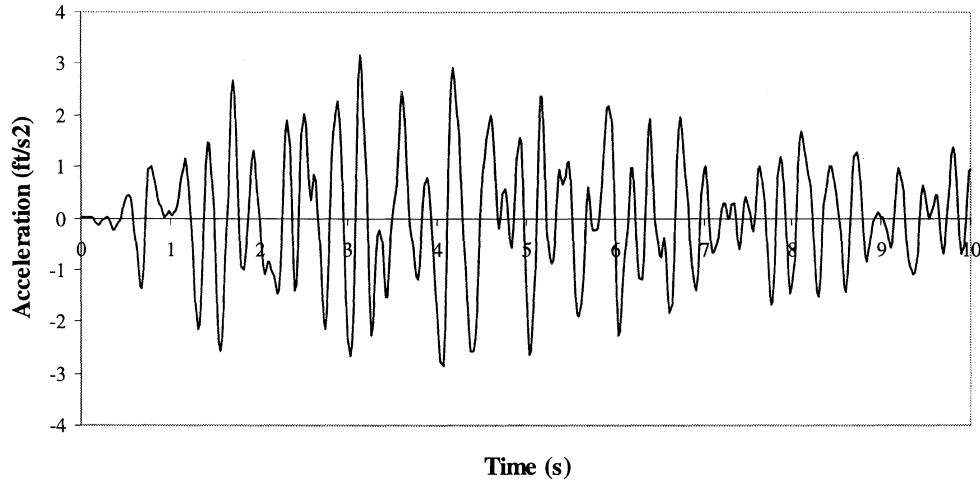
FIGURE 9-5 Ground motion sample 1

by the envelope function

$$a(t) = w(t) \sum_{k=1}^{n} \sqrt{g(\omega_k, \boldsymbol{\theta}) \Delta \omega} \left(A_k \cos(\omega_k t) + B_k \sin(\omega_k t) \right) \tag{9-1}$$

where $w(t)$ is the envelope function, $\boldsymbol{\theta} = [M \; r \; V_{30}]$, ω_c is a cut-off frequency, $\Delta \omega = \frac{\omega_c}{n}$; $\omega_k = (k - \frac{1}{2}) \Delta \omega$; and A_k and B_k are independent standard Gaussian random variables.

The derivative of a realization of the ground motion with respect to a general parameter x in $\boldsymbol{\theta}$ is

$$\frac{\partial a(t)}{\partial x} = \sum_{k=1}^{n} \frac{\sqrt{\Delta \omega}}{2\sqrt{g(\omega_k, \boldsymbol{\theta})}} \frac{\partial g(\omega_k, \boldsymbol{\theta})}{\partial x} \left(A_k \cos(\omega_k t) + B_k \sin(\omega_k t) \right) \tag{9-2}$$

where the same realizations of $A_k, B_k, k = 1, 2, 3, \ldots, n$ are used in equations 9-1 and 9-2. $\frac{\partial a(t)}{\partial x}$ is then used to calculate $\frac{\partial \boldsymbol{f}(t)}{\partial x}$ in the governing equation of the sensitivity factor (equation 3-4).

For real analysis, design or selection of retrofit strategies, a suite of ground motions should be considered, each with a different realization of $A_k, B_k, k = 1, 2, \ldots, n$. For the example in this section, two ground motion samples are considered (figures 9-5 and 9-6). The samples are independent and are applied separately at the base of the primary system. Results for displacement and sensitivity factors are calculated for both samples and compared.

164
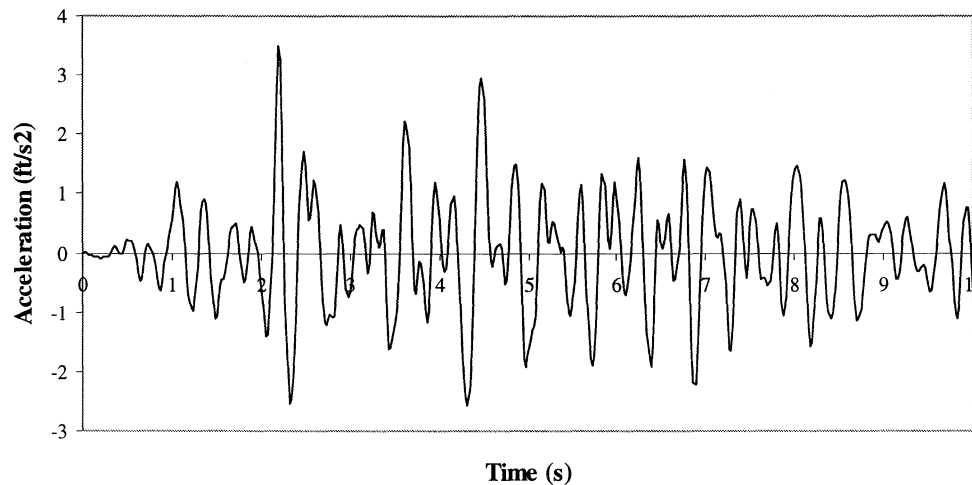
FIGURE 9-6 Ground motion sample 2

9.3 Primary system

The primary system is the structural frame of the hospital. It is a 14 story steel frame structure (figure 9-7). A SAP2000 computer model of the structure was prepared at the State University of New York at Buffalo. The model was converted to DIANA for the sensitivity analysis. It has 10678 elements, 551 different element geometries and 46845 degrees of freedom. The model uses beam elements and the Rayleigh damping parameters were selected to allow 5% damping in the first two modes. The system remained linear when subjected to the given ground motions. It is possible to increase the ground motion to cause nonlinear behavior, but it was decided to keep the linear behavior for the following reasons:

1. The original SAP2000 model of the structure was intended for linear analysis only and necessary data for nonlinear analysis was not included.

2. An approach that will be used for analysis of the secondary system uses the linear modes of the primary system to generate the motion of the support points of the secondary system without performing a time-history analysis of the primary system [45]. The method assumes that the primary system remains linear.

3. The model is intended to illustrate the concepts of sensitivity analysis, which are the same for both linear and nonlinear structures. Nonlinear behavior is not essential for the example.

When analyzing the structure it is necessary to identify the critical outputs of the analysis, and the criteria that must be met by the critical outputs. Examples of critical outputs

165
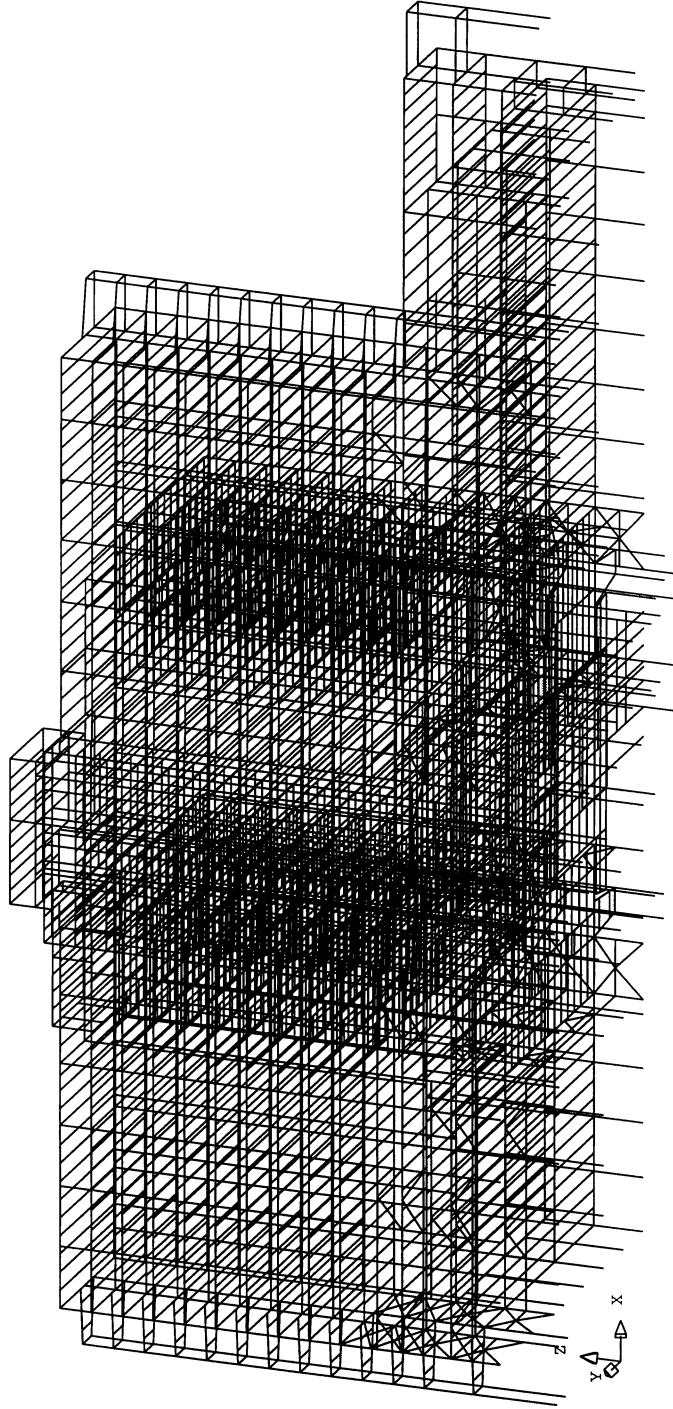
FIGURE 9-7 Primary system
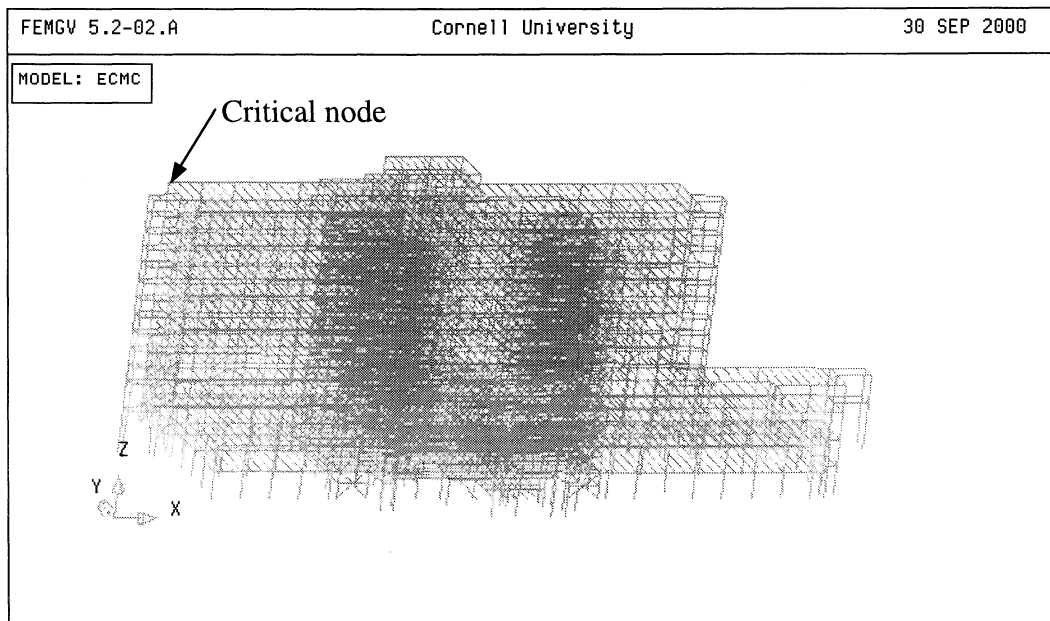
FIGURE 9-8 Node for critical displacement

are roof displacement, interstory drift and damage indices based on functions of the displacements. One common example of a criterion is that the maximum absolute value, or peak, output should be less than a specified threshold. For the purposes of this analysis, the displacement in the X-direction of a node on the roof is selected as the critical output (figure 9-8). Typical limits for the displacement are $1/400 - 1/600$ of the height of the building [47]. The calculated displacements under the given ground motions are shown in figure 9-9. They are approximately $1/2000$ of the building height, which is satisfactory.

9.3.1 Identification of critical parameters

The first use of the sensitivity factors is the evaluation of the effects of the various input and system parameters on the output or response. Suppose that we wish to evaluate the sensitivity of the response to the following parameters: the Young's modulus E of the steel sections in the structure, the coefficient b of the global stiffness matrix in the specification of Rayleigh damping, the earthquake magnitude M, or the soil shear wave velocity V_{30}. The evaluation of the sensitivity will be demonstrated using ground motion sample 1 as the input.

The sensitivity factors for the displacement of the roof with respect to each of the parameters were calculated by DIANA and are shown in figures 9-10–9-13. However, as pointed out in Section 2.3, *two* factors must be considered when evaluating the sensitivity: (1) the sensitivity factors themselves, and (2) the uncertainty in the parameter values. The uncertainty in a
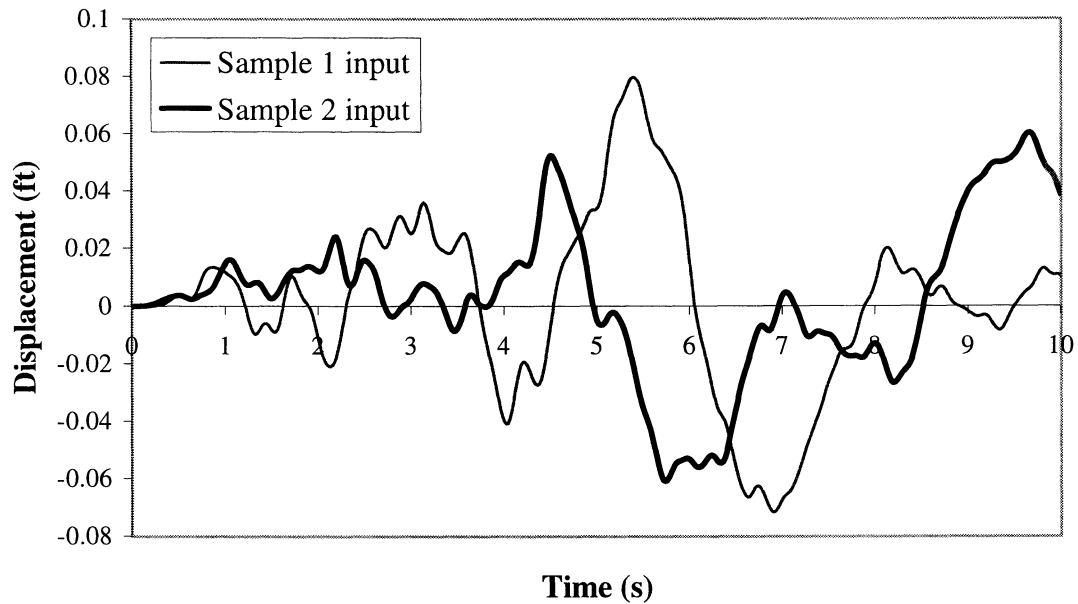
FIGURE 9-9 Displacement

parameter value is the amount by which the value may reasonably be expected to vary from the nominal value. This will in general be different for each parameter, as some parameters are inherently less uncertain than others. For example, the uncertainty in the Young's modulus of steel is typically less than the uncertainty in the damping or in the seismic loading. The uncertainties may also vary from case to case. For example, the uncertainty in the soil shear wave velocity will be substantially less if it is based on tests at the site than if it is based solely on the estimated soil conditions.

The assumed uncertainties in the parameter values for the demonstration project are described below.

- The Young's modulus E of the steel is usually known within 3% [44].

- The damping of the structure is less accurately known. An uncertainty of 20% is assumed [13].

- The average soil shear wave velocity V_{30} can typically only be estimated within 20% given the soil conditions at the site.

- The earthquake magnitude M is highly uncertain. However, for illustration an uncertainty of 20% is assumed.

Three methods are suggested to evaluate the sensitivity with respect to the different parameters:

1. One often suggested method of comparison is to multiply the sensitivity factors by the nominal parameter values (figure 9-14) [68]. This results in a factor that indicates the sensitivity of the output to changes in the *percentage* of the parameter values. For example, if the factor in figure 9-14 with respect to b is larger than that with respect to E, this indicates that the output is more sensitive to a 1% change in b than to a 1% change in E. In fact, multiplying the factor by 0.01 gives an estimate of the difference between the original displacement and the displacement found after changing the parameter value by 1%. However, this method of comparison is valid *only if* the uncertainty in the parameter value is the same percentage of the nominal value for each parameter. In general, the uncertainties in the parameters are very different so the method is not valid. For example, the uncertainty in E is 3% while the uncertainty in b is 20%.

2. A second and possibly more useful way to evaluate the sensitivity is to use the first order Taylor series approximation to estimate the effect of changes in the parameter values, as in equation 2-4 which is repeated here

$$\boldsymbol{u}(t, \boldsymbol{x}_0 + h\boldsymbol{e}_i) \approx \boldsymbol{u}(t, \boldsymbol{x}_0) + \boldsymbol{v}_i(t)h \qquad (9\text{-}3)$$

   The advantages of this method are (1) the magnitude of the uncertainty h in the parameter value is explicitly considered; and (2) the original displacement is also taken into account. The second point is important as, for example, we may be more interested in the sensitivity at the time of the peak displacement than in the sensitivity when the displacement is small. This information is not considered in figures 9-10–9-14.

   The effects of increasing E by 3%, b by 20%, V_{30} by 20% and M by 20% are shown in figure 9-15, and the effects of decreasing the parameters by the same amounts in figure 9-16. The figures show that the output is more sensitive to the input parameters V_{30} and M than to the system parameters E and b.

3. A different approach to identifying the critical parameters is to consider them to be random and to calculate the contribution of each to the variance of the response. Using upper case letters for random variables, assume that the parameter vector $\boldsymbol{X} \in \mathbb{R}^m$ is a random vector and that element X_i has variance $\sigma_i^2, i = 1, 2, 3, \ldots, m$. From the first-order Taylor approximation (equation 9-3), it can be shown that the variance of u_j can be approximated by

$$\mathrm{Var}[u_j(t, \boldsymbol{X})] \approx \sum_{i=1}^{m} v_{ji}^2(t)\sigma_i^2 \qquad (9\text{-}4)$$

   provided that the nominal parameter vector value at which the sensitivity factors are calculated is equal to the mean value, $E[\boldsymbol{X}]$. One possible assumption about the coefficients of variation of the random parameters is that they are the same as the uncertainties defined previously, that is, 0.03 for E, 0.2 for b, 0.2 for V_{30} and 0.2 for M. This assumption is followed here. Figure 9-17 shows the variance of the displacement of the critical node, calculated by equation 9-4. The total variance is subdivided

169
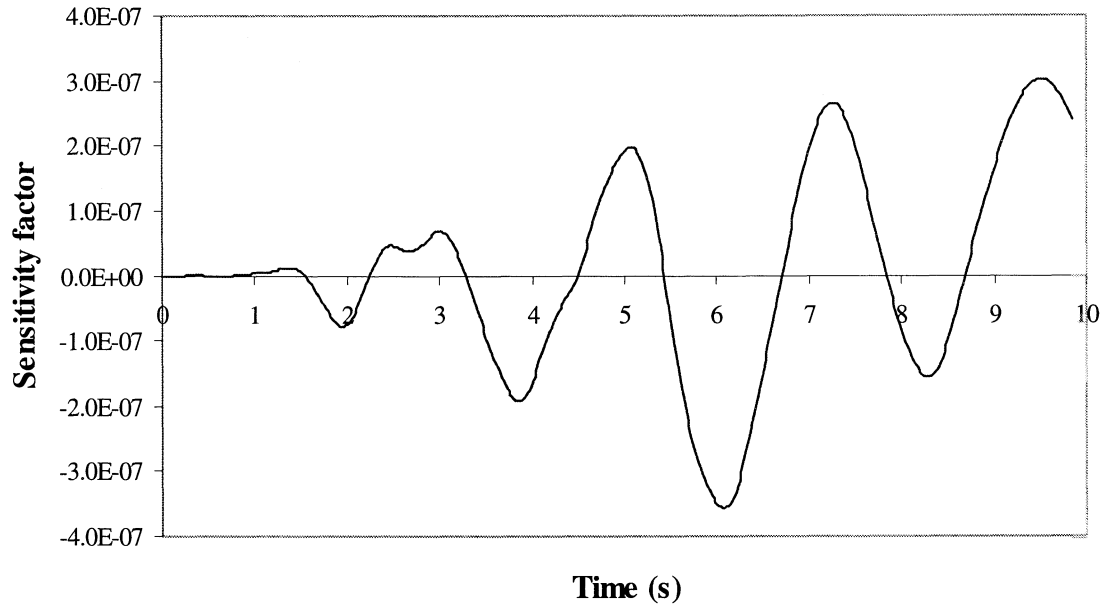
FIGURE 9-10 Sensitivity factor with respect to Young's modulus E

into different bands showing the contribution of each term on the right-hand side of equation 9-4 to the total. A critical parameter is one which has a large contribution to the total variance. Inspection of figure 9-17 shows that the earthquake magnitude M is the most critical parameter. Among the system parameters, it is clear that b is more critical than E.

Similar conclusions are reached after considering ground motion sample 2. The sensitivity factors multiplied by the nominal parameter values are shown in figure 9-18, and the variance of the displacement in figure 9-19. Comparison between figures 9-14 and 9-18, and figures 9-17 and 9-19 indicates similar relative magnitudes of sensitivity factors, except that the displacement is even more sensitive to M for this ground motion. As stated earlier, in real design several ground motions should be considered and conclusions made after considering all of the results.

The sensitivity factors can also be used to identify the most critical elements of the system. Consider the line of columns indicated in figure 9-20. It may be useful to identify the column in that line to which the roof displacement is most sensitive. This information can be used in selecting columns for retrofit, in improving the design, or just to give insight into the behavior of the structure. The sensitivity factors with respect to the stiffnesses of four of the ten columns are plotted in figure 9-21 for ground motion sample 1. Interestingly, the roof displacement is most sensitive to the stiffness of the top column. It appears to be roughly equally sensitive to the stiffnesses of the two columns in the middle, and less sensitive to the bottom column.
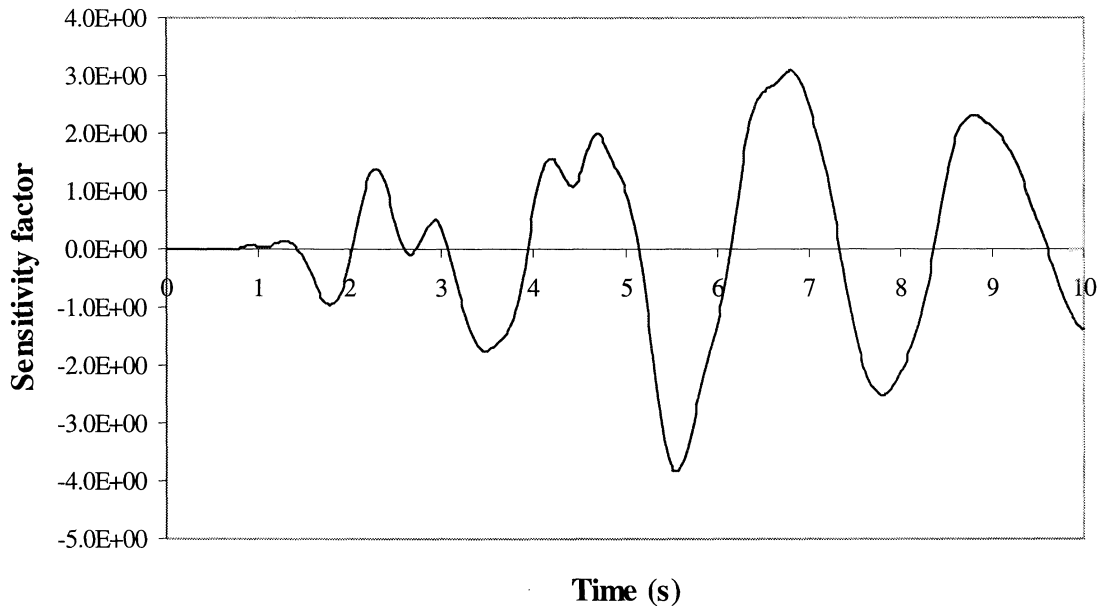
FIGURE 9-11 Sensitivity factor with respect to coefficient of stiffness in damping b
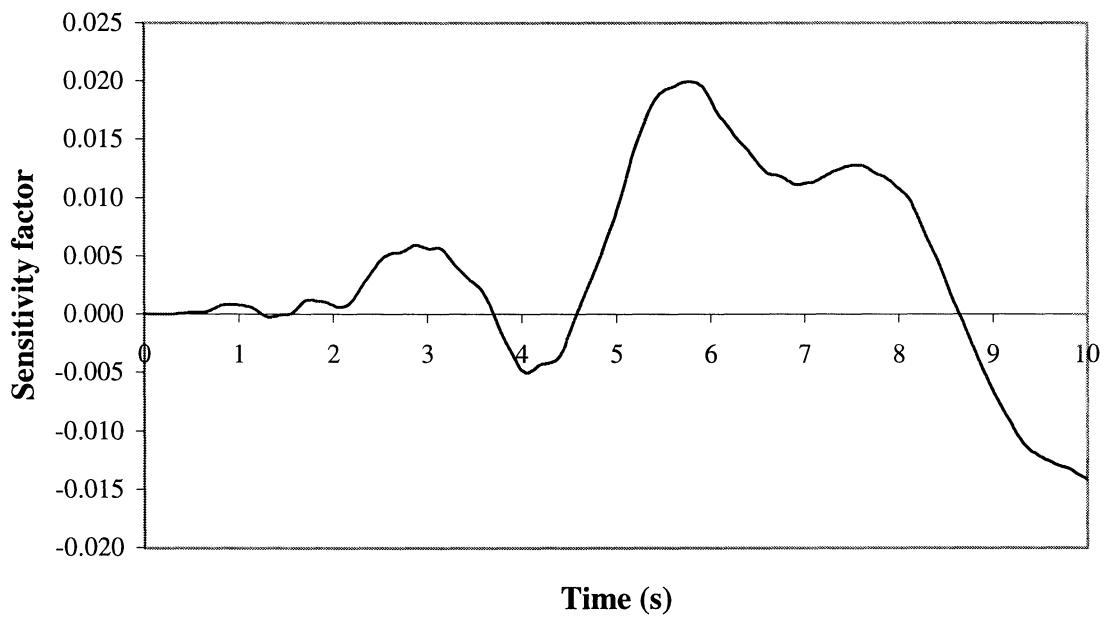
FIGURE 9-12 Sensitivity factor with respect to earthquake magnitude M
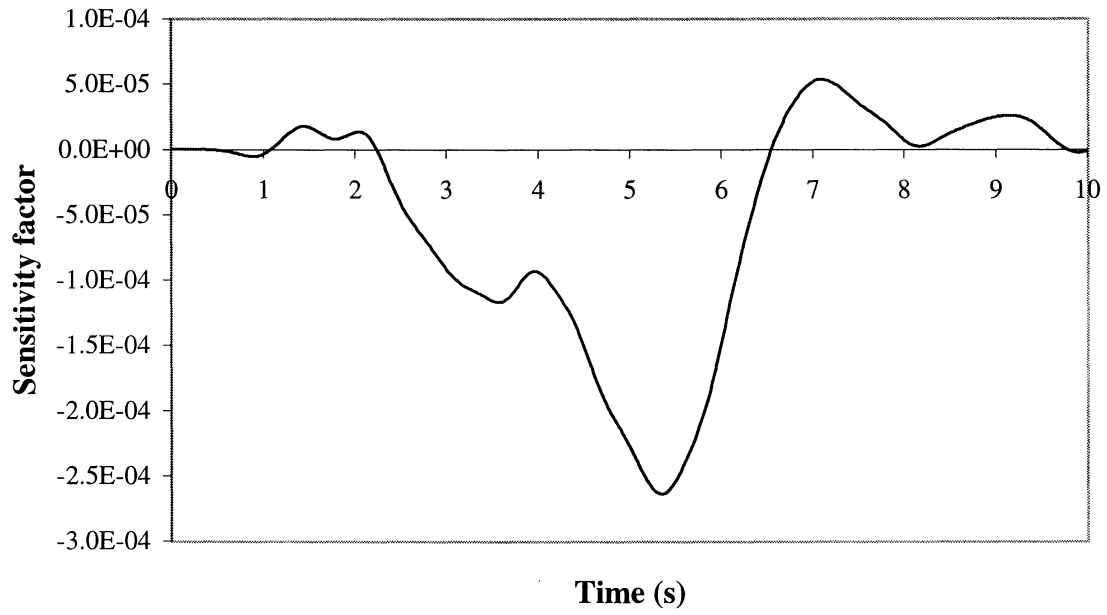
FIGURE 9-13 Sensitivity factor with respect to average shear wave velocity V_{30}
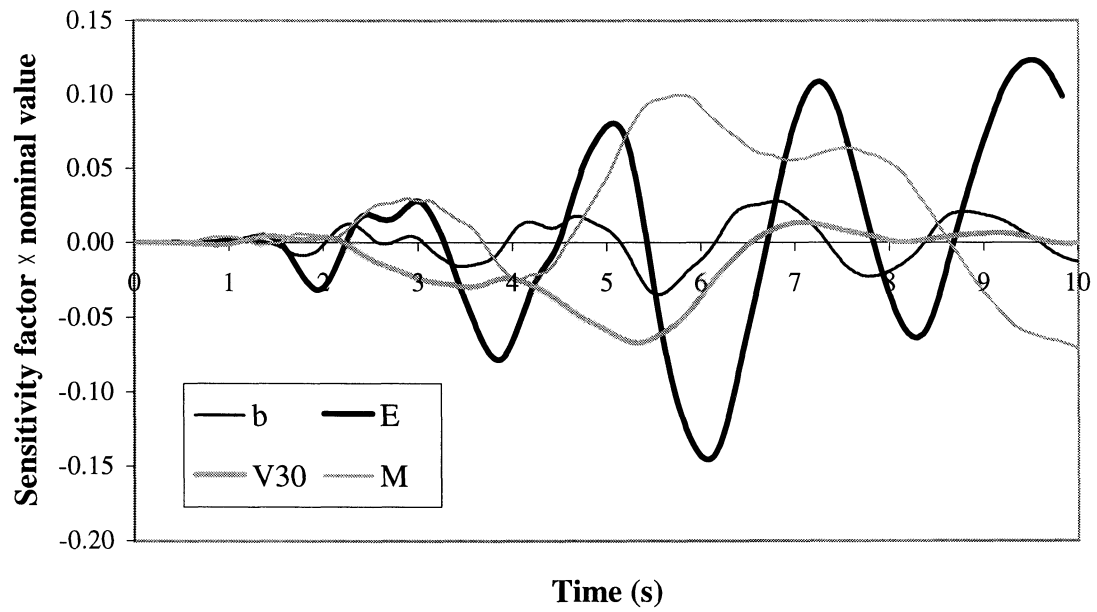
FIGURE 9-14 Sensitivity factors scaled by nominal parameter values

172
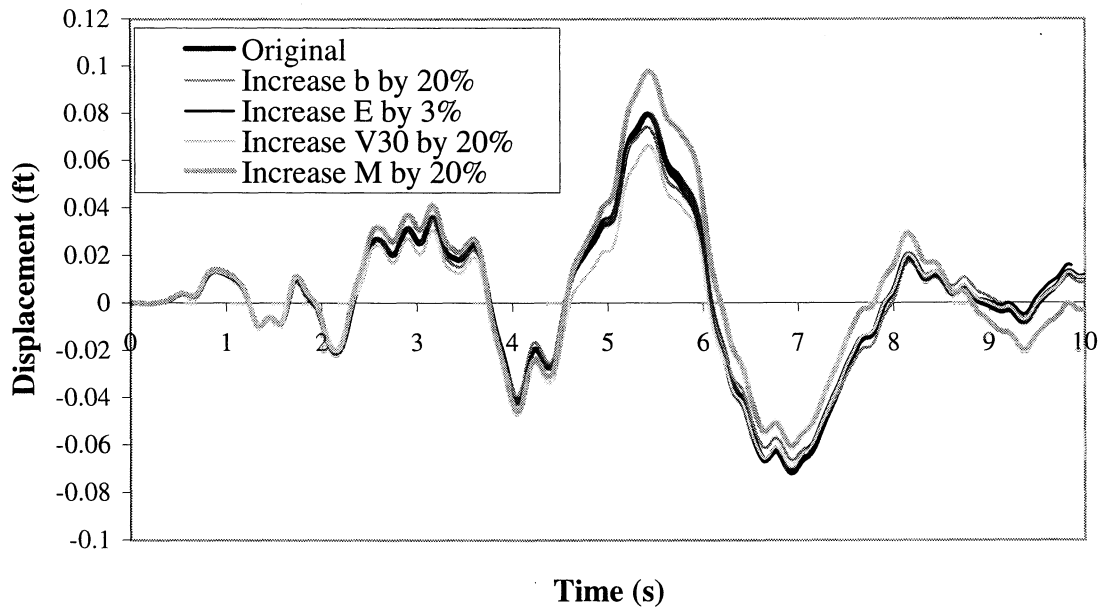
FIGURE 9-15 Effects of increasing parameters
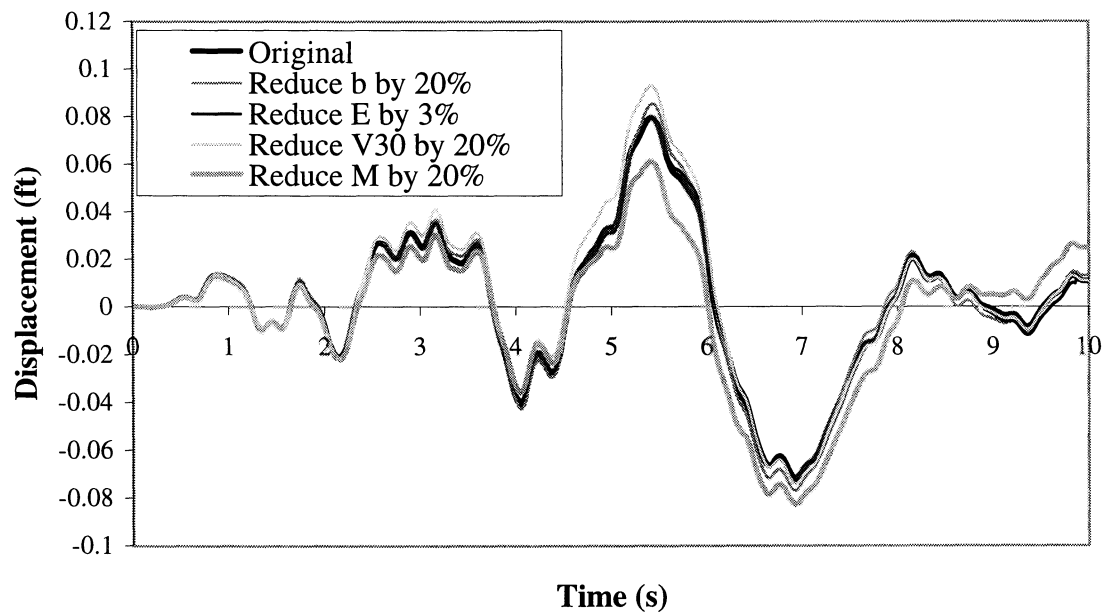
FIGURE 9-16 Effects of decreasing parameters

173
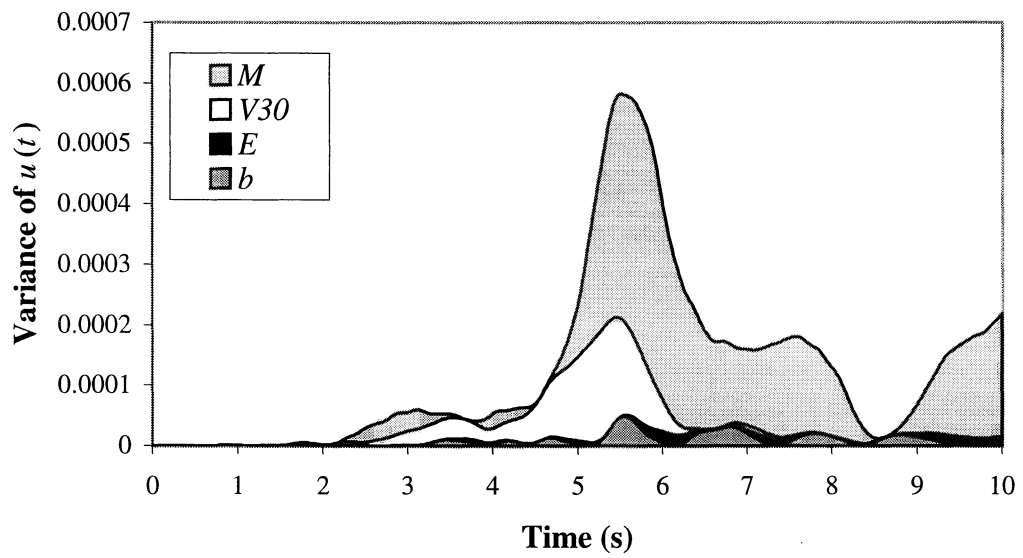
FIGURE 9-17 Variance of displacement
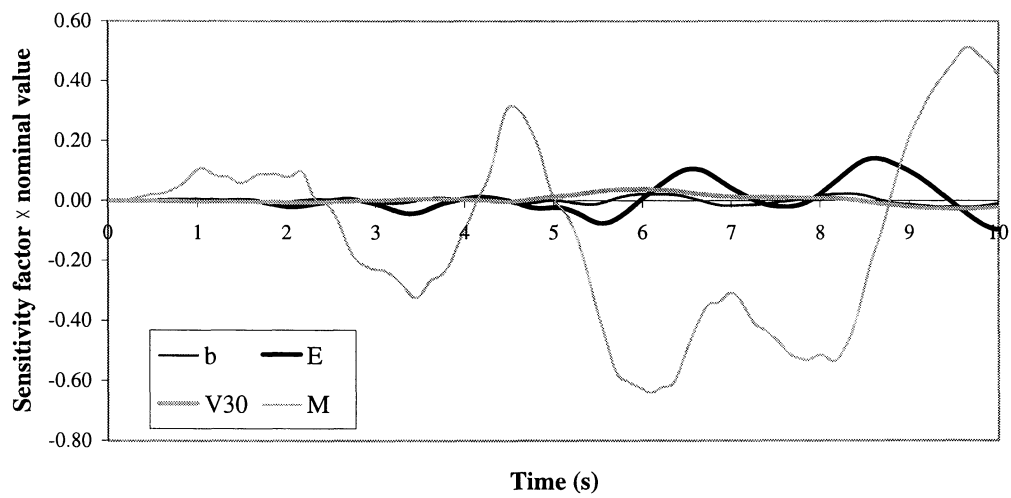
FIGURE 9-18 Sensitivity factors for ground motion sample 2

174
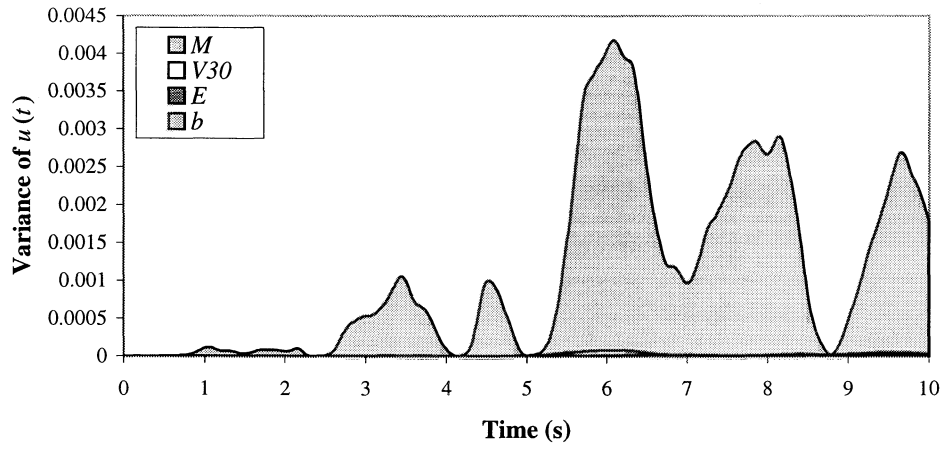
FIGURE 9-19 Variance of displacement for ground motion sample 2
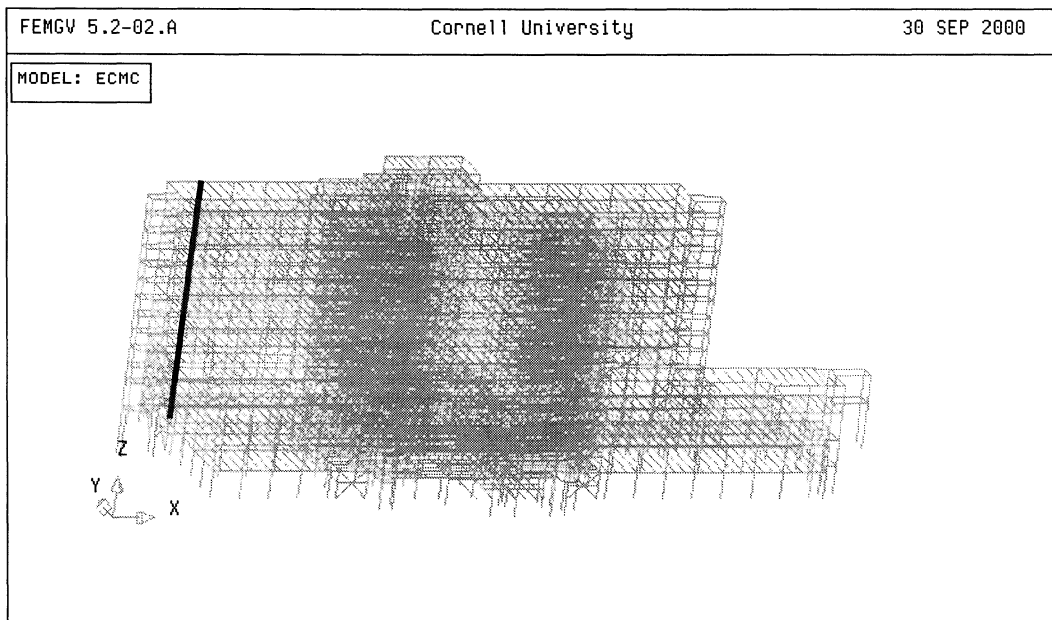
FIGURE 9-20 Columns considered
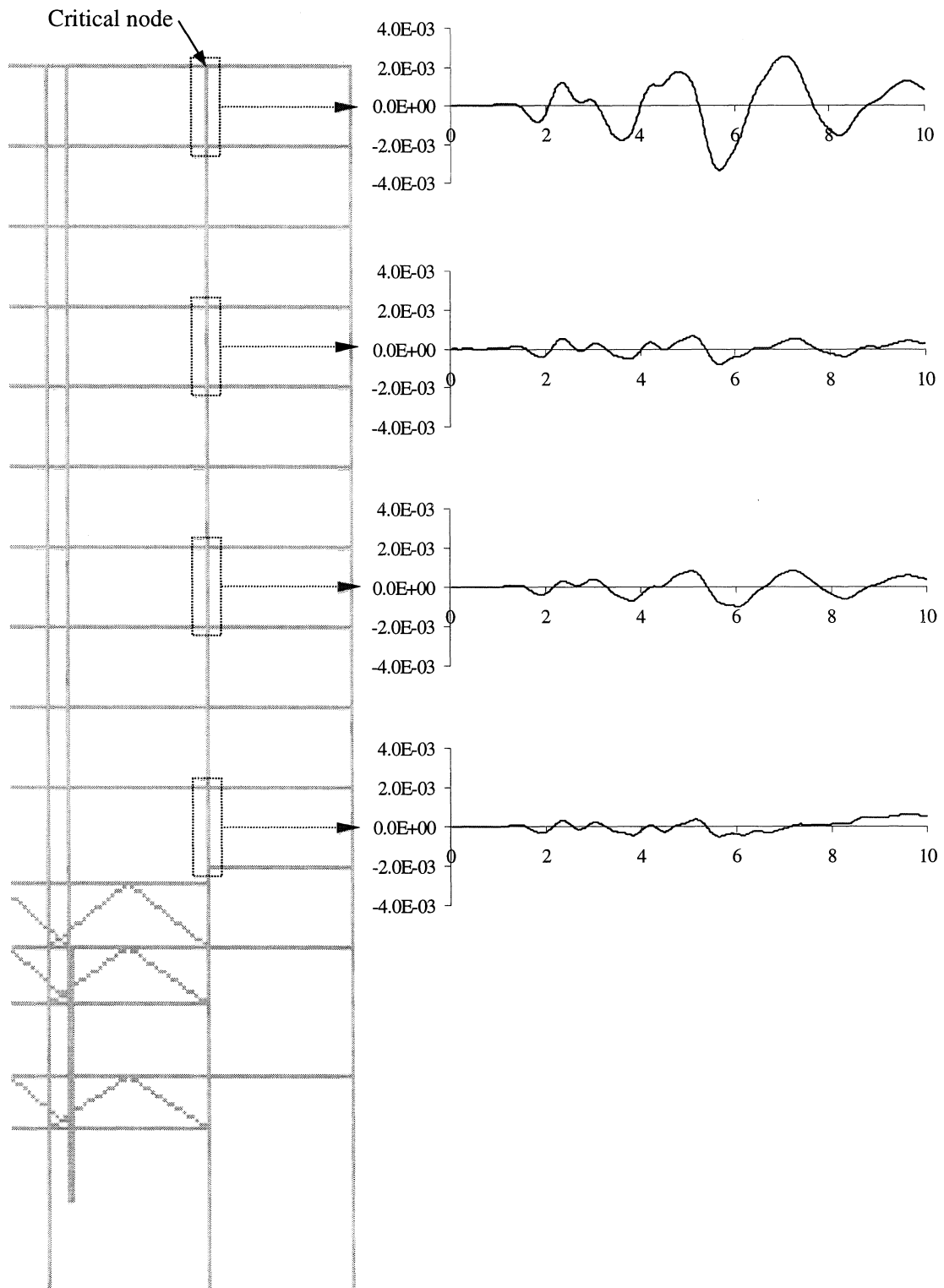
FIGURE 9-21 Sensitivity factors with respect to column stiffnesses

176

9.3.2 Improvement of design

The sensitivity factors can be used during design to assist in determining parameter values for which the structure satisfies the design criteria. For illustration, assume that the top floor houses a sensitive piece of medical equipment and that the design criterion is that the drift at the roof must be less than 1 inch for all ground motions. From figure 9-9, for sample 1 the peak displacement is 0.088 feet or 1.05 inches at $t = 5.40$ seconds. For sample 2 the peak displacement is -0.061 feet or -0.73 inches at $t = 5.74$ seconds. As the peak displacement exceeds 1 inch for sample 1, the current design is unsatisfactory. The sensitivity factors can be used to estimate whether a satisfactory design can be obtained by changing the parameters of the system.

At the time of the peak displacement for sample 1 the the sensitivity factors are

- 3×10^{-9} with respect to E

- -0.3 with respect to b

For comparison, for sample 2 the sensitivity factors at the time of the peak displacement are

- -1×10^{-8} with respect to E

- 0.1 with respect to b

Factors for both ground motions suggest that to reduce the peak value, E should be reduced or b increased. Of course, it is not realistic to reduce E of the steel, but the same effect on the structure stiffness can be obtained by using steel sections with lower moments of inertia. The damping can be increased through passive control measures such as hydraulic dampers. Suppose that it is possible to either reduce the stiffness of the structure by 10% or to increase the damping coefficient b by 10%. Both of these strategies should improve the design. The effects of the changes can be estimated by using equation 9-3. The new displacements are shown in figures 9-22 and 9-23. The new peak displacements for sample 1 are 0.084 feet if E is reduced, and 0.079 feet if b is increased. For sample 2, the peak displacements are -0.063 feet if E is reduced and -0.060 feet if b is increased. This indicates that a design that satisfies the criteria for both ground motions is obtained if the damping is increased by 10%, but not if the stiffness is reduced by 10%. The same approach can be used to evaluate different retrofit strategies.

Another potential use of the sensitivity factors is to select the optimum value of a parameter of a design or retrofit strategy by using an optimization routine as suggested in Section 4. For example, the optimum slip-load of a friction damper is often difficult to determine [62] and can be found using the sensitivity information. The procedure will be illustrated in Section 9.4 for the secondary system.
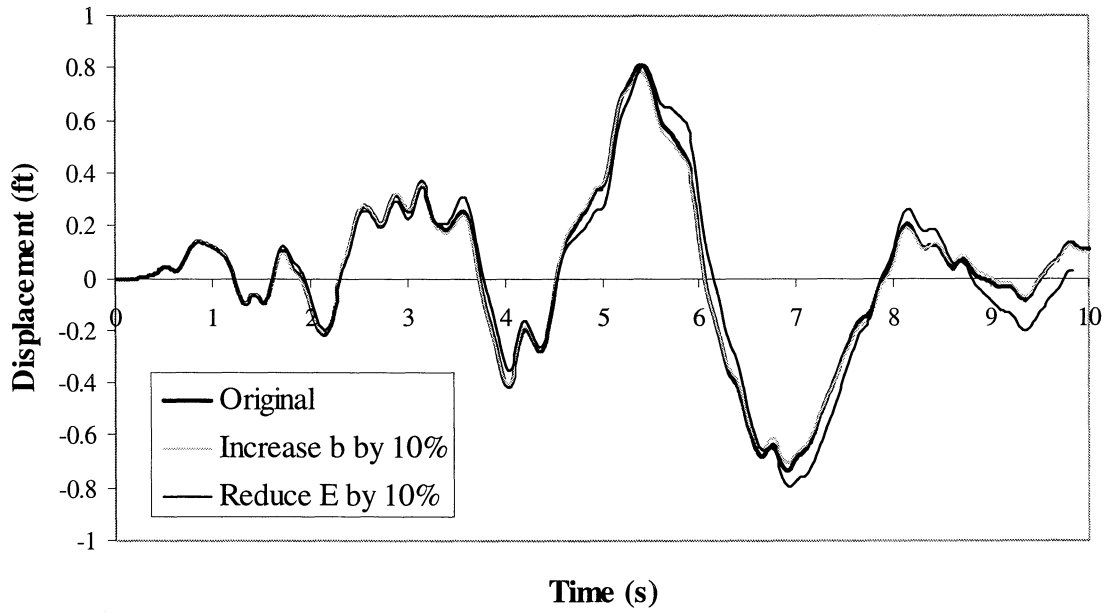
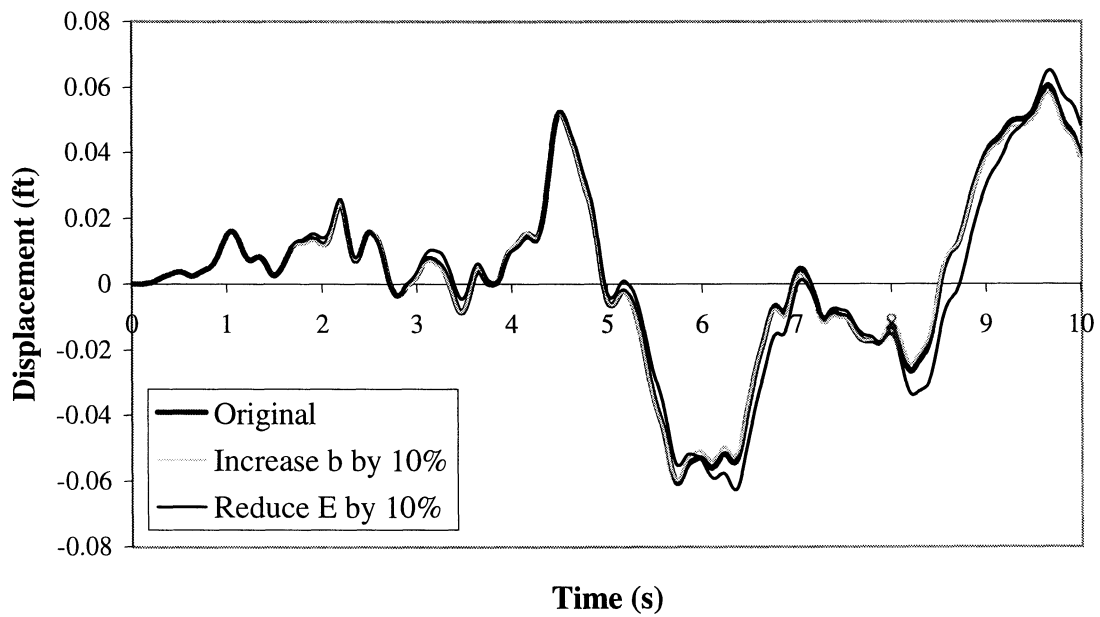**FIGURE 9-22 Displacement for ground motion sample 1**

FIGURE 9-23 Displacement for ground motion sample 2

9.4 Secondary system

The secondary system considered is the hospital fire suppression piping system. It is a steel piping system that runs from a tank in the hospital basement to a standpipe on the roof. On floors 6–14, branches split off from the main riser pipe to supply water to ceiling-mounted sprinklers in the hospital wards. The riser pipe and connection to the basement tank are 6 inches in diameter, while the branches are 2 inches in diameter reducing to 1 inch at the ends. To reduce the size of the model, only two of the branches were analyzed: the branch on the top floor, where the maximum displacement and damage to piping is expected [48], and the branch at a typical intermediate floor. The system is shown in figure 9-24, where the axis units are inches. It was modeled in SABER-3D using linear pipe elements for the straight pipe runs and nonlinear elbow hinge elements for the pipe elbows. The parameters for the hinge elements were obtained from DIANA shell element analyses of the elbows.

The assumed boundary conditions were (figure 9-25):

- Tank: the pipe was assumed to be fully fixed to the tank on the basement level.

- Pipe clamps: the vertical pipe sections were assumed to be attached to the primary system at each floor by means of pipe clamps constraining translation of the pipe in all directions. This was based on evidence obtained from a visit to the site.

- Pipe hangers: the horizontal pipes were assumed to be suspended from pipe hangers from the floor beams. The pipe hangers provide only vertical support.

The input to the secondary system is the motion of the hospital structure from the primary system analysis. As the structure does not move as a rigid body, the motion is different at each support point of the secondary system. There are two methods of determining the input to the secondary system:

- Perform a time-history analysis of the primary system, and use the motion at the attachment points as input to the secondary system. If the primary system is nonlinear, this method must be used.

- If the primary system remains linear, it is possible to determine the motion at the attachment points without performing a time history analysis of the primary system. The method is based on modal analysis and is covered in Appendix A.
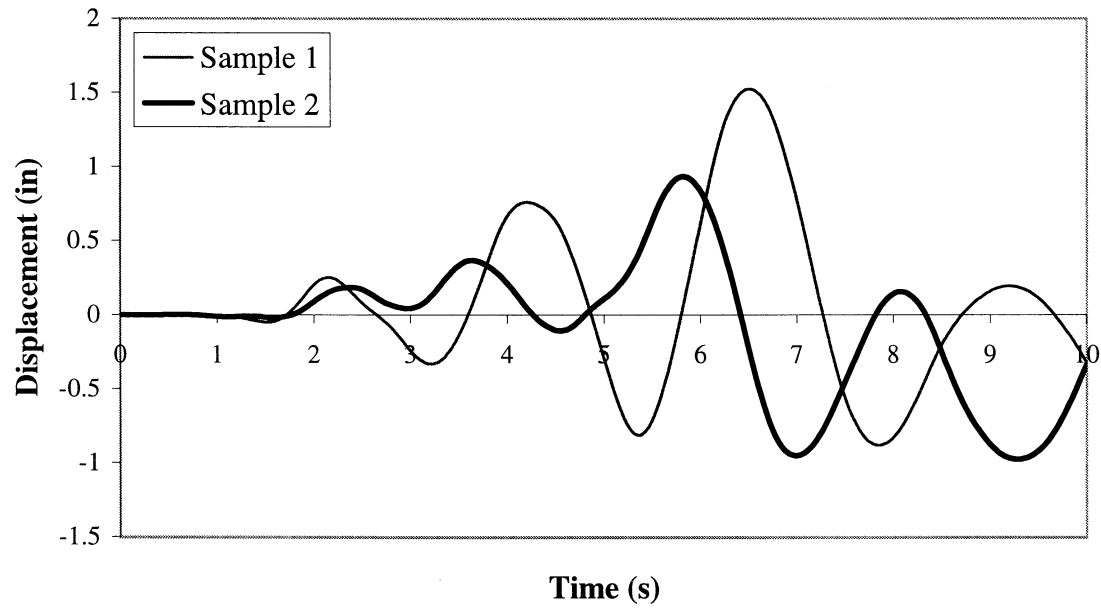
The corresponding methods of determining the sensitivity of the input to the secondary system to a parameter of the input to the primary system are:
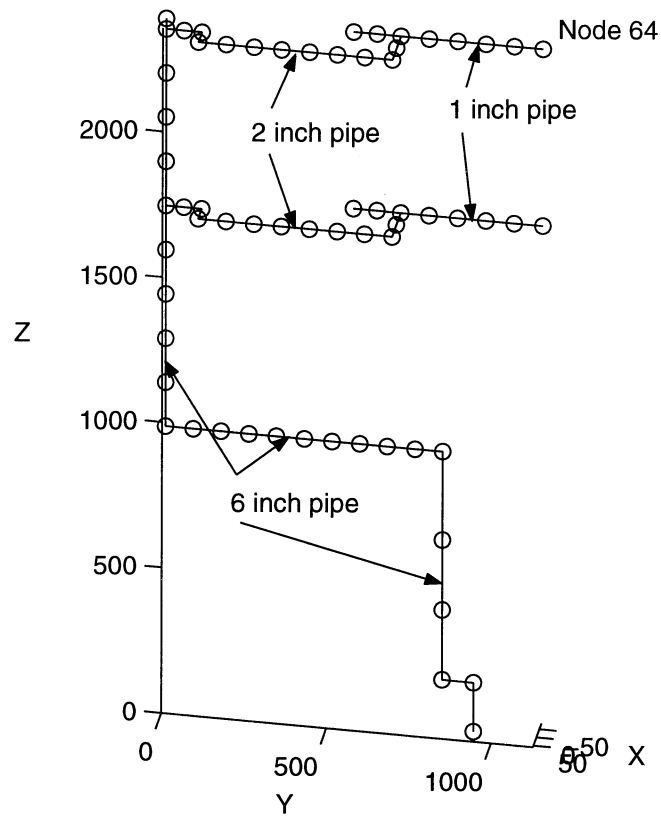
FIGURE 9-24 Secondary system

↑	Pipe hanger: vertical support
←→	Pipe clamp: applied horizontal motion, vertical support
⁄⁄⁄	Tank: applied horizontal motion, fixed against rotation
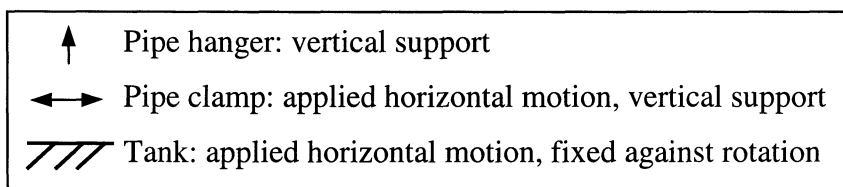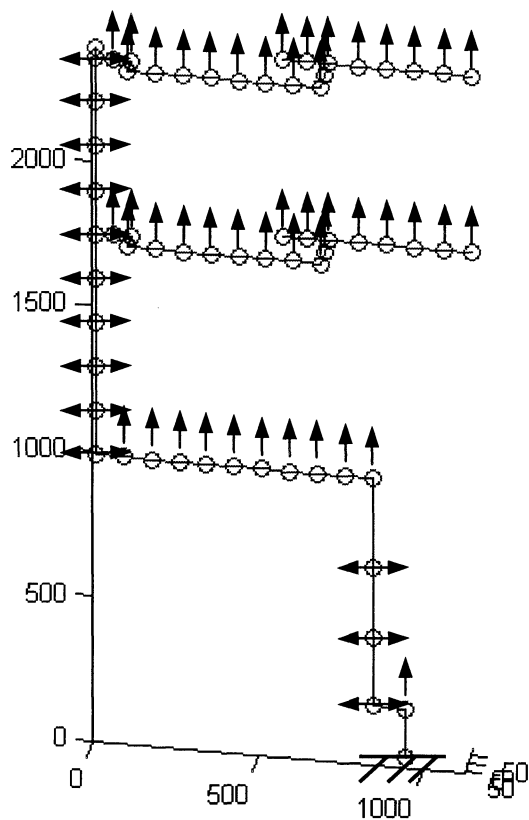
FIGURE 9-25 Boundary conditions

181

FIGURE 9-26 Relative Y-displacement of node 64

- Calculate the sensitivity factors for the time-history analysis of the primary system. For example, if the acceleration at degree of freedom j, $\ddot{u}_j(t)$, is used as the acceleration of an attachment point of the secondary system, the sensitivity is $\frac{\partial}{\partial x}\ddot{u}_j(t) = \frac{\partial^2}{\partial t^2}\left(\frac{\partial}{\partial x}u_j(t)\right) = \ddot{v}_j(t)$, which is calculated in the sensitivity analysis.

- The modal analysis approach can be used directly with the derivatives of the primary system input. Details are given in Appendix A.

As displacements and sensitivity factors have been calculated for the primary system, the first method is generally used here. The second method is used to generate input to the secondary system for Monte Carlo analysis.

The critical output for the secondary system was assumed to be the relative displacement between the structure and the pipe where sprinklers are located, that is, the 1 and 2 inch pipes. This output was selected as sprinkler damage due to relative motion between the pipe and hard ceilings was found to be a common problem for hospital piping systems in the Northridge earthquake [5]. The relative displacement in the Y-direction of node 64 was found to be the most critical and is plotted in figure 9-26. It was assumed that the sprinklers would be damaged if the displacement exceeded 1 in. The peak displacement in figure 9-26 is 1.52 in for sample 1, which is unsatisfactory.

182
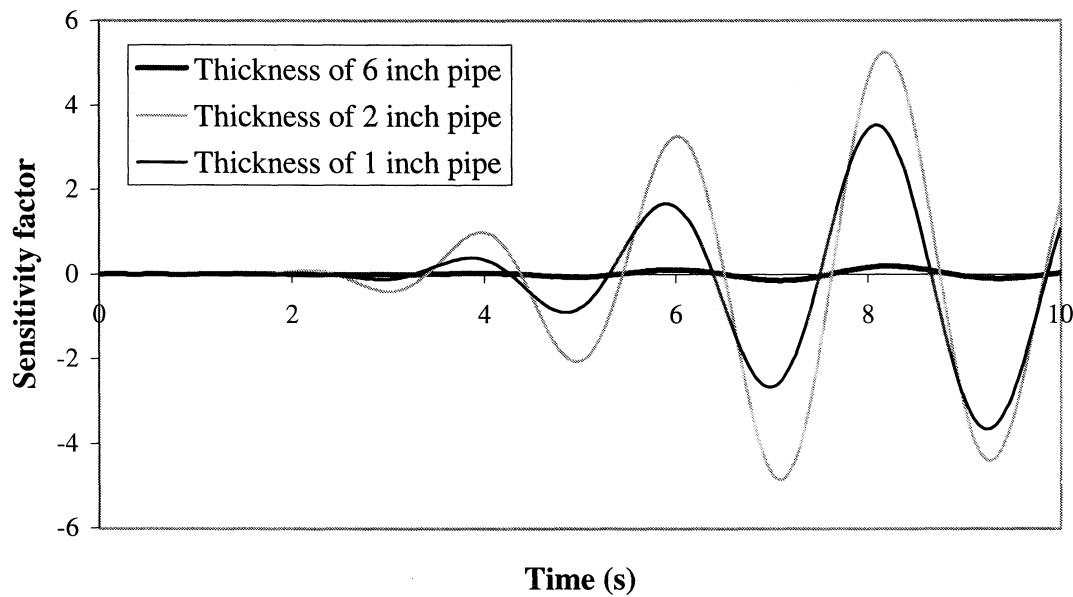
FIGURE 9-27 Sensitivity factors with respect to pipe thicknesses for sample 1

9.4.1 Identification of critical parameters

The parameters of the system that can be changed are the thicknesses of the pipes, which can be increased by selecting a stronger pipe; the strength and stiffness of the elbow and tee connections; and the mass. It is assumed that the Young's modulus of the steel is difficult or impossible to change and that the pipe diameters are fixed by the water flow requirements. Consider the problem of evaluating the sensitivity of the displacement of node 64 to the thicknesses of the three sizes of pipes. The sensitivity factors with respect to the three pipe thicknesses are shown in figures 9-27 and 9-28. As the uncertainty in the thickness is likely to be a similar percentage of the nominal value for each pipe, the first method described in Section 9.3.1 can be used to evaluate the sensitivity. The sensitivity factors multiplied by the nominal parameter values are in figures 9-29 and 9-30. It appears that for a similar percentage change in pipe thickness, the displacement is more sensitive to the thickness of the 2 inch pipe than to the 1 inch pipe, and not very sensitive to the thickness of the 6 inch pipe. This seems reasonable as the Y-displacement of node 64 is governed by the motion of the support where the 2 inch branch meets the riser, and is transferred to node 64 by axial and flexural behavior in the 2 inch pipe, and axial behavior in the 1 inch pipe. The flexural behavior in the 2 inch pipe is probably more critical than the axial behavior, and is affected by the thickness of that pipe.

For comparison, the sensitivity factor with respect to the soil average shear wave velocity for sample 1 is plotted in figure 9-31. The sensitivity of the displacement of node 64 to the different parameters can be compared by equation 9-4. Assuming coefficients of variation of
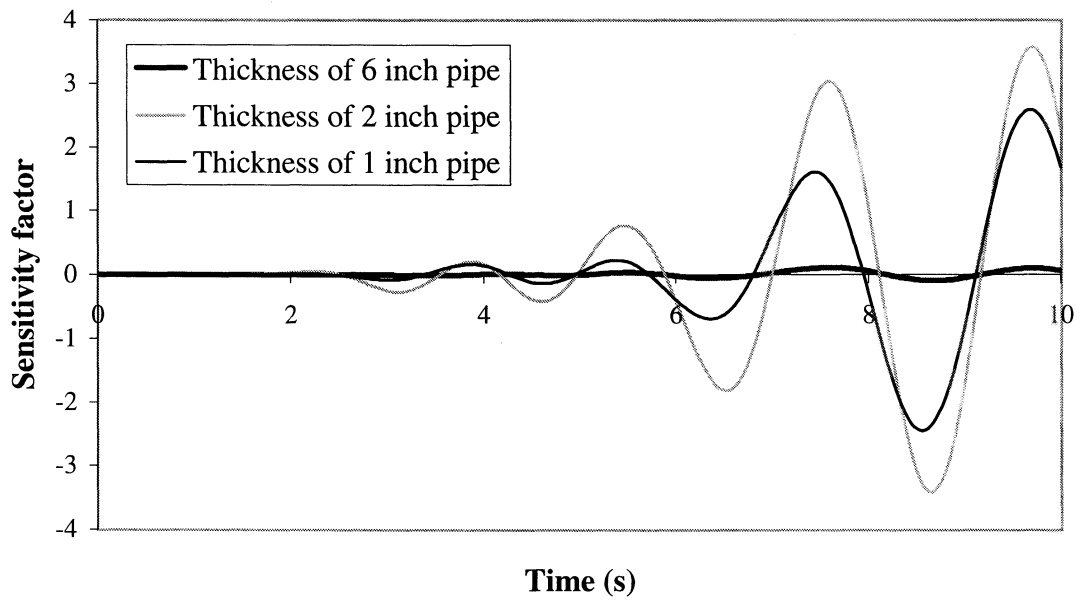
183

FIGURE 9-28 Sensitivity factors with respect to pipe thicknesses for sample 2
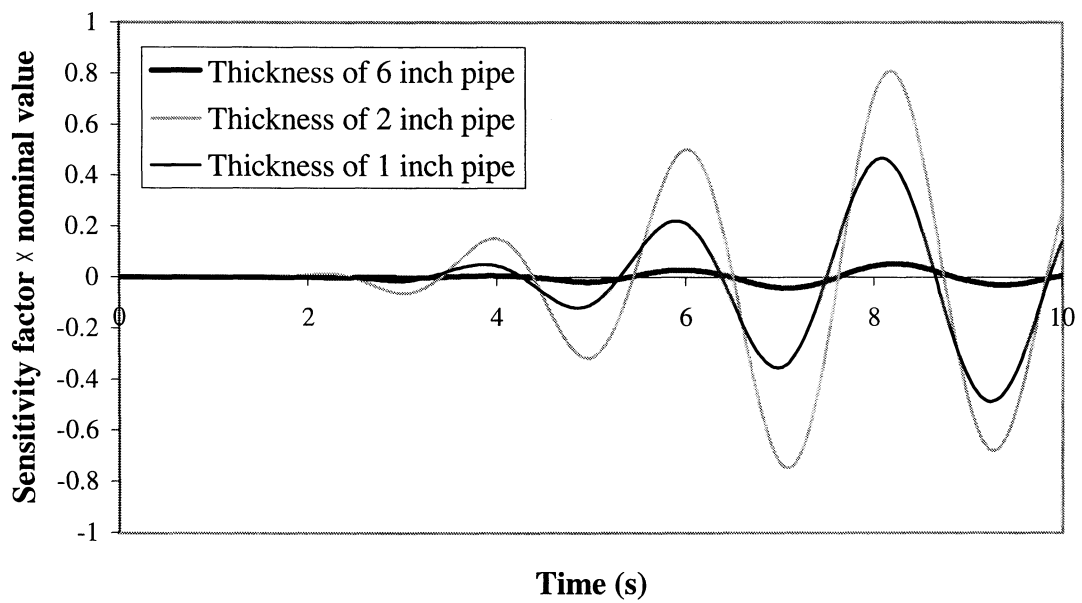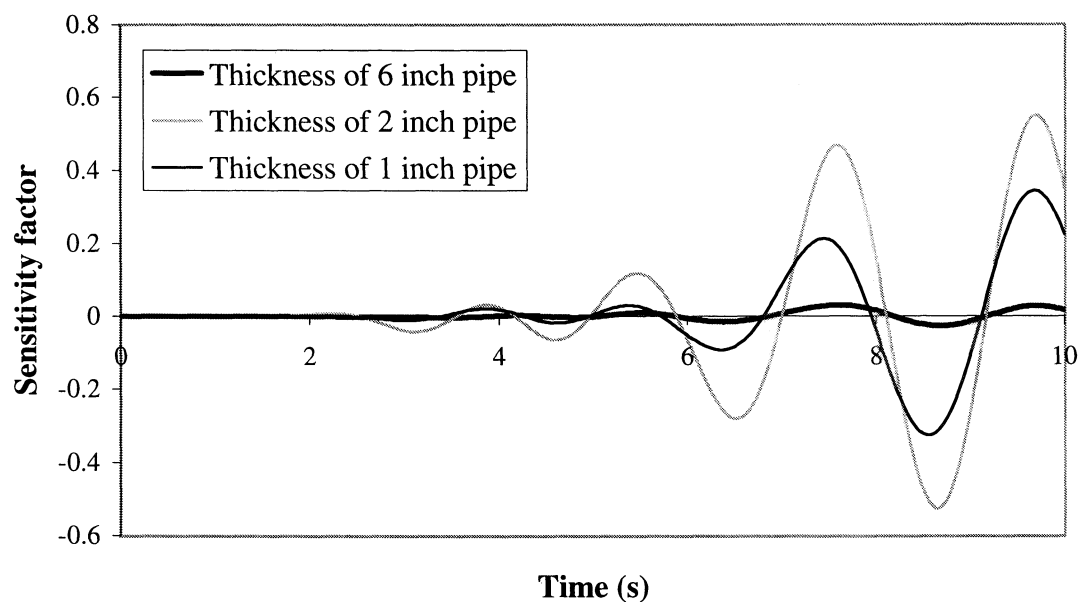

FIGURE 9-29 Sensitivity factors scaled by nominal parameter values for sample 1

184

FIGURE 9-30 Sensitivity factors scaled by nominal parameter values for sample 2

0.1 for the pipe thicknesses and 0.2 for the average shear wave velocity, the variance of the displacement is shown in figure 9-32. The displacement is substantially more sensitive to the soil parameter than to the pipe thicknesses.

To improve the behavior of the system it is necessary to reduce the displacement of node 64 to less than 1 inch. We can estimate whether this can be done by increasing any of the pipe thicknesses by using the sensitivity factors and the linear approximation. The approximate effects of increasing the thickness of the 1 inch pipe from 0.133 in to 0.179 in, the thickness of the 2 inch pipe from 0.154 in to 0.218 in, and the thickness of the 6 inch pipe from 0.280 in to 0.432 in are shown in figure 9-33 for ground motion sample 1. The thickness changes correspond to use of a stronger pipe section [49]. The behavior is not significantly affected. The peak displacements, to be compared with the original peak displacement of 1.52 in, are 1.50 in if the thickness of the 1 inch pipe is increased, 1.56 in if the thickness of the 2 inch pipe is increased, and 1.52 in if the thickness of the 6 inch pipe is increased. The new peak displacements are only approximate, but they do indicate that increasing the pipe thicknesses will not reduce the peak displacement sufficiently. It is necessary to consider retrofit strategies.

9.4.2 Retrofit strategies

Consider the often recommended retrofit strategy of installing braces to restrict the horizontal movement of the pipe [5]. The question of where the braces should be installed can be tackled
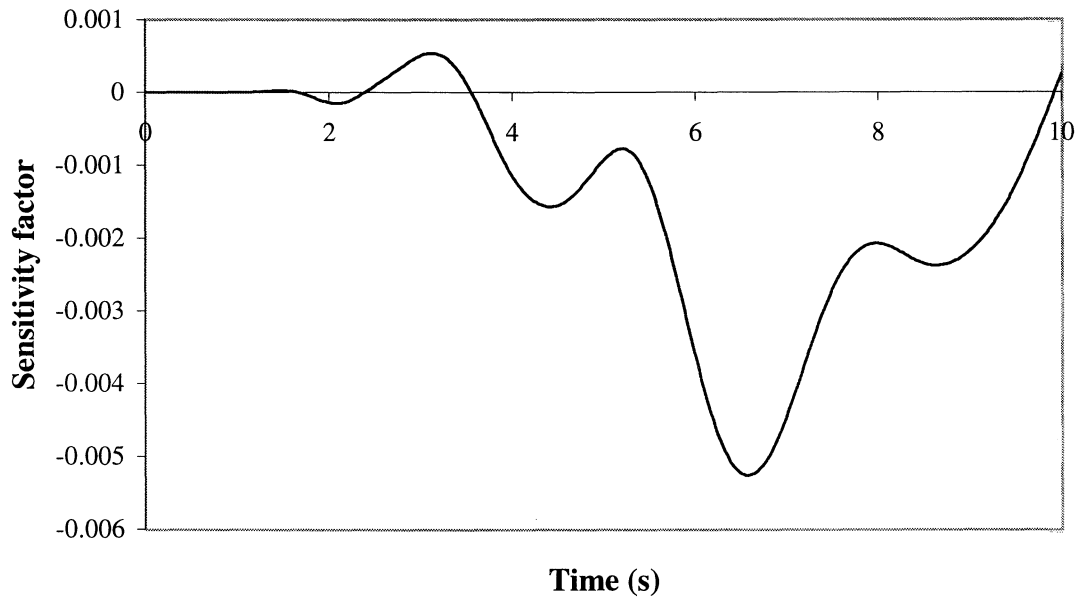
185

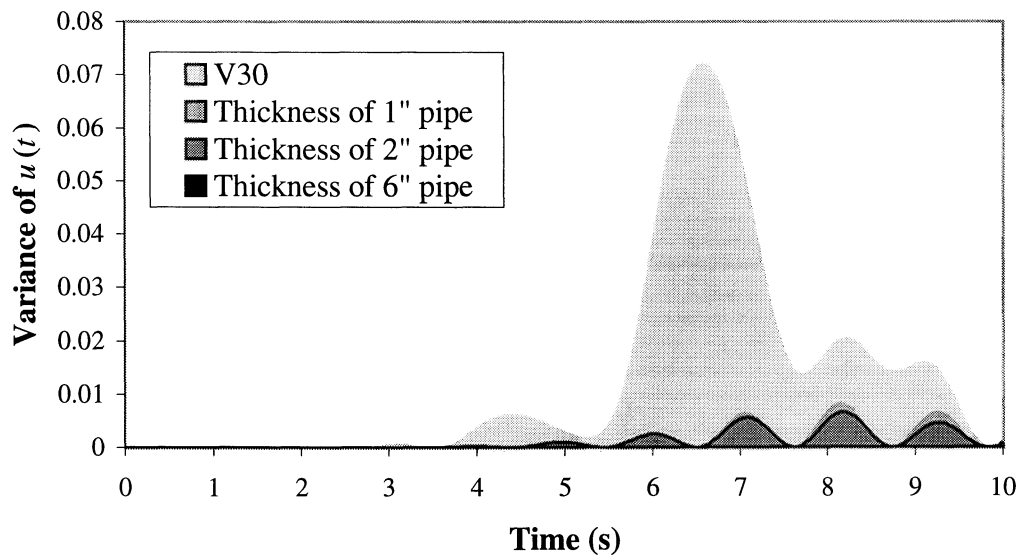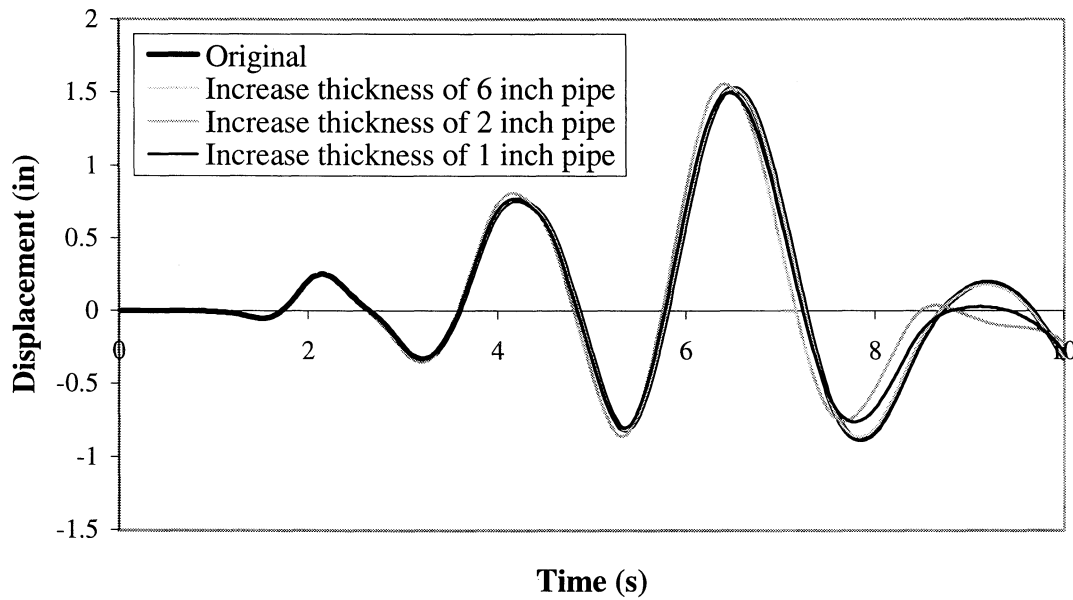**FIGURE 9-31 Sensitivity factor with respect to soil shear wave velocity**

**FIGURE 9-32 Variance of displacement**

186

**FIGURE 9-33 Displacements after increasing pipe thicknesses**

using the sensitivity factors. An initial estimate of the effect of braces on the displacement can be obtained by adding elements with zero Young's modulus to the unbraced system and calculating the sensitivity of the displacement of node 64 with respect to the Young's modulus of each of the new elements. This should give an estimate of the relative effects of adding restraints at different points to the unbraced system. Provided that all of the degrees of freedom at the supported end of the brace are fixed, the zero modulus will not cause numerical problems as stiffness in the degrees of freedom at the piping system end of the brace is provided by the existing system.

Five locations were considered as shown in figure 9-34. The sensitivity factors for ground motion sample 1 are shown in figure 9-35. The braces on the 1 inch pipe have the greatest effect on the displacement of node 64, indicating that these are the best locations to install braces.

At this point it is possible to add stiffness to the braces and reanalyze the system to confirm that the performance is satisfactory. However, to illustrate another use of the sensitivity factors, we will investigate another retrofit strategy as well. Consider replacing the rigid pipe clamp connections between the structure and the riser section of the pipe by snubbers. Snubbers are hydraulic or mechanical devices used as flexible supports for piping systems. A snubber can be modeled as a spring and a dashpot in series [11]; however, for simplicity it is modeled here as a spring [60]. The locations of the snubbers are shown in figure 9-36. The spring stiffness that minimizes the displacement of node 64 needs to be determined so that a snubber can be selected. The sensitivity factors can be used for this purpose. The approach is based on nonlinear optimization as mentioned in Section 4 and is programmed in SABER.

187
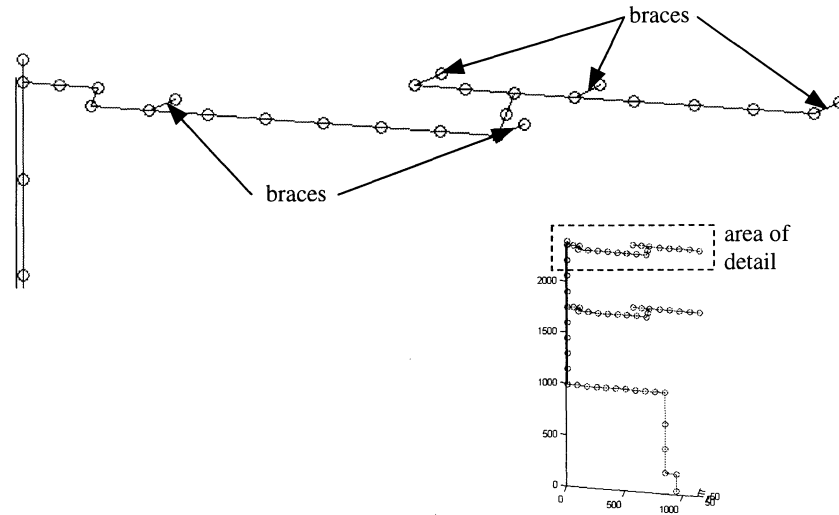
FIGURE 9-34 Brace locations
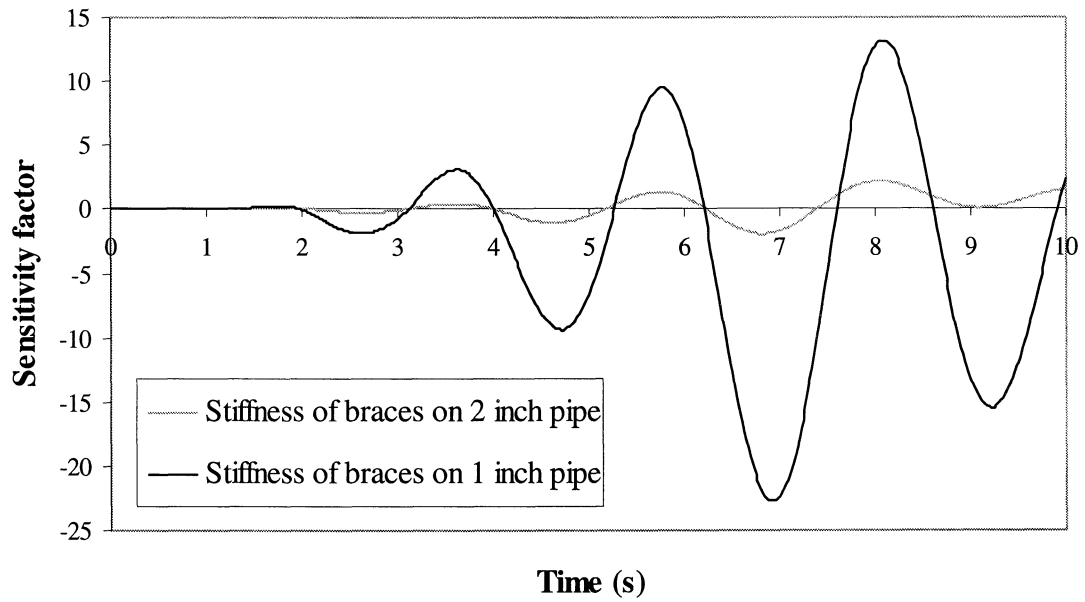
FIGURE 9-35 Sensitivity factors with respect to brace stiffnesses

188
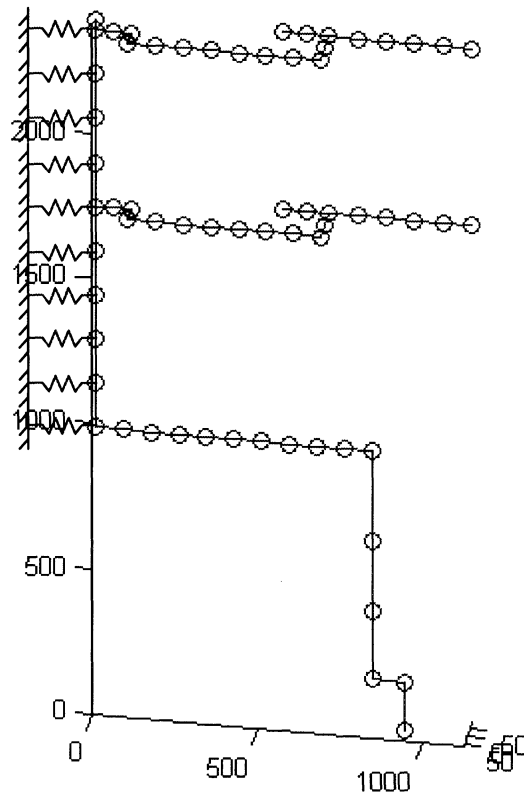
FIGURE 9-36 Snubber locations

The optimization routine indicates that the optimum stiffness is 0.0032 kip/inch, which reduces the peak displacement to 0.62 in. This value is less than 1 inch so the performance is satisfactory.

The optimization procedure is automated in SABER and it is not strictly necessary to monitor the progress or provide any further input once the routine has started. However, it may be useful here to take a more detailed look at the results. Figure 9-37 illustrates the progress of the optimization. For spring stiffnesses less than 0.0032 kip/inch, the peak displacement over the whole 10 second range occurs at around 6 seconds. The peak is not necessarily exactly at 6 sec, but varies continuously from 5.98 seconds to 6.08 seconds as the stiffness increases from 0.001 to 0.0032 kip/inch. For spring stiffnesses greater than 0.0032 kip/inch, the peak displacement over the 10 second range occurs at around 9 seconds. Again, the time of the peak actually varies continuously from 9 seconds to 8.54 seconds as the stiffness varies from 0.0032 to 0.006 kip/inch. The values of the peaks at around 6 seconds and 9 seconds are shown in figure 9-37. The peak over the entire 10 second range is the larger of the two. The minimum possible peak displacement is found where the two lines intersect. At each iteration of the optimization routine, the derivative of the peak displacement with respect to the spring stiffness is calculated and used to guide the routine. The progress of the routine is shown in the figure. It satisfactorily converges to the stiffness value which

189
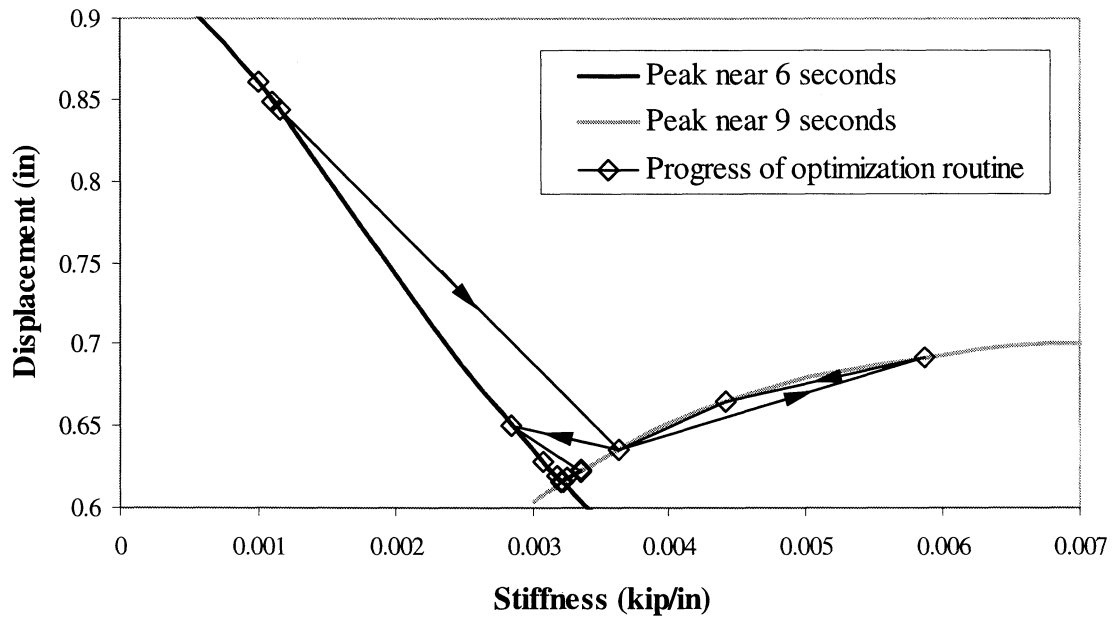
FIGURE 9-37 Progress of optimization

minimizes the peak displacement.

9.4.3 Fragility curves

Fragility curves show the probability of failure of a system as a function of a parameter of the input ground motion. As mentioned in Section 4, the sensitivity factors can be used to generate fragility curves using the approximate first-order Monte Carlo method. This section illustrates the generation of fragility curves for the secondary system using traditional Monte Carlo analysis as well as the approximate method. The failure criterion assumed is a relative Y-direction displacement of node 64 of 1.75 inches.

Fragility curves are often plotted as functions of the peak ground acceleration (PGA) of the input motion. However, PGA is not an entirely satisfactory index. As described in Section 9.2, the power spectral density of the motion is a function of the magnitude M and distance R of the earthquake event causing the motion. A better option than plotting a fragility curve against PGA may be to plot a fragility *surface* as a function of both M and R (figure 9-38). The joint probability density of M and R, obtained from a seismic hazard analysis of the site, can then be used with the surface to determine a probability of failure for the system over a predetermined lifetime. However, as this section is only intended as a demonstration of the methodology for generating fragility curves, it is not necessary to generate an entire surface. It will be assumed that the distance R is fixed at 50 km and the fragility curves will be plotted against magnitude M. The resulting fragility curve forms one

190
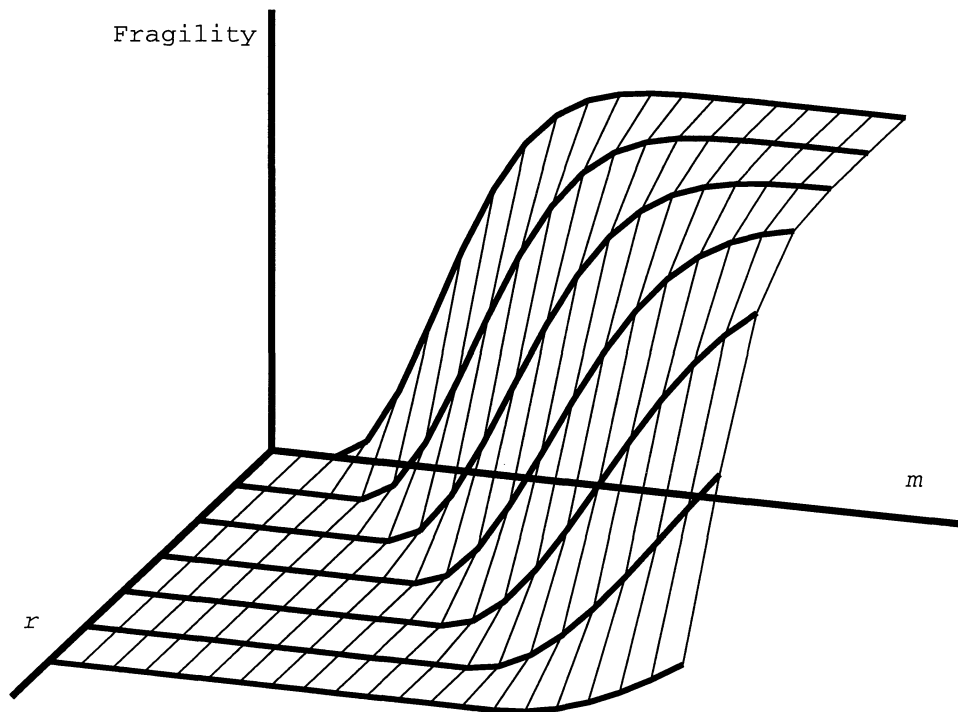
FIGURE 9-38 Fragility surface

of the lines at fixed r on the fragility surface of figure 9-38.

For a given (m, r) pair the power spectral density from which a ground motion can be generated is fixed. However, infinitely many realizations are possible for a fixed power spectral density so the input ground motion used to generate the fragility curves is random. In the terms of the parametric representation used to generate the motion (equation 9-1), the variables $A_k, B_k,\ k = 1, 2, 3 \dots$ are random.

System parameters assumed random are the diameter and Young's modulus of the pipes, and the damping. The coefficients of variation used are 0.2 for the pipe diameters, 0.06 for the Young's modulus and 0.5 for the damping.

One possible procedure for generating the fragility curve is the following, referred to here as **Method A**:

1. Select a value of M.

2. Generate a predetermined number N_s samples of the input and N_s samples of the

secondary system.

3. Perform a time-history analysis of the primary system using one of the input samples.

4. Perform a time-history analysis of one of the secondary system samples using the results from the primary system analysis. Determine whether failure occurs in the secondary system.

5. Repeat steps 2–4 for each of the N_s samples.

6. If the number of failures in the N_s analyses is N_f, the probability of failure at this value of M is approximately $\frac{N_f}{N_s}$.

7. Repeat steps 2–6 for several different values of M.

8. Fit a regression curve through the resulting points. The curve must be monotonically increasing over the range $[0, 1]$.

However, in this procedure N_s time-history analyses of the primary system must be performed at each M-value. This may be a problem if these analyses are time-consuming. A better procedure may be **Method B**, in which only *one* realization of the ground motion at each M-value is used. The probability of failure is then calculated using the N_s secondary system samples. This probability is conditional on the particular ground motion realization used. However, a different realization is used at each M-value, so the fitted fragility curve will reflect the average probability of failure of all of the realizations. Method B is quicker than Method A, particularly if a time-history analysis of the primary system is substantially more time-consuming than a time-history analysis of the secondary system.

Corresponding approximate methods in which the sensitivity factors and the procedure of Section 4 are used instead of traditional Monte Carlo simulation to determine the probability of failure will be termed Methods A' and B'.

For the hospital demonstration project, it was found that Methods A and A' were impractical, so Methods B and B' were used to generate the fragility curves. Method A requires several analyses of the primary system at each M-value, which is extremely time-consuming. Method A' requires only one analysis of the primary system at each M-value, but requires that sensitivity factors be calculated for all of the random variables A_k, B_k, $k = 1, 2, 3 \ldots$ used in the input to the primary system. Approximately 650 were used and calculating sensitivity factors for each one would also be extremely time-consuming.

The fragility curves calculated by Methods B and B' are shown plotted against M in figure 9-39 and PGA in figure 9-40. Fragility curves of the following form were fitted by the weighted least squares method:

$$y = 1 - \exp\left(-ax^b\right) \tag{9-5}$$

192

where y is the fragility, x is the ground motion parameter, and a and b are regression constants.

The following comments can be made about the fragility curves:

1. In both figures 9-39 and 9-40, the curves generated by Methods B and B′ are reasonably similar and the approximate B′ curves may be accurate enough for most applications. The advantage of the approximate method is in the time taken. To illustrate the order of magnitude difference, the total time required for a 256 MHz computer to complete the calculations was less than one minute for Method B′ compared with two days for Method B.

2. Comparison of figures 9-39 and 9-40 indicates that magnitude M is a better ground motion parameter than PGA for the fragility curves. In this context, a good ground motion parameter is one against which the points on a fragility curve show a clear increasing trend. It appears from inspection of figure 9-39 that higher fragilities coincide with higher values of M. It is less apparent from figure 9-40 that higher fragilities coincide with higher values of PGA, indicating empirically that M is a better parameter. More precisely, in figure 9-39 the sum of squared residuals for the B and B′ curves are 0.06 and 0.05 respectively, while in figure 9-40 they are 0.14 and 0.12. This indicates that the data points fit the increasing curves against M better than they fit the curves against PGA.
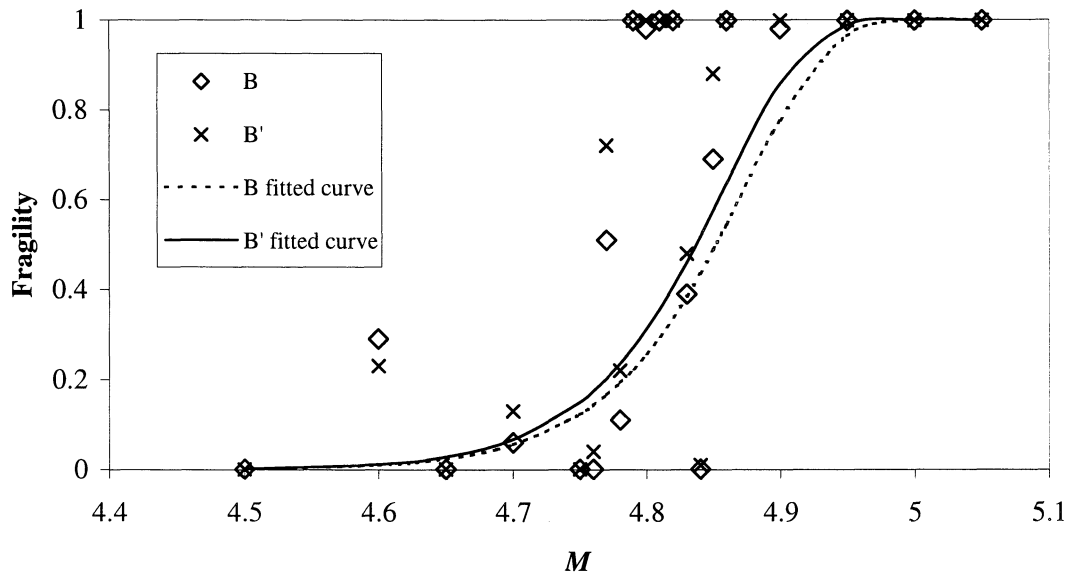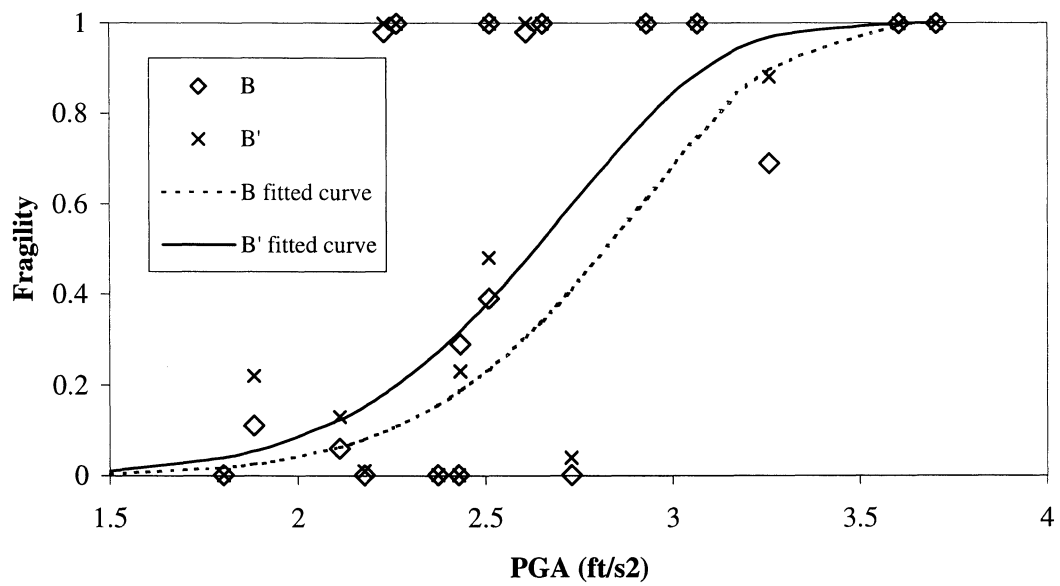
FIGURE 9-39 Fragility curves versus M

FIGURE 9-40 Fragility curves versus PGA

194

SECTION 10
CONCLUSIONS

There appears to be no limit to the application of the direct differentiation method to calculate sensitivity factors for dynamic systems subjected to seismic loads. The basic framework and approach has been laid out and implemented in two computer programs: a relatively simple MATLAB program and a more detailed DIANA finite element analysis program. The approach works well and no major numerical problems were experienced. If required, derivatives can be calculated for other material models. Some effort is required to derive the relevant equations, which can then be used in the existing computer program framework.

An example was presented to illustrate the application of the sensitivity factors to the primary and secondary systems of a hospital in Buffalo. The sensitivity factors were used to identify critical parameters, estimate the variance of the response of the systems, select retrofit strategies and generate approximate fragility curves.

10.1 Future work

The following points can be considered for future work:

- Derivation and implementation of sensitivity equations for other DIANA material models such as the smeared cracking model.

- Derivation and implementation of sensitivity equations for geometrically nonlinear behavior.

- A new type of shell finite element for analysis of pipes. The hybrid shell and beam model is not entirely satisfactory as it is difficult to generate and enforces a plane section at the shell/beam interface. The problem with a full shell element analysis is that at least twenty elements are required around the circumference of the pipe to ensure accuracy. Current shell elements are required to be approximately square, so that the longitudinal dimensions of the elements have to be very small relative to the longitudinal dimensions of typical piping systems. This means that unnecessarily high numbers of elements have to be used for a full shell analysis. An elongated type of shell element would thus be useful.

SECTION 11
REFERENCES

[1] H Adelman and R Haftka. Sensitivity analysis of discrete structural systems. *AIAA Journal*, 24(5):823–832, 1986.

[2] M Arad, G Ben-Dor, and A Yakhot. High-order-accurate discretization of a second-order equation with discontinuous coefficients. *Applied Mathematical Modelling*, 22:69–79, 1998.

[3] J Arora and J Cardoso. A design sensitivity analysis principle and its implementation into ADINA. *Computers & Structures*, 32(3–4):691–705, 1989.

[4] G Ayala and Y Xianguo. Analytical evaluation of the structural seismic damage of reinforced concrete frames. *Proceedings of the 7th Canadian Conference on Earthquake Engineering*, 1995.

[5] Ayres and Ezer Associates. *Northridge Earthquake Hospital Water Damage Study*. Ayres and Ezer Associates, Inc., Los Angeles, California, 1996.

[6] S Benfratello, S Caddemi, and G Muscolino. Gaussian and non-Gaussian stochastic sensitivity analysis of discrete structural system. *Computers & Structures*, 78(1–3):425–434, 2000.

[7] J Besseling. A theory of elastic, plastic and creep deformations of an initially isotropic material showing anisotropic strain-hardening, creep recovery and secondary creep. *Journal of Applied Mechanics, ASME*, 25:529–536, 1958.

[8] M Bykhovskiy. The accuracy of mechanisms for which the state (or position) of the components (links) are described by differential equations. *Izvestiya AN SSSR*, 11, 1947.

[9] M Bykhovskiy. Sensitivity and dynamic accuracy of control systems. *Engineering Cybernetics*, 2:121–134, 1964.

[10] F Casciati and L Faravelli. Plastic zone spread and seismic reliability of reinforced concrete frames. *Proceedings of the Eighth World Conference on Earthquake Engineering*, IV:567–574, 1984.

[11] T Chiba and H Kobayashi. A study of modeling the mechanical snubber for dynamic analysis. *8th International Conference on Structural Mechanics in Reactor Technology*, K(b):189–194, 1985.

[12] K Choi, J Santos, and M Frederick. Implementation of design sensitivity analysis with existing finite element codes. *Journal of Mechanisms, Transmissions, and Automation in Design, ASME*, 109:385–391, 1987.

[13] A Chopra. *Dynamics of Structures: Theory and Applications to Earthquake Engineering*. Prentice-Hall, Englewood Cliffs, New Jersey, 1995.

[14] M Constantinou, P Tsopelas, and W Hammel. *Testing and Modeling of an Improved Damper Configuration for Stiff Structural Systems*, Technical Report, State University of New York at Buffalo, Buffalo, New York, 1997.

[15] M Cook, D Malkus, and M Plesha. *Concepts and Applications of Finite Element Analysis*. John Wiley and Sons, New York, New York, 1989.

[16] R de Borst. The zero-normal-stress condition in plane-stress and shell elastoplasticity. *Communications in Applied Numerical Methods*, 7:29–33, 1991.

[17] F de Witte and J Jansen. *DIANA User's Manual*. TNO Building and Construction Research, Delft, The Netherlands, 1998.

[18] C Edwards and E Penney. *Elementary Differential Equations with Applications*. Prentice Hall, Englewood Cliffs, New Jersey, 1985.

[19] M Eslami. *Theory of Sensitivity in Dynamic Systems*. Springer-Verlag, Berlin, Germany, 1994.

[20] P Feenstra. *Computational Aspects of Biaxial Stress in Plain and Reinforced Concrete*. PhD thesis, Delft University of Technology, 1993.

[21] A Frankel. Mapping seismic hazard in the central and eastern United States. *Seismological Research Letters*, 66(4):8–21, 1995.

[22] T Fung. Higher order time-step integration methods with complex time steps. *Journal of Sound and Vibration*, 210(1):69–89, 1998.

[23] D Fylstra, L Lasdon, J Watson, and A Waren. Design and use of the microsoft excel solver. *Interfaces*, 28(5):29–55, 1998.

[24] M Greenberg. *Advanced Engineering Mathematics*. Prentice Hall, Upper Saddle River, New Jersey, 1998.

[25] W Greene and R Haftka. Computational aspects of sensitivity calculations in transient structural analysis. *Computers & Structures*, 32(2):433–443, 1989.

[26] T Hien and M Kleiber. Stochastic design sensitivity in structural dynamics. *International Journal for Numerical Methods in Engineering*, 32(6):1247–1265, 1991.

[27] T Hughes. *The Finite Element Method: Linear Static and Dynamic Finite Element Analysis*. Prentice-Hall, Englewood Cliffs, New Jersey, 1987.

[28] S Jao and J Arora. Design optimization of non-linear structures with rate-dependent and rate-independent constitutive models. *International Journal for Numerical Methods in Engineering*, 36(16):2805–2823, 1993.

[29] M Kleiber. Shape and non-shape structural sensitivity analysis for problems with any material and kinematic non-linearity. *Computer Methods in Applied Mechanics and Engineering*, 108:73–97, 1993.

198

[30] M Kleiber, T Hien, and E Postek. Incremental finite element sensitivity analysis for non-linear mechanics applications. *International Journal for Numerical Methods in Engineering*, 37:3291–3308, 1994.

[31] M Kulkarni and A Noor. Sensitivity analysis for the dynamic response of viscoplastic shells of revolution. *Computers & Structures*, 55(6):955–969, 1995.

[32] M Kulkarni and A Noor. Sensitivity analysis of the non-linear dynamic viscoplastic response of 2-D structures with respect to material parameters. *International Journal for Numerical Methods in Engineering*, 38(2):183–198, 1995.

[33] B Lee and O Lim. Design sensitivity analysis extended to perturbation treatment in problems of uncertain structural system. *Computers & Structures*, 62(4):757–762, 1997.

[34] B Lee and O Lim. Application of stochastic finite element method to optimal design of structures. *Computers & Structures*, 68(5):491–497, 1998.

[35] I Lee, G Jung, and J Lee. Numerical method for sensitivity analysis of eigensystems with non-repeated and repeated eigenvalues. *Journal of Sound and Vibration*, 195(1):17–32, 1996.

[36] Femsys Limited. *FEMGV User Manual*. Femsys Limited, Leicester, United Kingdom, 1997.

[37] X Liu and D Begg. Sensitivity analysis of smart structures. *Computer Methods in Applied Mechanics and Engineering*, 163(1–4):311–322, 1998.

[38] D Luenberger. *Linear and Nonlinear Programming*. Addison-Wesley, Reading, Massachusetts, 1984.

[39] A Ma, S Chen, and X Li. Design sensitivity analysis of non-linear response for large deflection forced vibrations of beams. *Journal of Sound and Vibration*, 187(4):683–693, 1995.

[40] H Madsen, S Krenk, and N Lind. *Methods of Structural Safety*. Prentice-Hall, Englewood Cliffs, New Jersey, 1986.

[41] P Marchand. *Graphics and GUIs with MATLAB*. CRC Press, Boca Raton, Florida, 1996.

[42] The MathWorks. *MATLAB Student Version*. The MathWorks, Inc., Natick, Massachusetts, 1999.

[43] W McGuire and R Gallagher. *Matrix Structural Analysis*. John Wiley and Sons, New York, New York, 1979.

[44] S Mirza and J MacGregor. Variability of mechanical properties of reinforcing bars. *Journal of the Structural Division, ASCE*, 105(ST5):921–937, 1979.

[45] E Mostafa and M Grigoriu. *Fragility curves for non-structural systems*, Technical Report 99-2, School of Civil and Environmental Engineering, Cornell University, Ithaca, New York, 1999.

[46] N Newmark. A method of computation for structural dynamics. *Journal of the Engineering Mechanics Division, ASCE*, 85(3):67–94, 1959.

[47] American Society of Civil Engineers. *Minimum design loads for buildings and other structures*. ANSI/ASCE 7-95. American Society of Civil Engineers, New York, New York, 1996.

[48] Office of Statewide Health Planning and Development. *The Northridge Earthquake: A Report to the Hospital Building Safety Board on the Performance of Hospitals*. Facilities Development Division, Office of Statewide Health Planning and Development, Sacramento, California, 1995.

[49] American Institute of Steel Construction. *Manual of Steel Construction*. American Institute of Steel Construction, Chicago, Illinois, 1995.

[50] Y Ohtori and B Spencer. A MATLAB-based tool for nonlinear structural analysis. *Proceedings of the 13th ASCE Engineering Mechanics Division Specialty Conference*, 1999.

[51] A Papageorgiou and K Aki. A specific barrier model for the quantitative description of inhomogeneous faulting and the prediction of strong ground motion. *Bulletin of the Seismological Society of America*, 73(3):693–722, 1983.

[52] D Phelan, C Vidal, and R Haber. An adjoint variable method for sensitivity analysis of non-linear elastic systems. *International Journal for Numerical Methods in Engineering*, 31:1649–1667, 1991.

[53] W Press. *Numerical Recipes in Fortran 90 : the Art of Parallel Scientific Computing*. Cambridge University Press, Cambridge, United Kingdom, 1996.

[54] D Ray. *Sensitivity Analysis for Hysteretic Dynamic Systems*, EERC74-5, Earthquake Engineering Research Center, University of California, Berkeley, California, 1974.

[55] D Ray, K Pister, and E Polak. Sensitivity analysis for hysteretic dynamic system: theory and applications. *Computer Methods in Applied Mechanics and Engineering*, 14:179–208, 1978.

[56] C Roth. *Sensitivity analysis of dynamic systems subjected to seismic loads*. PhD thesis, Cornell University, 2001.

[57] C Roth and M Grigoriu. *SABER User's Manual*, Technical Report 00-2, School of Civil and Environmental Engineering, Cornell University, Ithaca, New York, 2000.

[58] M Saiidi. Hysteresis models for reinforced concrete. *Journal of the Structural Division, ASCE*, 108(ST5):1077–1087, 1982.

[59] O Sergeyev and Z Mróz. Sensitivity analysis and optimal design of 3D frame structures for stress and frequency constraints. *Computers & Structures*, 75(2):167–185, 2000.

[60] G Sharma, M Manna, G Ghosh, and S Chatterjee. Seismic analysis of main primary heat transport system for Kakrapar atomic power project. *8th International Conference on Structural Mechanics in Reactor Technology*, K(b):229–234, 1985.

[61] J Simo, J Kennedy, and S Govindjee. Non-smooth multisurface plasticity and viscoplasticity. Loading/unloading conditions and numerical algorithms. *International Journal for Numerical Methods in Engineering*, 26:2161–2185, 1988.

[62] T Soong and G Dargush. *Passive Energy Dissipation Systems in Structural Engineering*. John Wiley and Sons, New York, New York, 1997.

[63] T Soong and M Grigoriu. *Random Vibration of Mechanical and Structural Systems*. P T R Prentice Hall, Englewood Cliffs, New Jersey, 1993.

[64] J Tang, W Ni, and W Wang. Eigensolutions sensitivity for quadratic eigenproblems. *Journal of Sound and Vibration*, 196(2):179–188, 1996.

[65] J Tang and W Wang. On calculation of sensitivity for non-defective eigenproblems with repeated roots. *Journal of Sound and Vibration*, 225(4):611–631, 1999.

[66] J Tsay and J Arora. Nonlinear structural design sensitivity analysis for path dependent problems. Part 1: general theory. *Computer Methods in Applied Mechanics and Engineering*, 81(2):183–208, 1990.

[67] J Tsay, J Cardoso, and J Arora. Nonlinear structural design sensitivity analysis for path dependent problems. Part 2: analytical examples. *Computer Methods in Applied Mechanics and Engineering*, 81(2):209–228, 1990.

[68] Y Zhang and A Der Kiureghian. Dynamic response sensitivity of inelastic structures. *Computer Methods in Applied Mechanics and Engineering*, 108:23–36, 1993.

[69] Y Zhang and A Der Kiureghian. First-excursion probability of uncertain structures. *Probabilistic Engineering Mechanics*, 9:135–143, 1994.

[70] O Zienkiewicz and Y Xie. A simple error estimator and adaptive time stepping procedure for dynamic analysis. *Earthquake Engineering and Structural Dynamics*, 20(9):871–887, 1991.

APPENDIX A
CALCULATION OF RESPONSE OF LINEAR PRIMARY SYSTEM

The input to the primary system is a Gaussian stochastic process with the amplitude modulated through time by an envelope function $w(t)$. The process is simulated by [63]

$$a(t) = w(t) \sum_{k=1}^{n} \sqrt{g(\omega_k, \boldsymbol{\theta}) \Delta\omega} \left(A_k \cos(\omega_k t) + B_k \sin(\omega_k t) \right) \tag{A-1}$$

where $\boldsymbol{\theta}$ is a vector of parameters of the power spectral density $g(\omega)$, ω_c is a cut-off frequency, $\Delta\omega = \frac{\omega_c}{n}$; $\omega_k = (k - \frac{1}{2})\Delta\omega$; and A_k and B_k are independent standard Gaussian random variables.

The displacement at any degree of freedom i of the primary system is [13]

$$u_i(t) = \sum_{j=1}^{m} \phi_{ij} q_j(t) \tag{A-2}$$

where ϕ_{ij} is the displacement at degree of freedom i in mode j and $q_j(t)$ is the j-th modal coordinate. It is typically not necessary to consider all of the modes — only the m modes that have significant contributions need be included. The modal coordinate is governed by

$$\ddot{q}_j(t) + 2\zeta_j \omega_j \dot{q}_j(t) + \omega_j^2 q_j(t) = \Gamma_j a(t) \tag{A-3}$$

where ω_j, ζ_j and Γ_j are the frequency, damping ratio and modal participation factor for mode j respectively.

The solution to equation A-3 is

$$q_j(t) = \frac{\Gamma_j}{\omega_{dj}} \int_0^t e^{-\zeta_j \omega_j (t-s)} \sin\left(\omega_{dj}(t-s)\right) a(s) \, ds \tag{A-4}$$

where $\omega_{dj} = \omega_j \sqrt{1 - \zeta_j^2}$.

Substituting equations A-1 and A-4 into A-2

$$u_i(t) = \sum_{j=1}^{m} \phi_{ij} \frac{\Gamma_j}{\omega_{dj}} \int_0^t e^{-\zeta_j \omega_j (t-s)} \sin\left(\omega_{dj}(t-s)\right) a(s) \, ds$$

$$= \sum_{j=1}^{m} \phi_{ij} \frac{\Gamma_j}{\omega_{dj}} \int_0^t e^{-\zeta_j \omega_j (t-s)} \sin\left(\omega_{dj}(t-s)\right)$$

$$\cdot w(s) \sum_{k=1}^{n} \sqrt{g(\omega_k, \boldsymbol{\theta}) \Delta\omega} \left(A_k \cos(\omega_k s) + B_k \sin(\omega_k s)\right) \, ds$$

$$= \sum_{k=1}^{n} \sqrt{g(\omega_k, \boldsymbol{\theta}) \Delta\omega}$$

$$\cdot \left[A_k \sum_{j=1}^{m} \phi_{ij} \frac{\Gamma_j}{\omega_{dj}} \int_0^t e^{-\zeta_j \omega_j (t-s)} \sin\left(\omega_{dj}(t-s)\right) w(s) \cos(\omega_k s) \, ds \right.$$

$$\left. + B_k \sum_{j=1}^{m} \phi_{ij} \frac{\Gamma_j}{\omega_{dj}} \int_0^t e^{-\zeta_j \omega_j (t-s)} \sin\left(\omega_{dj}(t-s)\right) w(s) \sin(\omega_k s) \, ds \right]$$

$$= \sum_{k=1}^{n} \sqrt{g(\omega_k, \boldsymbol{\theta}) \Delta\omega} \left[A_k \sum_{j=1}^{m} \phi_{ij} \frac{\Gamma_j}{\omega_{dj}} I_1(t) + B_k \sum_{j=1}^{m} \phi_{ij} \frac{\Gamma_j}{\omega_{dj}} I_2(t) \right] \qquad \text{(A-5)}$$

The integrals

$$I_1(t) = \int_0^t e^{-\zeta_j \omega_j (t-s)} \sin\left(\omega_{dj}(t-s)\right) w(s) \cos(\omega_k s) \, ds$$

$$I_2(t) = \int_0^t e^{-\zeta_j \omega_j (t-s)} \sin\left(\omega_{dj}(t-s)\right) w(s) \sin(\omega_k s) \, ds$$

can be solved in closed form for certain forms of the envelope function $w(s)$. An often used function has the form

$$w(s) = a s^b e^{-cs} \qquad \text{(A-6)}$$

However, in this case no closed form exists for $I_1(t)$ and $I_2(t)$. A better option is to use

$$w(s) = c_1 e^{c_2 s} \sin(c_3 s) \qquad \text{(A-7)}$$

and select the values of c_1, c_2 and c_3 to match equation A-6 as closely as possible. In this case closed form solutions can be found for $I_1(t)$ and $I_2(t)$ [56].

If x is a parameter in $\boldsymbol{\theta}$, then the derivative of $u_i(t)$ with respect to x is

$$\frac{\partial u_j(t)}{\partial x} = \sum_{k=1}^{n} \frac{\sqrt{\Delta\omega}}{2\sqrt{g(\omega_k, \boldsymbol{\theta})}} \frac{\partial g(\omega_k, \boldsymbol{\theta})}{\partial x} \left[A_k \sum_{j=1}^{m} \phi_{ij} \frac{\Gamma_j}{\omega_{dj}} I_1(t) + B_k \sum_{j=1}^{m} \phi_{ij} \frac{\Gamma_j}{\omega_{dj}} I_2(t) \right] \qquad \text{(A-8)}$$